OCRWM	SCIENTIFIC ANALYSIS COVER SHEET	1. QA: QA Page 1 of 80

2. Scientific Analysis Title:	
Advection versus Diffusion in the Invert	
3. DI (including Revision Number):	
ANL-EBS-MD-000063 REV 00	
4. Total Attachments: Nineteen (19)	5. Attachment Numbers - Number of pages in each: I-4; II-4; III-10; IV-14; V-14; VI-16; VII-10; VIII-4; IX-4; X-22; XI-12; XII-4; XIII-6; XIV-8; XV-4; XVI-4; XVII-6; XVIII-8; XIX-CD-ROM-2 8/18/03

	Printed Name:	Signature:	Date:
6. Originator:	John B. Case	SIGNATURE ON FILE	8/23/03 JBC 8/23/03
7. Checker:	Junghun Leem	SIGNATURE ON FILE	8/23/03
8. QER:	Darrell K. Svalstad	SIGNATURE ON FILE	8/23/03
9. Responsible Manager/Lead:	Dennis W. Thomas	SIGNATURE ON FILE	8/23/03
10. Responsible Manager:	Robert W. Andrews	SIGNATURE ON FILE	8/29/03

11. Remarks:

Added page number (2) to Attachment XIX-CD-Rom-, of Block 5.

SIGNATURE ON FILE 2/10/04

Revision History

12. Revision/ICN No.:	13. Description of Revision/Change:
00	Initial Issue.

INTENTIONALLY LEFT BLANK

CONTENTS

Page

CONTENTS (Continued)

Page

FIGURES

Page

TABLES

Page

ACRONYMNS

AC	Acceptance Criteria
DKM	Dual Permeability Model
DTN	Data Tracking Number
EBS	engineered barrier system
ECM	Equivalent Continuum Model
FEPS	features, events and processes
ICN	Interim Change Notice
LLNL	Lawrence Livermore National Laboratory
NBS	natural barrier system
NMR	Nuclear Magnetic Resonance
TDMS	Technical Data Management System
TSPA	Total System Performance Assessment
UFA	Unsaturated Flow Apparatus
YMP	Yucca Mountain Project

NOMENCLATURE

Am = Americium
b = Slope of the ln(ψ) versus ln(θ) retention curve
C = Solute concentration at location x, y, z and time t(mg/l)
C_L = Solute concentration of the solute at location L and time t (mg/l)
C_o = Solute concentration of the solute at location x =0 (mg/l)
D = Dispersion/Diffusion Coefficient (m^2/sec) (D_e/2)
d_g = Geometric mean particle diameter(-)
d_m = Mean Particle Diameter (mm)
D_e = Effective Dispersion/Diffusion Coefficient (m^2/sec)
D_{lh} = Hydrodynamic dispersion coefficient (m^2/sec)
D_x = Dispersion/Diffusion Coefficient in the x direction (m^2/sec)
D_y = Dispersion/Diffusion Coefficient in the y direction (m^2/sec)
D_z = Dispersion/Diffusion Coefficient in the z direction (m^2/sec)
D_{wl} = Binary diffusion coefficient (m^2/sec)
D_{sl} = solute diffusion coefficient of solute in water (m^2/sec)
erfc = Complementary error function
exp = Exponential function
g = Acceleration due to gravity
I = Iodine
J_l = Combined flux
J_{lc}= Liquid Advection flux (m/s)
J_{lh} = Hydrodynamic dispersion flux (m/s)
J_{sl} = Soil liquid flux (m/s)
J_w = Vertical Darcy flux rate (m/s)
K_d = Partition coefficient (m^3/kg)
K_s = Saturated hydraulic conductivity (cm/sec)
K_{us} = Unsaturated hydraulic conductivity (cm/sec)
k = Intrinsic permeability (m^2)
k_{us} = Unsaturated intrinsic permeability(m^2)
k_{vs} = Intrinsic permeability of volcanic sand (m^2)
k_{fs} = Intrinsic permeability of volcanic of fine sand (m^2)
k_{gb}= Intrinsic permeability of glass beads(m^2)
k_{tsl} = Intrinsic permeability of Touchet silt loam (m^2)
L = Length in the vertical direction (m)
M = van Genuchten parameter estimated from the water retention curve
n =van Genuchten n parameter
Np = Neptunium
Pu = Plutonium
R = Retardation Factor
S= Saturation
S_{bulk} = Bulk saturation of the rock
S_{matrix} = Saturation of the rock matrix in individual grains
$S_{intergrain}$ =Saturation of the large or coarse pore spaces between grains
S_r = Residual saturation
S_s = Saturation at saturation
t = Time (sec)
Tc = Technetium
Th = Thorium

NOMENCLATURE (Continued)

U = Uranium
V = Pore-water velocity or average linear velocity (m/s)
V_c = Volume of the voids in the coarse or intergranular void space (m^3)
V_{sm} =Volume of the Solids of the Crushed Tuff Matrix (m^3)
V_{tm}= Volume of the voids in the intragranular void space (m^3)
$V_{Grain,Total}$ = Total volume of the grains
V_{Total} = Total volume of grains and pore space(m^3)
VW_c=Volume of water in the intergranualr void space (m^3)
VW_{tm}= Volume of water in the intragranular void space(m^3)
V_v= Total volume of the voids (m^3)
W_s= Weight of the Solids(kg)
W_w= Weight of the Water (kg)
v_c = Average Pore-water Velocity (m/s)
v_x = Pore-water velocity in the x direction (m/sec)
v_y= Pore-water velocity in the y direction (m/sec)
v_z= Pore-water velocity in the z direction (m/sec)
x = Horizontal coordinate
y = Horizontal Coordinate (m)
z = Vertical Coordinate (m)
α = van Genuchten air-entry parameter (Pa^{-1}) or (cm^{-1}) or ($bars^{-1}$)
ϕ = Porosity
ϕ_{bulk} = Bulk Porosity of the rock
ϕ_{matrix} = Porosity of the rock matrix in an individual grain
$\phi_{intergrain}$ = Porosity of the large pore spaces between grains
ω= Tortuosity
ϕ_{Total} = Total Porosity of the Crushed Tuff
ψ = Moisture potential (m)
ψ_e = Air-entry water potential or the potential at which the largest water filled pores just drain (J/kg)
ψ_{es} = Air-entry water potential or the potential at which the largest water filled pores just drain at a standard density (J/kg)
ψ_{ND} = Nondimensionalized moisture potential
λ = Dispersivity based upon pore water velocity (m)
μ = Absolute viscosity of water($N \cdot s/m^2$)
ρ = Mass density of water (kg/m^3)
ρ_b= Bulk density of the tuff matrix(kg/m^3) or bulk density (kg/m^3)
ρ_s = Solids density of the tuff matrix (kg/m^3)
θ = Volumetric moisture content
θ_{matrix} = Volumetric moisture content of the tuff matrix
θ_{bulk} = Bulk Volumetric moisture content
θ_r = Residual Volumetric moisture content
θ_s = Saturated Volumetric moisture content
$\xi(\theta)$ = Liquid tortuosity factor
σ_g = Geometric standard deviation(mm)
σ_w = Interfacial tension between the pore water and mineral surface (dyne/cm)

1. PURPOSE

The purpose of this analysis report is to provide supporting analyses to several other reports regarding Engineered Barrier System (EBS) Flow and Transport as described in *Technical Work Plan for: Engineered Barrier System Department Modeling and Testing FY03 Work Activities* (BSC 2003a). These reports include revisions to *Multiscale Thermohydrologic Model* (BSC 2001a) and *EBS Radionuclide Transport Abstraction* (BSC 2003b). *Multiscale Thermohydrologic Model* (BSC 2001a) requires hydrological properties for a dual-porosity material in the invert comprised of crushed tuff. This report develops the retention and unsaturated flow properties for a dual-porosity media that includes an intragranular porosity for crushed tuff and an intergranular porosity between particles for crushed tuff:

- Intergranular permeability of the crushed tuff
- Intergranular saturated moisture content
- Intergranular porosity
- van Genuchten properties
- Residual moisture content
- Maximum saturation
- Residual saturation.

This analysis report also supports *EBS Radionuclide Transport Abstraction* (BSC 2003b) in determining whether advection or diffusion in each media is the dominant transport mechanism. The analysis of advection or unsaturated flow through the invert requires that the retention and flow properties of the invert be used in a flow analysis in conjunction with initial conditions and boundary conditions. For this purpose, the NUFT software code was used to analyze the dual-continuum media. The resulting analysis indicates the degree to which the fine intragranular porosity and the coarse intergranular porosity retain and flow water, and thus it provides an estimate of advection through the invert. A NUFT analysis at ambient temperature uses a refined mesh to determine advection within the invert in cases where no dripping in the drift occurs other than what has been used in other previous analyses (BSC 2001a; BSC 2001b).

Engineered Barrier System Features, Events, and Processes (CRWMS M&O 2001a) examines coupled processes and provides a list of the EBS features, events, and processes (FEPs) and supporting analyses. However, this analysis report examines the processes of advection, dispersion, and diffusion in the invert for the breakthrough of radionuclides. These processes require an assessment of the following properties based upon the treatment of the invert as a dual-porosity medium:

- Intergranular porosity
- Bulk volumetric moisture content
- Dispersivity
- Effective diffusion coefficient.

The work contained in this analysis falls within the scope of work described by *Technical Work Plan for: Engineered Barrier System Department Modeling and Testing FY03 Work Activities* (BSC 2003a). Primary tasks include performing sensitivity studies to quantify the importance of

uncertainty in key parameters, such as the bulk permeability of the host rock and invert hydrological and diffusion properties.

2. QUALITY ASSURANCE

This analysis has been prepared in accordance with the Quality Assurance program. The direction for preparing the analysis was obtained from AP-SIII.9Q, *Scientific Analyses.*

The work scope described in this report has been determined to be subject to *Quality Assurance Requirements and Description* (DOE 2003). The work scope of this report involves conducting investigations or analyses of the invert barrier that have been classified as Quality Level 2 by *Q-List* (YMP 2001). Furthermore, this report provides analysis of data indirectly supporting performance assessment activities for the Multiscale Thermohydrologic Model non-dripping case, and directly supporting the dripping case as presented in Section 6.10. Since the work scope provides supporting analyses to *EBS Radionuclide Transport Abstraction* (BSC 2003b), the activity provides analysis of the data used to assess the potential dispersion of radioactive materials from the licensed facility.

Electronic data used as inputs in the preparation of this document were obtained from the Yucca Mountain Project (YMP) Technical Data Management System (TDMS) as appropriate, in accordance with controls specified in Section 8 of *Technical Work Plan for: Engineered Barrier System Department Modeling and Testing FY03 Work Activities* (BSC 2003a).

3. USE OF SOFTWARE

3.1 DESCRIPTION OF SOFTWARE

The software described in this section is used to develop the diagrams, graphs, and tables used in Chapter 6 and the Appendices. The computer software used was run on computers located at Bechtel SAIC Company, Las Vegas, Nevada.

3.1.1 NUFT v3.0s

NUFT v3.0s (NUFT V3.0s, STN: 10088-3.0s-01) is classified as a qualified software program per AP-SI.1Q, *Software Management*. It is used in this scientific analysis to calculate pore-water velocities and saturation in the invert. NUFT provides a numerical solution of a nonisothermal unsaturated-saturated flow and transport in porous media, with application to subsurface contaminant transport problems.

NUFT v3.0s was obtained from Software Configuration Management and was run on a Sun Workstation computer. NUFT v 3.0s is appropriate for use in this analysis, and has been used only within the range of validation as identified in its user documentation (CRWMS M&O 2000a).

3.1.2 XTOOL V10.1

XTOOL V10.1 (XTOOL V10.1, STN: 10208-10.1-00) is classified as a qualified software program per AP-SI.1Q, *Software Management*. XTOOL v10.1 was obtained from Software Configuration Management for use on the SUN Ultra Sparc operating platform. This software has been used within the range of validation defined for the software, and is appropriate for use in this analysis.

XTOOL V10.1 is a post-processor for NUFT. It is used to plot the time history of the liquid saturation (S) and moisture potential (ψ) computed by NUFT V3.0s, and provides an approximated liquid flow pattern showing the direction (but not the magnitude) of flow.

3.2 DESCRIPTION OF THE USE OF OFF-THE-SHELF SOFTWARE

3.2.1 Mathcad 2001 Professional

Mathcad 2001 Professional was used in this analysis to calculate the pore water velocity through the invert and to generate the contaminant transport breakthrough curves. Mathcad 2001 Professional was also used in Attachment VI in the derivation of the invert "packed bed" properties from the data by Brooks and Corey (1964). Mathcad 2001 Professional is an off-the-shelf software program that performs calculations using standard functions, the results of which are not dependent on the software itself. The results are documented sufficiently that they can be reproduced and checked by hand calculation. Therefore, in accordance with Section 2.1.6 of AP-SI.1Q, *Software Management*, Mathcad 2001 Professional is software that does not need to be qualified.

3.2.2 Microsoft Excel 97

Microsoft Excel 97 is classified as a commercial off-the-shelf program per AP-SI.1Q, *Software Management*. Microsoft Excel is designed as a spreadsheet program to assist in routine calculations. Microsoft Excel was used to perform van Genuchten retention relationship curve fitting (results in Attachments IV, V, VII, XIII, and XVI). The Solver is an add-in function in Microsoft Excel. The Solver can minimize a target cell that involves multiple cell variables that might be subject to multiple constraints. The Solver is used specifically to solve for several variables under the constraint for a target value. In this case, the constraint is the minimization of the least squares of the volumetric moisture content for curve fitting.

4. INPUTS

4.1 DIRECT INPUTS

This section presents the direct inputs to the analysis. Section 6.11 presents the uncertainty analysis for these parameters.

4.1.1 Retention Data for Volcanic Sand, Fine Sand, Glass Beads, and Touchet Silt Loam

The input data for determining the retention and flow parameters for the invert include the permeability, the porosity, and the retention data for volcanic sand, fine sand, glass beads, and Touchet silt loam used to calculate retention characteristics from the measurements by Brooks and Corey (1964, Appendix 3, Table 1). Table 4-1 presents the permeability data (k) and the porosity data (ϕ) of various unconsolidated materials. These inputs are used in Section 6.3 to calculate the hydrologic flow and retention properties of crushed tuff. Table 4-2 presents the retention data for the same materials. These properties are used in Section 6.4 of this analysis.

Table 4-1. Summary of Permeability and Porosity of Various Unconsolidated Materials

Material [a]	Porosity	Value (-)	Intrinsic Permeability (m^2)	Value (m^2)
Volcanic Sand	ϕ_{vs}	0.351	k_{vs}	1.80E-11
Fine Sand	ϕ_{fs}	0.377	k_{fs}	2.50E-12
Glass Beads	ϕ_{gb}	0.37	k_{gb}	6.30E-12
Touchet Silt Loam	ϕ_{ts}	0.485	k_{ts}	6.00E-13

Source: Brooks and Corey 1964, Appendix 3, Table 1

NOTE: [a] See Section 6.4 for a description of these materials.

The data presented by Brooks and Corey (1964, Appendix 3, Table 1) is prominent data from reputable soil scientists whose work is widely recognized. The data, and an analysis of curve-fit parameters derived from the data, are corroborated by the analysis presented in Sections 6.5 and 6.8. The data for various size particles (as subsequently presented), as well as the curve-fits to that data, are in agreement with the Campbell retention relation for the same-size particles.

4.1.2 Retention Data for Topopah Spring Tuff at the Repository Horizon

Tuff matrix retention and flow hydrologic properties for the TSw35 and the TSw36 units of the Topopah Spring Formation are used in Section 6.3 of this analysis. Table 4-3 presents hydrologic properties (DTN: LB990861233129.001) that were used in the NUFT analysis runs reported in Section 6.0. A comparison of this data with data in DTN: LB0207REVUZPRP.002 is provided in Table 4-4 and in Attachment IX. Note that this DTN is unqualified and is used for reference only.

Table 4-2. Retention Data for Various Materials

Volcanic Sand			Fine Sand			Glass Beads			Touchet Silt Loam		
Saturation	Capillary Rise(cm) Hydrocarbon	Capillary Rise(cm) Water	Saturation	Capillary Rise(cm) Hydrocarbon	Capillary Rise(cm) Water	Saturation	Capillary Rise(cm) Hydrocarbon	Capillary Rise(cm) Water	Saturation	Capillary Rise(cm) Hydrocarbon	Capillary Rise(cm) Water
0.99	12	24	0.99	12.8	25.6	0.995	5.9	11.8	0.998	32.8	65.6
0.986	13.5	27	0.98	27.8	55.6	0.989	11.8	23.6	0.995	42.8	85.6
0.98	14.5	29	0.962	30.8	61.6	0.985	17.8	35.6	0.992	52.8	105.6
0.974	15.5	31	0.95	31.8	63.6	0.98	23.8	47.6	0.984	62.8	125.6
0.948	16	32	0.926	34.8	69.6	0.971	26.9	53.8	0.978	67.8	135.6
0.895	17	34	0.901	36.8	73.6	0.938	28.8	57.6	0.967	72.5	145
0.875	17.2	34.4	0.855	39.8	79.6	0.912	29.3	58.6	0.946	77.8	155.6
0.638	21	42	0.788	42.8	85.6	0.764	30.4	60.8	0.892	82.3	164.6
0.479	24.8	49.6	0.716	45.8	91.6	0.681	31	62	0.821	87.7	175.4
0.277	36.9	73.8	0.627	48.8	97.6	0.579	32.1	64.2	0.719	97.8	195.6
0.188	67.7	135.4	0.503	52.8	105.6	0.465	32.7	65.4	0.641	107.6	215.2
0.158	136.6	273.2	0.393	57.7	115.4	0.337	33.9	67.8	0.562	123	246
—	—	—	0.314	64.8	129.6	0.269	35.7	71.4	0.492	142.6	285.2
—	—	—	0.273	71.7	143.4	0.19	39	78	0.424	177	354
—	—	—	0.262	74.4	148.8	0.13	43.8	87.6	0.383	207.2	414.4
—	—	—	0.217	92.1	184.2	0.099	53.5	107	—	—	—
—	—	—	0.174	150.1	300.2	0.097	150.4	300.8	—	—	—

Source: Brooks and Corey 1964, Appendix 3, Table 1

Table 4-3. Tuff Matrix Hydrologic Properties for TSw35 and TSw36

Parameter	TSw36	TSw35
Porosity of the rock matrix in an individual granule (ϕ_{matrix})	0.112	0.131
Full Saturation * (S_s)	1.0	1.0
Residual Saturation (S_r)	0.18	0.12
van Genuchten Air-Entry Parameter (α) 1/Pa	3.55E-6	6.44E-6
van Genuchten Parameter (m)	0.380	0.236
Intrinsic Permeability (k) m^2	5.71E-18	3.04E-17

DTN: LB990861233129.001

Table 4-4. Summary Tuff Matrix Hydrologic Properties for TSw35 and TSw36

Statigraphic Unit	TSw36 [a]	TSw35 [a]	TSw35 (Tptpll) [b]	Cell Reference [c]	TSw36 (Tptpln)	Cell Reference [d]
Porosity of the rock matrix in an individual grain (ϕ_{matrix})	0.112	0.131	0.131	C20	0.103	C21
Residual Saturation (S_r)	0.18	0.12	0.12	V20	0.20	V21
van Genuchten Air-Entry Parameter (α) 1/Pa	3.55×10^{-6}	6.44×10^{-6}	1.66×10^{-5} [e]	O20	2.84×10^{-7}	O21
van Genuchten Parameter (m)	0.380	0.236	0.216	S20	0.442	S21
Intrinsic Permeability (k) m^2	5.71×10^{-18}	3.04×10^{-17}	3.70×10^{-17}	H20	2.3×10^{-20}	H21

NOTES: [a] DTN: LB990861233129.001.
[b] DTN: LB0207REVUZPRP.002. Values reported in BSC 2003c. Note that this DTN is unqualified and is used for reference only. The retention data from this DTN are obtained from the Microsoft Excel workbook Matrix_Props from worksheet Matrix Hydrologic Properties Row 20.
[c] For the TSw35 (Tptpll) of DTN: LB0207REVUZPRP.002.
[d] For the TSw36 (Tptpln) of DTN: LB0207REVUZPRP.002.
[e] This value is obtained by inverting the value shown in the DTN as 6.01×10^{4} Pa.

4.1.3 Retention Measurements of the Crushed Tuff Invert

Measurements by the U.S. Geological Survey (USGS) (DTN: GS980808312242.015) are used to assess porosity and retention for crushed tuff. The measurements provide retention data for calculating a combined porosity of the intergranular porosity ($\phi_{intergrain}$, i.e., between the crushed tuff particles) and an intragranular porosity (ϕ_{matrix}, i.e., within crushed tuff particles). This input is based upon measurements used in Section 6.3, 6.8 and Attachments XI and XVI.

4.1.4 Porosity of Poorly Graded Sands in the Loose State

Winterkorn and Fang report an intergranular porosity (ϕ_{matrix}) range of 0.40 to about 0.48 (Winterkorn and Fang 1975, p. 257). These values are used in Section 6.3 to assess the range of intergranular porosity.

4.1.5 Geometry of the Invert

The emplacement drift configuration is shown on *Repository Design Project, Repository/PA IED Emplacement Drift Configuration 1 of 2* (BSC 2003d). The configuration in this drawing is not

to scale, but references *Repository Design, Emplacement Drift Steel Invert Plan and Details* (BSC 2001c), which illustrates the invert geometry. The current design for the repository shows that the maximum depth of the invert is 0.806 m at the drift centerline. This value is used in Attachment XV to develop the path length for breakthrough analysis presented in Section 6.9.

4.1.6 Percolation Rate at the Repository Horizon

Percolation fluxes from the PTn to the TSw unit for mean infiltration-flux, the upper-bound infiltration flux and the lower-bound infiltration flux cases for the various climates are presented in DTN: LB0302PTNTSW9I.001, as discussed in Section 6 of *UZ Flow Models and Submodels* (BSC 2003e). This analysis uses the upper bound distribution for the glacial climate. This input is used for comparison to the NUFT analysis in Section 6.6.

4.1.7 Thermal and Hydrologic Properties of Stratigraphic Units

The thermal and hydrologic properties of stratigraphic units used to calculate the hydrologic properties of the tuff matrix (TSw36) were based on DTN: LB990861233129.001 and the calibrated one-dimensional property set (DTN: LB0207REVUZPRP.002) published in *Calibrated Properties Model* (BSC 2003c). The properties for the other stratigraphic units are presented in Tables 4-4 through 4-7. These inputs are used in Section 6.6, and Attachments IX and X.

4.1.8 Thermal Properties of Crushed Tuff

Additional measurements of geotechnical and thermal properties (DTN: GS000483351030.003) have been performed. These inputs are used in the statistical analysis of the data presented in Table XI-1 of Attachment XI.

4.1.9 Properties of Water

The properties of water at ambient temperature are given by Incropera and DeWitt (1996). The water density (ρ) equals approximately 1000 kg/m^3, and the absolute viscosity (μ) equals 8.935×10^{-4} N·s/(m^2). The surface tension of water equals 72 dynes/cm. These data are used in Sections 6.4, 6.5, and Attachments IV, V, VI, VII, and VIII.

Table 4-5. Summary of the Matrix Hydrologic Properties for the NUFT Analysis

Model Layer	Permeability k_m (m^2)	Porosity ϕ_m (-)	van Genuchten α α_m (1/Pa)	van Genuchten M (λ) m_m (-)	Residual Saturation S_{lrm} (-)	Satiated Saturation S_{lsm} (-)
tcw11	3.98E-15	0.253	4.27E-5	0.484	0.07	1.00
tcw12	3.26E-19	0.082	2.18E-5	0.229	0.19	1.00
tcw13	1.63E-16	0.203	2.17E-6	0.416	0.31	1.00
ptn21	1.26E-13	0.387	1.84E-4	0.199	0.23	1.00
ptn22	5.98E-12	0.439	2.42E-5	0.473	0.16	1.00
ptn23	3.43E-13	0.254	4.06E-6	0.407	0.08	1.00
ptn24	3.93E-13	0.411	5.27E-5	0.271	0.14	1.00
ptn25	1.85E-13	0.499	2.95E-5	0.378	0.06	1.00
ptn26	6.39E-13	0.492	3.54E-4	0.265	0.05	1.00
tsw31	9.25E-17	0.053	7.79E-5	0.299	0.22	1.00
tsw32	5.11E-16	0.157	4.90E-5	0.304	0.07	1.00
tsw33	1.24E-17	0.154	1.97E-5	0.272	0.12	1.00
tsw34	7.94E-19	0.110	3.32E-6	0.324	0.19	1.00
tsw35	1.42E-17	0.131	7.64E-6	0.209	0.12	1.00
tsw36	1.34E-18	0.112	3.37E-6	0.383	0.18	1.00
tsw37	7.04E-19	0.094	2.70E-6	0.447	0.25	1.00
ch1v	4.36E-14	0.273	4.23E-5	0.363	0.03	1.00
ch2z	1.16E-17	0.331	1.13E-6	0.229	0.28	1.00
ch4z	1.16E-17	0.331	1.13E-6	0.229	0.28	1.00

DTN: LB990861233129.002

Table 4-6. Summary of the Fracture Hydrologic Properties for the NUFT Analysis

Model Layer	Permeability K_f (M^2)	Porosity ϕ_F (-)	van Genuchten α α_F (1/Pa)	van Genuchten M (λ) M_f (-)	Residual Saturation S_{lrf} (-)	Satiated Saturation S_{lsf} (-)	Active Fracture Parameter γ (-)	Frequency F (1/M)	Fracture To Matrix Connection Area A (M^2/M^3)
tcw11	2.75E-12	2.8E-2	4.67E-3	0.636	0.01	1.00	0.31	0.92	1.56
tcw12	1.00E-10	2.0E-2	2.18E-3	0.633	0.01	1.00	0.31	1.91	13.39
tcw13	2.26E-12	1.5E-2	1.71E-3	0.631	0.01	1.00	0.31	2.79	3.77
ptn21	1.00E-11	1.1E-2	2.38E-3	0.611	0.01	1.00	0.08	0.67	1.00
ptn22	1.00E-11	1.2E-2	1.26E-3	0.665	0.01	1.00	0.08	0.46	1.41
ptn23	1.96E-13	2.5E-3	1.25E-3	0.627	0.01	1.00	0.08	0.57	1.75
ptn24	4.38E-13	1.2E-2	2.25E-3	0.631	0.01	1.00	0.08	0.46	0.34
ptn25	6.14E-13	6.2E-3	1.00E-3	0.637	0.01	1.00	0.08	0.52	1.09
ptn26	3.48E-13	3.6E-3	3.98E-4	0.367	0.01	1.00	0.08	0.97	3.56
tsw31	2.55E-11	5.5E-3	1.78E-4	0.577	0.01	1.00	0.09	2.17	3.86
tsw32	7.08E-12	9.5E-3	1.32E-3	0.631	0.01	1.00	0.38	1.12	3.21
tsw33	1.50E-12	6.6E-3	1.50E-3	0.631	0.01	1.00	0.38	0.81	4.44
tsw34	4.63E-13	1.0E-2	4.05E-4	0.579	0.01	1.00	0.38	4.32	13.54
tsw35	5.09E-12	1.1E-2	9.43E-4	0.627	0.01	1.00	0.38	3.16	9.68
tsw36	1.48E-12	1.5E-2	8.21E-4	0.623	0.01	1.00	0.38	4.02	12.31
tsw37	1.48E-12	1.5E-2	8.21E-4	0.623	0.01	1.00	0.38	4.02	12.31
ch1v	7.90E-13	6.9E-4	1.66E-3	0.656	0.01	1.00	0.10	0.10	0.30
ch2z	2.64E-14	4.3E-4	8.45E-4	0.628	0.01	1.00	0.10	0.14	0.43
ch4z	2.64E-14	4.3E-4	8.45E-4	0.628	0.01	1.00	0.10	0.14	0.43

DTN: LB990861233129.002

Table 4-7. Summary of the Thermal Properties for the NUFT Analysis

Model Layer	Rock Grain Density ρ_G (Kg/M^3)	Rock Grain Specific Heat C_p (J/Kg K)	Dry Conductivity λ_{Dry} (W/M K)	Wet Conductivity λ_{Wet} (W/M K)	Tortuosity τ (-)
tcw11	2550	823	1.60	2.00	0.7
tcw12	2510	851	1.24	1.81	0.7
tcw13	2470	857	0.54	0.98	0.7
ptn21	2380	1040	0.50	1.07	0.7
ptn22	2340	1080	0.35	0.50	0.7
ptn23	2400	849	0.44	0.97	0.7
ptn24	2370	1020	0.46	1.02	0.7
ptn25	2260	1330	0.35	0.82	0.7
ptn26	2370	1220	0.23	0.67	0.7
tsw31	2510	834	0.37	1.00	0.7
tsw32	2550	866	1.06	1.62	0.7
tsw33	2510	882	0.79	1.68	0.7
tsw34	2530	948	1.56	2.33	0.7
tsw35	2540	900	1.20	2.02	0.7
tsw36	2560	865	1.42	1.84	0.7
tsw37	2560	865	1.42	1.84	0.7
ch1v	2310	1060	0.70	1.31	0.7
ch2z	2350	1150	0.61	1.20	0.7
ch4z	2350	1150	0.61	1.20	0.7

DTN: LB990861233129.002

4.2 CRITERIA

Section 1.2.4 of *Technical Work Plan for: Engineered Barrier System Department Modeling and Testing FY03 Work Activities* (BSC 2003a) has identified the scope for analyses such as this one:

> The EBS flow and transport models and analyses are used to quantify the post-closure release of radionuclides from the EBS. . . Advection and diffusion may transport radionuclides mobilized as dissolved or colloidal species (BSC 2003a, Section 1.2.4).

The scope of this analysis is specifically defined in Section 1.2.4.1 of the technical work plan (BSC 2003a).

In addition, the following acceptance criteria (AC), based on the requirements listed in *Project Requirements Document* (Canori and Leitner 2003) and *Yucca Mountain Review Plan, Final Report* (NRC 2003) apply:

1. System Description and Demonstration of Multiple Barriers (NRC 2003, Section 4.2.1.1.3; Canori and Leitner 2003, PRD-002/T-014, PRD-002/T-016)

   Specific requirements involve identification of multiple barriers (natural and engineered), describing the capabilities of these barriers to isolate waste, and providing

technical bases for capabilities descriptions consistent with the post-closure performance objectives. To comply with these requirements, the following acceptance criteria are identified in *Technical Work Plan for: Engineered Barrier System Department Modeling and Testing FY03 Activities* (BSC 2003a).

- AC1: Identification of Barriers is Adequate.
- AC2: Description of the Capability of Identified Barriers is Acceptable.
- AC3: Technical Basis for Barrier Capability is Adequately Presented.

2. Scenario Analysis and Event Probability (NRC 2003, Section 4.2.1.2.1.3; Canori and Leitner 2003, PRD-002/T-015)

   Specific requirements include providing technical bases for inclusion or exclusion of specific FEPs. In order to meet these requirements, the following acceptance criteria are identified in the EBS Department *Technical Work Plan for: Engineered Barrier System Department Modeling and Testing FY03 Activities* (BSC 2003a).

   - AC1: The Identification of the Initial List of Features, Events, and Processes is Adequate.
   - AC2: Screening of the Initial List of FEPs is Appropriate.
   - AC3: Formation of Scenario Classes Using the Reduced Set of Events is Adequate.
   - AC4: Screening of Scenario Classes is Appropriate.

3. Degradation of Engineered Barriers (NRC 2003, Section 4.2.1.3.1.3; Canori and Leitner 2003, PRD-002/T-015):

   Specific requirements include describing deterioration or degradation of engineered barriers and modeling degradation processes using data for performance assessment, including total system performance assessment (TSPA). Consideration of uncertainties and variabilities in model parameters and alternative conceptual models is also required. To fulfill these requirements, the following acceptance criteria are identified in the EBS Department *Technical Work Plan for: Engineered Barrier System Department Modeling and Testing FY03 Activities* (BSC 2003a).

   - AC1: System Description and Model Integration are Adequate.
   - AC2: Data are Sufficient for Model Justification.
   - AC3: Data Uncertainty is Characterized and Propagated Through the Model Abstraction.
   - AC4: Model Uncertainty is Characterized and Propagated Through the Model Abstraction.
   - AC5: Model Abstraction Output is Supported by Objective Comparisons.

4. Quantity and Chemistry of Water Contacting Waste Packages and Waste Forms (NRC 2003, Section 4.2.1.3.3.3; Canori and Leitner 2003, PRD-002/T-015):

   Specific requirements include quantifying the amount and chemistry of water contacting the waste package and the waste forms. To comply with these

requirements, the following acceptance criteria are identified in the EBS Department *Technical Work Plan for: Engineered Barrier System Department Modeling and Testing FY03 Activities* (BSC 2003a).

- AC1: System Description and Model Integration are Adequate.
- AC2: Data are Sufficient for Model Justification.
- AC3: Data Uncertainty is Characterized and Propagated Through the Model Abstraction.
- AC4: Model Uncertainty is Characterized and Propagated Through the Model Abstraction.
- AC5: Model Abstraction Output is Supported by Objective Comparisons.

4.3 CODES AND STANDARDS

No codes or standards were used in the preparation of this document.

5. ASSUMPTIONS

The following assumptions have been used in this analysis.

5.1 DIRECTION OF ADVECTIVE TRANSPORT

Assumption: It is assumed that advective transport in the invert occurs in the vertical direction at constant flux rates for purposes of breakthrough analysis.

Rationale: The technical basis for this assumption is that the general flow in the vadose zone is in the vertical direction, and that any tendency for flow to occur locally in the invert's horizontal direction would tend to decrease the breakthrough time in the vertical direction. Therefore, the assumption of one-dimensional flow in the vertical direction is a bounding, conservative assumption, and requires no further confirmation.

Confirmation Status: This assumption does not require further confirmation.

Use in the Model: This assumption is used in Sections 6.1 and 6.9.5.

5.2 EFFECTS OF TRANSVERSE DISPERSION NEGLECTED

Assumption: It is assumed that only longitudinal dispersion is important to consider in this analysis, and that the effects of transverse dispersion can be neglected.

Rationale: The basis for using this assumption is the fact that analyzing breakthrough to neglect transverse dispersion is conservative, since transverse dispersion results in a lateral dispersion perpendicular to the direction of flow, and is slow compared to longitudinal dispersion.

Confirmation Status: This assumption does not require further confirmation.

Use in the Model: This assumption is used in Sections 6.1 and 6.9.5.

5.3 TRAVEL TIME OF CONTAMINANTS THROUGH HOMOGENEOUS INVERT MATERIAL

Assumption: The shortest travel time for breakthrough of a contaminant through a homogeneous material is one-dimensional flow along a straight line.

Rationale: The technical basis for this assumption is that if flow were directed along a path other than a straight line, the travel time would be longer.

Confirmation Status: This assumption does not require further confirmation.

Use in the Model: This assumption is used in Section 6.1.

5.4 RADIONUCLIDE CONCENTRATION RELEASED OVER TIME IS CONSTANT AND AT THE CENTERLINE OF THE DRIFT

Assumption: The concentration of radionuclides released after waste package failure is assumed to be constant over time and at the centerline of the drift.

Rationale: This is a bounding assumption; therefore, it is adequate for the purpose of performing sensitivity studies. Therefore, an analytical solution for comparing advection to diffusion can be used.

Confirmation Status: This assumption does not require further confirmation**.**

Use in the Model: This assumption is used in Section 6.1.

5.5 THE EFFECTS OF RADIOACTIVE DECAY IS NEGLECTED

Assumption: It is assumed that the effects of radioactive decay can be neglected.

Rationale: The technical basis for this assumption is that the contaminant breakthrough will occur rapidly relative to the half-life of long-lived radionuclides. This is a conservative assumption for analyzing breakthrough times.

Confirmation Status: This assumption does not require further confirmation.

Use in the Model: This assumption is used in Section 6.1.

5.6 MOLECULAR DIFFUSION OCCURS AT A CONSTANT TEMPERATURE

Assumption: It is assumed that the breakthrough occurs at a common temperature in the sensitivity studies presented in this analysis.

Rationale: Previous models and analyses have characterized the environment of the repository to be near ambient temperature in the invert at a time when a drip shield failure and the first waste package breach potentially occurs (~11,000 years). *Multiscale Thermohydrologic Model* (BSC 2001a, Figure 6-68) indicates the temperatures in the repository might be about 40°C at that time (~11,000 years). Note that the analysis considers waste package failure except for juvenile failures that would occur over an extended period of time where temperatures are

slightly elevated. The analysis does not consider juvenile waste package failure over shorter periods of time where repository temperatures would be higher.

In addition, based on measurements by Mills (1973, pp. 687 and 688) and Fetter (1993, p. 44), values for molecular diffusion or binary diffusion coefficient are well known, and fall in the range of 1×10^{-5} to 2×10^{-5} cm^2/sec. Section 6.2 provides a more detailed discussion on reported values for diffusion, and the technical basis for this assumption. The analysis uses a reasonable bounding value of 1.707×10^{-7} cm^2/sec or 5.388×10^{-4} m^2/yr for the molecular diffusion coefficient of water at 45°C. The calculations are presented in Attachment III. The measurements show a 1.1×10^{-5} to 3.5×10^{-5} cm^2/sec (0.11×10^{-9} – 0.35×10^{-9} m^2/yr) for 1°C and 45°C range, respectively. Based on this information, the foregoing correction of the molecular diffusion coefficient of water for temperature is not expected to have an impact on the contaminant breakthrough time analysis.

Confirmation Status: This assumption does not require further confirmation.

Use in the Model: This assumption is used in Section 6.9 and Attachment III.

5.7 SOLUTE VAPOR PHASE NEGLIGIBLITY

Assumption: It is assumed that the vapor phase of the solute is negligible for advection or dispersion in the invert material.

Rationale: The technical basis for this assumption is that while it is possible for contaminants to be transported by vapor diffusion, the critical radionuclides from the standpoint of individual release are not volatile, particularly at ambient temperatures. They may be soluble in water, however, and therefore would only be carried by the liquid phase. This is a bounding assumption.

Confirmation Status: This assumption does not require further confirmation.

Use in the Model: This assumption is used in Section 6.1

5.8 INVERT MATERIAL

Assumption: For the purpose of this analysis, it is assumed that the crushed tuff is from any of the TSw2 thermal/mechanical units that comprise the repository horizon.

Rationale: This assumption is based on the fact that crushed tuff will be taken from the surface of the muckpile that may be obtained from several lithostratigraphic units (e.g., the Tptpul, Tptpmn, Tptpll, and Tptpln units). The technical basis for this assumption is that the matrix retention and flow properties of the Tptpmn, Tptpll, and the Tptpln units are very similar, since the mineralogic composition and matrix porosity are similar. Therefore, the results of analysis for any of these units are similar.

Confirmation Status: This assumption is used throughout the calculation and does not require further confirmation.

Use in the Model: This assumption is used throughout the report.

5.9 THE CRUSHED TUFF PARTICLE SIZE DISTRIBUTION FOLLOWS A LOG NORMAL DISTRIBUTION

Assumption: The particle sizes in the Campbell retention relation used to calculate the moisture retention relationship are assumed to follow a log normal distribution (Campbell 1985, pp. 9 and 10).

Rationale: The technical basis for this assumption is that the data for the soil texture diagram presented by Campbell (1985) follows a log normal distribution.

Confirmation Status: This assumption does not require further confirmation.

Use in the Model: This assumption is used in Section 6.5.

6. SCIENTIFIC ANALYSIS DISCUSSION

Section 6.1 develops the governing relationships for the scientific analysis discussion of the advection-dispersion at the centerline of the drift. The degree to which either diffusion or advection/dispersion dominates the flow system depends on the fundamental mass transport properties, and on the hydrological environment in the invert. In turn, the fundamental mass transport properties depend on other more fundamental geotechnical properties of the invert.

Section 6.2 presents the effective dispersion-diffusion and solute properties of the invert, and develops these properties as a function of the porosity, and the degree of saturation in the invert. Advection through the invert occurs by unsaturated flow that depends on the fundamental retention and unsaturated hydraulic conductivity properties of the invert.

Section 6.3 develops the retention and unsaturated hydraulic conductivity properties of the invert based upon a dual-porosity medium that consists of the intragranular porosity within the crushed tuff particles, and the intergranular porosity between the crushed tuff particles. The development of the fundamental retention and unsaturated hydraulic properties is assisted by the use of phase diagrams.

Section 6.4 presents the non-dimensionalized van Genuchten retention relationship based upon the original work of Brooks and Corey (1964) for a given range of conditions. The scientific analysis uses an alternate approach for developing the retention properties of the crushed tuff medium. Section 6.5 presents this alternate approach analysis using the Campbell retention relationship for a similar range of conditions that corroborates the non-dimenionalized van Genuchten retention relationships.

Sections 6.6 through 6.8 present the NUFT advection calculation using the non-dimensionalized van Genuchten retention relation and the Campbell retention relation. Table 6-9 present the comparison of invert conditions at steady state for the van Genuchten method. Table 6-10 presents the same information for the Campbell method that provides corroborating or supporting technical information on the constitutive relations.

Section 6.9 presents containment transport results, including calculations of bulk porosity, diffusion and dispersion coefficients, breakthrough analyses, and an analysis of retardation.

Sections 6.10 through 6.12 present the TSPA-LA uncertainties and limitations, as well as the YMRP acceptance criteria addressed in this analysis.

6.1 ADVECTION-DISPERSION-DIFFUSION AT THE CENTERLINE OF THE DRIFT

The three-dimensional advection-dispersion-diffusion relation for transport or breakthrough of a solute is shown in the general Equation 6-1 (Fetter 1993, p. 53):

$$\left[\frac{\partial}{\partial x}\left(D_x \cdot \frac{\partial C}{\partial x}\right)+\frac{\partial}{\partial y}\left(D_y \cdot \frac{\partial C}{\partial y}\right)+\frac{\partial}{\partial z}\left(D_z \cdot \frac{\partial C}{\partial z}\right)\right]-\left[\frac{\partial}{\partial x}(v_x \cdot C)+\frac{\partial}{\partial y}(v_y \cdot C)+\frac{\partial}{\partial z}(v_z \cdot C)\right]=\frac{\partial C}{\partial t} \qquad \text{(Eq. 6-1)}$$

where

D_x = dispersion/diffusion coefficient in the x direction (m^2/sec)
D_y = dispersion/diffusion coefficient in the y direction (m^2/sec)
D_z = dispersion/diffusion coefficient in the z direction (m^2/sec)
C = solute concentration at location x, y, z and time t(mg/l)
v_x = pore-water velocity in the x direction (m/sec)
v_y = pore-water velocity in the y direction (m/sec)
v_z = pore-water velocity in the z direction (m/sec)
t = time (sec)

The dispersion coefficients (i.e., D_x, D_y, and D_z in the x, y, and z directions) include the process of both advection and hydrodynamic dispersion (which includes molecular diffusion and mechanical dispersion combined) (Fetter 1993, p. 51). This equation has been applied to homogeneous, anisotropic, saturated media. Jury et al. (1991, pp. 221 to 223) extend the application of the general equation to unsaturated media.

Applying Assumptions 5.1 through 5.4, the radionuclides are released at the centerline of the drift and flow occurs in the vertical direction. Transverse-flux and transverse-dispersion are neglected (see Assumptions 5.1 and 5.2). Three-dimensional Equation 6-1 reduces to the one-dimensional Equation 6-2a:

$$\left[\frac{\partial}{\partial z}\left(D_z \cdot \frac{\partial C}{\partial z}\right)\right]-\left[\frac{\partial}{\partial z}(v_z \cdot C)\right]=\frac{\partial C}{\partial t} \qquad \text{(Eq. 6-2a)}$$

Expanding the expression for advection according to the chain rule, the following partial differential equation (Equation 6-2b) for mass transport is obtained:

$$\left[\left(D_z \cdot \frac{\partial^2 C}{\partial z^2}\right)\right]-\left[C\frac{\partial v_z}{\partial z}\right]-\left[v_z\frac{\partial C}{\partial z}\right]=\frac{\partial C}{\partial t} \qquad \text{(Eq. 6-2b)}$$

Consider a uniform velocity (v_z) in the media in which the velocity gradient is zero ($\partial v_z / \partial z = 0$). The above equation reduces to the one-dimensional advection-diffusion-dispersion equation that can then be solved using a closed form analytical solution. This equation can be written with the effective Dispersion/Diffusion Coefficient (D_z) being independent of position (Jury et al. 1991, p. 223):

$$\left[\left(D_z \cdot \frac{\partial^2 C}{\partial z^2}\right)\right] - \left[v_z \frac{\partial C}{\partial z}\right] = \frac{\partial C}{\partial t} \qquad \text{(Eq. 6-3)}$$

Since the centerline of the drift represents a line of symmetry, the horizontal Darcy flux is zero. The vertical Darcy flux increases with depth into the invert and the host rock because, for an unsaturated flow in the vadose zone to occur in the absence of localized indrift seepage, the drift acts as a capillary barrier to flow. The flow pattern is then similar to the problem of fluid flow around an inclusion in which a stagnation point forms on the downstream side. Note that while the release of the radionuclides might advect, disperse or diffuse in the radial direction from the point of release, it is conservative to assume flow in the vertical direction. If the concentration is set to equal one at the top of the invert (Assumption 5.4), and the Darcy flux is constant for a steady state flow, then the one-dimensional advection-dispersion equation (Equation 6-3) can be solved using a closed form analytical solution.

A solution to the above relation is presented for non-retarded transport in one dimension, with initial concentration (C_o) moving at a continuous rate where the vapor phase transport is negligible (see Assumption 5.7) (Freeze and Cherry 1979, p. 391).

$$\frac{C_l}{C_0} = \frac{1}{2} \cdot \left(erfc\left(\frac{L - V \cdot t}{2\sqrt{D \cdot t}}\right) + \exp\left(\frac{V \cdot L}{D}\right) \cdot erfc\left(\frac{L + V \cdot t}{2 \cdot \sqrt{\mathrm{D} \cdot \mathrm{t}}}\right)\right) \qquad \text{(Eq. 6-4)}$$

The pore water velocity (V) presented above equals the Darcy Flux (J_w) (the vertical Darcy flux rate) divided by the porosity (ϕ) in the vertical direction of flow or the porewater velocity (V) for saturated flow. For unsaturated flow, the average linear velocity, or the porewater velocity, equals the Darcy Flux (J_w) divided by the volumetric moisture content (θ) (Jury et al. 1991, p. 221).

6.2 EFFECTIVE DISPERSION-DIFFUSION AND SOLUTE TRANSPORT PROPERTIES

The flux/transport of a dissolved solute is governed by the processes of advection and hydrodynamic dispersion. Liquid advection is the bulk transport (also referred to as convection) of solutes moving with a flowing soil solution. The hydrodynamic dispersion process includes both molecular diffusion and mechanical dispersion (Fetter 1993, pp. 43 to 51). Molecular diffusion is characterized by transport due to a concentration gradient, and is expressed by Fick's First Law in which the mass flux of solute per unit area per unit time is the product of the diffusion coefficient and the concentration gradient. When liquid advection is characterized as "plug flow," the mass transport yields a sharp concentration front (Fetter 1993, p. 48). However, for systems where concentrations are changing with time, and in the absence of liquid advection, the governing equation (Equation 6-3) reduces to Fick's Second Law which is the transient partial differential equation governing diffusion (Equation 6-5) (Fetter 1993, p. 44).

$$\frac{\partial C}{\partial t} = D_d \cdot \frac{\partial^2 C}{\partial x^2} \qquad \text{(Eq. 6-5)}$$

In porous media, diffusion is slower than it is in water because solutes must follow longer pathways around mineral grains/particles in the invert, which introduces the coefficient related to the tortuosity (ω) into the equation where, in porous media, the effective diffusion coefficient, D* must be used (Fetter 1993, p. 44):

$$D^* = \omega D d \quad \text{(Eq. 6-6)}$$

Groundwater containing solute does not all travel at the same velocity due to the mixing that occurs along the flow path. This mixing is called mechanical dispersion, and is a result of solute dilution at the advancing edge of the flow. The mixing that occurs along the direction of the flow path is called longitudinal dispersion. Where the solute tends to spread and mix in the normal flow path direction, it is referred to as transverse dispersion (Fetter 1993, p. 49, Figure 2.4). Factors causing longitudinal dispersion on the scale of individual pores are:

1. As fluid moves through the pore space, fluid moves more rapidly in the pore space centers rather than along the edges.

2. Some flow paths through a porous media are longer than other flow paths due to flow tortuosity.

3. Some flow paths are larger due to grain size effects.

These causal factors combined together result in dispersive flux. The three fluxes (liquid advection, soil-liquid diffusion, and hydrodynamic dispersion) can be expressed mathematically as follows (Jury et al. 1991, pp. 220 to 223):

Liquid Advection (Bulk Flow or Convection)

$$J_{lc} = J_w \cdot C_L \quad \text{(Eq. 6-7)}$$

where

J_{lc} is the liquid advection flux (kg/s/m^2)
J_w is the vertical Darcy flux rate (m/s)
C_L is the solute concentration of the solute at location x = 0 (kg/m^3 or mg/L)

Soil-Liquid Diffusion

$$J_{sl} = -D_{sl} \cdot \frac{dC_L}{dz} \quad \text{(Eq. 6-8)}$$

where

J_{sl} is the soil liquid flux (kg/s/m^2)
D_{sl} is the solute diffusion coefficient of the solute in water (m^2/sec)

Hydrodynamic Dispersion Flux

$$J_{lh} = -D_{lh} \cdot \frac{dC_L}{dz} \quad \text{(Eq. 6-9)}$$

where

J_{lh} is the hydrodynamic dispersion flux (kg/s/m^2)
D_{lh} is the hydrodynamic dispersion coefficient (m^2/sec)

The combined flux (J_l), which is the sum of liquid advection (J_k), soil-liquid diffusion (D_{sl}), and hydrodynamic dispersion flux (J_{lh}) (Equations 6.7 through 6.9) is expressed as:

$$J_l = J_w \cdot C_L + J_k = J_w \cdot C_L - D_{sl} \cdot \frac{dC_L}{dz} - D_{lh} \cdot \frac{dC_L}{dz} \quad \text{(Eq. 6-10)}$$

It is important to understand the properties associated with soil-liquid diffusion (D_{sl}) and hydrodynamic dispersion (D_{lh}), and their dependence on other parameters. Jury et al. (1991, pp. 220 to 223) combine the last two terms in Equation 6-10 to express the combined flux (J_l) as:

$$J_l = J_w \cdot C_L - D_e \cdot \frac{dC_L}{dz} \quad \text{(Eq. 6-11)}$$

in which the effective dispersion-diffusion coefficient (D_e) equals the sum of the hydrodynamic dispersion (D_{lh}) and soil-liquid diffusion coefficients (D_{sl}) (Jury et al. 1991, p. 222):

$$D_e = D_{lh} + D_{sl} \quad \text{(Eq. 6-12)}$$

Further, the dispersion-diffusion coefficient (D) in m^2/sec equals the effective dispersion-diffusion coefficient (D_e) divided by the volumetric moisture content (θ) (Jury et al. 1991, p. 223).

The hydrodynamic dispersion coefficient (D_{lh}) has frequently been observed to be proportional to the pore-water velocity V, also known as the average linear velocity, where λ is the dispersivity in cm and $V = J_w/\theta$ (Jury et al. 1991, p. 221):

$$D_{lh} = \lambda \cdot V \quad \text{(Eq. 6-13)}$$

Dispersivity (λ) is defined as the degree of kinematic dispersion in a porous medium. Fetter provides a relationship between dispersivity and length that shows a conservative estimate of dispersivity to be 0.1 m (10 cm) for a path length (L) of one meter (Fetter 1993, p. 73, Figure 2.18). Jury et al. discuss a range from 0.5 to 2 cm for packed laboratory columns, and from 5 to 20 cm in field experiments (Jury et al. 1991, p. 222). Jury et al. state that the dispersivity can be considerably larger for regional groundwater flow. However, due to the scale of the invert, these values would not apply. Based upon information provided by Jury et al. (1991, p. 222) and Fetter (1993, p. 73), a reasonable bounding range of values for dispersivity would be 0.4 to 10 cm. Note that a value of 10 cm was used in the analysis in Attachment III to provide an upper bounding analysis for hydrodynamic dispersion.

The soil-liquid diffusion coefficient (D_{sl}) is also a function of the binary diffusion coefficient ($D_{wl)}$ in water, and a function of $\xi(\theta)$, the liquid tortuosity factor, which accounts for the increased path length and decreased cross-sectional area of solute diffusion in the invert. The soil-liquid diffusion coefficient (D_{sl}) is given by Equation 6-14 (Jury et al. 1991, p. 221) and applying Assumption 5.6.

$$D_{sl}(\theta) = \xi(\theta) D_{wl} \quad \text{(Eq. 6-14)}$$

The soil-liquid diffusion coefficient (D_{sl}) is applied to crushed tuff, assumed to be the composition of the invert in Assumption 5.8. The dependence of the soil-liquid diffusion coefficient on the saturation (S), the porosity (ϕ), and the binary diffusion coefficient of water is represented mathematically in *EBS Radionuclide Transport Abstraction* (BSC 2003b) as:

$$D_{sl}(S,\phi) = D_{wl} \cdot \phi^{1.863} \cdot S^{1.863} \quad \text{(Eq. 6-15)}$$

Substituting in the volumetric moisture content (θ) for the saturation (S) and the porosity (ϕ) values yields:

$$D_{sl}(\theta) = D_{wl} \cdot \theta^{1.863} \quad \text{(Eq. 6-16)}$$

In the solution of the contaminant transport equation for porous media flow, de Marsily writes several basic contaminant transport equations that are based upon the flow through the pore space that entails the porosity (ϕ) for saturated flow, and that includes the Darcy Flux (J_w) (de Marsily 1986, p. 267). The form of the soil-liquid diffusion coefficient as presented in the advection-dispersion-diffusion contaminant equations by de Marsily (1986) is similar to the relationships presented above.

As noted in Section 5.6, variations in temperature do not significantly change the diffusion. The solute diffusion coefficient (D_{sl}) is calculated on the basis of Archie's Law in Section 4.1.1 of *Invert Diffusion Properties Model* (CRWMS M&O 2000b) that modifies the binary diffusion/molecular diffusion coefficient of water (D_{wl}) and on a diffusion versus temperature relationship presented in Attachment III. The self-diffusion coefficients of tritiated water in normal and heavy water were measured over a temperature range from 1°C to 45°C using the diaphragm-cell technique (Mills 1973, p. 685). These coefficients have been tabulated at various temperatures with the molecular mass for water taken into account. The measurements were compared with the molecular dynamics and Nuclear Magnetic Resonance (NMR) data. The measurements show temperature dependence from 1.1×10^{-5} to 3.5×10^{-5} cm^2/sec (0.11×10^{-9} to 0.35×10^{-9} m^2/y) for 1°C and 45°C, respectively. Recent NMR studies provided values at different temperatures that were in reasonable agreement with measurements by Mills (1973, pp. 687 to 688). Fetter (1993, p. 44) states that the values for molecular diffusion or a binary diffusion coefficient are well known, and fall in the range of 1×10^{-5} to 2×10^{-5} cm^2/sec. Based upon Mills (1973, pp. 687 to 688), a reasonable bounding value of 2.30×10^{-5} cm^2/sec or 0.073 m^2/yr for the molecular diffusion coefficient of water at 25°C is used. Based on the relationship for correcting the molecular diffusion coefficient of water for temperature, the calculated value for diffusion at 45°C is 1.707×10^{-7} cm^2/sec (5.388×10^{-4} m^2/yr). The reduction in temperature

does not have a significant effect on breakthrough times, particularly when advection is the dominant mechanism of radionuclide transport through the invert (e.g., after drip shield failure). In addition, greater uncertainty exists with parameters of greater significance to radionuclide transport (i.e., volumetric moisture content, and Darcy flux) than the molecular diffusion coefficient for water. For example, the molecular diffusion coefficient for water at 45°C is only approximately three times greater than the value at 1°C (Mills 1973, pp. 687 to 688).

6.3 RETENTION AND UNSATURATED HYDRAULIC CONDUCTIVITY PROPERTIES OF THE INVERT

Inputs to the various models (Section 4.0) require an evaluation of the retention and hydraulic properties of the crushed tuff that comprise the invert. In Attachment XI, the retention and hydraulic properties were determined for a single-porosity material. For the calculations used in this analysis, the invert is characterized as a dual-porosity material in which the properties for each component of the material are determined. NUFT is run in this analysis using the new retention and hydraulic properties of the crushed tuff based on its characterization as a dual-porosity invert material. This is done in order to demonstrate the concept of a fully-saturated matrix intragranular space and an unsaturated intergranular space in the invert.

Prior analyses have estimated the intragranular porosity ($\phi_{inatrix}$) of crushed tuff to be 0.112 (Table 4-3) (DTN: LB990861233129.001). However, the total porosity includes both the intergranular porosity ($\phi_{intergrain}$), related to the voids between the crushed tuff particles, as well as the intragranular porosity, related to the voids within the crushed tuff particles (ϕ_{matrix}). A total porosity of 0.55 has been calculated (Attachment XI) for sieved samples of crushed tuff ranging from 2 to 4.75 mm from TSw (DTN: GS980808312242.015) and as presented in detail in Attachment XI.

The phase diagram for crushed tuff is shown in Figure 6-1. The diagram has been developed to illustrate and characterize a matrix made up of tuff solids, intragranular voids, and intergranular voids. This phase diagram and the relationship between void volume and porosity are used to calculate the intergranular porosity ($\phi_{intergrain}$) based upon the reported values of 0.112 for intragranular porosity, and 0.55 for the total porosity.

In this analysis, V_{tm} equals the volume of the voids in the intragranular void space. V_c is equal to the volume of the voids in the intergranular void space and the total volume of the solids (V_{sm}) is equal to 1 cm^3, in accordance with standard soil mechanics conventions. Using this relationship, the void volume of the tuff matrix can be calculated. The porosity, ϕ_{matrix}, as defined in Equation 6-17 and 6-18, is the volume of the voids divided by the total volume of solids. The volume of the voids within the tuff matrix (V_{tm}) can be determined by Equation 6-19.

$$\phi_{matrix} = \frac{V_{tm}}{V_{sm} + V_{tm}} = 0.112 \qquad \text{(Eq. 6-17)}$$

$$\frac{V_{tm}}{1 + V_{tm}} = 0.112 \qquad \text{(Eq. 6-18)}$$

$$V_{tm} = \frac{0.112}{1-0.112} = 0.126 \quad \text{(Eq. 6-19)}$$

When the total porosity (ϕ) is set to 0.55, the volume of the coarse fraction is calculated as follows:

$$\frac{V_{tm}+V_c}{1.0+V_{tm}+V_c} = 0.55 \quad \text{(Eq. 6-20)}$$

$$\frac{0.126+V_c}{1.0+0.126+V_c} = 0.55$$

$$V_c = 1.10 \text{ cm}^3 \quad \text{(Eq. 6-21)}$$

Having calculated the volume of the coarse pore space (V_c) to be 1.10 cm^3, the calculated intergranular porosity ($\phi_{intergrain}$) that pertains to this coarse void space is equal to 0.49. This value is relatively high, and indicates that the samples laboratory tested by the USGS using the unsaturated flow apparatus were high (DTN: GS980808312242.015). Winterkorn and Fang evaluated uniformly graded or poorly sorted sands and measured intergranular porosity (ϕ_{matrix}) ranges from 0.40 to about 0.48 when considering the maximum void ratio or porosity (Winterkorn and Fang 1975, p. 257). Because the intergranular porosity value of 0.49 exceeds the range 0.40 to 0.48, it can be concluded that the USGS values for measured bulk porosity (DTN: GS980808312242.015) are consistent with a poorly graded sand in a loose state. Considering that crushed tuff may settle over time, a median value of 0.45 is adopted for the intergranular porosity ($\phi_{intergrain}$) for purposes of analysis.

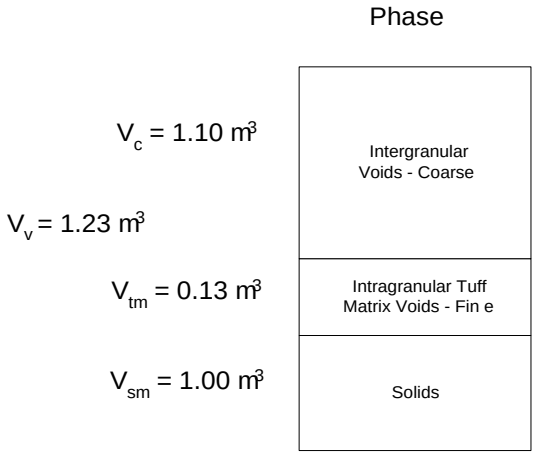

Figure 6-1. Phase Diagram for Crushed Tuff

An estimation of the water retention properties for the coarse intergranular porosity ($\phi_{intergrain}$) requires developing a retention relationship. This is for the following reasons. First, the retention characteristics obtained in the laboratory from the Unsaturated Flow Apparatus (UFA) measurements in Attachment XI (DTN: GS980808312242.015) were not tested above a

moisture potential (ψ) of approximately 0.04 bars (-40 cm). The measurements reported previously for the 2 mm to 4.75 mm had a minimum moisture potential of -100 cm. Since the higher negative pressures indicate that the intragranular pore space would retain water while the intergranular pore space would not (Attachment XI), these measurements reflect near saturation of the intragranular pore space but no retention of water in the intergranular pore space.

6.4 NON-DIMENSIONALIZED VAN GENUCHTEN RETENTION RELATION

Brooks and Corey retention data were obtained for such materials as volcanic sand, fine sand, and glass beads data (Brooks and Corey 1964). Figure 6.2 presents the capillary rise of these unconsolidated samples. Figure 6-3 presents the normalized capillary rise for various materials using the combined nondimensional van Genuchten retention relation measurements. The Brooks and Corey moisture potential measurements include a range of particle sizes. The measurements are combined by transforming the capillary pressures to nondimensional capillary pressures (Attachment IV). This is accomplished by using a nondimensional relationship dependent on particle size for moisture potential and for transforming volumetric moisture content to saturation for the respective materials (Leverett 1941, p. 159). (Volumetric moisture content is converted to saturation by dividing the volumetric moisture content by the porosity.) A description of these data sets follows:

- **Volcanic Sand**–This material comes from a wind-blown deposit along Crab Creek in Washington State. It consists of dark-colored aggregates that can be broken down into finer particles by pressure. It is not known to what degree these aggregates are themselves permeable, but they undoubtedly have some permeability. This sand has a degree of structure and has both primary and secondary porosity.

- **Fine Sand**–This sand was supplied by the Hanford Laboratories of General Electric Company at Richland, Washington, and apparently contains some volcanic minerals. This material contains a wide range of particle sizes, ranging down to silt size. Most of the particles are angular and not as rounded as most river bed sands.

- **Glass Beads**–This material is an example of media having a very narrow range of pore sizes. In this respect, however, it is not much different from many clean river sands.

- **Touchet Silt Loam**–This soil comes from the Columbia River basin and as also supplied by the Hanford Laboratory. It is extremely fine-textured in that it contains practically no coarse sand, but it is somewhat unusual in that it contains a smaller amount of clay than would be expected in such a fine-textured soil. It is, in fact, nearly pure silt mixed with some extremely fine sand. It contains enough clay, however, to create a structure with secondary porosity.

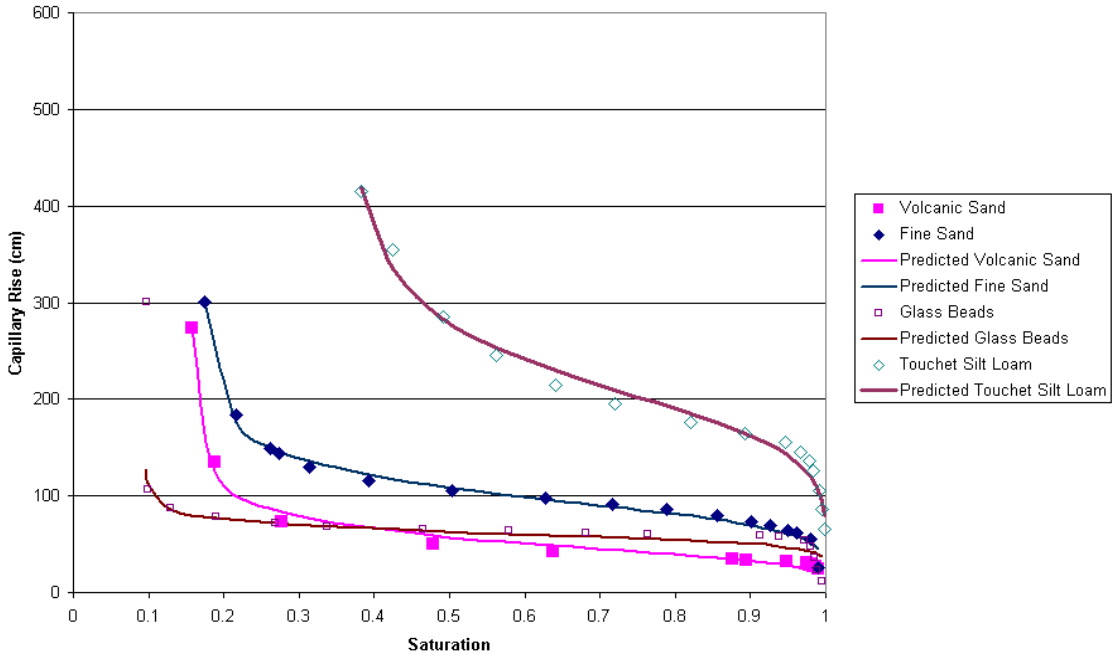

Source: Brooks and Corey 1964

Figure 6-2. Capillary Rise of Unconsolidated Samples

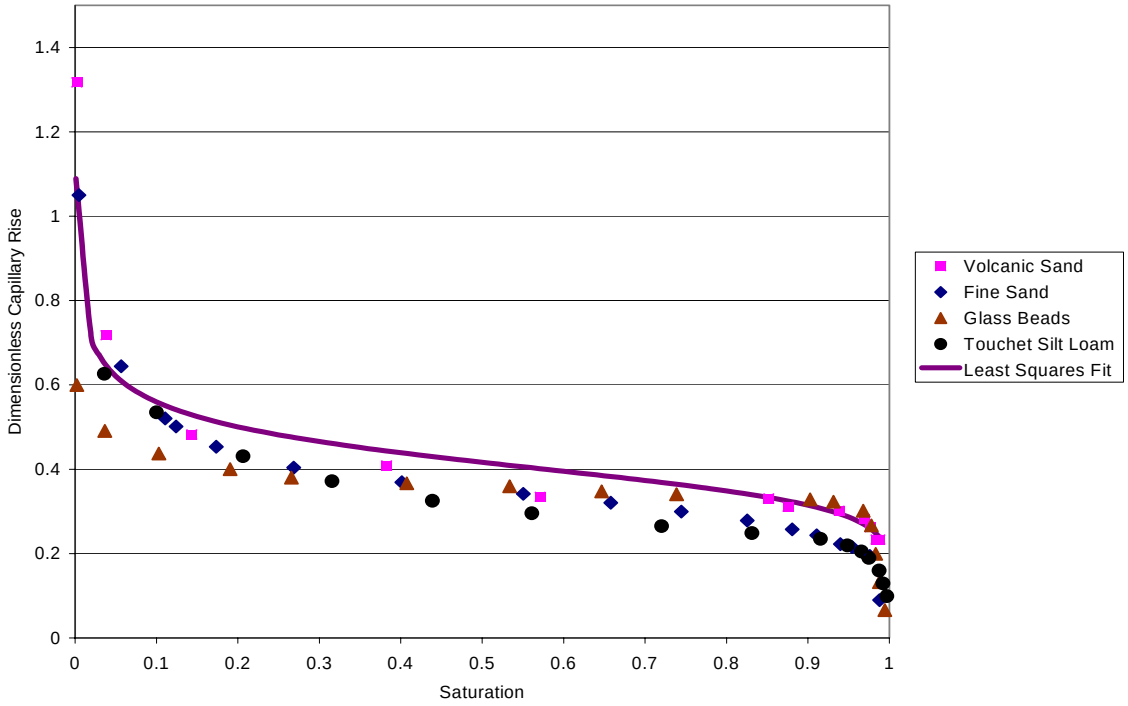

Source: Brooks and Corey 1964
DTN: MO0307SPAVGHYD.000

Figure 6-3. Normalized Capillary Rise for Various Materials

The methodology for determining the relationship of unsaturated hydraulic conductivity (K_{us}) from the retention curve using the two-parameter nondimensional van Genuchten relationship

and the size of the crushed tuff is provided in Attachment IV. The intrinsic permeability (k) is determined from the Kozeny-Carman formula shown by Equation IV-4 (Bear 1972, p. 166) that relates intrinsic permeability (k) to the grain size or pore diameter (d_m) and porosity (ϕ). On the basis of the selected grain size, the saturated hydraulic conductivity (K_s) and the van Genuchten relationship for relative permeability, the relationship of unsaturated hydraulic conductivity (K_{us}) to moisture potential (ψ) can be determined.

A qualitative assessment can be made over the range of moisture potentials (ψ) of interest (0.01 to 0.1 bars) as to whether liquid flow or advection in the coarse fraction of the crushed tuff would occur for a range of particle diameters. The analysis is performed for grain size diameters of 0.317 mm, 3 mm, 10 mm, and 20 mm for the intergranular porosity ($\phi_{intergrain}$), respectively, to cover a broad range of particle diameters. The equations used in these derivations are shown in Attachment VI.

The van Genuchten parameters can be used to determine the moisture retention relationship for the tuff matrix and the intergranular pore space. Table 6-1 presents the tuff matrix hydrologic properties used for these determinations for TSw36 (DTN: LB990861233129.001).

Additional analyses were performed for grain sizes of 3 mm, 10 mm, and 20 mm and these calculations are summarized in Tables 6-2 through 6-4, respectively, for each particle size evaluated. The detailed calculations for developing the parameters for the van Genuchten moisture retention relationships are presented in Tables IV-1 through IV-5 of Attachment IV. Figure 6-4 presents the retention relationships for the intergranular and intragranular pore space for comparison to the retention relationship for the tuff matrix. Figure 6-5 presents the unsaturated hydraulic conductivity relationship.

An intrinsic permeability (k) of 1.68×10^{-10} m^2 corresponds to a grain size diameter of 0.317 mm and a saturated hydraulic conductivity (K_s) of 0.165 cm/sec (see footnote 5 to Table 6-1 for conversion factor). The relative permeability function scales the saturated conductivity (K_s) allowing the unsaturated hydraulic conductivity (K_{us}) function to be determined. The unsaturated hydraulic conductivity relationships are presented in Figure 6-5.

The retention relationship (Equation IV-2) shows that for a fine intergranular porosity ($\phi_{intergrain}$) associated with a particle size of 0.317 mm over the range of moisture potentials (ψ) of 0.01 to 0.1 bars, water would be retained and would flow in the fine intergranular void space. If the unsaturated hydraulic conductivity (K_{us}) for the intergranular porosity ($\phi_{intergrain}$) is higher than the tuff matrix over the range of moisture potential of interest (0.01 to 0.1 bars), it can be concluded that the water flowing in the intergranular pore space would be the dominant flow path. However, if K_{us} for the intergranular porosity is lower than the K_{us} of the tuff matrix over the range of moisture potential of interest (0.01 to 0.1 bars), it can be concluded that water would not be retained in the intergranular porosity ($\phi_{intergrain}$), and the flow of water would not occur.

Table 6-1. Summary of Tuff Matrix Hydrologic Properties for TSw36

Parameter	Value
Porosity of the rock matrix in an individual grain (ϕ_{matrix})	0.112
Saturation at saturation (S_s)	1.0
Residual Saturation (S_r)	0.18
Saturated Volumetric moisture content (θs)[1]	0.112
Residual Volumetric moisture content (θr)[2]	0.02016
van Genuchten air-entry parameter (α)	3.55×10^{-6} $(Pa)^{-1}$
van Genuchten air-entry parameter (α)	0.355 $bars^{-1}$
van Genuchten parameter estimated from the water retention curve (m)	0.380
van Genuchten n parameter (n)[3]	1.61
Intrinsic permeability (k)	6×10^{-18} m^2
Saturated hydraulic conductivity (K_s)[4]	6×10^{-9} cm/sec

DTN: LB990861233129.001

NOTES: [1] The saturated volumetric moisture content (θ_s) equals the porosity (ϕ_{matrix}).

[2] The residual volumetric moisture content (θ_r) equals the residual saturation (S_r) times the porosity (ϕ)

[3] The value of n is given by 1/(1-m) (Fetter 1993, p. 172).

[4] The value of the saturated hydraulic conductivity (K_s) is obtained by the equation that converts an saturated intrinsic permeability (k) to a saturated hydraulic conductivity (K_s) (Freeze and Cherry 1979, p. 27).

$$K_s = \frac{\rho \cdot g}{\mu} \cdot k$$

The properties of water at ambient temperature are given by Incropera and DeWitt (1996, p. 846). The water density (ρ) equals 1000 kg/m^3 and the absolute viscosity (μ) equals 8.935×10^{-4} $N\cdot s/(m^2)$.

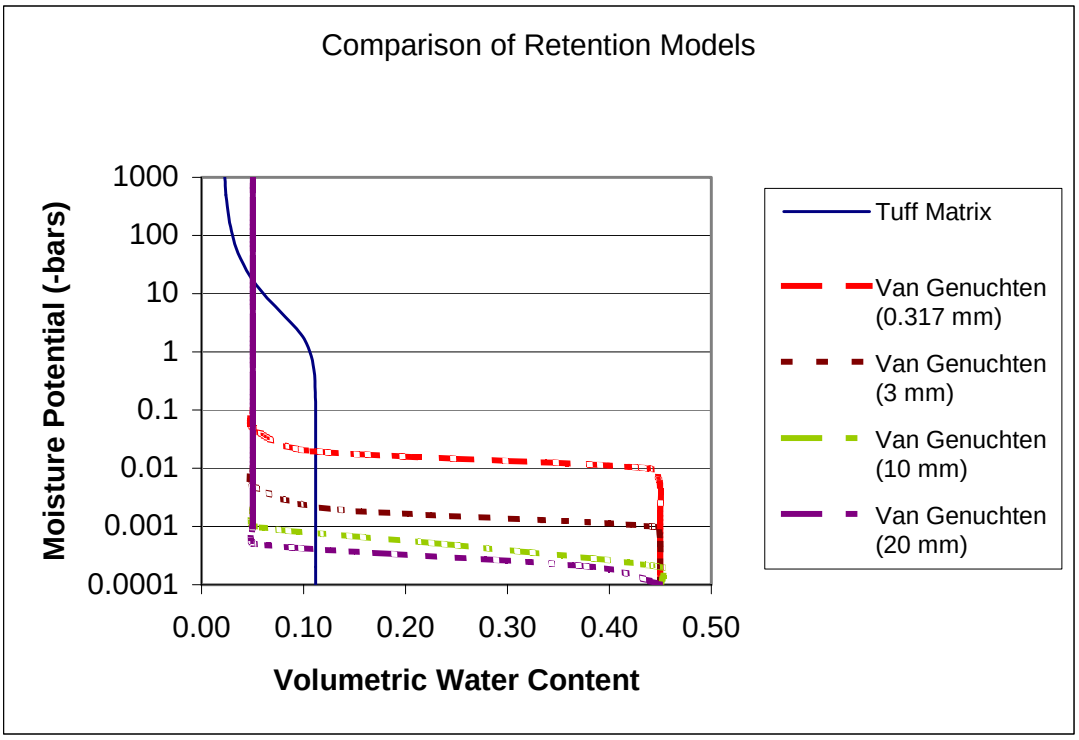

NOTE: See Tables 6-1 and 6-3.

Figure 6-4. Retention Relationships Based Upon the Non-Dimensionalized van Genuchten Retention Relation

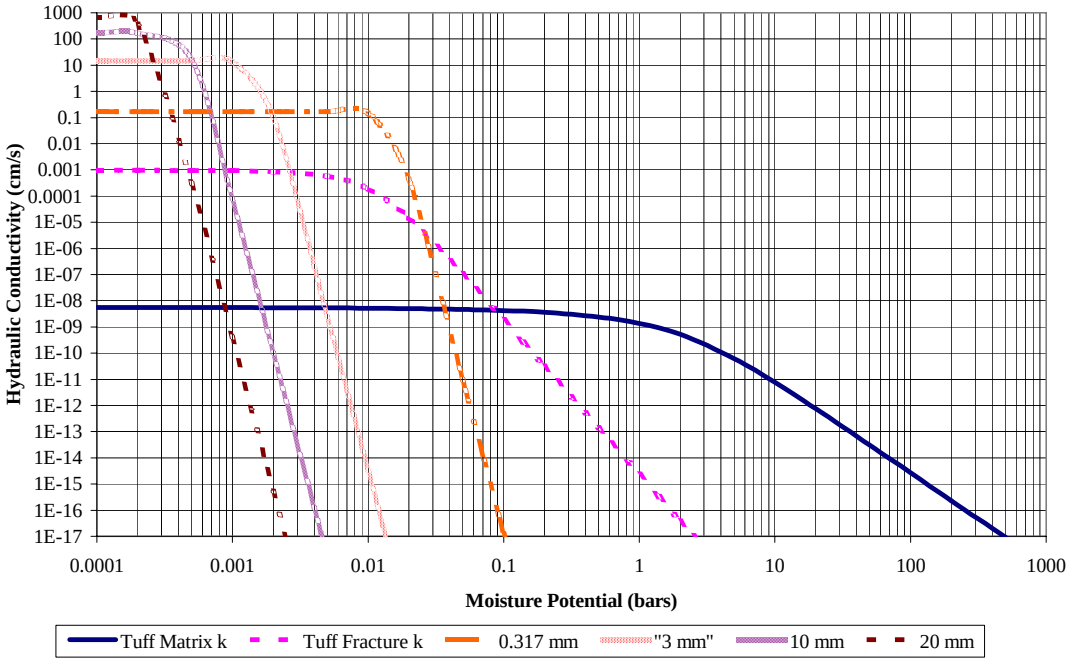

NOTE: See Table 6-4.

Figure 6-5. Comparison of Conductivity Relationships Non-Dimensionalized van Genuchten Retention Relation

Table 6-2. Summary of Hydrologic Properties Based on the Non-Dimensionalized Moisture Potential Retention Relation

Parameter	Particle Size (d_m)			
	0.317 mm	**3 mm**	**10 mm**	**20 mm**
Saturated Volumetric Moisture Content (θ_s)[2]	0.450	0.450	0.450	0.450
Residual Volumetric Moisture Content (θ_r)	0.050	0.050	0.050	0.050
van Genuchten Air-entry Parameter ($bars^{-1}$) (α)[1]	65.9	624.	2080.	4160.
van Genuchten Air-entry Parameter (cm^{-1}) (α)	0.0647	0.612	2.04	4.08
van Genuchten n Value (n)	8.013	8.013	8.013	8.013
van Genuchten m Value (m)[3]	0.875	0.875	0.875	0.875
Saturated Intrinsic Permeability(m^2) (k)[4]	1.68E-10	1.51E-08	1.67E-07	6.69E-07
Saturated Hydraulic Conductivity (cm/sec) (K_s)[5]	0.184	16.48	183.1	732.5

DTN: MO0307SPAVGSUM.000

NOTES: [1]See text and Table IV-1 for the calculation of the van Genuchten Air-Entry Parameter (α).
[2]The saturated volumetric moisture (θ_s) content equals the porosity (ϕ).
[3]The value of n is given by 1/(1-m) (Fetter 1993, p. 172).
[4]The intrinsic permeability (k) is calculated from Equation IV-4.
[5]The value of the saturated hydraulic conductivity (K_s) is obtained by the equation that converts an saturated intrinsic permeability (k) to a saturated hydraulic conductivity (K_s) (Freeze and Cherry 1979, p. 27).

$$K_s = \frac{\rho \cdot g}{\mu} \cdot k$$

The properties of water at ambient temperature are given by Incropera and DeWitt (1996, p. 846). The water density (ρ) equals 997 kg/m^3 and the absolute viscosity (μ) equals 8.935×10^{-4} $N \cdot s/(m^2)$. Note that these values compare well with the values for sands and gravels from Freeze and Cherry (1979, p. 29).

Table 6-3. Moisture Retention Calculations for the Non-Dimensionalized Moisture Potential Retention Relation

Moisture Potential(ψ) (bars)	Volumetric Moisture Content (θ)			
	Particle Size (d_m)			
	0.317 mm	**3 mm**	**10 mm**	**20 mm**
0.0001	0.450	0.450	0.450	0.450
0.0002	0.450	0.450	0.450	0.384
0.001	0.450	0.450	0.238	0.052
0.001	0.450	0.442	0.052	0.050
0.002	0.450	0.124	0.050	0.050
0.005	0.450	0.050	0.050	0.050
0.010	0.438	0.050	0.050	0.050
0.020	0.103	0.050	0.050	0.050
0.050	0.050	0.050	0.050	0.050
0.100	0.050	0.050	0.050	0.050
0.200	0.050	0.050	0.050	0.050
0.500	0.050	0.050	0.050	0.050

DTN: MO0307SPAVGHYD.000

NOTE: The detailed calculations for developing the moisture retention relationships are presented in Tables IV-1 through IV-5 of Attachment IV.

Table 6-4. Unsaturated Hydraulic Conductivity (K_{us}) Calculations for the Non-Dimensionalized Moisture Potential (ψ) Retention Relation

Moisture Potential (ψ) (bars)	Unsaturated Hydraulic Conductivity (K_{us}) (cm/sec)[1]				
	Particle Size (d_m)				
	Welded Tuff Matrix	0.317 mm	3 mm	10 mm	20 mm
0.0001	6.23E-09	1.84E-01	1.65E+01	1.83E+02	7.29E+02
0.0002	6.21E-09	1.84E-01	1.65E+01	1.82E+02	3.97E+02
0.001	6.15E-09	1.84E-01	1.52E+01	8.60E-05	4.56E-10
0.0015	6.13E-09	1.84E-01	4.54E+00	3.15E-08	1.66E-13
0.002	6.10E-09	1.84E-01	1.16E-01	1.14E-10	6.01E-16
0.005	5.99E-09	1.84E-01	2.81E-09	1.93E-18	1.01E-23
0.01	5.86E-09	1.63E-01	3.71E-15	2.54E-24	1.36E-29
0.02	5.66E-09	5.02E-04	4.89E-21	3.41E-30	2.02E-34
0.05	5.24E-09	1.08E-11	8.27E-29	1.22E-35	5.45E-36
0.1	4.74E-09	1.42E-17	1.57E-34	1.36E-36	5.92E-37
0.2	4.02E-09	1.86E-23	7.34E-37	1.48E-37	6.30E-38

DTN: MO0307SPAVGSUM.000

NOTES: [1]The values for the saturated hydraulic conductivity (K_s) (cm/sec) as a function of the moisture potential (ψ) are obtained by calculating the intrinsic permeability (k) for a given set of van Genuchten parameters from Equation IV-4 and then applying the conversion from intrinsic permeability (k) to saturated hydraulic conductivity (K_s) (Freeze and Cherry 1979, p. 27)

$$K_s = \frac{\rho \cdot g}{\mu} \cdot k$$

The properties of water at ambient temperature are given by Incropera and DeWitt (1996, p. 846). The water density (ρ) equals 1000 kg/m^3 and the absolute viscosity (μ) equals 8.935×10^{-4} N·s/(m^2). The values for the unsaturated hydraulic conductivity are then determined by scaling the saturated hydraulic conductivity relationship by the relative permeability relationship presented in Equation IV-11 for a given moisture potential.

Subsequent analyses were developed based upon a grain sizes of 3 mm, 10 mm, and 20 mm particles that correspond approximately to the average grain size of the material used in Attachment XI.

The value of the van Genuchten air-entry parameter (α) for the 3 mm diameter grain size in terms of bars^{-1} is calculated to be 624 (bars)$^{-1}$ (see Attachment IV, Equation IV-10). The intrinsic permeability (k) corresponding to a grain size of 3 mm is equal to 1.51×10^{-8} m^2. This corresponds to a saturated hydraulic conductivity (K_s) value of 14.76 cm/s (see footnote 5 to Table 6-1 for conversion). The hydraulic conductivity relationship suggests that, over the range of moisture potential (ψ) of interest, the coarse intergranular porosity ($\phi_{intergrain}$) would not retain water, and matrix flow would be dominant.

6.5 CAMPBELL RETENTION RELATION

In the following discussion, a moisture retention relation proposed by Campbell (1985, pp. 45 to 47) is used to develop the moisture potential relation. The prediction is based upon developing parameters for soil texture. Campbell presents a texture diagram for clays, silts, and sands that is based upon the assumption that the particle size distribution in soil is approximately a log-normal distribution (Assumption 5.9) characterized by the geometric mean and a geometric standard deviation (Campbell 1985, pp. 9 and 10). For sands that have diameters greater than 0.8 mm, the approximate geometric standard deviation is approximately one.

Two components of the soil-water potential depend on volumetric moisture content; these include the matrix and the osmotic potentials. Campbell (1985) terms the relationship between moisture potential (ψ) and volumetric water or moisture content (θ) as the soil moisture characteristic or moisture release curve. For the moisture potential $\psi<\psi_e$, Campbell states that the relationship is determined by the function (Campbell 1985, p. 43):

$$\psi = \psi_e \cdot (\theta / \theta_s)^{-b} \quad \text{(Eq. 6-22)}$$

The air-entry moisture potential (ψ_e) is the water potential at which the largest water filled pore in the soil will drain. As the mean pore diameter becomes smaller the air-entry moisture potential decreases (becomes more negative). Note that the "b" parameter increases as the standard deviation (σ_g) of the pore size increases. The following approximate relationships can be used to develop a moisture retention relationship based on the assumption that particle sizes follow a log-normal distribution (Assumption 5.9) (Campbell 1985, p. 45):

$$\psi_{es} = -0.5 \cdot d_g^{-1/2} \quad \text{(Eq. 6-23)}$$

$$b = -2 \cdot \psi_{es} + 0.2 \cdot \sigma_g \quad \text{(Eq. 6-24)}$$

According to Campbell, the geometric mean diameter (σ_g) can be calculated for any combination of sand, silt, and clay particle sizes (Campbell 1985, p. 8). The log normal distribution can be represented by a geometric mean particle diameter (d_g), and a geometric standard deviation (σ_g). The "b" parameter (i.e., the slope) increases with the geometric standard deviation of the pore size. The geometric standard deviation depends on the soil texture. For sand particles, the geometric standard deviation can be estimated from a soil texture diagram as equal to 1 (Campbell 1985, p. 10). Further, Campbell provides an empirical correction for the effects of bulk density (Campbell 1985, p. 46):

$$\psi_e = \psi_{es} \cdot (\rho_b / 1.3)^{0.67b} \quad \text{(Eq. 6-25)}$$

The results for the Campbell retention relation for particle diameters of 0.317 mm, 3 mm, 10 mm, and 20 mm are presented in Tables 6-5 through 6-8, based upon the detailed calculations in Attachment V. Table 6-5 presents a summary of the calculations for the parameters for the Campbell retention relation based upon the relations presented in Equations 6-22 through 6-25. Table 6-6 presents a summary of the van Genuchten curve fit parameters (α, n) based upon the van Genuchten curve fit to the Campbell retention relation. Table 6-7 presents the moisture

retention calculations for the Campbell retention relation. Table 6-8 presents the unsaturated hydraulic conductivity calculations for the Campbell retention relation. The coarse fraction will have low hydraulic conductivity over the range of the absolute values of moisture potentials from 0.01 to 0.1 bars.

Table 6-5. Summary of Parameter Determinations for the Campbell Retention Relation

Parameter		Particle Size (d_g)			
		0.317 mm	**3 mm**	**10 mm**	**20 mm**
Saturated Volumetric Moisture Content	(θ_s)	4.50×10^{-1}	4.50×10^{-1}	4.50×10^{-1}	4.50×10^{-1}
Air-entry water potential or the potential at which the largest water filled pores just drain	(ψ_{es}) (J/kg)[1]	-8.88×10^{-1}	-2.89×10^{-1}	-1.58×10^{-1}	-1.12×10^{-1}
Standard Deviation (σg)	(-)	5	1	1	1
Slope of the ln(ψ) versus ln(θ) retention curve (b)[2]		2.78	7.77×10^{-1}	5.16×10^{-1}	4.24×10^{-1}
Air-entry water potential or the potential at which the largest water filled pores just drain	(ψ_{es}) (Bars)[3]	-8.88×10^{-3}	-2.89×10^{-3}	-1.58×10^{-3}	-1.12×10^{-3}
	ψ_{es} (cm)[4]	-9.06	-2.94	-1.61	-1.14
Corrected Air-entry water potential or the potential at which the largest water filled pores just drain	(ψ_e) (Bars)	1.006×10^{-2}	2.99×10^{-3}	1.62×10^{-3}	$1.141.006\times10^{-3}$

NOTES: [1] Air-entry water potential or the potential at which the largest water filled pores just drain (J/kg) is calculated from Equation 6-23.
[2] The b value is calculated from Equation 6-24 with σ_g equal to 5 for a fine grained material (0.317 mm), and 1 for the coarser materials (Campbell 1985, Figure 2.1).
[3] The conversion from (J/kg) is performed by multiplying by the density (ρ = 1000 kg/m^3), and then expressing the pressure in bars.
[4] The conversion from bars to cm is performed by dividing the pressure by the product of the mass density (ρ = 1000 kg/m^3), and the acceleration due to gravity.

Table 6-6. Summary of van Genuchten Curve Fit Parameters Based Upon the Campbell Retention Relation[1]

Parameter	Particle Size (d_g)			
	0.317 mm	**3 mm**	**10 mm**	**20 mm**[2]
Saturated Volumetric Moisture Content (θ_s)	0.450	0.450	0.450	0.450
Residual Volumetric Moisture Content (θ_r)	0.020	0.010	0.010	0.010
van Genuchten Air-entry Parameter (α) (bars^{-1})	47.64	230.84	476.91	561.61
van Genuchten Air-entry Parameter (α) (cm^{-1})	0.06	0.24	0.48	0.56
van Genuchten (n) Value	1.53	3.04	4.03	11.11
van Genuchten (m) Value	0.35	0.67	0.752	0.91
Saturated Intrinsic Permeability (k)(m^2)	1.68E-10	1.51E-08	1.67E-07	6.69E-07
Saturated Hydraulic Conductivity (K_s)(cm/sec)	0.184	16.48	183.1	732.5

NOTES: [1] See Attachment V for the details of the van Genuchten curve fit to the Campbell retention relation.
[2] Note that the hydraulic conductivity under saturated conditions may have a Reynolds Number that exceeds the range of validity for Darcy's Law.

Table 6-7. Moisture Retention Calculations for the Campbell Retention Relation [1]

Moisture Potential (ψ) bars	Volumetric Moisture Content[2]			
	Particle Size (d_g)			
	0.317 mm	3 mm	10 mm	20 mm
0.0001	0.450	0.450	0.450	0.450
0.0002	0.450	0.450	0.450	0.450
0.0005	0.450	0.450	0.449	0.450
0.001	0.449	0.447	0.434	0.449
0.002	0.446	0.424	0.290	0.119
0.005	0.435	0.245	0.041	0.010
0.01	0.410	0.086	0.014	0.010
0.02	0.363	0.029	0.010	0.010
0.05	0.271	0.013	0.010	0.010
0.1	0.203	0.011	0.010	0.010
0.2	0.149	0.010	0.010	0.010
0.5	0.100	0.010	0.010	0.010
1	0.076	0.010	0.010	0.010
2	0.059	0.010	0.010	0.010
5	0.044	0.010	0.010	0.010
10	0.037	0.010	0.010	0.010
20	0.032	0.010	0.010	0.010
50	0.027	0.010	0.010	0.010
100	0.025	0.010	0.010	0.010
200	0.023	0.010	0.010	0.010
500	0.022	0.010	0.010	0.010
1000	0.021	0.010	0.010	0.010

NOTES: [1] See Attachment V for the detailed calculations.
[2] Note that Tables V-3, V-5, V-7, and V-9 present the calculations for the retention data presented above based upon the curve fit to the Campbell relationship and determination of van Genuchten parameters.

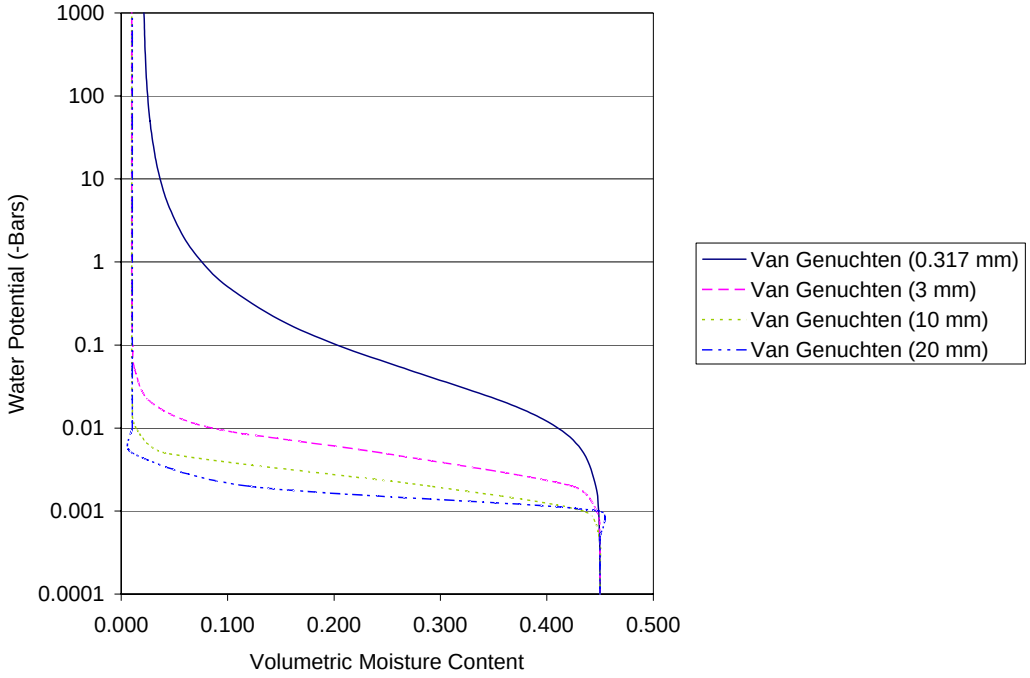

Figure 6-6. Retention Relationships Based Upon a Normalized Moisture Potential for the Campbell Retention Relation (Attachment V)

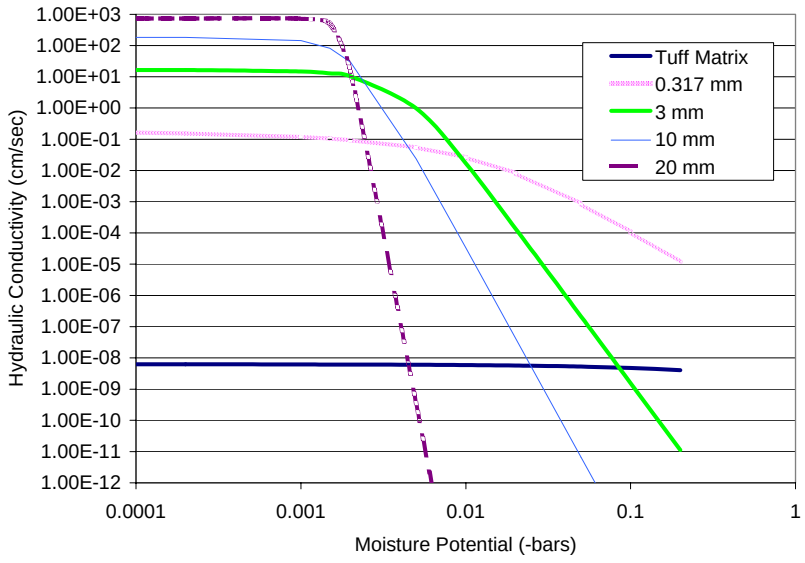

NOTE: The hydraulic conductivity for 20 mm under saturated conditions may have a Reynolds Number that exceeds the range of validity for Darcy's Law.

Figure 6-7. Comparison of Conductivity Relationships Based Upon the Campbell Retention Relation (Attachment V)

Table 6-8. Unsaturated Hydraulic Conductivity (K_{us}) Calculations for the Campbell Retention Relation

Moisture Potential (ψ) (bars)	Unsaturated Hydraulic Conductivity (K_{us}) (cm/sec)[1]			
	Particle Size (d_g)			
	0.317 mm	3 mm	10 mm	20 mm[2]
0.0001	1.65E-01	1.48E+01	1.64E+02	6.53E+02
0.0002	1.65E-01	1.48E+01	1.63E+02	3.56E+02
0.001	1.65E-01	1.48E+01	1.64E+01	3.08E-04
0.001	1.65E-01	1.36E+01	7.70E-05	4.09E-10
0.002	1.65E-01	1.04E-01	1.02E-10	5.39E-16
0.005	1.65E-01	2.52E-09	1.72E-18	9.09E-24
0.010	1.46E-01	3.32E-15	2.27E-24	1.22E-29
0.020	4.50E-04	4.38E-21	3.04E-30	1.81E-34
0.050	9.65E-12	7.40E-29	1.10E-35	4.88E-36
0.100	1.27E-17	1.40E-34	1.22E-36	5.30E-37
0.200	1.68E-23	6.58E-37	1.60E-37	6.72E-38
0.500	2.84E-31	3.27E-38	7.68E-39	2.70E-39
1.000	7.15E-37	3.48E-39	7.93E-40	3.72E-40
2.000	3.67E-39	3.64E-40	9.29E-41	3.27E-41
5.000	2.44E-40	1.99E-41	3.74E-42	1.89E-42
10.000	2.65E-41	2.02E-42	4.22E-43	1.49E-43
20.000	2.82E-42	2.02E-43	4.64E-44	1.47E-44
50.000	1.59E-43	1.03E-44	2.07E-45	8.82E-46
100.000	1.86E-44	1.12E-45	2.01E-46	7.76E-47
200.000	1.63E-45	9.82E-47	1.94E-47	7.46E-48
500.000	7.48E-47	4.36E-48	7.80E-49	3.55E-49
1000.000	9.28E-48	4.21E-49	8.87E-50	3.38E-50

NOTE: [1] The values for the saturated hydraulic conductivity (K_s) (cm/sec) as a function of the moisture potential (ψ) are obtained by calculating the intrinsic permeability (k) for a given set of van Genuchten parameters from Equation IV-4 and then applying the conversion from intrinsic permeability (k) to saturated hydraulic conductivity (K_s) (Freeze and Cherry 1979, p. 27):

$$K_s = \frac{\rho \cdot g}{\mu} \cdot k$$

The properties of water at ambient temperature are given by Incropera and DeWitt (1996, p. 846). The water density (ρ) equals 1000 kg/m^3 and the absolute viscosity (μ) equals 8.935×10^{-4} N·s/(m^2). The values for the unsaturated hydraulic conductivity are then determined by scaling the saturated hydraulic conductivity relationship by the relative permeability relationship presented in Equation IV-11 for a given moisture potential.

6.6 NUFT ADVECTION CALCULATION

In *In-Drift Thermal-Hydrological-Chemical Model* (BSC 2001b), a single-continuum approximation was used to represent hydrologic properties and performance of the invert ballast material.

The invert ballast material is comprised of crushed tuff. Crushed tuff contains two types of porosity, an intragranular matrix porosity (ϕ_{matrix}) component (within the grains) and an intergranular porosity ($\phi_{intergrain}$) (between the grains). Each of these porosity components has distinct intrinsic hydrologic properties. The single-continuum approach, generally referred to as Equivalent Continuum Model (ECM), does not explicitly represent the hydrologic properties for each porosity component, but instead represents hydrologic behavior of the crushed tuff with a single set of average properties (Attachment XI).

An alternate analysis approach is to assess invert hydrologic performance with a dual permeability model (DKM) approach wherein each porosity component is represented explicitly. This approach allows the intragranular and intergranular porosities to behave in a manner consistent with their respective intrinsic hydrologic properties (e.g., capillary suction potentials). In general, when the grain size is small, the intragranular and intergranular component behave like a porous matrix medium and thus the single-continuum approach may be justified. However, as the grain size increases, the intergranular and intragranular components would tend to behave more independently of each other and accordingly, the DKM approach is a more appropriate method to use in modeling.

A series of NUFT simulations have been performed to corroborate the hydrologic performance of the invert using the van Genuchten and Campbell retention relations for different grain sizes as examined by this analysis. The input parameters to the DKM model of NUFT are porosity (ϕ), van Genuchten air-entry parameter (α) and "m" values, residual and maximum saturation (S_r and S_s), and intrinsic permeability (k) for the intergranular and intergranular components, as derived in Section 6.3.

The percolation flux at the PTn/TSw contact for the analysis was selected as 35 mm per year or 70 mm per year. Percolation fluxes for the upper bound glacial climate that represents most extreme case for nine cases analyzed are presented in DTN: LB0302PTNTSW9I.001. The nine cases are for the three climate conditions, and the lower, mean, and upper bound distributions for each climate. The mean value for the upper bound glacial is 35.63 mm per year. A value of 35 mm per year was selected for analysis. The distribution function approximately follows an exponential distribution in which the mean equals the standard deviation (Hahn and Shapiro 1967, pp. 122 to 124). To provide a more extreme condition that corresponds approximately to the mean, plus one standard deviation (70 mm per year) was applied. Note that, as discussed subsequently in Section 6.8, in the coarse pore space, the results were not sensitive to the percolation flux.

The matrix properties for the crushed tuff grains are the same as those of the host rock surrounding the drift (TSw36). Simulations are conducted for different intergranular pore space properties based on a uniform grain diameter size of 0.317, 3, 10, or 20 mm. The 0.317-mm size tends to wick more liquid into the invert than the larger grain size and thus is conservative for radionuclide transport.

The hydraulic response of the intergranular pore space is represented as a relationship between moisture potential and moisture content. This relationship is based on the van Genuchten retention relation (Fetter 1993, p. 172) discussed previously in Section 6.4, and the Campbell retention relation (Campbell 1985, p. 45) discussed previously in Section 6.5. Figures 6-4 and 6-6 present the van Genuchten and Campbell curve fit to moisture retention data for the different grain sizes. The corresponding van Genuchten and Campbell relationships (Fetter 1993, p. 182) between unsaturated hydraulic conductivity (K_{us}) and moisture potential are presented in Figures 6-5 and 6-7. Although the van Genuchten and the Campbell curves show the same saturated hydraulic conductivity (K_s) for a given grain size, the van Genuchten relationship, in general, provides a lower unsaturated hydraulic conductivity, for the same moisture potential for the invert material.

6.7 NUFT SIMULATIONS

The key changes for the current calculations are the use of a dual-continuum approach and better spatial resolution for EBS components. Attachment I presents a list of the NUFT input file names. These and other minor modifications are listed below:

- Backfill is not present in the space between the drip shield and the drift wall.
- Heating from the waste package is ignored since the purpose of this analysis is to predict a steady-state liquid saturation (S) and flux distribution in the invert.
- An approximate-round shape for the waste package and a letter-box shape for the drip shield are included in the model.
- The air gap below the drip shield extends through the space between the waste package and the invert. That is, the waste package is not in contact with the invert.
- A Dual-Permeability Model (DKM), as discussed in *Water Distribution and Removal Model* (CRWMS M&O 2001b, Section 6.2.1), has been used rather than a single-continuum or equivalent continuum model. DKM is used to describe the permeability for the geologic media surrounding the drift and for the invert ballast material (DTN: LB990861233129.001). It is appropriate to model the invert with the dual-permeability approach because the crushed tuff has an intragranular matrix component and an intergranular pore space component. The dual-permeability approach is consistent with the anticipated response of the tuff grains, where the matrix component will behave like the host rock and the large, intergranular pore spaces will act as a capillary barrier to incoming flow from the host rock.
- The depth of the invert of 0.806 m is used to determine the path length, as discussed in Attachment XV. Note that, as discussed in Attachment XV, the path length of 0.5 was selected to account for possible variations in the location of contaminants entering the invert from the waste package, and to account for settlement with time.
- The simulation grid is finer than that used in *In-Drift Thermal-Hydrological-Chemical Model* (BSC 2001b) to provide more spatial resolution in the invert and to provide better definition of the shapes of the waste package, drip shield, invert, and the air gap between waste package and invert.

The thermal and hydrologic properties of stratigraphic units of the Natural Barrier System (NBS) from the ground surface to the water table were developed in *Calibrated Properties Model* (BSC 2003c) as presented in DTN: LB990861233129.002. These properties (Tables 4-5, 4-6, and 4-7) are the same as those used in *In-Drift Thermal-Hydrological-Chemical Model* (BSC 2001b). Attachment VIII presents the hydrologic properties of other EBS components used in the NUFT runs. For the specific location of the repository used in the In-Drift Thermal-Hydrological-Chemical Model, the drift would be surrounded by the Tptpln (TSw36) formation even though the majority of the repository elsewhere will be in the Tptpll (TSw35) formation. Similarly in these calculations, it is assumed that the TSw36 unit surrounds the drift. The sensitivity of replacing TSw36 by the TSw35 units around the drift on the fluxes in the invert is analyzed in Section 6.8.

The calculations were performed with an ambient geothermal gradient (no heating from waste package) because the purpose of the analyses is to predict the steady-state liquid saturation (S) and flux distribution in the invert at late times, after waste package failure, when the thermal pulse has passed through the repository system.

6.8 NUFT RESULTS

The detailed NUFT results are presented in Attachment X. Attachment II presents a list of the NUFT output files. A model simulation grid is presented on Figure X-1. All discussions here will pertain to steady state conditions. Figures X-2a and X-2b show the general flow directions in the rock fractures and matrix, respectively, around the drift. They both show essentially identical pattern. The flow directions as displayed by XTOOL, a post-processor of NUFT, are only approximate. The size of the vector does not reflect the magnitude of flow and the vectors may extend slightly to a neighboring cell that may not have any flow at all. This description applies to Figures X-3 through X-18 that show liquid flux directions in the intergranular and intragranular components of the invert for different grain sizes using the van Genuchten and Campbell models. The blank space on these figures represents areas with zero flux. The exact flow direction and magnitude of flux in a cell, as computed by NUFT, can be displayed on a monitor by positioning the cursor in that cell while running XTOOL.

6.8.1 NUFT Analyses with the Nondimensionalized van Genuchten and Campbell Relationships

Tables 6-9 and 6-10 summarize the computational results at steady state for a grain size varying from 0.317-mm diameter to 20-mm diameter for the two retention relations. The tables compare conditions in the invert in the intergranular, and intragranular components. The data in Tables 6-9 and 6-10 and Figures X-2 through X-17 demonstrate that:

- The saturation of the rock matrix in individual grains (S_{matrix}) of the grain matrix is approximately equal to the saturation of the host rock. This is a reasonable response because the tight pores in the tuff grains have high capillarity that draws water from the fractures of the host rock into the grains.

- The vertical pore-water velocity (V) in the matrix component is low and is controlled by the saturated hydraulic conductivity (K_s), the pressure gradient in the matrix, and also by the pressure gradient across the intergranular and intragranular components.

- The Campbell retention relation predicts that for a grain size of 0.317-mm in diameter, the intergranular component behaves similarly to the intragranular matrix component, and the moisture potential equilibrates across the two components. As the grain size increases to 3-mm diameter or larger, the intergranular component breaks away and behaves as a capillary barrier, as shown by a sharp difference in pressure potential across the two components. This pressure gradient steepens as the grain size increases from 3-mm to 20-mm diameter, inducing a slightly higher flux in the matrix component. This matrix flux tends to stabilize between the 10- and 20-mm grain size models.

- The van Genuchten retention relation predicts that for all grain sizes of the crushed tuff 0.317-mm diameter or larger, the intergranular component acts as a capillary barrier, whereas the intragranular component behaves as a matrix medium, as expected in a DKM model.

- For those cells in the invert showing zero intergranular fluxes (represented by blank space in the figures), the saturation ($S_{intergrain}$) of the intergranular pore spaces is zero, confirming that the pore space acts like a capillary barrier to flow.

- Except for the 0.317-mm Campbell retention relation, the intergranular components of all other models behave as a capillary barrier to flow from the rock to the invert.

6.8.2 NUFT Sensitivity Analyses

Sensitivity analyses were conducted to evaluate the impact of: 1) different grain/void contact areas, 2) host-rock properties, 3) infiltration rates, 4) invert thickness, and 5) grid spacing in the invert on fluxes in the invert for the van Genuchten retention relation. These analyses are discussed in Attachment X and presented in Figures X-2 through X-19. The analyses show that:

1. An increase of the specific grain/void contact area from 90 m^{-1} to 8,517 m^{-1} would increase the matrix fluxes by only a factor of 1.2 to 1.4. The intergranular fluxes are the same (pr2D35rmntinvrs in Attachment I).

2. A change of the host-rock properties from tsw36 (Tptpln) to tsw35 (Tptpll) and the corresponding invert matrix properties would increase the matrix fluxes by a factor of 1.3 to 1.5. Intergranular fluxes are essentially the same (pr2D35rmntinv35 in Attachment I).

3. An increase of infiltration rate at the ground surface from 35- to 70-mm per year (Section 3.14) would increase the intergranular fluxes by a factor of 3 to 5 along the outer edge of the invert. Matrix fluxes remain practically unchanged (pr2D70rmni in Attachment I).

4. An increase of invert thickness from 0.5 to 0.6 meters would not change the fluxes (pr2D35rmntinv2 in Attachment I).

5. Refinement of grid spacing in the invert would not significantly change the fluxes in the invert. This indicates that the mesh is fine enough to produce reasonable results (pr2D35rmnt2 in Attachment I).

The NUFT_Input.txt file (Attachment I) contains information from the output of the NUFT calculation. The first line states the number of grid points minus one (n-1) at the centerline of the NUFT model that are input. The program then loops from 0 to (n-1) to read in each line the elevation (m), depth(m), pore-water velocity (V) (m/sec), the degree of saturation (S), and the Darcy flux (J_w) (m/sec) for each grid point. Note that the Darcy flux for the invert material equals the pore-water velocity times the degree of saturation (S) times the porosity (ϕ).

6.8.3 Corroboration of the NUFT Analyses

The following presents a discussion of the retention measurements made on crushed tuff presented in Attachment XI based upon the Unsaturated Flow Apparatus (UFA) as described in Appendix C of *Engineered Barrier System Performance Requirements Systems Study Report* (CRWMS M&O 1996). The measurements are from DTN: GS980808312242.015.

The UFA mainly consists of an ultracentrifuge in which a soil sample is subject to centrifugal force. The volumetric moisture content (θ) as a function of the moisture potential (ψ) as discussed subsequently below can be determined by allowing the sample to drain until the moisture potential equals the centrifugal force per unit area divided by the unit weight in a state of equilibrium. The volumetric moisture content (θ) is determined gravimetrically using the bulk density of the sample. The UFA represents an efficient method for testing fine-grained soils at higher moisture potential (ψ).

As discussed Attachment XI, the van Genuchten curve-fitting parameters were determined by fitting the curve to the retention data for crushed tuff (Section 4.1.5). Attachment XVI presents the Microsoft Excel 97 spreadsheet that uses the Equation Solver to calculate the curve-fitting parameters. The results from the curve-fitting process presented in Attachment XVI (p. XVI-22) are:

$$\theta_r = 0.05$$

$$\alpha_i = 0.12 \text{ (1/cm)}$$

$$n_i = 2.75$$

The results of the analysis as shown in Figure XI-1 show that over a broad range of moisture potential that would be expected in the repository that the measured volumetric moisture content was approximately equal to the matrix porosity. The UFA measurements indicate that the fine pore space as represented by the intragranular porosity was nearly saturated while the intergranular porosity was free of water. The UFA measurements provide a corroboration of the NUFT analysis results.

6.9 CONTAMINANT TRANSPORT RESULTS

The results of the NUFT calculations, as summarized in Tables 6-9 and 6-10, show in general that the coarse intergranular pore space is drained and free of water while the intragranular pore space is near saturation. If consideration is given to the advection-dispersion-diffusion relation presented in Equation 6-4, with calculation of the diffusion coefficient by the relationship presented in Equation 6-11 to flow, bounding calculations can be performed to estimate the range of breakthrough times near the centerline of the model. The NUFT results suggest that

diffusion would be the dominant mass transport mechanism in the intergranular pore space that is drained of water, and near the top surface of the invert. As depth into the invert increases, the NUFT results suggest that advection becomes more dominant.

The diffusion relation (Equation 6-12) is used to estimate the invert liquid diffusion property. Note that the experiments performed, as presented in *Invert Diffusion Properties Model* (CRWMS M&O 2000b, Figure 3), did not distinguish between intergranular and intragranular porosities in the calculation of the diffusion coefficient. The following presents a calculation of the bulk porosity (ϕ), and the bulk volumetric moisture content (θ) based upon the summary material parameters.

6.9.1 Calculation of Bulk Porosity

Using the following definitions for the total volume, V_{total}, of grains and pore space and for the total volume of the grains, $V_{Grain,Total}$, the total volume and the grain total volume can be expressed as, respectively:

$$\begin{aligned} V_{Total} &\equiv V_s + V_{tm} + V_c, \\ V_{Grain,Total} &\equiv V_s + V_{tm} \\ &= V_{Total} - V_c, \end{aligned} \qquad \text{(Eq. 6-26)}$$

The detailed calculations for the dripping case and the nondripping case are presented in Attachment XIII. The bulk moisture content for the dripping case can be expressed as (Attachment XIII)

$$\theta_{Bulk} := \frac{\phi_{intergrain} \cdot \left(1 + \frac{\phi_{matrix}}{1-\phi_{matrix}}\right) \cdot \frac{1}{1-\phi_{intergrain}} \cdot \left(\frac{\theta - \theta_r}{\phi_{intergrain} - \theta_r}\right) + \frac{\phi_{matrix}}{1-\phi_{matrix}}}{1 + \left[\phi_{intergrain} \cdot \left(1 + \frac{\phi_{matrix}}{1-\phi_{matrix}}\right) \cdot \frac{1}{1-\phi_{intergrain}}\right] + \frac{\phi_{matrix}}{1-\phi_{matrix}}} \qquad \text{(Eq. 6-27)}$$

For the nondripping case, the coarse pore space has a zero percent saturation as determined from the NUFT analysis, and the fine pore space may be partially saturated at a fairly high saturation. The bulk volumetric moisture content can be expressed as (Attachment XIII):

$$\theta_{Bulk} := \frac{S_{matrix} \cdot \frac{\phi_{matrix}}{1-\phi_{matrix}}}{1 + \phi_{intergrain} \cdot \left[\left(1 + \frac{\phi_{matrix}}{1-\phi_{matrix}}\right) \cdot \frac{1}{1-\phi_{intergrain}}\right] + \frac{\phi_{matrix}}{1-\phi_{matrix}}} \qquad \text{(Eq. 6-28)}$$

Table 6-9. Comparison of Invert Conditions at Steady State for the van Genuchten Method of Formulating Retention Data

Intragranular (Matrix) Component				Intergranular Component				Component Parameters
Vertical Pore Velocity (V) Along Centerline (m/s)	Moisture Potential (ψ) at Center (Pa)	Saturation at Center of Invert (S_{matrix})	Porosity (ϕ_{matrix})	Vertical Pore Velocity (V) Along Centerline (m/s)	Moisture Potential (ψ) at Center (Pa)	Saturation at Center of Invert ($S_{intergrain}$)	Porosity ($\phi_{intergrain}$)	Grain Diameter (d_m) (mm)
7.6E-11 to 1.8E-10	9368	0.999	0.112	0.0	3377	0.0	0.450	0.317
5.9E-11 to 1.3E-10	1.41E4	0.998	0.112	0.0	357	0.0	0.450	3
5.8E-11 to 1.3E-10	1.52E4	0.997	0.112	0.0	111	0.0	0.450	10
5.9E-11 to 1.3E-10	1.54E4	0.997	0.112	0.0	56	0.0	0.450	20

Table 6-10. Comparison of Invert Conditions at Steady State for the Campbell Method of Formulating Retention Data

Intragranular (Matrix) Component				Intergranular Component				Component Parameters
Vertical Pore Velocity (V) Along Centerline (m/s)	Moisture Potential (ψ) at Center (Pa)	Saturation at Center of Invert (S_{matrix})	Porosity (ϕ_{matrix})	Vertical Pore Velocity (V) Along Centerline (m/s)	Moisture Potential (ψ) at Center (Pa)	Saturation at Center of Invert ($S_{intergrain}$)	Porosity ($\phi_{intergrain}$)	Grain Diameter (d_m) (mm)
4.4E-14 to 2.1E-13	7370	0.999	0.112	5.5E-10 to 1.6E-9	7370	0.487	0.450	0.317
3.7E-11 to 8.3E-11	1.16E4	0.998	0.112	0.0	2981	0.0	0.450	3
5.7E-11 to 1.3E-10	1.50E4	0.997	0.112	0.0	830	0.0	0.450	10
5.8E-11 to 1.3E-10	1.54E4	0.997	0.112	0.0	267	0.0	0.450	20

Table 6-11. Summary of Material Parameters

Parameter	Symbol	Value	Source
Porosity of the rock matrix in an individual grain	ϕ_{matrix}	0.112	DTN: LB990861233129.001
Porosity of the large pore spaces between grains	$\phi_{intergrain}$	0.45	See Section 6.3
Saturation of the rock matrix in an individual grain	s_{matrix}	0.999	Table 6-9
Saturation of the large pore spaces between grains	$s_{intergrain}$	0.0	Table 6-9

The calculated volumetric moisture contents for the dripping and nondripping cases are presented in Attachment XIII as 0.073 and 0.058, respectively, for purposes of illustration are presented in Attachment XIII.

6.9.2 Calculation of the Diffusion and Dispersion Coefficient

The calculated diffusion coefficient is based on a freewater diffusion coefficient of 2.3×10^{-5} cm^2/sec (Assumption 5.6) and near saturation of the intergranular pore space from Attachment III. Equation III.7 is 1.7×10^{-7} cm^2/sec for the dripping case, as presented in the breakthrough analysis in Attachment III.

The hydrodynamic dispersion coefficient for each of the breakthrough analyses is calculated by taking the pore-water velocities from Tables 6-9 and 6-10 of this calculation, and multiplying by the dispersivity of 10 cm or 0.1 m, as presented in Attachment III. The effective dispersion coefficient is then the sum of the diffusion coefficient, and the hydrodynamic dispersion for each case analyzed, as presented in Attachment III.

Attachment XII presents a range of diffusion coefficients for the dripping case for a broad range of waste package flow rates. The results of the analysis shows that diffusion rates are on the order of 10^{-8} to 10^{-7} cm^2/sec.

6.9.3 Breakthrough Analysis

The closed form analytical solution for the one-dimensional advection-dispersion equation (Equation 6-4) is used to develop breakthrough curves for a range of conditions. Figure 6-8 presents the breakthrough analysis for 0.317 mm grain diameter with the retention properties given by the van Genuchten retention relation. Attachment III presents the detailed calculations. The analysis is subject to the assumptions that the direction of the advective flux is in the vertical direction (Assumption 5.1); the effects of lateral dispersion are neglected (Assumption 5.2); and the invert is homogeneous (Assumption 5.3). The radionuclides are assumed to be released at the centerline of the drift (Assumption 5.4), and that the effects of radioactive decay are neglected (Assumption 5.5). Solute vapor phase is assumed to be negligible (Assumption 5.7). The range of pore water velocities for the intergranular pore space was from 7.6×10^{-11} m/s to 1.8×10^{-10} m/s for the low and high advection cases, respectively (Table 6-9). For comparison, the breakthrough curve for diffusion is presented. The breakthrough analysis for the case of variable pore-water velocity would fall between these extremes for high and low advection. The

results of the analysis show that breakthrough would occur within a time frame of 400 to 1,000 years while a diffusion dominated process in the intergranular pore space would occur within a time frame of 1,000 to 10,000 years.

The closed form analytical solution for the one-dimensional advection-dispersion equation (Equation 6-4) is used to develop breakthrough curves for grain diameters from 3 to 20 mm with the retention properties given by the van Genuchten and Campbell retention relations (Section 6.3). Figures 6-9 through 6-10 present breakthrough curves for high and low advection for the nondimensionalized van Genuchten and Campbell relations, respectively. The range of pore water velocities for the intergranular pore space was from 5.9×10^{-11} m/s to 1.3×10^{-10} m/s for the low and high advection cases, respectively (Table 6-9). The breakthrough analysis for the case of variable pore-water velocity would fall between these extremes for high and low advection. The results of the analysis show that breakthrough would occur again within the same time frame of 600 to 2,000 years while a diffusion dominated process such as would occur in the intergranular pore space would be of the order of a 1,000 to 10,000 years. Since advection through the intergranular pore space of the tuff matrix is not affected by pore size, the range for breakthrough for grain sizes between 3 to 20 mm is very similar.

The closed form solution for (Equation 6-4) is used to develop breakthrough curves for grain diameters from 3 to 20 mm with the retention properties given by the Campbell retention relation. The range of pore water velocities for the intergranular pore space was from 3.7×10^{-11} m/s to 1.3×10^{-10} m/s for the low and high advection cases, respectively (Table 6-10). For this range of grain sizes, the results of the breakthrough analysis for the intergranular pore space are nearly identical to the range given by the van Genuchten retention relation.

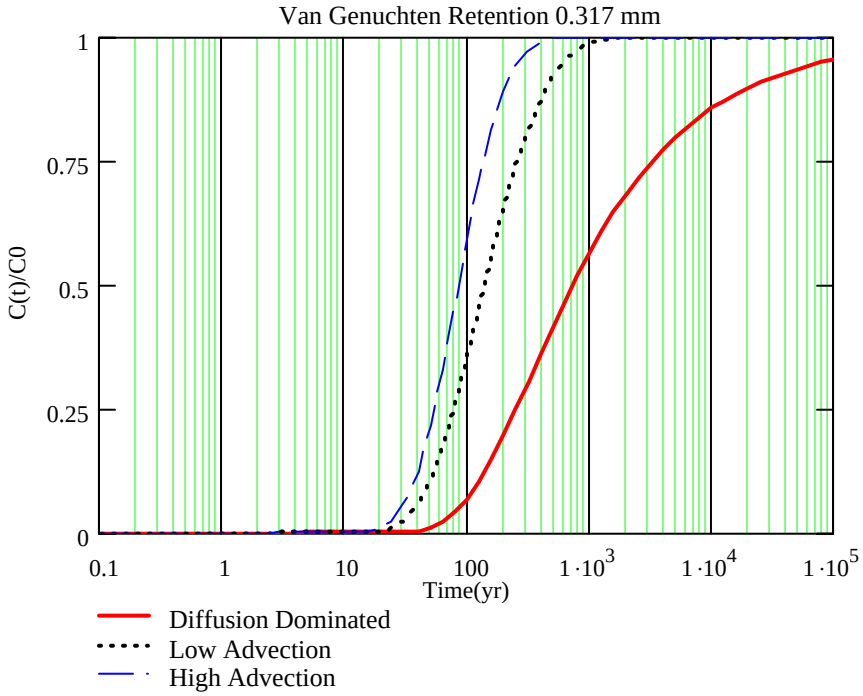

Figure 6-8. Breakthrough Curves for the 0.317 mm van Genuchten Retention Relation (Attachment III)

6.9.4 Retardation

This section provides a sensitivity analysis for radionuclide transport in solute or radionuclides adsorbed onto colloidal particles in the invert. This section applies the solution to the one-dimensional solute transport equation (Equation 6-4) for a range of retardation.

The retardation factor for unsaturated flow is obtained from Jury et al. (1991, p. 227):

$$R = 1 + \frac{\rho_b \, K_d}{\theta} \qquad \text{(Eq. 6-29)}$$

The bulk density used above is taken as the saturated bulk density. The following calculation is used to estimate the saturated bulk density. The volume of the voids (V_{tm}) is calculated in Equation 6-19 as 0.126 m^3. The grain density is given as 2560 kg/m^3 for TSW36 (DTN: LB990861233129.001). The saturated bulk density is the weight of the water (W_w) and the weight of the solids (W_s) divided by the volume of the solids (V_s = 1 m^3) and the volume of the water (VW_{tm}):

$$\rho_b = \frac{1000 \cdot \frac{kg}{m^3} \cdot 0.126 \cdot m^3 + 2560 \cdot \frac{kg}{m^3}}{1 \cdot m^3 + 0.126 \cdot m^3} = 2385 \cdot \frac{kg}{m^3} \qquad \text{(Eq. 6-30)}$$

Sheppard and Thibault (1990, Tables A-1 through A-4) present data on the mean and standard deviation of the natural logarithm of the partition coefficient for individual elements for sands, loams, clays, and organic soils that would have application to the invert. This information includes the number of measurements. Sheppard and Thibault (1990, p. 472) also cite previous work in which the partition coefficients are log normally distributed. Finally, Sheppard and Thibault (1990, p. 472) calculated the geometric mean and the geometric standard deviation for each element by soil texture for the mineral soils and also for organic soils. All distributions developed were log-uniform because the partition coefficient (K_d) data is often observed to be logarithmically distributed, because a log-distribution maintains uniformity of sampling in each decade, and because little is known about the distribution of partition coefficient (K_d) values throughout a given range.

To take into account a broad range of values, the partition coefficients, an analysis was performed using the closed form solution presented in Equation 6-4 for partition coefficient (K_d) values of 1, 10, 100, and 1,000 ml/gram. The calculated values for the retardation coefficients are presented in Table 6-12 using Equation 6-29.

Equation 6-4 is used to calculate breakthrough curves taking the pore-water velocity, and the diffusion coefficient as calculated above, and dividing by the retardation factor as calculated in Table 6-12. The results of these calculations are presented in Figures 6-11 through 6-14. The results of the calculations show that for the case of low sorption (K_d = 1.0 ml/gm), the retardation factor is low, and breakthrough is delayed to 1,000 to 5,000 years. For the case of intermediate and high sorption (10 - 100 ml/gm), the delay in breakthrough time is more substantial. In the case of the intermediate sorption, breakthrough would be delayed from 1,000 to 10,000 years. In the case of high sorption (1,000 ml/gm), breakthrough is delayed by at least one million years.

Table 6-12. Retardation Calculations

Partition Coefficient (K_d)		Saturation (S)	Volumetric Moisture Content (θ)	Bulk Density (ρ_b)	Retardation Factor R	Figure No.
ml/gm	m^3/kg	(-)	(-)	(kg/m^3)	(-)	
1	0.001	0.997	0.11	2385	22.7	6-11
10	0.01	0.997	0.11	2385	217.8	6-12
100	0.1	0.997	0.11	2385	2169.2	6-13
1000	1	0.997	0.11	2385	21682.8	6-14

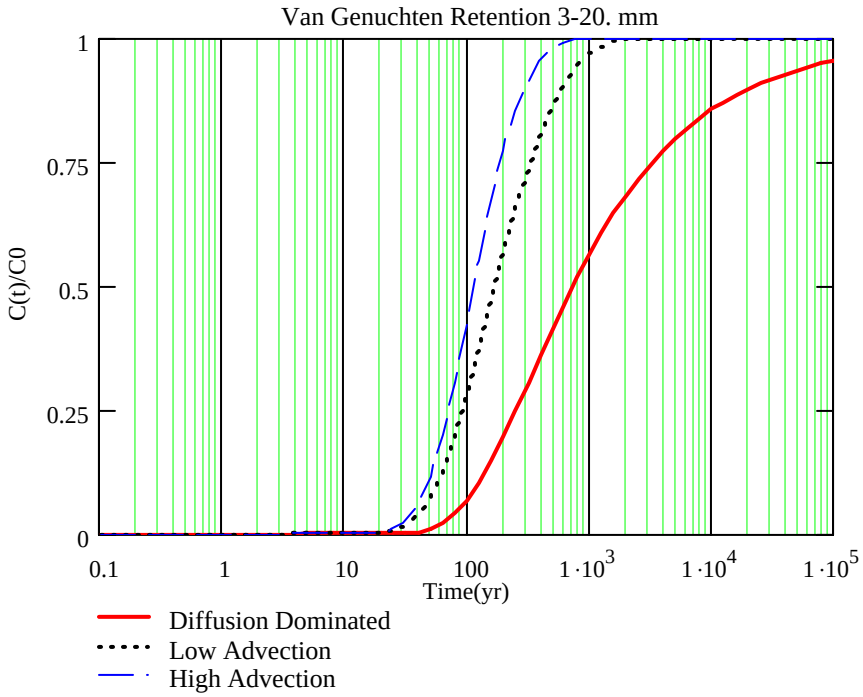

Figure 6-9. Breakthrough Curves for High and Low Advection (3-20 mm van Genuchten Retention Relation)

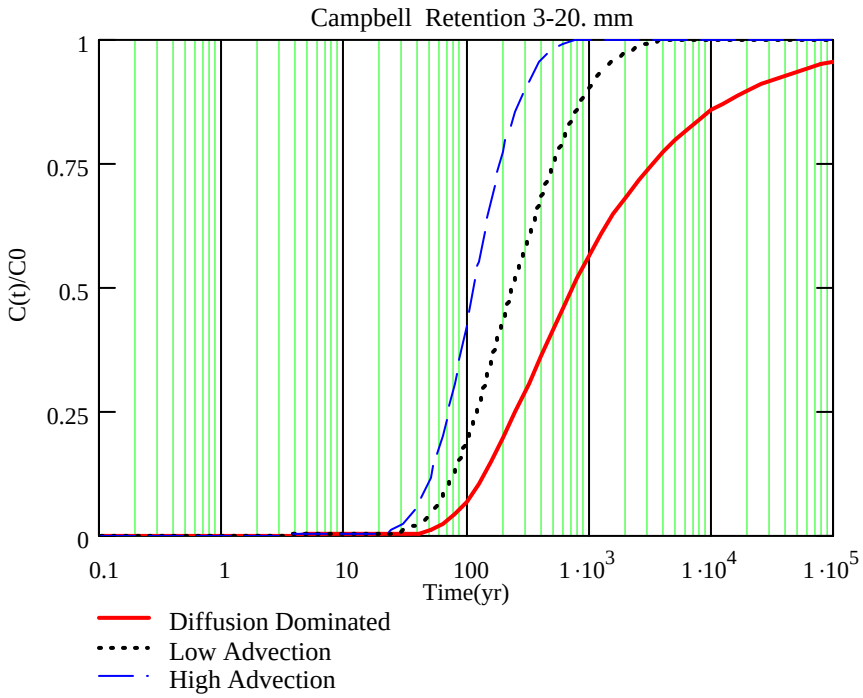

Figure 6-10. Breakthrough Curves for High and Low Advection (3-20 mm Campbell Retention Relation)

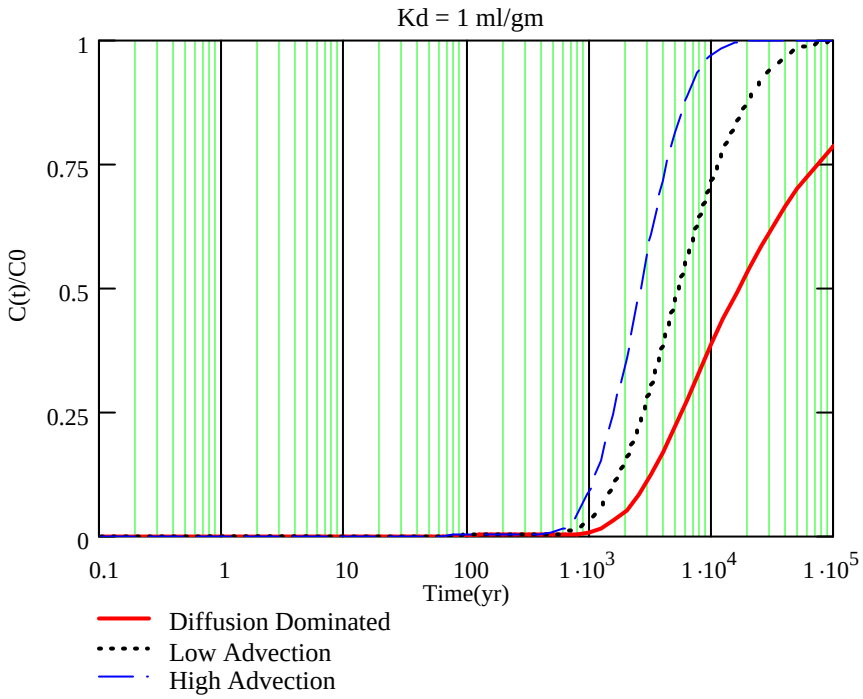

Figure 6-11. Breakthrough Curves for the Case of Low Partition Coefficient (K_d = 1.0 ml/gm)

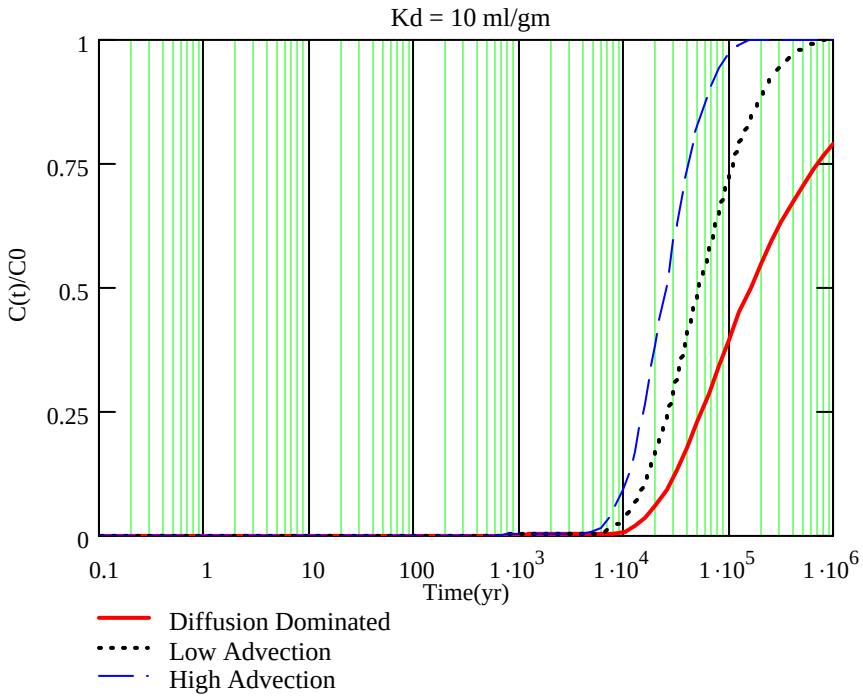

Figure 6-12. Breakthrough Curves for the Case of Low Partition Coefficient (K_d = 10.0 ml/gm)

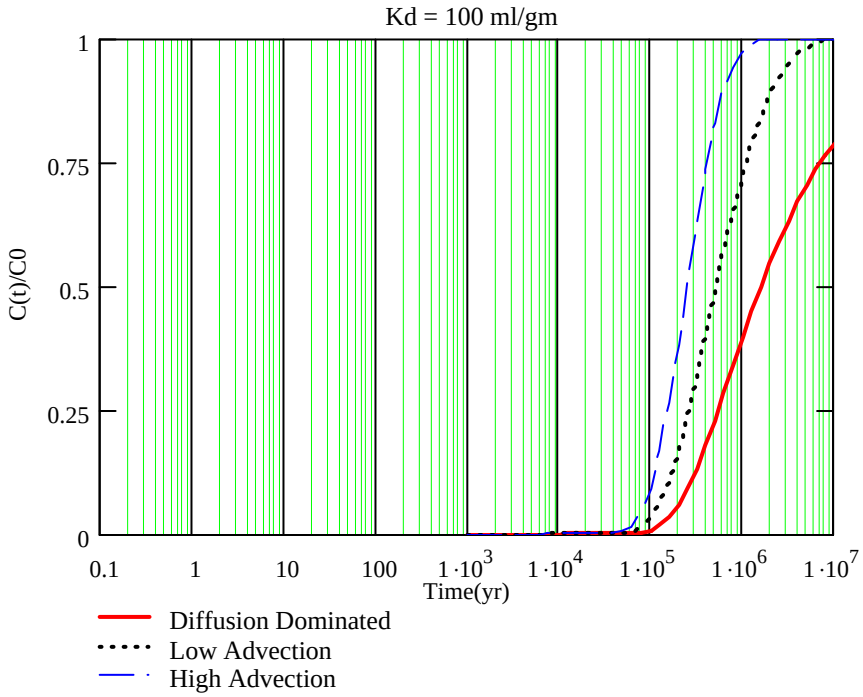

Figure 6-13. Breakthrough Curves for the Case of High Partition Coefficient (K_d = 100 ml/gm)

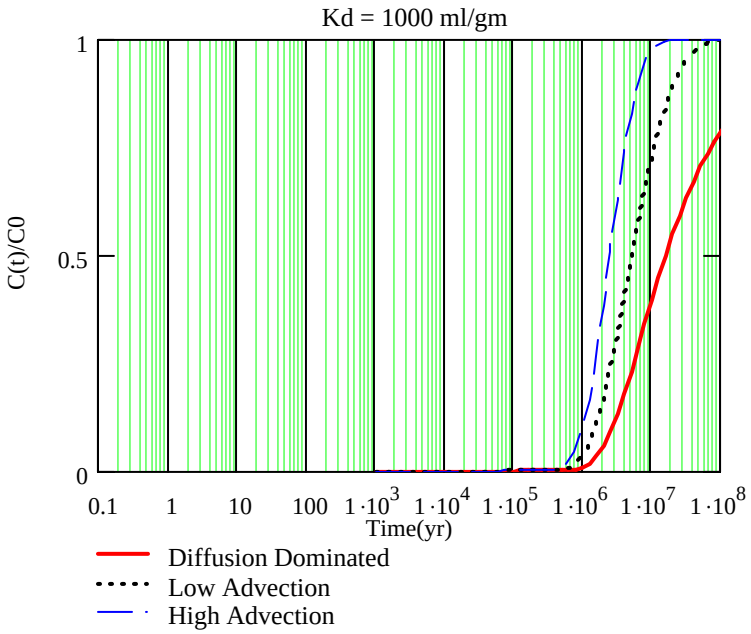

Figure 6-14. Breakthrough Curves for the Case of High Partition Coefficient (K_d = 1000 ml/gm)

6.10 TOTAL SYSTEM PERFORMANCE ASSESSMENT LICENSE APPLICATION ABSTRACTION FOR THE DRIPPING CASE

The following analysis presents a method for assessment of the breakthrough for radionuclides in the invert for the dripping case and the nondripping case. As discussed in Section 6.9.3, and as summarized in Tables 6-9 and 6-10, the results of the analysis show that if the grain sizes were equal or greater than 3 mm that the intergranular porosity is free of water, while the intragranular porosity is near saturation. If consideration is given to the moisture potential for the cases in which the grain sizes are 3 mm or greater, then an estimate of the vertical porewater velocity is obtained from the relationship presented by Jury et al. (1991, p. 127):

$$J_w = -K(\theta) \qquad \text{(Eq. 6-31)}$$

Considering the retention relationship presented by Fetter (1993, p. 172), this relationship can be restated as:

$$J_w = -K(\psi) \qquad \text{(Eq. 6-32)}$$

As stated by Jury et al. (1991), for prolonged downward flow, the invert water content adjusts to that value necessary to drain the invert under gravity at the imposed rate. This provides a means of estimating the fluxes in the coarse and fine pore space, and on the basis of saturation, the moisture content, and diffusion rates from the basic constitutive relations:

- For the case of zero seepage within the drift, the results of the two-dimensional NUFT calculations in which saturations are determined in the coarse and fine pore space are used. The NUFT calculations provide the advective fluxes directly, and the pore

velocities can be determined from the advective fluxes and the volumetric moisture content.

- The estimate of the diffusion coefficient for the invert requires an assessment of the bulk volumetric moisture content. Attachment XIII presents several derived relationships for assessing the bulk volumetric moisture content. From Attachment XIII, the bulk volumetric moisture content is given by for the case of zero seepage into the drift:

$$\theta_{Bulk} := \frac{S_{matrix} \cdot \frac{\phi_{matrix}}{1-\phi_{matrix}}}{1+\phi_{intergrain} \cdot \left[\left(1+\frac{\phi_{matrix}}{1-\phi_{matrix}}\right) \cdot \frac{1}{1-\phi_{intergrain}}\right] + \frac{\phi_{matrix}}{1-\phi_{matrix}}} \qquad \text{(Eq. 6-33)}$$

- The diffusion relationship for the bulk saturation is given by (Section 6.2):

$$D_{sl}(\theta) = D_{wl} \cdot \theta_{bulk}^{1.863} \qquad \text{(Eq. 6-34)}$$

A solution is presented by Freeze and Cherry (1979, Equation 6-4) for non-retarded transport in one dimension with initial concentration (C_o) moving at a continuous rate where the vapor phase transport is negligible (Freeze and Cherry 1979, p. 391). This premise is supported by Assumptions 5.1, 5.2, 5.3, 5.4, 5.5, and 5.7 and is appropriate for use in this scientific analysis.

The effective dispersion-diffusion coefficient (D_e) equals the sum of the hydrodynamic dispersion (D_{lh}) and soil-liquid diffusion coefficients (D_{sl}) (Jury et al. 1991, p. 222) (Equation 6-12).

Further, the dispersion-diffusion coefficient (D) in m^2/sec, equals the effective dispersion-diffusion coefficient (D_e) divided by the volumetric moisture content (θ) (Jury et al. 1991, p. 223).

This hydrodynamic dispersion coefficient (D_{lh}) has frequently been observed to be proportional to the pore-water velocity V, also known as the average linear velocity, where λ is the dispersivity in cm and $V = J_w/\theta_{matrix}$ (Jury et al. 1991, p. 221) (Equation 6-13).

Note that for the dripping case, the unsaturated flow analysis takes into account any potential flow focusing to the emplacement drift that tends to increase saturation in the intergranular porosity. On the other hand the fine pore structure would result from wicking of water to the crushed tuff matrix. Further, the drip shield tends to divert flow around the waste package and would reduce the advective flux. For flow that occurs through the drip shield, and waste package, the flux to the invert for the dripping case can be approximated as:

$$J_w = \frac{Q_{WASTE\_PACKAGE}}{A_{WASTE\_PACKAGE\_PLAN}} \qquad \text{(Eq. 6-35)}$$

Attachment XIV presents the analysis over a range of waste package flow rates to illustrate calculations for the dripping case for the four different particle sizes. The attachment first inputs the unsaturated hydraulic conductivity relationships from Attachment IV. The following equation is solved through the use of an interpolation table:

$$J_w - K(\psi) = 0 \qquad \text{(Eq. 6-36)}$$

Or substituting in the unsaturated hydraulic conductivity as determined from the van Genuchten relationship (Fetter 1993, p. 182):

$$J_w - K_S \frac{\left[1-(|\alpha\psi|)^{(n-1)}\left[1+(|\alpha\psi|)^n\right]^{\left(-1+\frac{1}{n}\right)}\right]^2}{\left[\left[1+(|\alpha\psi|)^n\right]^{\left[\frac{1}{2}-\frac{1}{(2n)}\right]}\right]} = 0 \qquad \text{(Eq. 6-37)}$$

The lookup tables use logarithmic interpolation to solve for the moisture potential in the coarse intergranular pore space. Solving for ψ:

$$\psi = K^{-1}(J_w) \qquad \text{(Eq. 6-38)}$$

The moisture potential can then be used to determine the volumetric moisture content in the coarse pore space assuming the fine pore space is saturated, and then used with the dispersivity/diffusion relationships presented above to calculate the diffusion, and the dispersion coefficients. The breakthrough analysis then proceeds as presented above.

As a practical matter, the retention relationships show that there is a "wet" range of moisture potential near saturation, and a very broad "dry" range of moisture potential in which the intergranular porosity is completely devoid of water. It is much less likely that the invert would retain moisture at intermediate saturations. If dripping occurs to saturate the coarse pore space of the invert, both advection and diffusion would be high, and breakthrough would occur rapidly. On the other hand, if the intergranular porosity remains unsaturated then breakthrough occurs slowly as suggested by the analysis presented in Attachment XIV.

6.11 DISCUSSION ON UNCERTAINTIES AND LIMITATIONS

The analyses presented in this report develop the hydrological and thermal properties for crushed tuff in the invert for a dual-porosity media comprised of an intergranular porosity between crushed tuff particles, and an intragranular porosity within crushed tuff. The following discussion presents the breakthrough performance measure, the evolution of the results with time, and the range of results. It discusses uncertainties as they apply to the intergranular and intragranular porosities for percolation rate, and the range of crushed tuff particle sizes as they affect the intergranular porosity. Further, the discussion considers diffusion, and retardation. The relative importance of these uncertainties is ranked in terms of their importance.

The fundamental performance measure in this analysis is the time for breakthrough, as presented in Section 6.9.5. The radionuclides are released at a constant rate as a step function beginning at time zero, and breakthrough depending on the mechanisms of advection, dispersion, and diffusion. The breakthrough time performance measure provides an indication as to when a concentration front of radionuclides released at a constant rate at the top of the invert would travel from the top of the invert to the bottom of the invert through the active pore space, and be released into the unsaturated zone. The breakthrough analysis also presents the evolution of radionuclide breakthrough with time since a high advection, dispersion, and diffusion results in a more rapid breakthrough of radionuclides while a low advection, dispersion, and diffusion results in a slow breakthrough of radionuclides. Note that concentration fronts that are time varying can be analyzed by convolution or superposition methods to assess a time varying concentration front.

The NUFT sensitivity analysis presented in Section 6.8 considered the effect of percolation on advection in the invert. Percolation fluxes for the upper bound glacial climate that represents most extreme case were discussed in Section 6.6. The range discussed in that section was selected to cover a broad range of percolation rates and as discussed previously, the unsaturated flow the matrix was found to be insensitive to the percolation rate. The NUFT results show that the intragranular pore space within crushed tuff particles in the invert is near saturation with advection is bounded by the matrix saturated hydraulic conductivity (10^{-8} cm/sec) (see Figure 6-5), and independent of the percolation rate.

Uncertainties as they apply to the coarse intergranular porosity can be divided into uncertainty of the constitutive relations to be applied, and parameter uncertainty. Note that while the van Genuchten retention constitutive relationship was adopted for analysis, other constitutive relationships such as the Brook-Corey retention relationship would yield very similar results. Further, the analysis using the empirical relationships in Section 6.4 developed by Campbell corroborates the calculations using the non-dimensionalized van Genuchten retention relation. Both sets reflect the fact that for coarse pore sizes (greater than 3 mm), it is expected that water at the given moisture potential at the repository horizon would not be retained in the coarse interstices. The analysis shows that this would be true for even coarser pore spaces than those considered in this report.

The analyses were carried out with different uniform particle-size diameters ranging from 0.3 mm to 20 mm. These correspond to a broad range of particle sizes (Winterkorn and Fang 1975, p. 287, Figure 7.42) for sand and gravel. The results show that for larger particle sizes, water would not be retained in the coarse pore space while the intragranular pore space is near saturation. The dual-porosity invert material would restrict flow from the surrounding formation to the invert due to the combined capillarity of both the intragranular and the intergranular porosities of the crushed tuff. The flux rates through the intragranular porosity of the crushed tuff would be bounded by the matrix saturated hydraulic conductivity (10^{-8} cm/sec) and would be independent of crushed tuff particle size diameters.

The results of the analysis presented in this report have used the active fracture model for the welded tuff repository host horizon that are representative of the rock media surrounding the crushed tuff invert. The invert was analyzed with intragranular matrix retention and intrinsic matrix permeability equal to the properties of the host horizon, and with intergranular properties

selected on the basis of the data by Brooks and Corey (1964) that is named the nondimensionalized van Genuchten properties in this report. The Campbell properties were used as an alternate model, and the NUFT results (Section 6.8) showed very similar behavior to the nondimensionalized van Genuchten properties in which the crushed tuff intragranular matrix showed high saturation, and the intergranular porosity was free of water.

The results of this analysis are also consistent with the results presented in Figure 6.3.4 of *Drift-Scale Radionuclide Transport* (BSC 2003f) that shows similar behavior in the matrix host rock for similar hydrologic properties sets. In one analysis reported in Figure 6.3.4 (BSC 2003f), the far field flux rate was selected as 10 mm per year which is lower than the far field flux of 35 mm per year used in the NUFT analysis. The percolation rate of 10 mm per year according to Figure 6.3.4 (BSC 2003f) would result in a lower saturation than the higher saturation presented in this analysis. Figure 6.3.4 (BSC 2003f) shows that the saturation is approximately 0.87. Substituting into the van Genuchten relation for unsaturated hydraulic conductivity (Jury et al. 1991, p. 109):

$$K(S) = K_s \cdot \left[S^{\frac{1}{2}} \left[1 - (1 - S^{\frac{1}{M}})^M \right] \right]^2 \qquad \text{(Eq. 6-39)}$$

where

$$S = \frac{\theta - \theta_r}{\theta_s - \theta_r} \qquad \text{(Eq. 6-40)}$$

Now substituting in the relationship of hydraulic conductivity to intrinsic permeability that converts a saturated intrinsic permeability (k) to a saturated hydraulic conductivity (K_s) (Freeze and Cherry 1979, p. 27):

$$K_s = \frac{\rho \cdot g}{\mu} \cdot k \qquad \text{(Eq. 6-41)}$$

$$K(S) = \frac{\rho \cdot g}{\mu} \cdot k \cdot \left[S^{\frac{1}{2}} \left[1 - (1 - S^{\frac{1}{M}})^M \right] \right]^2 \qquad \text{(Eq. 6-42a)}$$

The calculated value for the saturated hydraulic conductivity is approximately 10^{-8} cm per second (2 mm per year). Substituting in the following properties from Table 4-4:

$\theta_r = 0.0157$
$\theta_s = 0.112$
m = 0.236

Solving for the volumetric moisture content:

$$\theta = \left[S + \frac{1}{(\theta_s - \theta_r)} \cdot \theta_r \right] \cdot (\theta_s - \theta_r)$$

$$\theta = 0.099$$

Solving for the hydraulic conductivity:

$$K(S) = K_s \cdot \left[S^{\frac{1}{2}} \left[1 - (1 - S^{\frac{1}{M}})^M \right] \right]^2 = 0.055 \cdot \frac{mm}{yr} \qquad \text{(Eq. 6-42b)}$$

The calculated value for matrix percolation flux is approximately 0.1 mm per year that is in approximate agreement with the matrix percolation flux of 0.15 mm per year reported in Figure 6.3-4 of *Drift-Scale Radionuclide Transport* (BSC 2003f). It should be noted that small variations in matrix saturation can result in large variations in flux since the unsaturated matrix hydraulic conductivity is a strong nonlinear function of volumetric moisture content or saturation.

The results reported in Figure 6.3-4 of *Drift-Scale Radionuclide Transport* (BSC 2003f) indicate that the open drift behaves like an impermeable inclusion with flow being diverted around the inclusion. The analysis results (Section 6.7 and Attachment IX) show a similar behavior in flow being diverted around the open drift.

The crushed tuff matrix flow results can be interpreted with the aid of a closed form analytical solution for flow around an inclusion (CRWMS M&O 2001b, Attachment XII). The report developed a closed form solution for flow. Figure 6-15 shows the results of a comparison of the fluxes in the invert to the closed form solution for far field matrix flow around an inclusion. This far field flow is approximately 1.3 mm per year consistent with NUFT analysis. The figure shows that the Darcy fluxes in the invert at a percolation rate of 35 mm per year are near saturation, and are responding to the impermeable inclusion as represented by the emplacement drift.

This discussion shows that with the upper percolation fluxes of 35 mm per year to 70 mm per year used in this analysis that flow within the invert would be of the order of several mm per year. If the lower percolation flux of 10 mm per year resulting in a matrix flux of 0.15 mm per year is considered as in *Drift-Scale Radionuclide Transport* (BSC 2003f), the fluxes in the invert would be of the order of tenths of a mm per year, and the system would be more diffusion dominated. This shows that the principal uncertainties affecting whether advection versus diffusion in the invert occurs or not includes the percolation flux, the intrinsic permeability of the matrix at the host horizon, and the retention characteristics of the crushed tuff matrix.

The results of the NUFT analysis presented in this report show that for a percolation flux of 35 mm per year that flow dominantly occurs in the fractures in the surrounding rock with the coarse intergranular porosity acting as a capillary barrier to flow at the drift invert boundary.

Fracture flow is affected by gravity to a more significant degree than for matrix flow. For fracture flow within the rock, a dry shadow forms below the invert with a lower degree of fracture flow. To the side of the drift fracture flow is dominated by gravity, and there is a tendency for "drip lobes" to occur as was the case in *Drift-Scale Radionuclide Transport* (BSC 2003f). Further, the flow through the fractures that comprises a large percentage of the percolation flux would be diverted around the crushed tuff invert as the coarse pore space forms a capillary barrier to flow within the intergranular pore space of the invert. The results also show that matrix flow enters the micopores or intragranular porosity of the crushed tuff from the sides. This flow exits the drifts along the base of the drift into the rock matrix.

However, it should be noted that a significant source of uncertainty in these calculations is the interface zone between the crushed tuff and the surrounding host formation. The actual boundary that would exist between the two media might provide resistance to flow, and reduce the potential advection occurring through the invert such that the invert is actually a part of the rigid inclusion as is modeled in *Drift-Scale Radionuclide Transport* (BSC 2003f). This would result in a diffusion-dominated process in the invert. At present, there exist a number of unquantified uncertainties affecting the interface zone of the invert. Among these include the degree of consolidation of the crushed tuff, stresses acting across the grain to rock contacts from a transfer of loads from the waste package support system; interface retention of zones that are subject to local crushing, and stress corrosion cracking of the crushed tuff particles under stress. Near saturation, the crushed tuff to rock interface might represent a preferential pathway for flow while at elevated temperature during drying, it might represent a capillary barrier to flow. This analysis has conservatively assumed the interface offers no resistance to flow in the absence of definitive data to the contrary.

Since advection through the invert is relatively independent of percolation rate, and crushed tuff particle size for larger crushed tuff particle sizes, the moisture potential in the invert is relatively constant. The analyses use the hydrologic properties of welded tuff rock for the intergranular porosity. *Calibrated Properties Model* (BSC 2003c, Section 6.4.2) presents a discussion on the quantification of parameter uncertainty that applies to the intragranular porosity and permeability for crushed tuff in this report. The uncertainties in advection then reflect uncertainties in the matrix retention properties of the crushed tuff that would account for variations in pore size, and the distribution of pore sizes within the intragranular porosity.

The depth of the invert represents the path length as discussed in Attachment XV. Note that as discussed in Attachment XV, the path length of 0.5 was selected to account for possible variations in the location of contaminants entering the invert from the waste package, and to account for settlement with time.

Hydrodynamic dispersion would reflect uncertainties in advection (Section 6.8) and uncertainty in the dispersivity (Equation 6-13). The hydrodynamic dispersion affects the degree of spreading of the concentration breakthrough curve. The analysis showed that advection dispersion was dominant over diffusion in the intragranular pore space in the invert since the concentration breakthrough times occurred more rapidly (100 years to 1,000 years) while the breakthrough for diffusion was from 1,000 to 100,000 years (see Section 6.9.5).

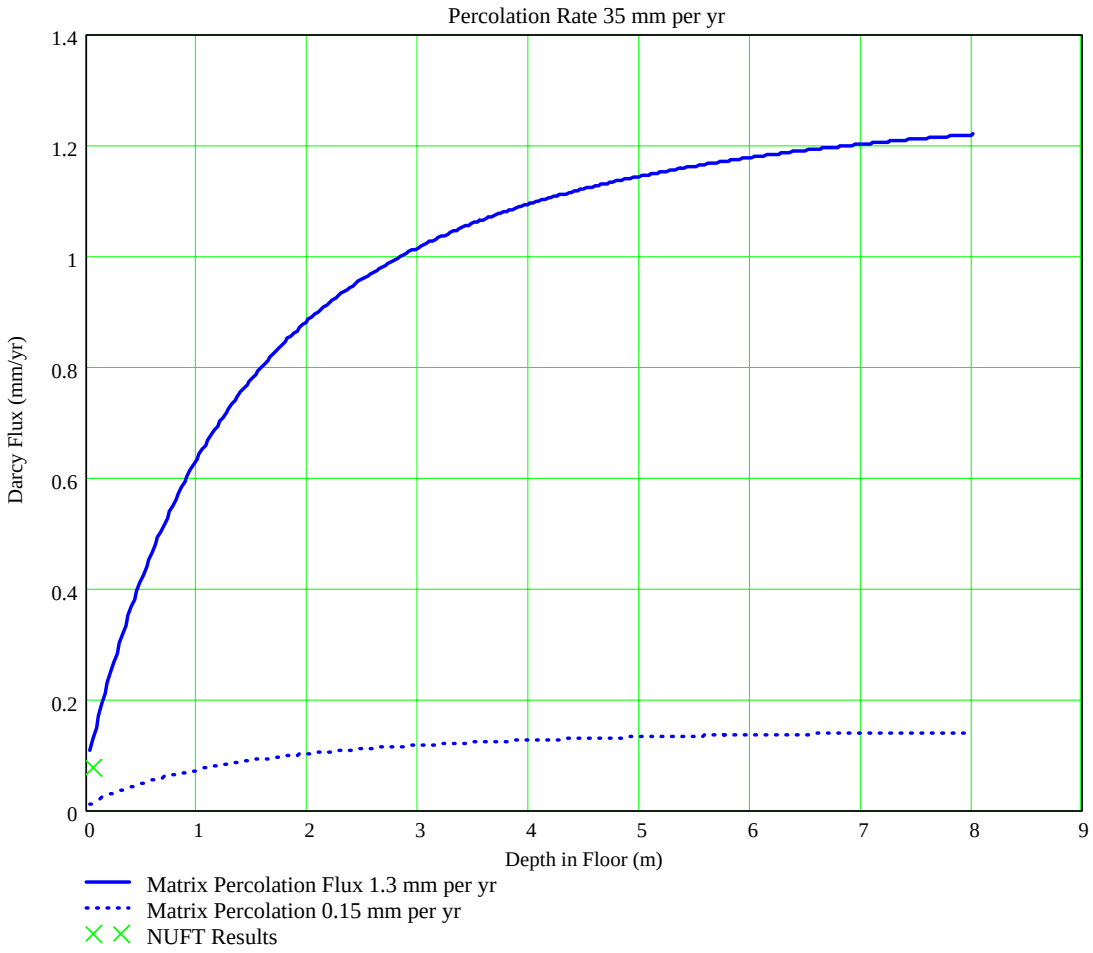

Figure 6-15. Comparison of a Closed Form Solution for Matrix Flow at Saturation with the Results of the NUFT Analysis

Since diffusion depends on the moisture content (Equation 6-16) in both the intragranular and intergranular porosity which has been found to be relatively insensitive to the effects of percolation rate, and crushed tuff pore size, diffusion is relatively constant with diffusion coefficients of the order of 10^{-7} cm^2/sec (see Attachment XII, Figure XII-1). As discussed in *EBS Radionuclide Transport Abstraction* (BSC 2003b, Section 6.3.4.1.1), the uncertainty approximates a normal distribution for the residuals in the log-log space. The log- normal distribution is truncated to plus or minus three standard deviations. The log-normal distribution has a mean value of 0.033, and a standard deviation of 0.218. A comparison of the results in Figure XII-1 over a broad range of percolation rates suggests that the principal source for uncertainty for diffusion is with the statistical curve fit, as presented in *EBS Radionuclide Transport Abstraction* (BSC 2003b, Section 6.3.4.1.1).

The analysis in this report presents a sensitivity analysis of the effects of retardation (Section 6.9.6). The retardation calculations considered a broad range of partition coefficients (Table 6-12). The results show that breakthrough is strongly dependent on retardation, and that concentration breakthrough could be retarded for very long periods of time.

The analysis presented in this model was performed for long periods of time and analyzes radionuclide migration after waste package failure due to corrosion. The results of the analysis presented in this report are weakly coupled to temperature after extended periods of time.

Juvenile failures have not been considered in the analysis. Such failures might occur at earlier periods of time when temperatures are more elevated, and potential dryout zone exists. Under these circumstances the potential flux through the invert are strongly coupled to elevated temperature. For temperatures above boiling, it would be expected that a dryout zone in the invert would form, and moisture potentials would be lower. This would mean that advection within the invert would be smaller. Also, diffusion would be smaller because of the lower moisture content.

In summary, the uncertainties in terms of the their rank importance on breakthrough time through the invert are:

- Uncertainties in retardation for individual radionuclides is the most significant source of uncertainty in these calculations. High partition coefficients (K_ds) have the potential of delaying the release of radionuclides for very long periods of time.

- Uncertainties in the matrix retention properties and saturated hydraulic conductivity is also a significant source of uncertainty. Variations in the unsaturated hydraulic conductivity as it is affected by retention in the fine intragranular pore space, and the saturated hydraulic conductivity has a significant effect on breakthrough times.

- Since the analysis shows that advection/dispersion dominates over diffusion in the invert in the intragranular porosity, a source of uncertainty of intermediate importance is the uncertainty in hydrodynamic dispersion.

- Since advection/dispersion is dominant over diffusion, uncertainties in diffusion, and the temperature dependence of diffusion is of low importance.

- Advection/dispersion occurs through the fine intergranular pore space and, therefore, the effects of particle size are of low importance provided that the particle sizes are coarse enough the intergranular porosity remains dry over the range of moisture potentials.

The properties and their uncertainties are adequately analyzed in this report because the van Genuchten flow properties are well documented. The retention relationship for the coarse pore space as determined from analysis of the data by Brooks and Corey (1964) corroborated by the Campbell relationship. Further, the results from the NUFT analysis is corroborated by the UFA flow measurements presented in Attachment XI. The analysis shows that advection/dispersion within the invert is the dominant transport mechanism with diffusion being of secondary importance. The analysis results show that the diffusion coefficient is relatively constant.

The finest pore space considered in the analysis was 0.3 mm. During the preclosure and postclosure periods, it is anticipated that fugitive dust from suspended particulates would settle at the top surface of the invert, and potentially migrate into the invert. It is unknown at the current time as to how much dust would settle, and migrate into the invert. While the formation of dust

would be expected to locally increase the retention of water within the coarse pore space, it is not expected to alter the retention characteristics of the intragranular porosity, and the predominance of flow within the fine pore space of the crushed tuff particles.

6.12 DISCUSSION OF YMRP ACCEPTANCE CRITERIA

The acceptance criteria from *Yucca Mountain Review Plan, Final Report* (NRC 2003) for the advection versus diffusion through the invert are summarized in Section 4.2. These criteria apply to system description and multiple barriers (Section 4.2.1); scenario analysis and event probability (Section 4.2.2); degradation of engineered barriers (Section 4.2.3); and quantity and chemistry of water contacting waste packages and waste forms (Section 4.2.4). Table 6-13 presents which criteria are addressed by this report; and which sections of the report present the detailed discussions addressing these criteria. A summary of how this report addresses the criteria is as follows:

6.12.1 System Description and Demonstration of Multiple Barriers

- The report describes the geometry, the relevant hydrologic material properties, and the advection-dispersion-diffusion transport phenomena in detail adequate for barrier identification (Sections 6.1 through 6.4, Section 6.7, and Attachment XV).

- The selection of engineered materials for the invert is made to make the performance of the barrier acceptable (Section 6.8).

- The technical basis for the relevant hydrologic properties is adequate and corroborated. The NUFT analysis presented is corroborated by experiments on samples of crushed tuff (Section 6.8.3).

6.12.2 Scenario Analysis and Event Probability

- Section 6.1 describes the physical processes of advection, dispersion, and diffusion for radionuclide transport through the invert. The descriptions of the transport phenomena are adequate.

6.12.3 Degradation of Engineered Barriers

- Model integration is adequate.

    - Section 6.4 provides the van Genuchten properties and the intrinsic permeability for intergranular porosity for the invert that are used in the Multiscale Thermohydrologic Model. When these properties for the dual-permeability media are input to NUFT for the nondripping case, along with the properties for other components within the EBS, and other initial and boundary conditions required for the thermal hydrological model, the analysis will produce the flows within both intergranular and intragranular porosities.

    - Section 6.10 provides the information for evaluating breakthrough for the dripping case. In this case, flux rates can be calculated using the method outlined

in Section 6.10 for the coarse intergranular porosity under the assumption that the intragranular porosity is saturated. Flows can be calculated for both components.

- Data are sufficient for the models supported. The models for the retention properties are well established, and accepted for use in vadose zone hydrology. The Campbell relationships provide corroboration of the nondimensionalized van Genuchten relationship. The NUFT analysis predicts that the coarse intergranular porosity is free of water over the range of expected moisture potentials in the repository.

- Data uncertainty is characterized and propagated through the model abstraction as described in Section 6.11. The report is a supporting analysis to *EBS Radionuclide Transport Abstraction* (BSC 2003b) and *Multiscale Thermohydrologic Model* (BSC 2001a).

- Analysis output is supported by objective comparisons. The measured retention on crushed tuff as reported in Attachment XI corroborates the NUFT analysis.

6.12.4 Quantity and Chemistry of Water Contacting Waste Packages and Waste Forms

- System description and model integration are adequate. Section 6.4 provides the van Genuchten properties for the invert used in the Multiscale Thermohydrologic Model. The quantity of water is calculated in that model. Section 6.10 presents a method for calculating water fluxes through the invert for the dripping case.

- The data for the calculation of the quantity of water are sufficient. The report is a supporting analysis to *EBS Radionuclide Transport Abstraction* (BSC 2003b) and *Multiscale Thermohydrologic Model* (BSC 2001a), where the quantities of water are calculated in detail.

- Data uncertainty is characterized and propagated through the model abstraction in Section 6.11. The report is a supporting analysis to *EBS Radionuclide Transport Abstraction* (BSC 2003b) and *Multiscale Thermohydrologic Model* (BSC 2001a).

Note that since this report is a supporting report to other models, Table 6-13 directs the reader to those model reports where the model criteria are addressed in detail. Further, the reader is directed to *Engineered Barrier System Features, Events, and Processes* (CRWMS M&O 2001a), which addresses scenario analysis and event probability in more detail.

Table 6-13. Report Sections that Address the YMRP Acceptance Criteria

Major Categories	YMRP Criteria No.	Criteria	Section Addressing Criteria	Remarks
1	System Description and Demonstration of Multiple Barriers (NRC 2003, Section 4.2.1.1.3; Canori and Leitner 2003, PRD-002/T-014, PRD-002/T-016):			
Specific requirements involve identification of multiple barriers (natural and engineered), describing the capabilities of these barriers to isolate waste, and providing technical bases for capabilities descriptions consistent with the post-closure performance objectives. To comply with these requirements, the following acceptance criteria are identified in *Technical Work Plan for: Engineered Barrier System Department Modeling and Testing FY03 Activities* (BSC 2003a).				
	AC1:	Identification of Barriers is Adequate.	1.0, 6.1,6.2,6.3,6.4,6.8	The report is a supporting analysis to *EBS Radionuclide Transport Abstraction* (BSC 2003b) and *Multiscale Thermohydrologic Model* (BSC 2001a).
	AC2:	Description of the Capability of Identified Barriers is Acceptable.	6.1, 6.9	The breakthrough analysis as presented in Section 6.9 describes the invert barrier's capability.
	AC3:	Technical Basis for Barrier Capability is Adequately Presented.	6	The technical basis for the hydrological properties for a dual-porosity material in the invert comprised of crushed tuff is presented in the supporting analysis.
2	Scenario Analysis and Event Probability (NRC 2003, Section 4.2.1.2.1.3; Canori and Leitner 2003, PRD-002/T-015):			
Specific requirements include providing technical bases for inclusion or exclusion of specific FEPs. In order to meet these requirements, the following acceptance criteria are identified in *Technical Work Plan for: Engineered Barrier System Department Modeling and Testing FY03 Activities* (BSC 2003a).				
	AC1:	The Identification of the Initial List of Features, Events, and Processes is Adequate.	6.1	Section 6.1 describes the processes of advection, dispersion, and diffusion for radionuclide transport through the invert.
	AC2:	Screening of the Initial List of FEPs is Appropriate.	NA	The screening of FEPs for EBS is presented in *Engineered Barrier System Features, Events, and Processes* (CRWMS M&O 2001a).
	AC3:	Formation of Scenario Classes Using the Reduced Set of Events is Adequate.	NA	The formation of FEPs for EBS is presented in *Engineered Barrier System Features, Events, and Processes* (CRWMS M&O 2001a).
	AC4:	Screening of Scenario Classes is Appropriate.	NA	The screening of scenario classes for EBS is presented in *Engineered Barrier System Features, Events, and Processes* (CRWMS M&O 2001a).

Table 6-13. Report Sections that Address the YMRP Acceptance Criteria (Continued)

Major Categories	YMRP Criteria No.	Criteria	Section Addressing Criteria	Remarks
3	Degradation of Engineered Barriers (NRC 2003, Section 4.2.1.3.1.3; Canori and Leitner 2003, PRD-002/T-015):			
Specific requirements include describing deterioration or degradation of engineered barriers and modeling degradation processes using data for performance assessment, including total system performance assessment (TSPA). Consideration of uncertainties and variabilities in model parameters and alternative conceptual models are also required. To fulfill these requirements, the following acceptance criteria are identified in *Technical Work Plan for: Engineered Barrier System Department Modeling and Testing FY03 Activities* (BSC 2003a).				
	AC1:	System Description and Model Integration are Adequate.	1.0,6.4,6.10	Section 6.4 provides the van Genuchten properties for the invert used in the Multiscale Thermohydrologic Model. Section 6.10 provides the information for evaluating breakthrough for the dripping case.
	AC2:	Data are Sufficient for Model Justification.	6.2-6.5, 6.8 and Attachment XI	The Campbell relationship provide corroboration of the nondimensionalized van Genuchten relationship. The NUFT analysis predict that the coarse intergranular porosity is free of water over the range of expected moisture potentials in the repository. The measured retention on crushed tuff as reported in Attachment XI corroborates the NUFT analysis.
	AC3:	Data Uncertainty is Characterized and Propagated Through the Model Abstraction.	6.11	The report is a supporting analysis to *EBS Radionuclide Transport Abstraction* (BSC 2003b).
	AC4:	Model Uncertainty is Characterized and Propagated Through the Model Abstraction.	6.11	The report is a supporting analysis to *EBS Radionuclide Transport Abstraction* (BSC 2003b).
	AC5:	Model Abstraction Output is Supported by Objective Comparisons.	NA	The report is a supporting analysis to *EBS Radionuclide Transport Abstraction* (BSC 2003b).

Table 6-13. Report Sections that Address the YMRP Acceptance Criteria (Continued)

Major Categories	YMRP Criteria No.	Criteria	Section Addressing Criteria	Remarks
4	Quantity and Chemistry of Water Contacting Waste Packages and Waste Forms (NRC 2003, Section 4.2.1.3.3.3; Canori and Leitner 2003, PRD-002/T-015):			
Specific requirements include quantifying the amount and chemistry of water contacting the waste package and the waste forms. To comply with these requirements, the following acceptance criteria are identified in *Technical Work Plan for: Engineered Barrier System Department Modeling and Testing FY03 Activities* (BSC 2003a).				
	AC1:	System Description and Model Integration are Adequate.	1.0,6.4,6.10	Section 6.4 provides the van Genuchten properties for the invert used in the Multiscale Thermohydrologic Model. Section 6.10 provides the information for evaluating breakthrough for the dripping case.
	AC2:	Data are Sufficient for Model Justification.	6.4,6.5,6.10	The report is a supporting analysis to *EBS Radionuclide Transport Abstraction* (BSC 2003b) and *Multiscale Thermohydrologic Model* (BSC 2001a).
	AC3:	Data Uncertainty is Characterized and Propagated Through the Model Abstraction.	6.11	Section 6.11 describes data uncertainties, and their propagation through the model abstraction.
	AC4:	Model Uncertainty is Characterized and Propagated Through the Model Abstraction.	NA	The report is a supporting analysis to *EBS Radionuclide Transport Abstraction* (BSC 2003b) and *Multiscale Thermohydrologic Model* (BSC 2001a).
	AC5:	Model Abstraction Output is Supported by Objective Comparisons.	NA	The report is a supporting analysis to *EBS Radionuclide Transport Abstraction* (BSC 2003b) and *Multiscale Thermohydrologic Model* (BSC 2001a).

7. CONCLUSIONS

Technical Work Plan for: Engineered Barrier System Department Modeling and Testing FY03 Work Activities (BSC 2003a) provides the basis for conducting an Advection versus Diffusion Analysis to support the development of several reports for *EBS Flow and Transport Model Development, Analyses and Testing.* These include *Multiscale Thermohydrologic Model* report and the *EBS Radionuclide Abstraction Analysis* report.

The *Advection versus Diffusion Analysis* presented in this analysis report is a supporting analysis to the *Multiscale Thermohydrologic Analysis* for the selection of hydrological properties for a dual-porosity material in the invert. The dual-porosity media for the invert required the development of retention and unsaturated hydraulic conductivity properties for the invert (Section 6.3). The dual-porosity media is comprised of the intragranular porosity of the crushed tuff that has retention properties equivalent to the tuff matrix that is characteristic of the site, and an intergranular porosity in which retention properties were developed.

Section 6.4 developed the retention and unsaturated flow properties for a dual-porosity media using the Non-Dimensionalized van Genuchten Retention Relation. The nondimensionalized van Genuchten Moisture Potential Retention relation was developed from the retention data for volcanic sand, fine sand, and glass beads. The basis for the nondimensional retention relationship for the first retention relation is a least squares curve fit for a series of retention measurements made on these materials that gives equal weighting to the several materials. The van Genuchten air-entry parameter "α" was determined from a scaling relationship while the "n" parameter is held constant. The saturated hydraulic conductivity (K_s) is determined from the Kozeny-Karmen formula (Bear 1972, p. 166) that relates saturated hydraulic conductivity (K_s) to grain size or pore diameter (d_m) and porosity (ϕ). The properties developed for the *Multiscale Thermohydrologic Analysis* include (Table 6-2):

- Intergranular permeability of the crushed tuff
- Intergranular saturated moisture content
- Intergranular porosity
- van Genuchten properties
- Residual moisture content
- Maximum saturation
- Residual saturation.

The Campbell retention relations provide an alternate method for the assessment of the hydrological properties for the intergranular porosity. This retention relation was developed from empirical relations presented by Campbell (1985, p. 43) based on the assumption that particle sizes in soils follow a log-normal distribution (Assumption 5.9). The analysis using the Campbell relation corroborates the nondimensionalized van Genuchten Moisture Potential relation. Tables 6-5 and 6-6 provide a summary of the Campbell hydrological properties.

In performing analysis of potential flow through the invert, the *Multiscale Thermohydrologic Model* would provide similar results using properties from the nondimensionalized van Genuchten relation based upon the data by Brooks and Corey (1964) as presented in Section 6.4

and the Campbell relation (Campbell 1985, p. 43) as presented in Section 6.5. The nondimensionalized van Genuchten relation based upon data by Brooks and Corey (1964) is selected for analysis for the reason that the hydrologic properties can be derived from fundamental data. Output DTNs (see Table 7-1) are included for the hydrological properties.

This analysis report also supports *EBS Radionuclide Transport Abstraction* (BSC 2003b) in determining whether advection or diffusion in each media is the dominant transport mechanism. NUFT analyses were performed to compare the contaminant breakthrough in the invert for advection versus dispersion-diffusion to assess the significance of advection to EBS radionuclide transport. NUFT simulations for flow through the invert used dual-porosity hydrological properties (Section 6.4) to estimate saturations and advection in the invert (Sections 6.6 through 6.8). A NUFT analysis at ambient temperature using a refined mesh in the invert (Sections 6.4 and 6.5) determined advection within the invert under the case of no seepage in the drift.

The NUFT results utilized a refined mesh and showed that the saturation of the grain matrix equals the matrix saturation. This response is reasonable because of the high capillarity that draws water from the fractures of the host rock into grains (Section 6.7). The NUFT results show that the vertical pore-water velocity in the matrix component is low and is controlled by the saturated hydraulic conductivity (K_s), the pressure gradient in the matrix, and the pressure gradient across the intergranular and intragranular components.

NUFT analyses were also performed using the Campbell hydrological properties. The Campbell retention relation predicted that for a grain size of 0.317 mm in diameter, the intergranular component behaves similarly to the intragranular matrix component, and the moisture potential equilibrates across the two components. As the grain size increases to 3-mm diameter or larger, the intergranular component breaks away and behaves as a capillary barrier, as shown by a sharp difference in pressure potential across the two components. This pressure gradient steepens as the grain size increases from 3-mm to 20-mm diameter inducing a slightly higher flux in the matrix component. This matrix flux tends to stabilize between 10- and 20-mm grain size models. The van Genuchten retention relation predicts that for all grain sizes of the crushed tuff 0.317-mm diameter or larger, the intergranular component acts as a capillary barrier whereas the intragranular component behaves as a matrix medium, as expected in a DKM model.

The one-dimensional contaminant transport equation (Section 6.1, Equation 6-4) was used to evaluate contaminant transport over the range of pore-water velocities and saturations from the NUFT calculation (Section 6.9.5). The closed form analytical solution for the one-dimensional advection-dispersion equation (Equation 6-4) was used to perform a sensitivity analysis of breakthrough times for a range of conditions in the invert. The sensitivity analysis is subject to the assumptions that the direction of the advective flux is in the vertical direction (Assumption 5.1); the effects of lateral dispersion are neglected (Assumption 5.2); and the invert is homogeneous (Assumption 5.3). The radionuclides are assumed to be released at the centerline of the drift (Assumption 5.4), and that the effects of radioactive decay are neglected (Assumption 5.5). Solute vapor phase is assumed to be negligible (Assumption 5.7). The range of pore water velocities for the intergranular pore space was from 7.6×10^{-11} m/s to 1.8×10^{-10} m/s for the low- and high-advection cases, respectively (Table 6-9). For comparison, the breakthrough curve for diffusion is presented. The breakthrough analysis for the case of variable pore-water velocity would fall between these extremes for high and low advection. The results

of the analysis show that breakthrough times would occur within a time frame of 400 to 1,000 years, while a diffusion-dominated process such as would occur in the intergranular pore space would occur within a time frame of 1,000 to 10,000 years (Figure 6-9).

Additional sensitivity studies using the one-dimensional advection-diffusion-dispersion equation were used to estimate the effects of retardation. Sheppard and Thibault (1990, Tables A-1 through A-4) present data on the mean and standard deviation of the natural logarithm of the partition coefficient for individual elements for sands, loams, clays, and organic soils. To take into account a broad range of values, the partition coefficients the sensitivity study for retardation used a range of partition coefficients from 1 to 1,000 ml/gm (Table 6-12). The results of the calculations show that for the case of low sorption (K_d = 1.0 ml/gm), the retardation factor is low, and the breakthrough time is delayed to 1,000 to 5,000 years. For the case of intermediate and high sorption (10 - 100 ml/gm), the delay in breakthrough time is more substantial. In the case of the intermediate sorption, breakthrough would be delayed from 1,000 to 10,000 years. In the case of high sorption (1,000 ml/gm), breakthrough is delayed by at least one million years.

The NUFT analysis presented in Sections 6.7 and 6.8 apply to the nondripping case in which flow is diverted around the open drift. Section 6.10 presents a method of analysis discussed in detail in Attachment XIV for the dripping case for estimating the flux and diffusion coefficient through invert. Table 7-1 presents the recommendations for the properties for the dripping and nondripping cases. Note that the properties for the nondripping case are implemented in the *Multiscale Thermohydrologic Model* that calculates flux rates through the invert. For the dripping case for flow through the matrix, the results of *Multiscale Thermohydrologic Model* can be used. For that portion of the flow carried by the large pore space, the moisture potential can be estimated from the flux from an interpolation table presented in Attachment XIV based upon the van Genuchten unsaturated hydraulic conductivity relation. This moisture potential can used to find the moisture content of the large pore space that then can be used to calculate the diffusive release. Noting that the results are not sensitive to the grain-size distribution, it is recommended that a particle size of 3 mm be adopted for TSPA analysis since the results of the analysis.

As noted in Section 6.11, uncertainties exist in the constitutive relations applied, and the calculated parameters. While the van Genuchten retention constitutive relationship was adopted for analysis, other constitutive relationships such as the Brooks-Corey relationship would yield similar results. Both the van Genuchten retention constitutive relationship and the Campbell retention relationship show that for pore sizes greater than 3 mm, it is expected that water at the given moisture potential at the repository horizon would not be retained in the coarse pore space.

The results of this analysis are also consistent with the results presented in Figure 6.3.4 of *Drift-Scale Radionuclide Transport* (BSC 2003f) that shows similar behavior in the matrix host rock for similar hydrologic properties sets. The calculated value for matrix percolation flux is approximately 0.1 mm per year that is in approximate agreement with the matrix percolation flux of 0.15 mm per year reported in Figure 6.3-4 of *Drift-Scale Radionuclide Transport* (BSC 2003f). It should be noted that small variations in matrix saturation can result in large variations in flux since the unsaturated matrix hydraulic conductivity is a strong nonlinear function of volumetric moisture content or saturation.

The crushed tuff matrix flow results can be interpreted with the aid of a closed form analytical solution for flow around an inclusion (CRWMS M&O 2001b, Attachment XII).

The report developed a closed form solution for flow. Figure 6-15 shows the results of a comparison of the fluxes in the invert to the closed form solution for far field matrix flow around an inclusion. This far field flow is approximately 1.3 mm per year consistent with NUFT analysis. The figure shows that the Darcy fluxes in the invert at a percolation rate of 35 mm per year are near saturation, and are responding to the impermeable inclusion as represented by the emplacement drift. The closed form solution presented in Attachment XVI represents an alternate method for evaluating the advection in the invert.

A significant source of uncertainty is the interface zone flow between the crushed tuff and the surrounding host rock. As discussed in Section 6.11, the actual boundary may provide more resistance to flow than what has been analyzed. This analysis has conservatively assumed the interface offers no resistance to flow in the absence of definitive data to the contrary.

The finest pore space considered in the analysis is 0.3 mm. During the preclosure and postclosure period, it is anticipated that fugitive dust from suspended particulates would settle at the top surface of the invert, and potentially migrate into the invert. It would be expected that such fugitive dust would locally increase the retention of water within the coarse pore space. However, fugitive dust would not be expected to alter the retention characteristics of the intragranular porosity, and the predominance of flow within the fine pore space of the crushed tuff particles.

This analysis has three output DTNs as summarized in Table 7-2. The first two DTNs support the Multiscale Thermohydrologic Model in providing van Genuchten curve fit parameters, and the intrinsic permeability. The last DTN supports TSPA for the dripping case within the invert.

Table 7-1. Recommended Values for TSPA Based Upon a Grain Size of 3mm

Parameter	Recommended Value for TSPA	Units
Porosity of the Rock Matrix in an Individual Grain for Crushed Tuff (ϕ_{matrix}) for the Dripping and Nondripping Cases	0.131	(-)
Porosity of Large Pore Spaces Between Grains ($\phi_{intergraqin}$) for the Dripping and Nondripping Cases	0.45	(-)
Residual Volumetric Moisture Content (θ_r) of Large Pore Spaces for the Dripping Case	0.05	(-)
Saturated Volumetric Moisture Content (θ_s) of Large Pore Spaces for the Dripping Case	0.45	(-)
van Genuchten Air-Entry Parameter of Large Pore Spaces for the Dripping and Nondripping Cases	624	$(bars)^{-1}$
van Genuchten n Parameter of Large Pore Spaces for the Dripping and Nondripping Cases	8.013	(-)
Saturated Intrinsic Permeability of the Large Pore Spaces for the Dripping and Nondripping Cases	1.51E-08	(m^2)

Table 7-2. Output DTNs

Output Name	Output Description	DTN	Sources of Uncertainty	Characteristic Values
van Genuchten Hydrologic Parameters	Retention and Unsaturated Hydraulic Conductivity Data	MO0307SPAVGHYD.000	See Section 6.11	See Attachment IV
van Genuchten Summary Parameters	Summary van Genuchten Parameters	MO0307SPAVGSUM.000	See Section 6.11	Table 6-2
TSPA Flow and Transport Abstraction	Lookup Table, and Technical Approach for Assessing Advection and Diffusion for the Dripping Case	MO0307SPAFTPDC.000	See Section 6.11	Attachment XIV

8. INPUTS AND REFERENCES

8.1 DOCUMENTS CITED

Bear, J. 1972. *Dynamics of Fluids in Porous Media.* Environmental Science Series. Biswas, A.K., ed. New York, New York: Elsevier. TIC: 217356.

Beyer, W.H., ed. 1987. *CRC Standard Mathematical Tables*. 28th Edition. 3rd Printing 1988. Boca Raton, Florida: CRC Press. TIC: 240507.

Brooks, R.H. and Corey, A.T. 1964. *Hydraulic Properties of Porous Media*. Hydrology Paper No. 3. Fort Collins, Colorado: Colorado State University. TIC: 217453.

BSC (Bechtel SAIC Company) 2001a. *Multiscale Thermohydrologic Model*. ANL-EBS-MD-000049 REV 00 ICN 02. Las Vegas, Nevada: Bechtel SAIC Company. ACC: MOL.20020123.0279.

BSC 2001b. *In-Drift Thermal-Hydrological-Chemical Model*. ANL-EBS-MD-000026 REV 00 ICN 02. Las Vegas, Nevada: Bechtel SAIC Company. ACC: MOL.20010406.0012.

BSC 2001c. *Repository Design, Emplacement Drift Steel Invert Plan and Details*. DWG-EDS-ST-000001 REV A. Las Vegas, Nevada: Bechtel SAIC Company. ACC: MOL.20020102.0323.

BSC 2001d. *Repository Multiple Waste Package Thermal Calculation.* CAL-WIS-TH-000010 REV 00. Las Vegas, Nevada: Bechtel SAIC Company. ACC: MOL.20010814.0330.

BSC 2002. *Repository Design Project, Repository/PA IED Emplacement Drift Configuration*. 800-IED-EBS0-00200-000-00A. Las Vegas, Nevada: Bechtel SAIC Company. ACC: MOL.20021031.0104.

BSC 2003a. *Technical Work Plan for: Engineered Barrier System Department Modeling and Testing FY03 Activities*. TWP-MGR-MD-000015 REV 04 ICN 01. Las Vegas, Nevada: Bechtel SAIC Company. ACC: DOC.20030728.0003.

BSC 2003b. *EBS Radionuclide Transport Abstraction*. ANL-WIS-PA-000001 REV 01A. Las Vegas, Nevada: Bechtel SAIC Company. ACC: MOL.20030617.0222.

BSC 2003c. *Calibrated Properties Model*. MDL-NBS-HS-000003 REV 01. Las Vegas, Nevada: Bechtel SAIC Company. ACC: DOC.20030219.0001.

BSC 2003d. *Repository Design Project, Repository/PA IED Emplacement Drift Configuration 1 of 2*. 800-IED-EBS0-00201-000-00A. Las Vegas, Nevada: Bechtel SAIC Company. ACC: ENG.20030630.0002.

BSC 2003e. *UZ Flow Models and Submodels*. MDL-NBS-HS-000006 REV 01. Las Vegas, Nevada: Bechtel SAIC Company. ACC: DOC.20030818.0002.

BSC 2003f. *Drift-Scale Radionuclide Transport*. MDL-NBS-HS-000016 REV 00C. Las Vegas, Nevada: Bechtel SAIC Company. ACC: MOL.20030804.0205.

Campbell, G.S. 1985. *Soil Physics with BASIC Transport Models for Soil-Plant Systems*. Developments in Soil Science 14. Amsterdam, The Netherlands: Elsevier. TIC: 214477.

Canori, G.F. and Leitner, M.M. 2003. *Project Requirements Document*. TER-MGR-MD-000001 REV 01. Las Vegas, Nevada: Bechtel SAIC Company. ACC: DOC.20030404.0003.

Chapman, A.J. 1974. *Heat Transfer*. 3rd Edition. New York, New York: Macmillan Publishing. TIC: 245061.

Crane, R.A.; Vachon, R.I.; and Khader, M.S. 1977. "Thermal Conductivity of Granular Materials - A Review." *Proceedings of the Seventh Symposium on Thermophysical Properties, held at National Bureau of Standards, Gaithersburg, Maryland, May 10-12, 1977*. Cezairliyan, A., ed. Pages 109-123. New York, New York: American Society of Mechanical Engineers. TIC: 246057.

CRWMS M&O (Civilian Radioactive Waste Management System Management and Operating Contractor) 1996. *Engineered Barrier System Performance Requirements Systems Study Report*. BB0000000-01717-5705-00001 REV 01. Las Vegas, Nevada: CRWMS M&O. ACC: MOL.19970407.0169.

CRWMS M&O 2000a. *NUFT 3.0S Users Manual*. 10088-UM-3.0s-00, Rev. 00. Las Vegas, Nevada: CRWMS M&O. ACC: MOL.20000920.0092.

CRWMS M&O 2000b. *Invert Diffusion Properties Model*. ANL-EBS-MD-000031 REV 01. Las Vegas, Nevada: CRWMS M&O. ACC: MOL.20000912.0208.

CRWMS M&O 2000c. *Water Diversion Model*. ANL-EBS-MD-000028 REV 00. Las Vegas, Nevada: CRWMS M&O. ACC: MOL.20000107.0329.

CRWMS M&O 2000d. *Seepage Model for PA Including Drift Collapse*. MDL-NBS-HS-000002 REV 00. Las Vegas, Nevada: CRWMS M&O. ACC: MOL.19990721.0525.

CRWMS M&O 2001a. *Engineered Barrier System Features, Events, and Processes*. ANL-WIS-PA-000002 REV 01. Las Vegas, Nevada: CRWMS M&O. ACC: MOL.20010312.0024.

CRWMS M&O 2001b. *Water Distribution and Removal Model*. ANL-EBS-MD-000032 REV 01. Las Vegas, Nevada: CRWMS M&O. ACC: MOL.20010214.0031.

Cussler, E.L. 1997. *Diffusion: Mass Transfer in Fluid Systems*. 2nd Edition. Cambridge, United Kingdom: Cambridge University Press. TIC: 241150.

de Marsily, G. 1986. *Quantitative Hydrogeology: Groundwater Hydrology for Engineers*. San Diego, California: Academic Press. TIC: 208450.

DOE (U.S. Department of Energy) 2003. *Quality Assurance Requirements and Description*. DOE/RW-0333P, Rev. 13. Washington, D.C.: U.S. Department of Energy, Office of Civilian Radioactive Waste Management. ACC: DOC.20030422.0003.

Fetter, C.W. 1993. *Contaminant Hydrogeology*. Upper Saddle River, New Jersey: Prentice Hall. TIC: 240691.

Freeze, R.A. and Cherry, J.A. 1979. *Groundwater*. Englewood Cliffs, New Jersey: Prentice-Hall. TIC: 217571.

Hahn, G.J. and Shapiro, S.S. 1967. *Statistical Models in Engineering*. New York, New York: John Wiley & Sons. TIC: 247729.

Holman, J.P. 1997. *Heat Transfer*. 8th Edition. New York, New York: McGraw-Hill. TIC: 239954.

Incropera, F.P. and DeWitt, D.P. 1996. *Fundamentals of Heat and Mass Transfer*. 4th Edition. New York, New York: John Wiley & Sons. TIC: 243950.

Jury, W.A.; Gardner, W.R.; and Gardner, W.H. 1991. *Soil Physics*. 5th Edition. New York, New York: John Wiley & Sons. TIC: 241000.

Leverett, M.C. 1941. "Capillary Behavior in Porous Solids." *AIME Transactions, Petroleum Development and Technology, Tulsa Meeting, October 1940*. *142*, 152-169. New York, New York: American Institute of Mining and Metallurgical Engineers. TIC: 240680.

Mills, R. 1973. "Self-Diffusion in Normal and Heavy Water in the Range 1-45°." *Journal of Physical Chemistry, 77*, (5), 685-688. Washington, D.C.: American Chemical Society. TIC: 246404.

NRC (U.S. Nuclear Regulatory Commission) 2003. *Yucca Mountain Review Plan, Final Report*. NUREG-1804, Rev. 2. Washington, D.C.: U.S. Nuclear Regulatory Commission, Office of Nuclear Material Safety and Safeguards. TIC: 254568.

Saxena, N.S.; Chohan, M.A.; and Gustafsson, S.E. 1986. "Effective Thermal Conductivity of Loose Granular Materials." *Journal of Physics D: Applied Physics*, *19*, (9), 1625-1630. London, England: The Institute of Physics. TIC: 249120.

Sheppard, M.I. and Thibault, D.H. 1990. "Default Soil Solid/Liquid Partition Coefficients, Kds, for Four Major Soil Types: A Compendium." *Health Physics*, *59*, (4), 471-482. New York, New York: Pergamon Press. TIC: 249329.

van Genuchten, M.T. 1980. "A Closed-Form Equation for Predicting the Hydraulic Conductivity of Unsaturated Soils." *Soil Science Society of America Journal*, *44*, (5), 892-898. Madison, Wisconsin: Soil Science Society of America. TIC: 217327.

Weast, R.C. and Astle, M.J., eds. 1981. *CRC Handbook of Chemistry and Physics*. 62nd Edition. Boca Raton, Florida: CRC Press. TIC: 240722.

Willhite, G.P.; Kunii, D.; and Smith, J.M. 1962. "Heat Transfer in Beds of Fine Particles (Heat Transfer Perpendicular to Flow)." *American Institute of Chemical Engineers Journal*, *8*, (3), 340-345. New York, New York: American Institute of Chemical Engineers. TIC: 249121.

Winterkorn, H.F. and Fang H-Y., eds. 1975. *Foundation Engineering Handbook*. Pages 37, 72, 78, 79, 117, 156, 256, 257, 266, and 267. New York, New York: Van Nostrand Reinhold. TIC: 241820.

YMP (Yucca Mountain Site Characterization Project) 2001. *Q-List*. YMP/90-55Q, Rev. 7. Las Vegas, Nevada: Yucca Mountain Site Characterization Office. ACC: MOL.20010409.0366.

8.2 CODES, STANDARDS, REGULATIONS, AND PROCEDURES

AP-SI.1Q, Rev. 5, ICN 1. *Software Management*. Washington, D.C.: U.S. Department of Energy, Office of Civilian Radioactive Waste Management. ACC: DOC.20030708.0001.

AP-SIII.9Q, Rev. 1, ICN 0. *Scientific Analyses*. Washington, D.C.: U.S. Department of Energy, Office of Civilian Radioactive Waste Management. ACC: DOC.20030708.0002.

8.3 SOURCE DATA, LISTED BY DATA TRACKING NUMBER

GS000483351030.003. Thermal Properties Measured 12/01/99 to 12/02/99 Using the Thermolink Soil Multimeter and Thermal Properties Sensor on Selected Potential Candidate Backfill Materials Used in the Engineered Barrier System. Submittal date: 11/09/2000.

GS980808312242.015. Water Retention and Unsaturated Hydraulic Conductivity Measurements for Various Size Fractions of Crushed, Sieved, Welded Tuff Samples Measured Using a Centrifuge. Submittal date: 08/21/1998.

LB0207REVUZPRP.002. Matrix Properties for UZ Model Layers Developed from Field and Laboratory Data. Submittal date: 07/15/2002.

LB0302PTNTSW9I.001. PTN/TSW Interface Percolation Flux Maps for 9 Infiltration Scenarios. Submittal date: 02/28/2003.

LB990861233129.001. Drift Scale Calibrated 1-D Property Set, FY99. Submittal date: 08/06/1999.

LB990861233129.002. Drift Scale Calibrated 1-D Property Set, FY99. Submittal date: 08/06/1999.

8.4 OUTPUT DATA, LISTED BY DATA TRACKING NUMBER

MO0307SPAFTPDC.000. Total System Performance Assessment (TSPA) Flow and Transport Parameters for the Dripping Case. Submittal date: 07/25/2003.

MO0307SPAVGHYD.000. van Genuchten Hydrologic Parameters. Submittal date: 07/25/2003.

MO0307SPAVGSUM.000. van Genuchten Hydrologic Parameters. Submittal date: 07/26/2003.

8.5 SOFTWARE CODES

Software Code: NUFT. V3.0s. Sun, Sun O.S. 5.8. 10088-3.0s-01.

Software Routine: XTOOL V10.1. V10.1. Sun Ultra10. 10208-10.1-00.

9. LIST OF ATTACHMENTS

Attachment I	List of NUFT Input File Names
Attachment II	List of NUFT Output File Names
Attachment III	EBS Radionuclide Transport Analysis
Attachment IV	Analysis of Nondimensionalized van Genuchten Moisture Potential Retention Relation
Attachment V	Analysis of the Campbell Retention Relation
Attachment VI	Derivation of Invert “Packed Bed” Properties from the Brooks and Corey Data
Attachment VII	Verification of the Mathcad Calculations Using Microsoft Excel
Attachment VIII	Hydrologic Properties of Engineered Barrier System Components Used for NUFT Runs
Attachment IX	Comparison of Tuff Matrix Hydrologic Properties

Attachment X	Liquid Flux Patterns in Matrix Component of Invert and Rock Matrix and in the Intergranular Component of Invert and Rock Fractures for the Campbell and van Genuchten Grain Size Retention Relations
Attachment XI	Hydrologic and Thermal Properties of the Invert
Attachment XII	Calculation of the Diffusion Coefficient for the Dripping Case
Attachment XIII	Derivation of the Formulas for the Calculation of the Bulk Volumetric Moisture Content
Attachment XIV	TSPA Calculation of the Diffusion Coefficient for the Dripping Case
Attachment XV	Calculation of the Thickness of the Invert for Analysis
Attachment XVI	Moisture Retention for Crushed Tuff
Attachment XVII	Estimate of the Boundary Between Advection and Diffusion
Attachment XVIII	Alternate Pore Water Velocity Calculation
Attachment XIX	CD-ROMs With Input and Output Files

ATTACHMENT I

LIST OF NUFT INPUT FILE NAMES

INTENTIONALLY LEFT BLANK

Attachment I - List of NUFT Input Files Names

These files are found in Directory “Input” of the CD-ROM.

File Name (size in kilobytes), date)	File Description
genmsh4rm 13 kb, Nov. 8, 2001	Grid spacing and material designation for initialization run (no EBS components).
genmsh4rm2 (13kb, Nov. 8, 2001)	Same as genmsh4rm except with refined mesh in the invert area.
genmsh4rm35 (13 kb, Nov. 8, 2001)	Same as genmsh4rm except using TSw35 properties around the drift.
genmsh5rmni (13 kb, Nov. 8, 2001)	Same as genmsh4rm but EBS components included for production run.
genmsh5rm2 (13kb, Nov. 8, 2001)	Same as genmsh5rmni except with refined mesh in the invert area.
genmsh5rmni35 (14kb, Nov. 8, 2001)	Same as genmsh5rmni except using tsw35 properties around the drift and with rounded outer invert boundary.
genmsh5rmnt (14kb, Nov. 8, 2001)	Same as genmsh5rmni except with rounded outer invert boundary.
genmsh5rmnt2 (14 kb, Nov. 8, 2001)	Same as genmsh5rmnt except with invert thickness increased from 0.5 to 0.6 meters.
dkm-afc-NBS-WDR4 (64 kb, Nov. 8, 2001)	Natural rock properties for initialization runs.
dkm-afc-EBS_Rev10-WDR4 (9 kb, Nov. 8, 2001)	EBS component properties specified but not used in initialization runs.
dkm-afc-NBS-WDR (65 kb, Nov. 8, 2001)	Natural Rock properties for production runs.
dkm-afc-EBS_Rev10-WDR (13 kb, Nov. 8,2001)	ECM invert properties and other EBS properties specified in production runs.
dkm-afc-EBS_Rev10-WDRinv135 (13 kb, Nov. 8, 2001)	TSw35 matrix properties for m-invert and 3mm-grain-size (van Genuchten) properties for f-invert (sensitivity analysis).
dkm-afc-EBS_Rev10-WDRinvrs (12 kb, Sept. 20, 2001)	DKM properties of invert for the .3 mm van Genuchten retention relation with contact area = 90 m^2/m^3.
ir2D35rm (2kb, Nov. 8, 2001)	Initialization run using 35 mm infiltration rate at ground surface.
ir2D35rm2 (2kb, Nov. 8, 2001)	Initialization run for 35 mm infiltration @ ground surface with refined mesh in invert.
ir2D70rm (2kb, Nov. 8, 2001)	Initialization run for 70 mm infiltration @ ground surface.
ir2D35rm35 (2 kb, Nov. 8, 2001)	Invert properties based on TSw35 rather than TSw36 (TSw35 surrounding drift).
pr2D35rmntinvr (4 kb, Sept. 19, 2001 - using genmsh5rmnt and dkm-afc-EBS_Rev10-WDRinv	Production run for van Genuchten 0.317 mm grain diameter for the invert.
pr2D35rmntinv (4 kb, Nov. 8, 2001) - using genmsh5rmnt and dkm-afc-EBS_Rev10-WDRinv1	Production run for van Genuchten 3 mm grain diameter for the invert.
pr2D35rmntinvr3 (4 kb, Oct. 26, 2001) - using genmsh5rmnt and dkm-afc-EBS_Rev10-WDRinvr3	Production run for van Genuchten 10 mm grain diameter for the invert.
pr2D35rmntinvr2 (4 kb, Oct. 26, 2001) - using genmsh5rmnt and dkm-afc-EBS_Rev10-WDRinvr2	Production run for van Genuchten 20 mm grain diameter for the invert.

File Name (size in kilobytes), date)	File Description
pr2D35rmntinvc (4 kb, Oct. 2, 2001) - using genmsh5rmnt and dkm-afc-EBS_Rev10-WDRinc	Production run for Campbell 0.317 mm grain diameter for the invert.
pr2D35rmntinc (4 kb, Nov. 8, 2001) - using genmsh5rmnt and dkm-afc-EBS_Rev10-WDRinvc	Production run for Campbell 3 mm grain diameter for the invert.
pr2D35rmntinc3 (4 kb, Nov. 8, 2001) - using genmsh5rmnt and dkm-afc-EBS_Rev10-WDRinvc3	Production run for Campbell 10 mm grain diameter for the invert.
pr2D35rmntinc2 (4 kb, Nov. 8, 2001) - using genmsh5rmnt and dkm-afc-EBS_Rev10-WDRinvc2	Production run for Campbell 20 mm grain diameter for the invert.
pr2D35rmntinvrs (4 kb, Sept. 20, 2001) - using genmsh5rmnt dkm-afc-EBS_Rev10-WDRinvrs	Sensitivity run on change of specific contact area to 90 m^2/m^3 for the .3-mm van Genuchten retention relation.
pr2D35rmni (4 kb, Aug. 1, 2001) - using genmsh5rmni and dkm-afc-EBS_Rev10-WDR	Production run with 35 mm/yr of infiltration rate, using ECM properties of invert.
pr2D70rmntinv (4 kb, Nov. 8, 2001) - using genmsh5rmnt and dkm-afc-EBS_Rev10-WDRinv1	Same as pr2D35rmntinv (3mm van Genuchten retention relation) except with 70 mm /yr Infiltration.
pr2D70rmni (4 kb, Aug. 3, 2001) - using genmsh5rmni and dkm-afc-EBS_Rev10-WDR	Sensitivity run similar to pr2D35rmni but using infiltration of 70mm/yr.
pr2D35rmnt2 (4 kb, Nov. 8, 2001) - using genmsh5rm2 dkm-afc-EBS_Rev10-WDR	Sensitivity run using refined mesh in center of invert.
pr2D35rmntinv2 (4 kb, Nov. 8, 2001) - using genmsh5rmnt2 dkm-afc-EBS_Rev10-WDRinv1	Sensitivity run using thicker invert (DKM Model).
pr2D35rmntinv35 (4 kb, Nov. 8, 2001) - using genmsh5rmni35 dkm-afc-EBS_Rev10-WDRinv135	Sensitivity run using TSw35 properties for the m-invert and around the drift (3 mm retention relation).

ATTACHMENT II

LIST OF NUFT OUTPUT FILE NAMES

INTENTIONALLY LEFT BLANK

Attachment II - List of NUFT Output File Names

Note: All **.ext** files may be graphically displayed by XTOOL to show saturations, moisture potentials, and liquid fluxes for different times of simulation. These files are found in Directory "Output" of the CD-ROM.

Table II-1. List of NUFT Files

File Name (size in megabytes, date)	File Description
ir2D35rm.res (4 mb, Nov. 9, 2001)	Output from ir2D35rm used as restart file for all production runs with 35 mm/yr infiltration rate.
ir2D35rm2.re1 (4 mb, Nov. 9, 2001)	Output from ir2D35rm2 used as restart file for sensitivity run with a finer mesh.
ir2D70rm.res (4 mb, Nov. 9, 2001)	Output from ir2D70rm used as restart file for sensitivity run with 70 mm/yr infiltration rate.
ir2D35rm35.re1 (4 mb, Nov. 9, 2001)	Output from ir2D35rm35 used as restart file for sensitivity run pr2D35rmntinv35.
pr2D35rmntinvr.f.ext (54 mb, Sept. 24, 2001)	Output for intergranular component for run pr2D35rmntinvr.
pr2D35rmntinvr.m.ext (54 mb, Sept. 24, 2001)	Output for intra-granular (matrix) component for run pr2D35rmntinvr.
pr2D35rmntinv.f.ext (54 mb, Nov. 9, 2001)	Output for intergranular component for run pr2D35rmntinv.
pr2D35rmntinv.m.ext (54 mb, Nov. 9, 2001)	Output for intra-granular (matrix) component for run pr2D35rmntinv.
pr2D35rmntinvr3.f.ext (54 mb, Nov. 1, 2001)	Output for intergranular component for run pr2D35rmntinvr3
pr2D35rmntinvr3.m.ext (54 mb, Nov. 1, 2001)	Output for intra-granular (matrix) component for run pr2D35rmntinvr3.
pr2D35rmntinvr2.f.ext (54 mb, Nov. 1, 2001)	Output for intergranular component for run pr2D35rmntinvr2.
pr2D35rmntinvr2.m.ext (54 mb, Nov. 1, 2001)	Output for intra-granular (matrix) component for run pr2D35rmntinvr2.
pr2D35rmntinvc.f.ext (54 mb, Oct. 26, 2001)	Output for intergranular component for run pr2D35rmntinvc.
pr2D35rmntinvc.m.ext (54 mb, Oct. 26, 2001)	Output for intra-granular (matrix) component for run pr2D35rmntinvc.
pr2D35rmntinc.f.ext (54 mb, Nov. 9, 2001)	Output for intergranular component for run pr2D35rmntinc.
pr2D35rmntinc.m.ext (54 mb, Nov. 9, 2001)	Output for intra-granular (matrix) component for run pr2D35rmntinc.
pr2D35rmntinc3.f.ext (54 mb, Nov. 9, 2001)	Output for intergranular component for run pr2D35rmntinc3.
pr2D35rmntinc3.m.ext (54 mb, Nov. 9, 2001)	Output for intra-granular (matrix) component for run pr2D35rmntinc3.
pr2D35rmntinc2.f.ext (54 mb, Nov. 9, 2001)	Output for intergranular component for run pr2D35rmntinc2
pr2D35rmntinc2.m.ext (54 mb, Nov. 9, 2001)	Output for intra-granular (matrix) component for run pr2D35rmntinc2.

Table II-2. List of Microsoft Excel Files in Directory “Excel” of CD-ROM

File Name	Description
Attachment IV REV01Ahm.xls (62 kb 5/23/2003)	Analysis of Nondimensionalized van Genuchten moisture potential retention relation.
Attachment V Rev01B.xls (133 kb 8/14/2003)	Analysis of the Campbell retention relation.
Attachment VII.xls (105 kb 5/28/2003)	Verification of the Mathcad Calculation Using Microsoft Excel.
Retention Property.xls (48 kb 8/11/2003)	Retention Properties for Welded Tuff (Attachment IX).
Total System Performance Abstraction.xls (21 kb 7/16/2003)	Calculation of the Diffusion Coefficient For The Dripping Case (Attachment XII).
Upper Bound Glacial Climate Percolation.xls (598 kb 8/09/2003	Statistical analysis of the Upper Bound Glacial Climate Percolation Flux.
Thermolink Properties of Crushed Tuff.xls(38 kb 8/09/2003)	Thermal properties and statistical analysis of crushed tuff.
Invert Velocity Profiles Rev – 1.xls (31 kb 8/09/2003)	Develops a plot of the Peclet Number in the Invert.
Attachment XVI.xls (31 kb 8/16/03)	Moisture Retention for Crushed Tuff

Table II-3. List of Mathcad Files in Directory “Mathcad” of CD-ROM

File Name	Description
Breakthrough Analysis Rev 01.mcd (48 kb 8/14/2003)	EBS Radionuclide Analysis (Attachment III).
Invert Properties mcad7.mcd (145 kb 7/24/2003)	Derivation of Invert "Packed Bed" Properties from Brooks and Corey Data (Attachment VI).
Total System Performance Assessment Abstraction Dripping Ca.mcd (59 kb 8/15/2003)	Attachment XIV TSPA Calculation of the Diffusion coefficient for the Dripping Case.
Calculation of the Bulk Volumetric Moisture Content.mcd (44 kb 6/28/2003)	Attachment XIII Derivation of the Formulas for Calculation of the Bulk Volumetric Moisture Content.
Attachment XVIII Alternate Pore Water Velocity Calculation Rev 01.mcd (47 kb 08/15/2003)	Attachment XVIII Alternate Pore Water Velocity Calculation.
Calculation of the Peclet Number for Diffusion Rev 01.mcd (10 kb 08/16/2003)	Calculation of the Peclet Number for Diffusion.

ATTACHMENT III

EBS RADIONUCLIDE TRANSPORT ANALYSIS

Attachment III - EBS Radionuclide Transport Analysis

This attachment presents the results of the EBS Radionuclide Transport Analysis. The model used for this calculation is documented in Attachment IV of the EBS Radionuclide Transport Model (CRWMS M&O, 2000 Attachment IV)[DIRS 150793]. The documentation and verification of the software routine is presented in this attachment. The attachment is incorporated by the Mathcad reference statement below.

Calculate breakthrough curves using the closed form analytical solution for contaminant transport (Equation 6 4) for the van Genuchten retention relation for the retention properties. Use the NUFT steady state results that considers the van Genuchten retention model and the Campbell model for the coarse intergranular pore space. The pore water velocities for the van Genuchten Model are presented in Table 6-9. Compare the results to the diffusion dominated process. Note that the saturation is nearly 1.0. Using the relationship developed for invert diffusion (Equation 6 16), calculate the soil-liquid diffusion constant using the free water diffusion coefficient (Section 5.6). The volumetric moisture content is calculated in Attachment XIII for the nondripping case as 0.058.

Note in the following calculation in Mathcad that := means an assignment of a constant to a variable, and = means to output the constant in the default SI units. Note that the constants can be output in alternate units.

Calculate the change in diffusivity D_T due to a change in temperature from 25°C to 45°C. The diffusivity D_T is proportional to the absolute temperature and inversely proportional to the viscosity η; i.e., D_T is proportional T/η_T (Cussler 1997, p. 114). It follows that if the diffusivity D_0 is known at some temperature T_0, the diffusivity at temperature T can be found by:

$$\frac{D_T}{D_0} = \frac{\frac{T}{T_0}}{\frac{\eta_T}{\eta_0}} \qquad \text{(Eq. III-1)}$$

where D_T is the diffusion coefficient (m^2/s) at temperature T(K), D_0 is the free water diffusion coefficient (m^2/s) at T_0(K), η_T is the viscosity of water (Pa s) at temperature T(K) and η_0 is the viscosity of water (Pa s) at temperature T_0. The temperature dependence of viscosity is given by Weast and Astle (1981, p. F-42):

$$\frac{\eta_T}{\eta_0} = \frac{10^{\frac{\left[1.3272\cdot(293.15-T)-0.001053\cdot(T-293.15)^2\right]}{T-168.15}}}{10^{\frac{\left[1.3272\cdot(293.15-T_0)-0.001053\cdot(T_0-293.15)^2\right]}{T_0-168.15}}} \qquad \text{(Eq. III-2)}$$

and the diffusion coefficient at temperature T is presented in *EBS Radionuclide Transport Abstraction* (BSC 2003b).

$$\left[\frac{D_T}{D_0} = 10^{\left[\frac{1.3272\cdot(293.15-T_0)-0.001053\cdot(T_0-293.15)^2}{T_0-168.15}-\frac{1.3272\cdot(293.15-T)-0.001053\cdot(T-293.15)^2}{T-168.15}\right]}\right] \quad \text{(Eq. III-3)}$$

Assign the temperatures for the calculation. The measured diffusion is at ambient temperature that equals 25°C.

$$T_0 := 25 + 273.15 \quad \text{(Eq. III-4)}$$

$$T := 45 + 273.15 \quad \text{(Eq. III-5)}$$

$$10^{\left[\frac{1.3272\cdot(293.15-T_0)-0.001053\cdot(T_0-293.15)^2}{T_0-168.15}-\left[\frac{1.3272\cdot(293.15-T)-0.001053\cdot(T-293.15)^2}{T-168.15}\right]\right]} = 1.494 \quad \text{(Eq. III-6)}$$

The diffusion coefficient is approximately fifty percent higher.

As discussed in Section 6.2, the dependence of the soil-liquid diffusion coefficient on the saturation (S_{matrix}), the porosity (ϕ_{matrix}), and the binary diffusion coefficient of water is represented mathematically in *EBS Radionuclide Transport Abstraction* (BSC 2003b, Equation 6-15) as:

$$D = D_0\cdot\phi_{matrix}^{1.863}\cdot S_{matrix}^{1.863} \quad \text{(Eq. III-7)}$$

From Attachment XIII, Section XIII.2 for the nondripping case, the bulk volumetric moisture content is calculated as 0.058. Calculate the solute diffusion coefficient at an elevated temperature of 45°C using the calculation presented above and the binary coefficient as given in Section 6.2 at ambient temperature. The diffusivity is increased by a factor of 1.494 as calculated above.

$$D_{sl} := 2.30\cdot 10^{-5}\cdot\frac{cm^2}{sec}\cdot 1.\cdot(0.058)^{1.863}\cdot 1.494$$

$$D_{sl} = 1.707\times 10^{-7}\ \frac{cm^2}{sec}$$

$$D_{sl} = 5.388\times 10^{-4}\ \frac{m^2}{yr}$$

Consider the case of the van Genuchten Model with 0.317 mm. From Table 6-9, the pore water velocities are given as:

$$V_L := 7.6\cdot 10^{-11}\cdot\frac{m}{sec}$$

$V_L = 2.398 \times 10^{-3} \frac{m}{yr}$

$V_L = 2.398 \frac{mm}{yr}$

$V_H := 1.8 \cdot 10^{-10} \cdot \frac{m}{sec}$

$V_H = 5.68 \times 10^{-3} \frac{m}{yr}$

$V_H = 5.68 \frac{mm}{yr}$

Calculate the effective diffusion coefficient using a dispersivity of 0.1 m (Section 6.2) based upon Equations 6-12 and 6-13.

$\lambda := 0.1 \cdot m$

$\lambda = 10 cm$

$D_L := D_{sl} + \lambda \cdot V_L$

$$D_L = 2.467 \times 10^{-7} \frac{cm^2}{sec} \quad \text{(Eq. III-8)}$$

$D_H := D_{sl} + \lambda \cdot V_H$

$D_H = 3.507 \times 10^{-7} \frac{cm^2}{sec}$

$$C_o := 1.0 \quad \text{(Eq. III-9)}$$

In the following analysis, the user defined function is defined by Equation 6-4 and Jury et al. (1991, p. 227, Equation 7.25) as:

$$C(V,t,L,R,D) := \frac{C_o}{2} \cdot erfc\left[\frac{\frac{1}{2} \cdot \left(L - \frac{V}{R} \cdot t\right)}{\sqrt{\frac{D}{R}} \cdot \sqrt{t}}\right] + \frac{C_o}{2} \cdot \exp\left(\frac{V}{1} \cdot \frac{L}{D}\right) \cdot erfc\left[\frac{\frac{1}{2} \cdot \left(L + \frac{V}{R} \cdot t\right)}{\sqrt{\frac{D}{R}} \cdot \sqrt{t}}\right] \quad \text{(Eq. III-10)}$$

where

- V = pore water velocity (m/yr)
- t = time (yr)
- λ = dispersivity (m)
- R = retardation factor
- D = effective dispersion/diffusion coefficient (m^2/yr)
- C = solute concentration at location x, y, z and time t (mg/l)
- C_0 = solute concentration of the solute at location x = 0 (mg/l)
- L = length in the vertical direction (m)

$$t(logt) := 10^{logt} \cdot yr \qquad logt := -1, -0.9 \ldots 6 \quad \text{(Eq. III-11)}$$

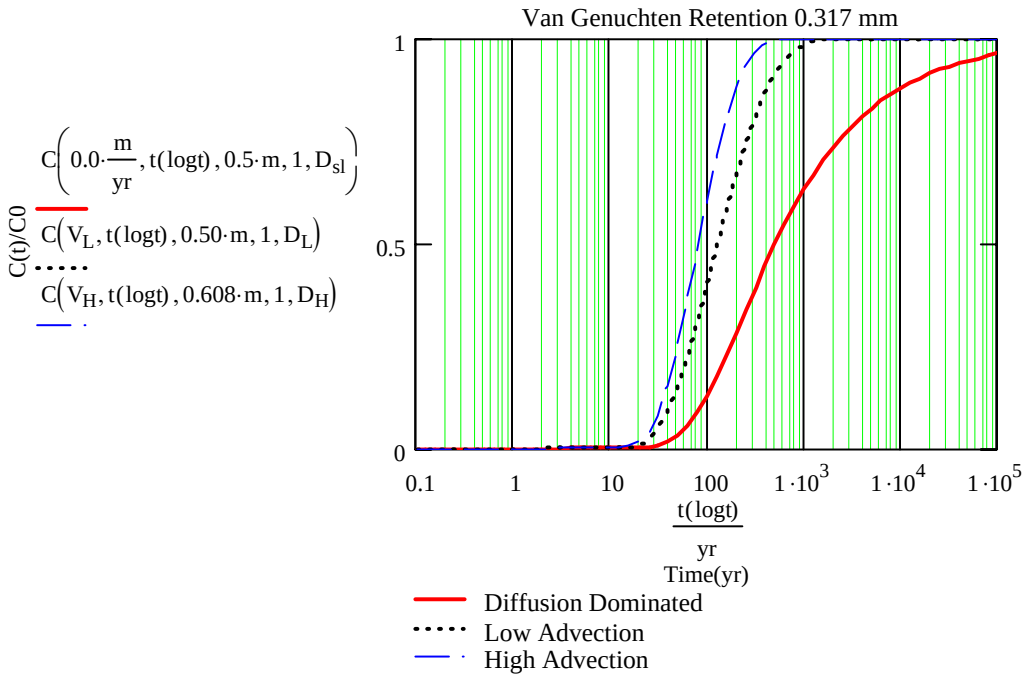

Figure III-1. Breakthrough Curves for the 0.317 mm van Genuchten Retention

Consider the case of the van Genuchten retention relation with 3-20 mm particles sizes (see Table 6-9).

$$V_L := 5.9 \cdot 10^{-11} \cdot \frac{m}{sec}$$

$$V_L = 1.862 \times 10^{-3} \frac{m}{yr}$$

$$V_L = 1.862 \frac{mm}{yr}$$

$$V_H := 1.3 \cdot 10^{-10} \cdot \frac{m}{sec}$$

$$V_H = 4.102 \times 10^{-3} \frac{m}{yr}$$

$$V_H = 4.102 \frac{mm}{yr}$$

$$D_L := D_{sl} + \lambda \cdot V_L$$

$$D_L = 2.297 \times 10^{-7} \frac{cm^2}{sec}$$

$$D_H := D_{sl} + \lambda \cdot V_H$$

$$D_H = 3.007\times 10^{-7}\ \frac{cm^2}{sec}$$

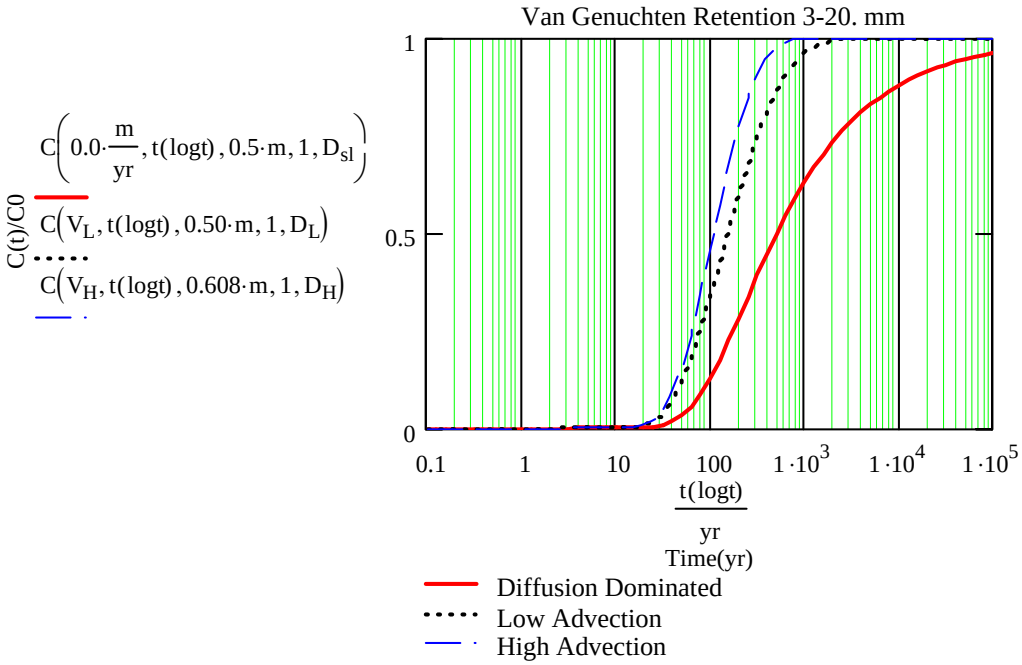

Figure III-2. Breakthrough Curves for the 3-20 mm van Genuchten Retention Relation

Consider the case of the 3 mm-20 mm Campbell retention relation (see Table 6-10).

$$V_L := 3.7\cdot 10^{-11}\cdot\frac{m}{sec}$$

$$V_L = 1.168\times 10^{-3}\ \frac{m}{yr}$$

$$V_L = 1.168\frac{mm}{yr}$$

$$V_H := 1.3\cdot 10^{-10}\cdot\frac{m}{sec}$$

$$V_H = 4.102\times 10^{-3}\ \frac{m}{yr}$$

$$V_H = 4.102\frac{mm}{yr}$$

$$D_L := D_{sl} + \lambda\cdot V_L$$

$$D_L = 2.077\times 10^{-7}\ \frac{cm^2}{sec}$$

$$D_H = 3.007\times 10^{-7}\ \frac{cm^2}{sec}$$

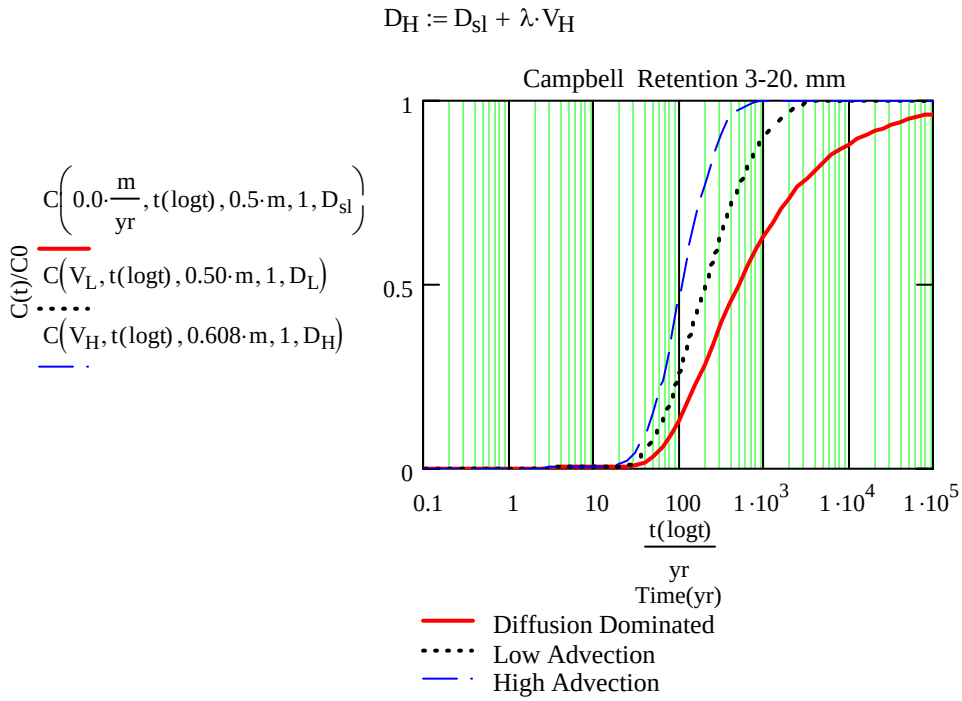

Figure III-3. Breakthrough Curves for the 3-20 mm Campbell Retention Relation

Define the units of ml for purposes of analysis.

$$ml := \frac{liter}{1000}$$

$$0.01 \cdot \frac{ml}{gm} = 1 \times 10^{-5} \frac{m^3}{kg}$$

$$1 \cdot \frac{ml}{gm} = 1 \times 10^{-3} \frac{m^3}{kg}$$

$$1000 \frac{ml}{gm} = 1 \frac{m^3}{kg}$$

Use Equation 6-9 to calculate the retardation factor for a low sorption coefficient of 1 ml/gm and 10 ml/gm. See Table 6-4 for properties.

$$R := 1 + \frac{2385 \frac{kg}{m^3} \cdot 1 \cdot \frac{ml}{gm}}{0.11}$$

$$R = 22.7$$

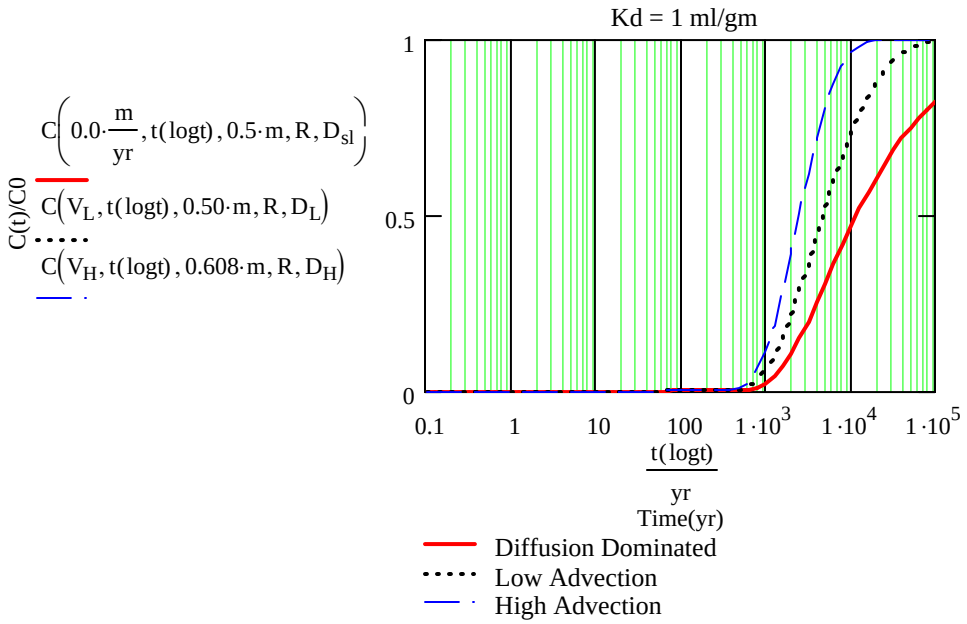

Figure III-4. Breakthrough Curves for the Case of Low Sorption Coefficient (K_d = 1.0 ml/gm)

$$R := 1 + \frac{2385 \cdot \frac{kg}{m^3} \cdot 10 \cdot \frac{ml}{gm}}{0.11}$$

$$R = 217.8$$

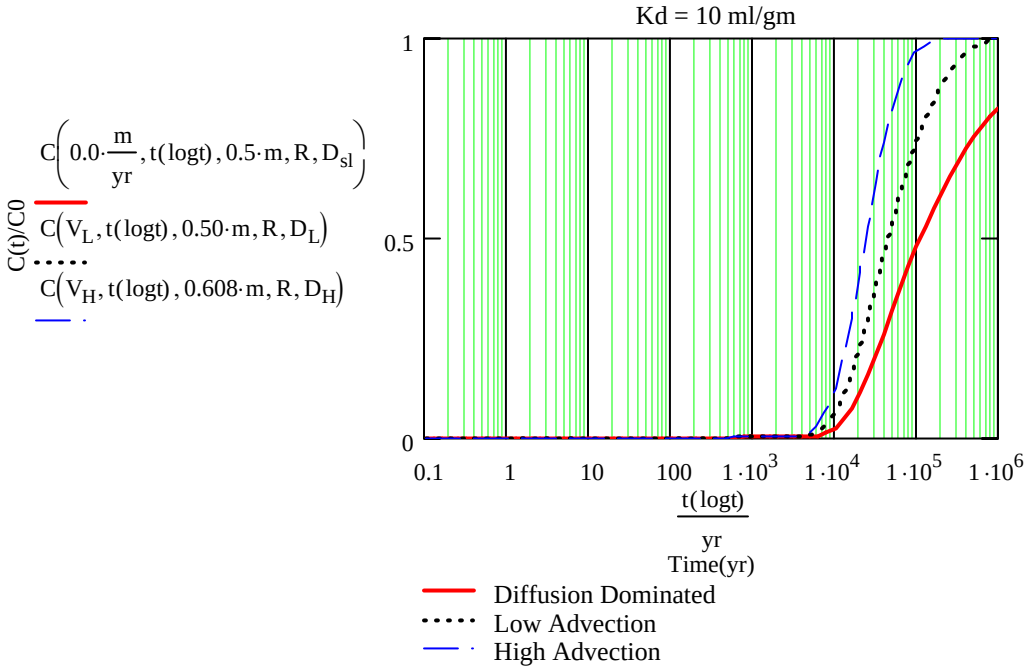

Figure III-5. Breakthrough Curves for the Case of Low Sorption Coefficient (K_d = 10.0 ml/gm)

Use Equation 6-9 to calculate the retardation factor for an intermediate sorption coefficient of 100 ml/gm. See Table 6-4 for properties.

$$logt := 3, 3.1 .. 8$$

$$R := 1 + \frac{2385 \frac{kg}{m^3} \cdot 100 \frac{ml}{gm}}{0.11}$$

$$R = 2169.2$$

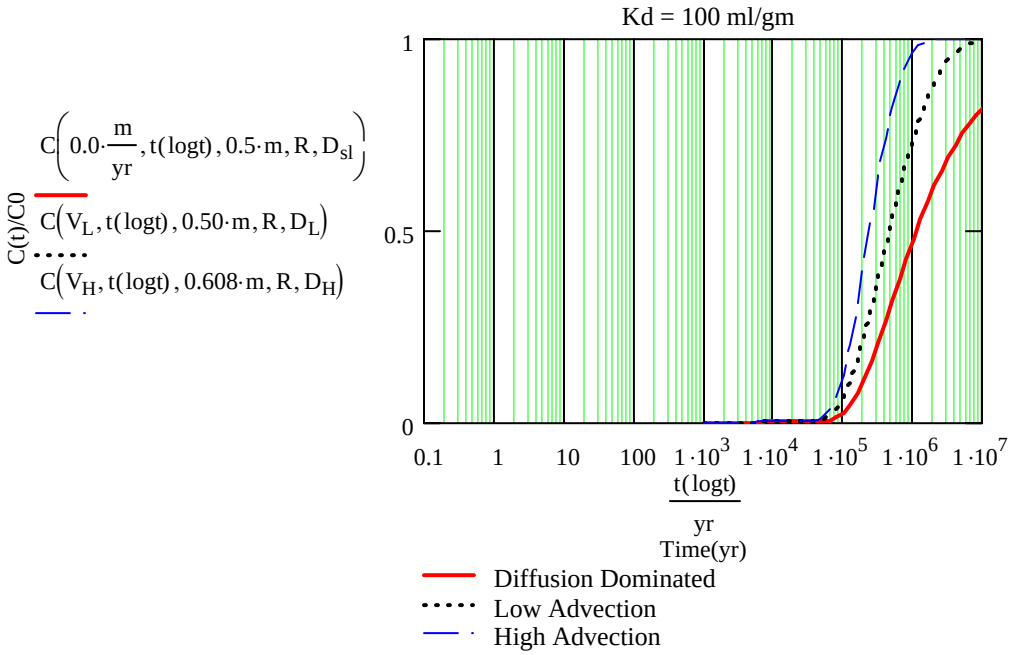

Figure III-6. Breakthrough Curves for the Case of Intermediate Sorption Coefficient (K_d = 100.0 ml/gm)

Use Equation 6-9 to calculate the retardation factor for an intermediate sorption coefficient of 1000 ml/gm. See Table 6-4 for properties.

$$R := 1 + \frac{2385 \frac{kg}{m^3} \cdot 1000 \frac{ml}{gm}}{0.11}$$

R = 21682.8

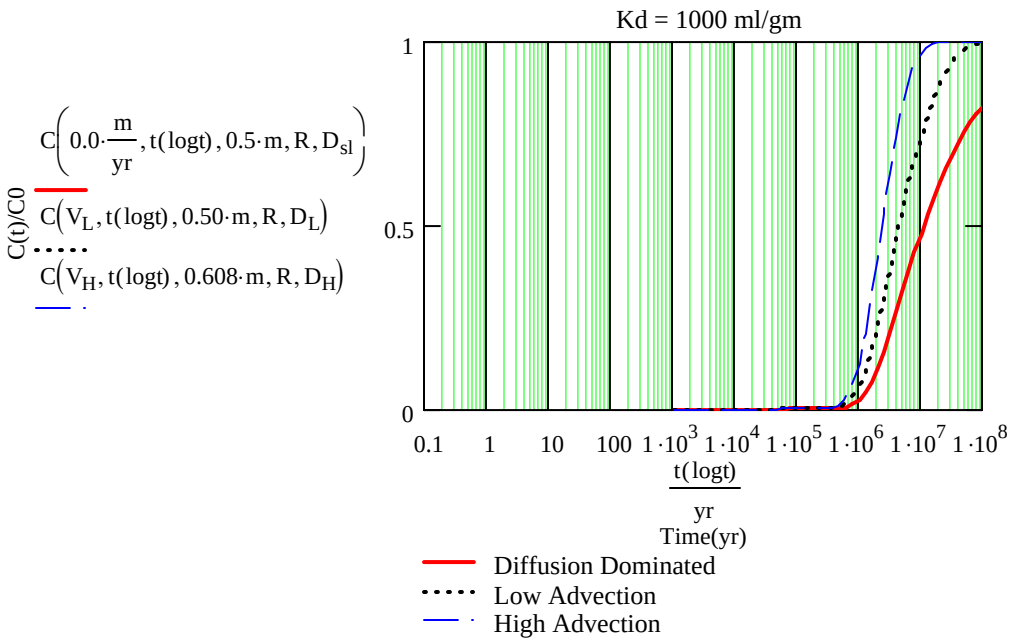

Figure III-7. Breakthrough Curves for the Case of High Sorption Coefficient (K_d = 1000.0 ml/gm)

ATTACHMENT IV

ANALYSIS OF NONDIMENSIONALIZED VAN GENUCHTEN MOISTURE POTENTIAL RETENTION RELATION

Attachment IV - Analysis of Nondimensionalized van Genuchten Moisture Potential Retention Relation

This attachment presents the calculations and plots of the retention curves for the nondimensionalized van Genuchten moisture potential retention relation. The summary of the calculations of the air entry parameters is presented in Table IV-1. The van Genuchten (n) value is 8.013 as discussed below. The individual retention curves with curve fits are presented in Tables IV-2 through IV-5 and are illustrated in Figures IV-1 through IV-4.

Table IV-1. van Genuchten Air Entry Parameter (α) Calculations

Parameter	Particle Diameter(d_m)			
	0.317 mm	**3 mm**	**10 mm**	**20 mm**
van Genuchten air-entry parameter(α) (cm)-1	0.0647[1]	0.612[3]	2.04	4.08
van Genuchten air entry parameter(bars)-1	65.9[2]	624[4]	2080	4160

NOTES: [1]See the calculation presented in Equation IV-6.
[2]See the calculation presented in Equation IV-7.
[3]See the calculation presented in Equation IV-10.
[4]See the calculation presented in Equation IV-11.

Table IV-2a. van Genuchten Curve Parameters for 0.317 mm Crushed Tuff

Parameter	Value	Units
Moisture Content at Saturation (θs)	0.45	(no units)
Residual Moisture Content (θr)	0.05	(no units)
Alpha (α)	65.91	$bars^{-1}$
n	8.01	(no units)
m	0.88	(no units)

NOTES: The alpha parameter is also equal to 0.07 cm^{-1}.

Table IV-2b. Retention Analysis for 0.317 mm Crushed Tuff

Moisture Potential y(bars)	Predicted Moisture Content (θ)
0.0001	0.450
0.0002	0.450
0.0005	0.450
0.001	0.450
0.002	0.450
0.005	0.450
0.01	0.438
0.02	0.103
0.05	0.050
0.1	0.050
0.2	0.050
0.5	0.050
1	0.050
2	0.050
5	0.050
10	0.050
20	0.050
50	0.050
100	0.050
200	0.050
500	0.050
1000	0.050

NOTE: Predicted moisture content obtained from Equation IV-1.

Table IV-3a. van Genuchten Curve Parameters for 3.0 mm Crushed Tuff

Parameter	Value	Units
Moisture Content at Saturation (θs)	0.45	(no units)
Residual Moisture Content (θr)	0.05	(no units)
Alpha (α)	624.00	$bars^{-1}$
n	8.01	(no units)
m	0.88	(no units)

NOTES: The alpha parameter is also equal to 0.62 cm^{-1}.

Table IV-3b. Retention Analysis for 3.0 mm Crushed Tuff

Moisture Potential y(bars)	Predicted Moisture Content (θ)
0.0001	0.450
0.0002	0.450
0.0005	0.450
0.001	0.442
0.002	0.124
0.005	0.050
0.01	0.050
0.02	0.050
0.05	0.050
0.1	0.050
0.2	0.050
0.5	0.050
1	0.050
2	0.050
5	0.050
10	0.050
20	0.050
50	0.050
100	0.050
200	0.050
500	0.050
1000	0.050

NOTE: Predicted moisture content obtained from Equation IV-1.

Table IV-4a. van Genuchten Curve Parameters for 10.0 mm Crushed Tuff

Parameter	Value	Units
Moisture Content at Saturation (θs)	0.45	(no units)
Residual Moisture Content (θr)	0.05	(no units)
Alpha (α)	2079.32	$bars^{-1}$
n	8.01	(no units)
m	0.88	(no units)

NOTES: The alpha parameter is also equal to 2.05 cm^{-1}.

Table IV-4b. Retention Analysis for 10.0 mm Crushed Tuff

Moisture Potential y(bars)	Predicted Moisture Content (θ)
0.0001	0.450
0.0002	0.450
0.0005	0.238
0.001	0.052
0.002	0.050
0.005	0.050
0.01	0.050
0.02	0.050
0.05	0.050
0.1	0.050
0.2	0.050
0.5	0.050
1	0.050
2	0.050
5	0.050
10	0.050
20	0.050
50	0.050
100	0.050
200	0.050
500	0.050
1000	0.050

NOTE: Predicted moisture content obtained from Equation IV-1.

Table IV-5a. van Genuchten Curve Parameters for 20.0 mm Crushed Tuff

Parameter	Value	Units
Moisture Content at Saturation (θs)	0.45	(no units)
Residual Moisture Content (θr)	0.05	(no units)
Alpha (α)	4158.80	$bars^{-1}$
n	8.01	(no units)
m	0.88	(no units)

NOTES: The alpha parameter is also equal to 4.09 cm^{-1}.

Table IV-5b. Retention Analysis for 20.0 mm Crushed Tuff

Moisture Potential y(bars)	Predicted Moisture Content (θ)
0.0001	0.450
0.0002	0.384
0.0005	0.052
0.001	0.050
0.002	0.050
0.005	0.050
0.01	0.050
0.02	0.050
0.05	0.050
0.1	0.050
0.2	0.050
0.5	0.050
1	0.050
2	0.050
5	0.050
10	0.050
20	0.050
50	0.050
100	0.050
200	0.050
500	0.050
1000	0.050

NOTE: Predicted Moisture content obtained from Equation IV-1.

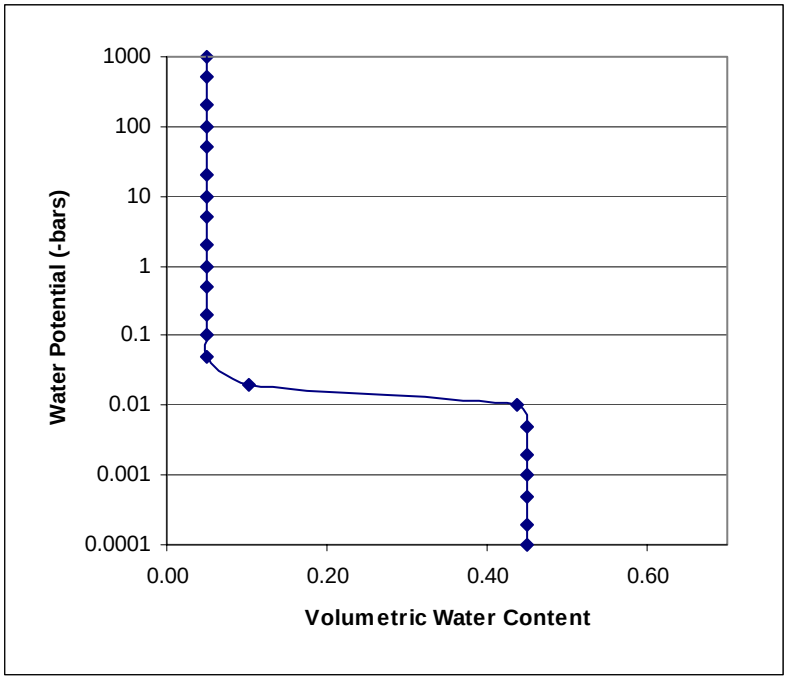

Figure IV-1. Nondimensionalized Model for Mean Particle Diameter of 0.317 mm

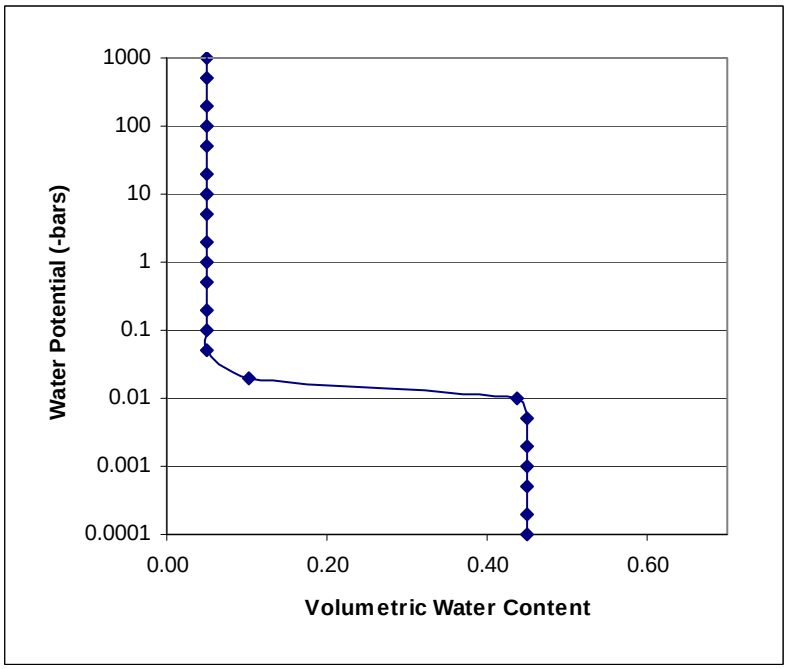

Figure IV-2. Nondimensionalized Model for Mean Particle Diameter of 3.0 mm

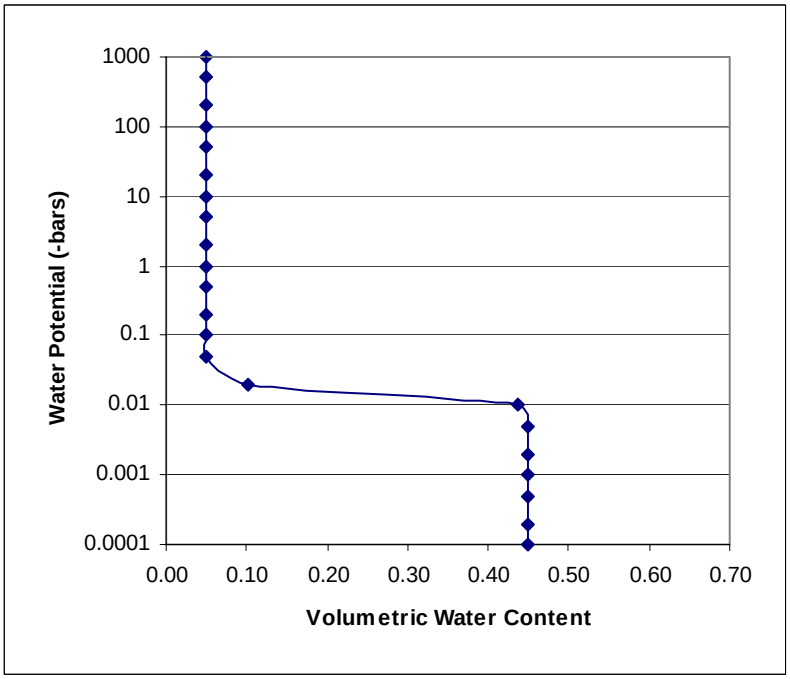

Figure IV-3. Nondimensionalized Model for Mean Particle Diameter of 10.0 mm

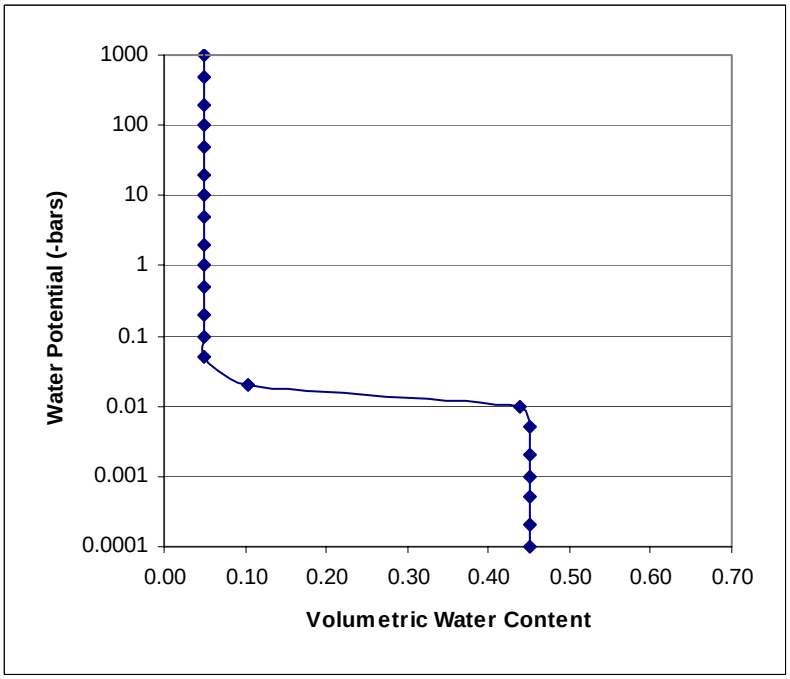

Figure IV-4. Nondimensionalized Model for Mean Particle Diameter of 20 mm

The following discussion presents the methodology and the analysis for determining the relationship of unsaturated hydraulic conductivity (K_{us}) from the retention curve using the two-parameter nondimensional van Genuchten relationship and the size of the crushed tuff. The basis for the nondimensional retention relationship is a least squares curve fit for a series of retention measurements made on the materials presented above. Equal weighting is given to these materials (Attachment VII). The nondimensional van Genuchten air-entry parameter (α) is determined from a scaling relationship while the nondimensional (n) parameter is constant. The intrinsic permeability (k) is determined from the Kozeny-Carman formula shown by Equation IV-4 (Bear 1972, p. 166) that relates intrinsic permeability (k) to the grain size or pore diameter (d_m) and porosity (ϕ). On the basis of the selected grain size, the saturated hydraulic conductivity (K_s) and the van Genuchten relationship for relative permeability, the relationship of unsaturated hydraulic conductivity (K_{us}) relationship to moisture potential (ψ) can be determined. It should be noted that the hydraulic conductivity under saturated conditions may have a Reynolds Number that exceeds the range of validity for Darcy's Law. Some other power law relating flow rate to hydraulic conductivity might apply under saturated conditions.

A qualitative assessment can be made over the range of moisture potentials (ψ) of interest (0.01 to 0.1 bars) as to whether liquid flow or advection in the coarse fraction of the crushed tuff would occur for a range of particle diameters. The analysis presented below is performed for grain size diameters of 0.317 mm, 3 mm, 10 mm, and 20 mm for the intergranular porosity ($\phi_{intergrain}$) respectively to cover a broad range of particle diameters.

Equation IV-1 is used to define the moisture potential (ψ) (capillary pressure divided by weight density) versus moisture content (θ) relation (Fetter 1993, p. 172):

$$\theta(\alpha, n, \theta_s, \theta_r, \psi) = \theta_r + \frac{(\theta_s - \theta_r)}{\left[1 + (|\psi\alpha|)^n\right]^m} \qquad \text{(Eq. IV-1)}$$

where

θ = Volumetric moisture/water content
α = van Genuchten air-entry parameter (Pa-1) or (fcm-1) or (bars-1)
n = van Genuchten nondimensional "n" parameter
θs = Saturated volumetric moisture content
θr = Residual volumetric moisture content
Ψ = Nondimensional moisture/matric potential
m = van Genuchten nondimensional "m" parameter

Fetter designates the (m) parameter for the van Genuchten relationship as: m = 1-1/n (Fetter 1993, p. 172). This value of "m" can be substituted into Equation IV-1 to derive the volumetric moisture content (θ) as shown in Equation IV-2. Figure IV-5 reflects this relationship. The parameter "n" is a van Genuchten nondimensional parameter estimated from the soil-water retention curve (van Genuchten 1980, p. 895).

$$\theta(\alpha, \mathrm{n}, \theta_s, \theta_r, \psi) = \theta_r + \frac{(\theta_s - \theta_r)}{\left[1 + (|\psi\alpha|)^n\right]^{(1-\frac{1}{n})}} \quad \text{(Eq. IV-2)}$$

Equation IV-3 is used to define the nondimensional moisture potential parameter (Ψ_{ND}) for analysis (Leverett 1941, p. 159). Figure IV-5 shows this relationship.

$$\psi_{ND} = \psi \cdot \frac{\rho \cdot g}{\sigma_W} \cdot \sqrt{\frac{k}{\phi}} \quad \text{(Eq. IV-3)}$$

where

Ψ = moisture potential
ρ = mass density of water ((kg/m^3)
g = acceleration due to gravity
k = intrinsic permeability
σ_w = interfacial tension between the pore water and mineral surface (dyne/cm)
ϕ = porosity

The least squares regression analysis of the data is presented in Attachment VI using the above relationship. Attachment VII presents independent verification of the Mathcad calculations using Microsoft Excel. The van Genuchten nondimensional parameter (n) is calculated, where the van Genuchten dimensionless air entry parameter, α_{ND} = 2.455 such that n = 8.01 (Attachments VI and VII). The original Brooks and Corey data have been plotted with a curve fit using Equation IV-3 (Brooks and Corey 1964). For specific sized grains, the Kozeny-Carman equation expresses the relationship of the intrinsic permeability (k) to the porosity (ϕ) as expressed in Equation 6-25 (Bear 1972, p. 166).

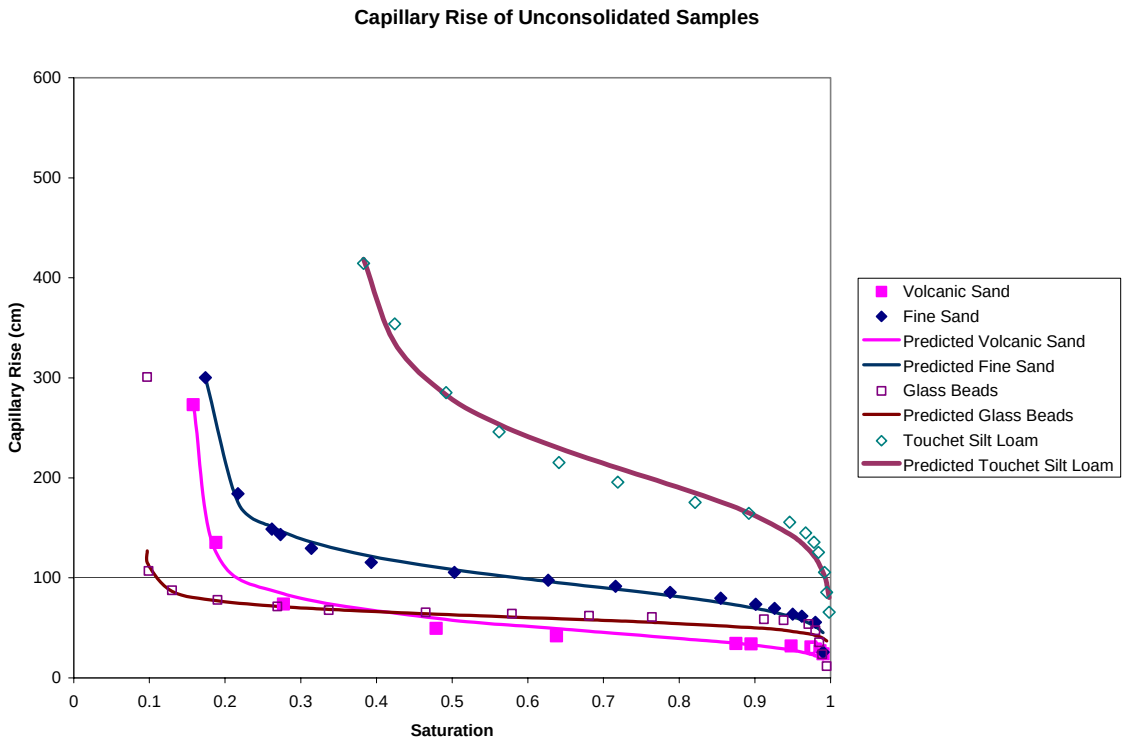

Figure IV-5. Capillary Rise of Unconsolidated Samples

$$\text{Intrinsic permeability} = k = \frac{d_m^{\,2}}{180} \cdot \frac{\phi^3}{(1-\phi)^2} \qquad \text{(Eq. IV-4)}$$

where

d_m = mean particle diameter
ϕ = porosity

This equation can be rearranged to obtain:

$$\sqrt{\frac{k}{\phi}} = \frac{d_m}{\sqrt{180}} \cdot \frac{\phi}{(1-\phi)} \qquad \text{(Eq. IV-5)}$$

The Leverett Equation, as presented in Equation IV-3, expresses the relationship of the nondimensional moisture potential to the dimensional moisture potential. Since the air-entry parameter α is inversely proportional to the moisture potential (see Equation IV-2), the relationship of the nondimensional air-entry parameter as determined from the regression analysis for Equation IV-2 is given by:

$$\frac{1}{\alpha_{ND}} = \frac{1}{\alpha} \cdot \frac{\rho \cdot g}{\sigma_w} \cdot \sqrt{\frac{k}{\phi}} \qquad \text{(Eq. IV-6)}$$

Solving for the air-entry parameter α in terms of the nondimensional air-entry parameter:

$$\alpha = \alpha_{ND} \cdot \frac{\rho \cdot g}{\sigma_w} \cdot \sqrt{\frac{k}{\phi}} \qquad \text{(Eq. IV-7)}$$

Substituting Equation IV-5 into Equation IV-7 to express the air-entry parameter α in terms of the particle diameter (d_m); the fluid density (ρ); the surface tension (σ_w); the porosity (ϕ), the gravitational constant (g); and the nondimensionless air entry parameter (α_{ND}) as determined from the curve fitting analysis in Attachments VI and VII:

$$\alpha = \alpha_{ND} \cdot \frac{\rho \cdot g}{\sigma_w} \cdot \frac{d_m}{\sqrt{180}} \cdot \frac{\phi}{(1-\phi)} = 2.455 \cdot \frac{\rho \cdot g}{\sigma_w} \cdot \frac{d_m}{\sqrt{180}} \cdot \frac{\phi}{(1-\phi)} \qquad \text{(Eq. IV-8)}$$

Substituting in the value of 0.317 mm as a particle size with an intergranular porosity ($\phi_{intergrain}$) of 0.45, the calculated value for the van Genuchten air-entry parameter (α) in cm^{-1} for this size material is given in Equation IV-7:

$$\frac{\rho \cdot g}{\sigma_w} \sqrt{\frac{k}{\phi}} 2.455 = \frac{\rho \cdot g}{\sigma_w} \frac{0.0317 \cdot cm}{\sqrt{180}} \cdot \frac{0.45}{(1-0.45)} 2.455 = 0.0647 \cdot cm^{-1} \qquad \text{(Eq. IV-9)}$$

This analysis uses the following referenced properties for water: mass density, ρ= 1000 kg/m^3, σ_g, geometric standard deviation, an interfacial tension between the pore water and mineral surface, σ_w = 72 dynes/cm at ambient temperature, and gravity, g = 9.81 m/sec^2 (Incropera and DeWitt 1996, p. 846). The air-entry parameter (α) in terms of $(bars)^{-1}$:

$$\alpha = \frac{0.06466 \cdot cm^{-1}}{1000 \cdot \frac{kg}{m^3} \cdot 9.81 \cdot \frac{m}{\sec^2}} = 65.9(bars)^{-1} \qquad \text{(Eq. IV-10)}$$

The wetting-phase relative permeability as a function of moisture potential (ψ) for van Genuchten curve fit is restated from Fetter (1993, p. 182). The unsaturated hydraulic conductivity (K_{us}) (wetting-phase relative permeability times saturated hydraulic conductivity) as a function of moisture potential (ψ) is derived using Equation IV-11 (Fetter 1993, Equation 4.17)

$$K_{us} = K(\alpha, n, \psi, K_s) = K_s \frac{\left[1 - (|\alpha\psi|)^{(n-1)}\left[1 + (|\alpha\psi|)^n\right]^{\left(-1+\frac{1}{n}\right)}\right]^2}{\left[\left[1 + (|\alpha\psi|)^n\right]^{\left[\frac{1}{2} - \frac{1}{(2n)}\right]}\right]} \qquad \text{(Eq. IV-11)}$$

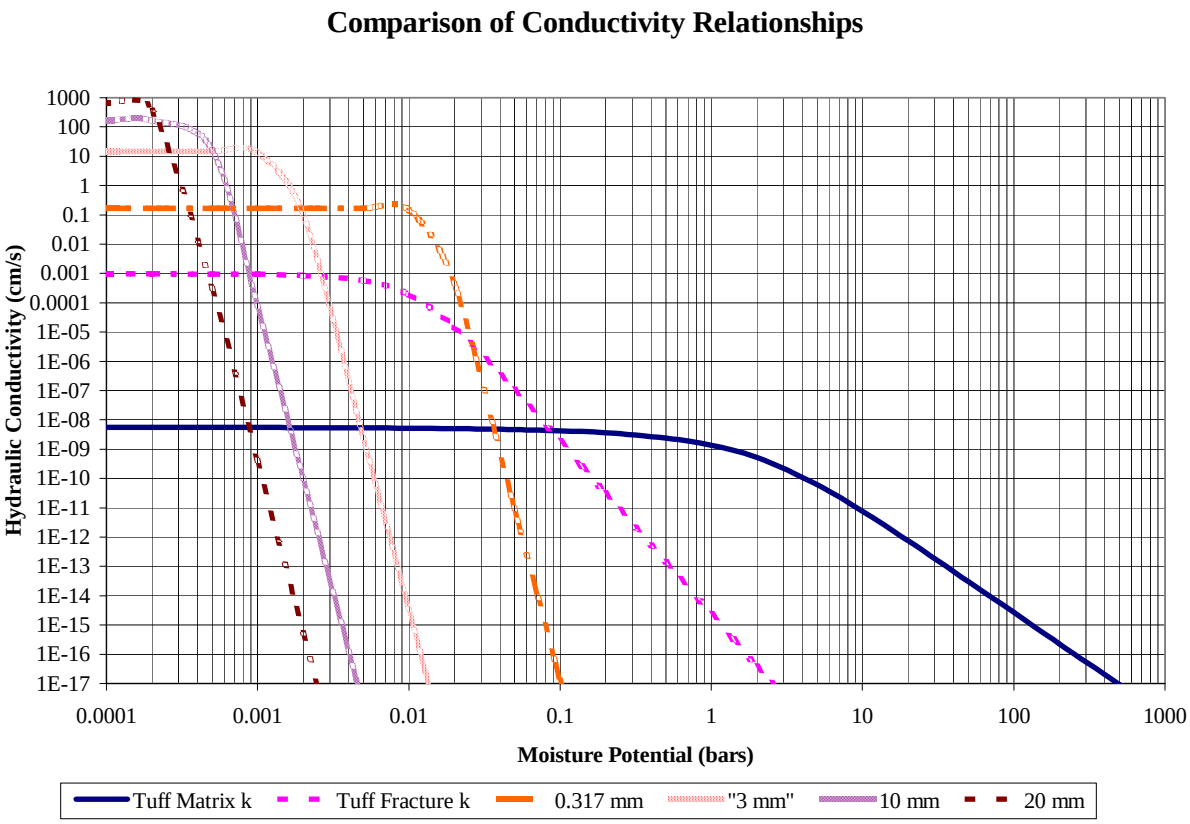

Figure IV-6. Unsaturated Hydraulic Conductivity Relationships

A second analysis was developed based upon a grain sizes of 3 mm. The van Genuchten air-entry parameter (α) for this grain size from Equations IV-3 and IV-5 is given as:

$$\frac{\rho \cdot g}{\sigma_w}\sqrt{\frac{k}{\phi}} \cdot 2.455 = \frac{\rho \cdot g}{\sigma_w}\frac{0.3 \cdot cm}{\sqrt{180}} \cdot \frac{0.45}{(1-0.45)} \cdot 2.455 = 0.612 \cdot cm^{-1} \qquad \text{(Eq. IV-12)}$$

The value of the van Genuchten air-entry parameter (α) for the 3 mm diameter grain size in terms of bars^{-1} is calculated using Equation IV-9 to be 624 (bars)$^{-1}$:

$$\alpha = \frac{0.612 \cdot \mathrm{cm}^{-1}}{1000 \cdot \frac{\mathrm{kg}}{\mathrm{m}^3} \cdot 9.81 \cdot \frac{\mathrm{m}}{\mathrm{sec}^2}} = 624 \cdot \mathrm{bars}^{-1} \qquad \text{(Eq. IV-13)}$$

The intrinsic permeability (k) corresponding to a grain size of 3 mm using Equation IV-4 as 1.51×10^{-8} m^2:

$$k = \frac{d_m^{\,2}}{180} \cdot \frac{\phi^3}{(1-\phi)^2} = 1.51 \cdot 10^{-8} \cdot m^2 \qquad \text{(Eq. IV-14)}$$

INTENTIONALLY LEFT BLANK

ATTACHMENT V

ANALYSIS OF THE CAMPBELL RETENTION RELATION

Attachment V - Analysis of the Campbell Retention Relation

This attachment presents calculations to develop the retention curve based upon the Campbell retention relation for the intergranular porosity. Based upon the retention data, the van Genuchten curve fit parameters (α, n) are estimated using Microsoft Excel Solver as outlined in *Water Diversion Model* (CRWMS M&O 2000c, Section 3 and Attachment IV). The Solver is an add-in function in Microsoft Excel. The Solver can minimize a target cell that involves multiple cell variables that might be subject to multiple constraints. The Solver is used specifically to solve for the van Genuchten curve fit parameters (α, n) based upon a minimization of the least squares of the volumetric moisture content for curve fitting to the Campbell retention relation. Table V-1 presents a summary of hydrologic properties based upon the Campbell retention relation. Tables V-2 through V-9 present the detailed calculations.

The following discussion presents a sample calculation for the purpose of calculating the retention relationship using the Campbell method. The first step is to calculate the air entry pressure for a particle diameter of 0.317 mm. Apply Equation 6-23 to the calculation of the air-entry moisture potential.

$$\psi_{es} = -0.5 \cdot d_g^{-1/2} = -0.5 \cdot (0.317)^{-0.5} = -0.888 \cdot J/kg$$

Calculate the value of b as reported in Table 6-5 from Equation 6-24:

$$b = -2 \cdot \psi_{es} + 0.2 \cdot \sigma_g = -2 \cdot -0.888 + 0.2 \cdot (5) = 2.78$$

For purposes of calculating the retention relationship, calculate the air-entry moisture potential for the crushed tuff using Equation 6-25. The dry unit weight is calculated from the phase diagram as:

$$\frac{V_v}{V_T} = 0.45$$

Using the soils mechanics convention of setting the volume of solids equal to one:

$$\frac{V_v}{1.0 + V_v} = 0.45$$

Solving for the volume of the voids:

$$V_V \cdot (1 - 0.45) = 0.45$$

$$V_V = 0.45/(1 - 0.45) = 0.818$$

The specific gravity of solids equals 2.52 gm/cm^3. Therefore, the dry mass density is calculated as:

$$\gamma_d = \frac{2.52}{1 + 0.818} = 1.39 \frac{gm}{cm^3}$$

Applying this correction to the air-entry moisture potential (Equation 6-25):

$$\psi_e = -0.888 \cdot (1.39/1.3)^{0.67b} = -1.006 \frac{J}{kg} = -0.01006 Bars$$

Calculate the volumetric moisture content by solving Equation 6-22 for volumetric moisture content for a value of moisture potential of 0.1 bars.

$$\theta = \left(\frac{\psi}{\psi_e} \right)^{\left(\frac{-1}{b}\right)} \cdot \phi = \left(\frac{0.1}{0.01006} \right)^{\left(\frac{-1}{2.776}\right)} \cdot \phi = 0.197$$

The results of this calculation are in agreement with the spreadsheet calculation presented in Table V-2.

Table V-1. Summary of Hydrologic Properties Based Upon the Campbell Retention Relation

Parameter	Particle Size (d_g)			
	0.317 mm	**3 mm**	**10 mm**	**20 mm**
Saturated Volumetric Moisture Content (θ_s)[1]	0.450	0.450	0.450	0.450
Residual Volumetric Moisture Content (θ_r)[2]	0.020	0.010	0.010	0.010
van Genuchten Air-entry Parameter (α) ($bars^{-1}$)[3]	47.64	230.84	476.91	561.61
van Genuchten Air-entry Parameter (α) (cm^{-1})	0.06	0.24	0.48	0.56
van Genuchten n Value[4]	1.53	3.04	4.03	11.11
van Genuchten m Value	0.35	0.67	0.752	0.91
Saturated Intrinsic Permeability (k)(m^2)[6]	1.68E-10	1.51E-08	1.67E-07	6.69E-07
Saturated Hydraulic Conductivity (K_s)(cm/sec)[7]	0.184	16.48	183.1	732.5

NOTES: [1] See Section 6.3 for the selection of the porosity (ϕ). The saturated volumetric moisture content (θ_s) equals the porosity.

[2] The residual volumetric moisture content (θ_r) is selected as 0.02 based upon a plot of the empirical retention curve.

[3] The van Genuchten air-entry parameter(α) is determined from a regression analysis using the Microsoft Excel Solver as explained in the text.

[4] The van Genuchten n value is determined from a regression analysis using the Microsoft Excel Solver as explained in the text. The value of n is given by 1/(1-m) (Fetter 1993, p. 172).

[5] Note that m = 1-1/n (Fetter 1993, p. 172).

[6] The intrinsic permeability (k) is calculated from Equation IV-4.

[7] The value of the saturated hydraulic conductivity (K_s) is obtained by the equation that converts an saturated intrinsic permeability (k) to a saturated hydraulic conductivity (K_s) (Freeze and Cherry 1979, p. 27):

$$K_s = \frac{\rho \cdot g}{\mu} \cdot k$$

The properties of water at ambient temperature are given by Incropera and DeWitt (1996, p. 846). The water density (ρ) equals 1000 kg/m^3 and the absolute viscosity (μ) equals 8.935×10^{-4} $N \cdot s/(m^2)$.

Table V-2a. Campbell Model Parameters[1] for 0.317 mm Crushed Tuff

Parameter	Value
Grain Diameter (d_g) (mm)	3.17E-01
Saturated Volumetric Water Content (θ_S)	4.50E-01
Air-entry water potential or the potential at which the largest water-filled pores just drain ψ_{es} (J/kg)[2]	-8.88E-01
Geometric Standard Deviation[3]	5.00E+00
Slope of the ln(ψ) versus ln(θ) retention curve (b)[4]	2.78E+00
ψ_e (bars)	-1.01E-02
ψ_e (cm)	-1.03E+01

NOTES: [1] See text and Table 6-5 for a description of the parameters.
[2] This value is calculated from Equation 6.23.
[3] This value is estimated from Campbell (1985, p. 10, Figure 2.1).
[4] This value is calculated from Equation 6.24.

Table V-2b. Campbell Model Moisture Data for 0.317 mm Crushed Tuff

Moisture Potential (bars)	Moisture Content
0.0001	0.450
0.0002	0.450
0.0005	0.450
0.001	0.450
0.002	0.450
0.005	0.450
0.01	0.450
0.02	0.351
0.05	0.253
0.1	0.197
0.2	0.153
0.5	0.110
1	0.086
2	0.067
5	0.048
10	0.037
20	0.029
50	0.021
100	0.016
200	0.013
500	0.009
1000	0.007

Table V-3a. van Genuchten Curve Fit Parameters for 0.317 mm Crushed Tuff

Parameter	Value	Units
Moisture Content at Saturation (θs)	0.45	(no units)
Residual Moisture Content (θr)	0.02	(no units)
Alpha (α)	47.64	$bars^{-1}$
n	1.53	(no units)
m	0.35	(no units)

NOTES: The alpha parameter is also equal to 0.06 cm^{-1}.
The sum of the residuals is 3.22E-03

Table V-3a. van Genuchten Retention Analysis Results for 0.317 mm Crushed Tuff

Volumetric Moisture Content[1]	Moisture Potential (bars)	Predicted Moisture Content[2]	Residuals Squared
0.450	0.0001	0.450	1.77E-09
0.450	0.0002	0.450	1.47E-08
0.450	0.0005	0.450	2.41E-07
0.450	0.001	0.449	1.99E-06
0.450	0.002	0.446	1.61E-05
0.450	0.005	0.435	2.39E-04
0.450	0.01	0.410	1.56E-03
0.351	0.02	0.363	1.29E-04
0.253	0.05	0.271	3.29E-04
0.197	0.1	0.203	3.85E-05
0.153	0.2	0.149	1.51E-05
0.110	0.5	0.100	9.53E-05
0.086	1	0.076	9.93E-05
0.067	2	0.059	6.56E-05
0.048	5	0.044	1.73E-05
0.037	10	0.037	7.52E-07
0.029	20	0.032	5.41E-06
0.021	50	0.027	3.74E-05
0.016	100	0.025	7.36E-05
0.013	200	0.023	1.14E-04
0.009	500	0.022	1.68E-04
0.007	1000	0.021	2.05E-04

NOTES: 1 The volumetric moisture content is determined from Equation 6-22 to the Campbell data.
2 The predicted moisture content is determined from the minimization of the least squares using the Microsoft Excel Solver as explained in the text.

Table V-4. Campbell Model Parameters[1] for 3.0 mm Crushed Tuff

Parameter	Value
Grain Diameter (d_g) (mm)	3
Saturated Volumetric Water Content (θ_S)	4.50E-01
Air-entry water potential or the potential at which the largest water-filled pores just drain ψ_{es} (J/kg)[2]	-2.89E-01
Geometric Standard Deviation[3]	1.00E+00
Slope of the ln(ψ) versus ln(θ) retention curve (b)[4]	7.77E-01
ψ_e (bars)	-2.99E-03
ψ_e (cm)	-3.05E+00

NOTES: [1] See text and Table 6-5 for a description of the parameters.
[2] This value is calculated from Equation 6-23.
[3] This value is estimated from Campbell (1985, p. 10, Figure 2.1).
[4] This value is calculated from Equation 6-24.

Table V-4. Campbell Model Moisture Data for 3.0 mm Crushed Tuff

Moisture Potential (bars)	Moisture Content
0.0001	0.450
0.0002	0.450
0.0005	0.450
0.001	0.450
0.002	0.450
0.005	0.232
0.01	0.095
0.02	0.039
0.05	0.012
0.1	0.015
0.2	0.012
0.5	0.011
1	0.010
2	0.010
5	0.010
10	0.010
20	0.010
50	0.010
100	0.010
200	0.010
500	0.010
1000	0.010

Table V-5a. van Genuchten Curve Fit Parameters for 3.0 mm Crushed Tuff

Parameter	Value	Units
Moisture Content at Saturation (θs)	0.45	(no units)
Residual Moisture Content (θr)	0.01	(no units)
Alpha (α)	230.84	$bars^{-1}$
n	3.04	(no units)
m	0.67	(no units)

NOTES: The alpha parameter is also equal to 0.24 cm^{-1}.
The sum of the residuals is 1.06E-03.

Table V-5a. van Genuchten Retention Analysis Results for 3.0 mm Crushed Tuff

Volumetric Moisture Content[1]	Moisture Potential (bars)	Predicted Moisture Content[2]	Residuals Squared
0.450	0.0001	0.450	9.48E-12
0.450	0.0002	0.450	6.45E-10
0.450	0.0005	0.450	1.70E-07
0.450	0.001	0.447	1.14E-05
0.450	0.002	0.424	6.78E-04
0.232	0.005	0.245	1.61E-04
0.095	0.01	0.086	9.06E-05
0.039	0.02	0.029	9.69E-05
0.012	0.05	0.013	9.21E-07
0.015	0.1	0.011	1.77E-05
0.012	0.2	0.010	3.40E-06
0.011	0.5	0.010	3.53E-07
0.010	1	0.010	6.15E-08
0.010	2	0.010	1.06E-08
0.010	5	0.010	1.02E-09
0.010	10	0.010	1.72E-10
0.010	20	0.010	2.90E-11
0.010	50	0.010	2.75E-12
0.010	100	0.010	4.62E-13
0.010	200	0.010	7.78E-14
0.010	500	0.010	7.37E-15
0.010	1000	0.010	1.24E-15

NOTES: 1 The volumetric moisture content is determined from Equation 6-22 to the Campbell data.
2 The predicted moisture content is determined from the minimization of the least squares using the EX Microsoft Excel Solver as explained in the text.

Table V-6a. Campbell Model Parameters for 10 mm Crushed Tuff [1]

Parameter	Value
Grain Diameter (d_g) (mm)	10
Saturated Volumetric Water Content (θ_S)	0.45
Air-entry water potential or the potential at which the largest water filled pores just drain ψ_{es} (J/kg)[2]	-0.158113883
Geometric Standard Deviation[3]	1
Slope of the ln(ψ) versus ln(θ) retention curve (b)[4]	0.516227766
ψ_{es} (Bars)	-0.001618173
ψ_{es} (cm)	-1.650787548

NOTES: [1] See text and Table 6-5 for a description of the parameters.
[2] This value is calculated from Equation 6.23.
[3] This value is estimated from Campbell (1985, p. 10, Figure 2.1)
[4] This value is calculated from Equation 6.24.

Table V-6b. Campbell Moisture Content Data for 10 mm Crushed Tuff

Moisture Potential (bars)	Moisture Content
0.0001	0.45
0.0002	0.450
0.0005	0.450
0.001	0.450
0.002	0.299
0.005	0.051
0.01	0.013
0.02	0.013
0.05	0.011
0.1	0.010
0.2	0.010
0.5	0.010
1	0.010
2	0.010
5	0.010
10	0.010
20	0.010
50	0.010
100	0.010
200	0.010
500	0.010
1000	0.010

Table V-7a. van Genuchten Curve Fit Parameters for 10 mm Crushed Tuff

Parameter	Value	Units
Moisture Content at Saturation (θs)	0.45	(no units)
Residual Moisture Content (θr)	0.01	(no units)
Alpha (α)	476.91	$bars^{-1}$
n	4.03	(no units)
m	0.75	(no units)

NOTES: The alpha parameter is also equal to 0.48 cm^{-1}.
The sum of the residuals is 3.42E-04.

Table V-7a. van Genuchten Curve Fit Parameters for 10 mm Crushed Tuff

Volumetric Moisture Content[1]	Moisture Potential (bars)	Predicted Moisture Content[2]	Residuals Squared
0.450	0.0001	0.450	2.51E-12
0.450	0.0002	0.450	6.65E-10
0.450	0.0005	0.449	1.06E-06
0.450	0.001	0.434	2.58E-04
0.285	0.002	0.290	1.87E-05
0.048	0.005	0.041	5.38E-05
0.013	0.01	0.014	1.59E-06
0.013	0.02	0.010	7.95E-06
0.011	0.05	0.010	2.80E-07
0.010	0.1	0.010	2.03E-08
0.010	0.2	0.010	1.42E-09
0.010	0.5	0.010	4.14E-11
0.010	1	0.010	2.84E-12
0.010	2	0.010	1.94E-13
0.010	5	0.010	5.57E-15
0.010	10	0.010	3.80E-16
0.010	20	0.010	2.59E-17
0.010	50	0.010	7.45E-19
0.010	100	0.010	5.08E-20
0.010	200	0.010	3.47E-21
0.010	500	0.010	9.95E-23
0.010	1000	0.010	6.79E-24

NOTES: [1] The volumetric moisture content is determined from Equation 6-22 to the Campbell data.
[2] The predicted moisture content is determined from the minimization of the least squares using the Microsoft Excel Solver as explained in the text.

Table V-8a. Campbell Model Parameters for 20 mm Crushed Tuff [1]

Grain Diameter (d_g) (mm)	20
Saturated Volumetric Water Content (θ_S)	0.45
Air-entry water potential or the potential at which the largest water filled pores just drain ψ_{es} (J/kg)[2]	-0.111803399
Geometric Standard Deviation[3]	1
Slope of the ln(ψ) versus ln(θ) retention curve (b)[4]	0.423606798
ψ_e (Bars)	-0.001139478
ψ_e (cm)	-1.162444233

NOTES: [1] See text and Table 6-5 for a description of the parameters.
[2] This value is calculated from Equation 6.23.
[3] This value is estimated from Campbell (1985, p. 10, Figure 2.1)
[4] This value is calculated from Equation 6.24.

Table V-8b. Campbell Moisture Content Data for 10 mm Crushed Tuff

Moisture Potential (bars)	Moisture Content
0.0001	0.4500000
0.0002	0.4500000
0.0005	0.4500000
0.001	0.4500000
0.002	0.1192454
0.005	0.0137099
0.01	0.0126693
0.02	0.0105197
0.05	0.0100598
0.1	0.0100116
0.2	0.0100023
0.5	0.0100003
1	0.0100001
2	0.0100000
5	0.0100000
10	0.0100000
20	0.0100000
50	0.0100000
100	0.0100000
200	0.0100000
500	0.0100000
1000	0.0100000

Table V-9a. van Genuchten Curve Fit Parameters for 20 mm Crushed Tuff

Parameter	Value	Units
Moisture Content at Saturation (θs)	0.45	(no units)
Residual Moisture Content (θr)	0.01	(no units)
Alpha (α)	561.61	$bars^{-1}$
n	11.11	(no units)
m	0.91	(no units)

NOTES: The alpha parameter is also equal to 0.56 cm^{-1}.
The sum of the residuals is 1.86E-05.

Table V-9a. van Genuchten Curve Fit Parameters for 20 mm Crushed Tuff

Volumetric Moisture Content[1]	Moisture Potential (bars)	Predicted Moisture Content[2]	Residuals Squared
0.450	0.0001	0.450	2.55E-29
0.450	0.0002	0.450	1.25E-22
0.450	0.0005	0.450	8.78E-14
0.450	0.001	0.449	4.30E-07
0.119	0.002	0.119	3.53E-10
0.014	0.005	0.010	1.08E-05
0.013	0.01	0.010	5.10E-06
0.011	0.02	0.010	1.20E-08
0.010	0.05	0.010	1.23E-07
0.010	0.1	0.010	1.59E-07
0.010	0.2	0.010	1.66E-07
0.010	0.5	0.010	1.68E-07
0.010	1	0.010	1.68E-07
0.010	2	0.010	1.68E-07
0.010	5	0.010	1.68E-07
0.010	10	0.010	1.68E-07
0.010	20	0.010	1.68E-07
0.010	50	0.010	1.68E-07
0.010	100	0.010	1.68E-07
0.010	200	0.010	1.68E-07
0.010	500	0.010	1.68E-07
0.010	1000	0.010	1.68E-07

NOTES: [1] The volumetric moisture content is determined from Equation 6-22 to the Campbell data.
[2] The predicted moisture content is determined from the minimization of the least squares using the Microsoft Excel Solver as explained in the text.

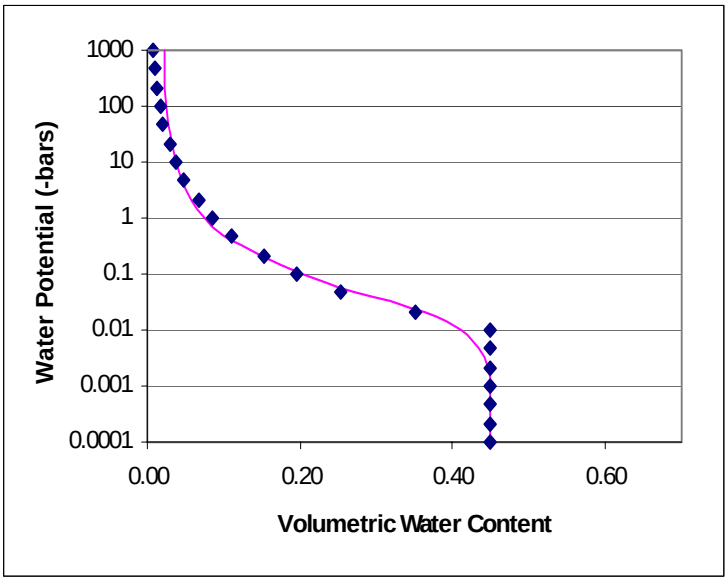

Figure V-1. Comparison of Data to Curve Fit Campbell Model (0.317 mm)

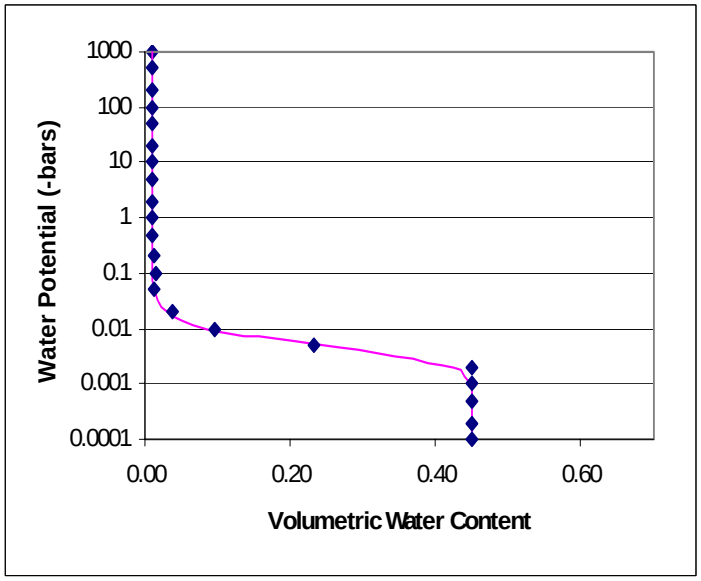

Figure V-2. Comparison of Data to Curve Fit Campbell Model (3 mm)

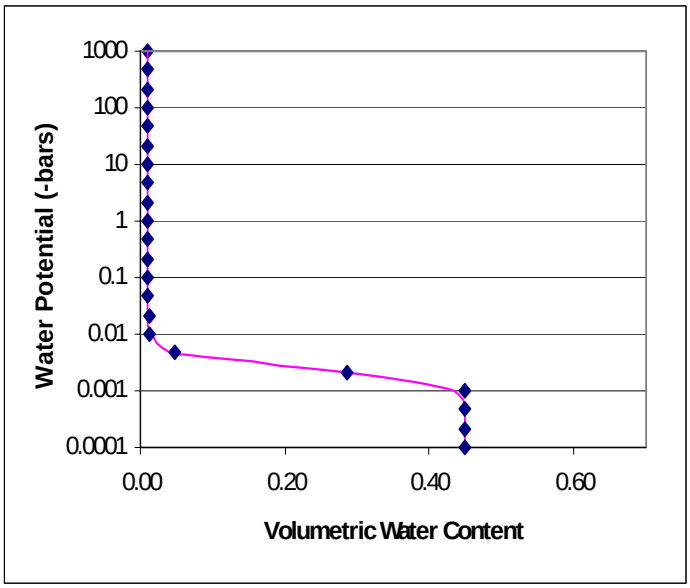

Figure V-3. Comparison of Data to Curve Fit Campbell Model (10 mm)

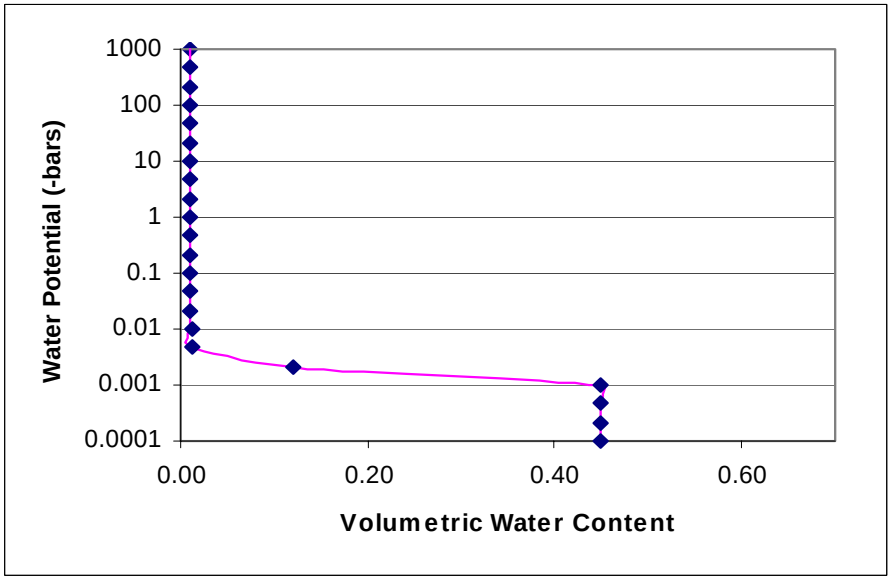

Figure V-4. Comparison of Data to Curve Fit Campbell Model (20 mm)

INTENTIONALLY LEFT BLANK

ATTACHMENT VI

DERIVATION OF INVERT "PACKED BED" PROPERTIES FROM BROOKS AND COREY DATA

INTENTIONALLY LEFT BLANK

Attachment VI - Derivation of Invert "Packed Bed" Properties from Brooks and Corey Data

This attachment uses the nondimensional form for the capillary pressure curve presented by Leverett (1941, p. 159) with the capillary pressure data generated by Brooks and Corey (1964) to provide a capillary pressure curve for the invert. The nondimensionalized data is then used to fit with a van Genutchen relationship (Equation 6-22) for use in developing retention curves for the coarse intergranular porosity of the invert.

The invert will consist of crushed tuff, probably supplied from the drift itself, crushed to a size of fine gravel to coarse "sand." The analysis using NUFT presented in Section 6.6 requires the permeability, capillary pressure, and relative permeability of the interparticle void space. Because the invert particle diameter is not fixed, a means of computing these properties as a function of particle diameter is desired.

VI.1 DEVELOPMENT OF PERMEABILITY AND RETENTION RELATIONSHIPS FOR THE INTERGRANULAR POROSITY

The permeability is supplied by the Kozeny-Carman equation (Bear 1972, p. 166). This equation relates the permeability to the mean particle diameter and the porosity. The mean particle diameter used in this analysis is based upon the specific surface area of the particle size distribution.

The dependence of the capillary pressure curve on particle diameter and porosity is analyzed in the same manner as Leverett (1941, p. 159). Leverett showed that capillary pressure data for various sands could be correlated using a nondimensional group that included the mean particle diameter and the porosity. This approach is applied to the data published by Brooks and Cory (1964) to produce a nondimensional capillary pressure/saturation curve (Brooks and Cory 1964). This nondimensional data is then fitted with the functional form posed by van Genuchten (1980, Equation 21).

The relative permeability is based upon the work of Mualem, as reported by van Genuchten (1980). Maulem developed a semi-empirical relationship between the capillary pressure curve and the relative permeability curve. Maulem's correlation coefficient is combined with the fit of the nondimensional capillary pressure to produce a liquid relative permeability curve appropriate for the invert interparticle porosity. The relative permeability of the gas phase is set to unity in anticipation of the very low interparticle saturation anticipated in the invert.

Specifically, the Brooks and Corey (1964) database (Attachment VI) for unconsolidated particulate media is most applicable to the proposed invert configuration. Both are composed of particles that are not consolidated together. Angularity of the particulate will be reflected in the data for sands. This, of course, presumes that the invert "rock" is "roughly" spherical, as opposed to a plate-like shape.

The assumed bed porosity should provide everything needed.

Input the properties for the four materials from Attachment VI (Brooks and Corey 1964, Appendix III and Table 1):

VS :=

	0	1
0	12.000	0.990
1	13.500	0.986
2	14.500	0.980
3	15.500	0.974
4	16.000	0.948
5	17.000	0.895
6	17.200	0.875

FS :=

	0	1
0	12.800	0.990
1	27.800	0.980
2	30.800	0.962
3	31.800	0.950
4	34.800	0.926
5	36.800	0.901
6	39.800	0.855

GB :=

	0	1
0	5.900	0.995
1	11.800	0.989
2	17.800	0.985
3	23.800	0.980
4	26.900	0.971
5	28.800	0.938

TSL :=

	0	1
0	32.800	0.998
1	42.800	0.995
2	52.800	0.992
3	62.800	0.984
4	67.800	0.978
5	72.500	0.967

Note that only the first few values are printed out in the Mathcad format.

Input the intrinsic permeability and porosity:

$$\begin{pmatrix} k_{VS} \\ k_{FS} \\ k_{FM} \\ k_{GB} \\ k_{TSL} \\ k_{FFH} \end{pmatrix} := \begin{pmatrix} 18 \\ 2.5 \\ 11.3 \\ 6.3 \\ 0.6 \\ 30 \end{pmatrix} \cdot \left(10^{-6} \cdot m\right)^2 \qquad \text{(Eq. VI-1)}$$

According to Brooks and Corey (1964, p. 9, Equation 17), the capillary rise of water was about twice that of the hydrocarbon used in the measurements. van Genuchten (1980) used the same factor in his analysis.

$$\begin{pmatrix} VS^{\langle 1\rangle} \\ FS^{\langle 1\rangle} \\ FM^{\langle 1\rangle} \\ GB^{\langle 1\rangle} \\ TSL^{\langle 1\rangle} \\ FFH^{\langle 1\rangle} \end{pmatrix} := \begin{pmatrix} VS^{\langle 1\rangle}\cdot 2 \\ FS^{\langle 1\rangle}\cdot 2 \\ FM^{\langle 1\rangle}\cdot 2 \\ GB^{\langle 1\rangle}\cdot 2 \\ TSL^{\langle 1\rangle}\cdot 2 \\ FFH^{\langle 1\rangle}\cdot 2 \end{pmatrix} \qquad \text{(Eq. VI-2)}$$

To completely specify the problem, we need the surface tension. Because Brooks and Corey (1964) do not specify surface tension or temperature, use an ambient temperature to represent laboratory conditions. Input the surface tension of 72 dynes/cm. The water density is set to 998 kg/m^3 (Incropera and DeWitt 1996, p. 846):

$$\sigma_w := 72\cdot\frac{dyne}{cm}$$

$$\rho := 998\cdot\frac{kg}{m^3}$$

$$\sigma_{HC} := \frac{\sigma_w}{2}$$

VI.2 DATA FITTING

In the following analysis, curve fits are developed for the four materials separately for comparison to the measured retention data. A function representing the van Genuchten function is defined. Error functions are defined that for a set of van Genuchten parameters (α, n, S_r) provide a summation of the residuals squared between the predicted value for capillary pressure, and the measured capillary pressure. After defining the error function, the Mathcad Minerr function is used to calculate the set of van Genuchten parameters (α, n, S_r) that minimizes the sum of the residuals squared. Define a vector of points for plotting purposes:

$$f_{plot} := \left| \begin{array}{l} \text{for } i \in 1..9999 \\ \quad s_i \leftarrow \dfrac{i}{10000} \\ s \end{array} \right. \qquad \text{(Eq. VI-3)}$$

The van Genuchten's fitting function (van Genuchten 1980, Equation 21) is:

$$\theta = \theta_r + \frac{\left(\theta_s - \theta_r\right)}{\left[1 + (\psi \cdot \alpha)^n\right]^m} \quad \text{(Eq. VI-4)}$$

van Genuchten includes the residual saturation in the fit. The van Genuchten m parameter is defined in terms of n (van Genuchten 1980, Equation 22):

$$m = 1 - \frac{1}{n} \quad \text{(Eq. VI-5)}$$

Equation VI-5 can be rewritten as follows to solve for the exponent:

$$\frac{1}{m} = \frac{n}{n-1} \quad \text{(Eq. VI-6)}$$

$$\frac{-1}{m} = \frac{n}{1-n} \quad \text{(Eq. VI-7)}$$

Substituting in the value of m into Equation VI-4:

$$\theta = \theta_r + \frac{\left(\theta_s - \theta_r\right)}{\left[1 + (\psi \cdot \alpha)^n\right]^{1-\frac{1}{n}}} \quad \text{(Eq. VI-8)}$$

Define the values for saturation:

$$S_s = \frac{\theta_s}{\theta_s}$$

$$S_s = 1$$

By definition, the value of Ss at saturation is one:

$$\theta = S \cdot \theta_s$$

$$\theta_r = S_r \cdot \theta_s$$

Substitute these definitions into Equation VI-5:

$$S \cdot \theta_s = S_r \cdot \theta_s + \frac{\left[-\theta_s \cdot \left(-1 + S_r\right)\right]}{\left[\left[1 + (\psi \cdot \alpha)^n\right]^{\left(1 - \frac{1}{n}\right)}\right]} \quad \text{(Eq. VI-9)}$$

Factor out θs from both sides of the equation:

$$S = S_r + \frac{\left[-1 \cdot \left(-1 + S_r\right)\right]}{\left[\left[1 + (\psi \cdot \alpha)^n\right]^{\left(1 - \frac{1}{n}\right)}\right]} \quad \text{(Eq. VI-10)}$$

Restating the equation:

$$\frac{S - S_r}{1 - S_r} = \frac{1}{\left[\left[1 + (\psi \cdot \alpha)^n\right]^{\left(1 - \frac{1}{n}\right)}\right]} \quad \text{(Eq. VI-11)}$$

Solve for the value of moisture potential as a function of saturation (S):

$$\left[\left[1 + (\psi \cdot \alpha)^n\right]^{\left(1 - \frac{1}{n}\right)}\right] = \frac{\left(1 - S_r\right)}{S - S_r} \quad \text{(Eq. VI-12)}$$

$$\left[\left[1 + (\psi \cdot \alpha)^n\right]^{\frac{n-1}{n}}\right] = \frac{\left(1 - S_r\right)}{S - S_r} \quad \text{(Eq. VI-13)}$$

$$\left[1 + (\psi \cdot \alpha)^n\right] = \left[\frac{\left(S - S_r\right)}{1 - S_r}\right]^{\frac{n}{n-1}} \quad \text{(Eq. VI-14)}$$

$$(\psi \cdot \alpha)^n = \left[\frac{\left(S - S_r\right)}{1 - S_r}\right]^{\frac{n}{n-1}} - 1$$

Solving for the moisture potential in terms of the satuation, and defining a function for the moisture potential:

$$G(S, S_r, \alpha, n) := \frac{1}{\alpha} \cdot \left[\left(\frac{S - S_r}{1 - S_r} \right)^{\frac{n}{1-n}} - 1 \right]^{\frac{1}{n}} \quad \text{(Eq. VI-15)}$$

VI.2.1 Volcanic Sand

Define a function in terms of the van Genuchten parameters that represents the sum of the residuals squared between the measured capillary pressure and the predicted capillary pressure for the volcanic sand:

$$error(Sr, \alpha, n) := \sum_{i=1}^{rows(VS)} \left[\left(G(VS_{i,2}, Sr, \alpha, n) - VS_{i,1} \right)^2 \right] \quad \text{(Eq. VI-16)}$$

Define an initial estimate of the parameters:

$$\begin{pmatrix} Sr \\ \alpha \\ n \end{pmatrix} := \begin{pmatrix} 0.1 \\ 0.02 \\ 6 \end{pmatrix} \quad \text{(Eq. VI-17)}$$

Use the Minerr function to obtain the lease squares fit to the volcanic sand data:

Given

$$error(Sr, \alpha, n) = 0 \quad \text{(Eq. VI-18)}$$

$$\begin{pmatrix} Sr_{VS} \\ \alpha_{VS} \\ n_{VS} \end{pmatrix} := Minerr(Sr, \alpha, n) \quad \text{(Eq. VI-19)}$$

$$\begin{pmatrix} Sr_{VS} \\ \alpha_{VS} \\ n_{VS} \end{pmatrix} = \begin{pmatrix} 0.156 \\ 0.021 \\ 4.413 \end{pmatrix} \quad \text{(Eq. VI-20)}$$

Output the sum of the residuals squared:

$$\text{error}\left(Sr_{VS}, \alpha_{VS}, n_{VS}\right) = 536.779 \quad \text{(Eq. VI-21)}$$

Define a function for plotting purposes:

$$Splot_{VS} := Sr_{VS} + \left(1 - Sr_{VS}\right) \cdot f_{plot} \quad \text{(Eq. VI-22)}$$

VI.2.2 Fine Sand

Define a function in terms of the van Genuchten parameters that represents the sum of the residuals squared between the measured capillary pressure and the predicted capillary pressure for the fine sand:

$$\text{error}(Sr, \alpha, n) := \sum_{i=1}^{\text{rows}(FS)} \left[\left(G\left(FS_{i,2}, Sr, \alpha, n\right) - FS_{i,1}\right)^2\right] \quad \text{(Eq. VI-23)}$$

Define an initial estimate of the parameters:

$$\begin{pmatrix} Sr \\ \alpha \\ n \end{pmatrix} := \begin{pmatrix} 0.01 \\ 0.1 \\ 2 \end{pmatrix}$$

Use the Minerr function to obtain the lease squares fit to the fine sand data:

Given

$$\text{error}(Sr, \alpha, n) = 0 \quad \text{(Eq. VI-24)}$$

$$\begin{pmatrix} Sr_{FS} \\ \alpha_{FS} \\ n_{FS} \end{pmatrix} := \text{Minerr}(Sr, \alpha, n) \quad \text{(Eq. VI-25)}$$

$$\begin{pmatrix} Sr_{FS} \\ \alpha_{FS} \\ n_{FS} \end{pmatrix} = \begin{pmatrix} 0.170 \\ 0.010 \\ 5.664 \end{pmatrix} \quad \text{(Eq. VI-26)}$$

Output the sum of the residuals squared:

$$error\left(Sr_{FS}, \alpha_{FS}, n_{FS}\right) = 675.283 \quad \text{(Eq. VI-27)}$$

Define a function for plotting purposes:

$$Splot_{FS} := Sr_{FS} + \left(1 - Sr_{FS}\right) \cdot f_{plot} \quad \text{(Eq. VI-28)}$$

VI.2.3 Glass Beads

Define a function in terms of the van Genuchten parameters that represents the sum of the residuals squared between the measured capillary pressure and the predicted capillary pressure for the glass beads:

$$error(Sr, \alpha, n) := \sum_{i=1}^{rows(GB)} \left[\left(G\left(GB_{i,2}, Sr, \alpha, n\right) - GB_{i,1}\right)^2\right] \quad \text{(Eq. VI-29)}$$

Define an initial estimate of the parameters:

$$\begin{pmatrix} Sr \\ \alpha \\ n \end{pmatrix} := \begin{pmatrix} 0.01 \\ 0.03 \\ 7 \end{pmatrix} \quad \text{(Eq. VI-30)}$$

Use the Minerr function to obtain the lease squares fit to the glass beads data:

Given

$$error(Sr, \alpha, n) = 0$$

$$\begin{pmatrix} Sr_{GB} \\ \alpha_{GB} \\ n_{GB} \end{pmatrix} := Minerr(Sr, \alpha, n) \quad \text{(Eq. VI-31)}$$

$$\begin{pmatrix} Sr_{GB} \\ \alpha_{GB} \\ n_{GB} \end{pmatrix} = \begin{pmatrix} 0.096991 \\ 0.016780 \\ 8.122966 \end{pmatrix} \quad \text{(Eq. VI-32)}$$

Output the sum of the residuals squared:

$$error\left(Sr_{GB}, \alpha_{GB}, n_{GB}\right) = 2.472 \times 10^{3} \quad \text{(Eq. VI-33)}$$

Define a function for plotting purposes:

$$Splot_{GB} := Sr_{GB} + \left(1 - Sr_{GB}\right) \cdot f_{plot} \quad \text{(Eq. VI-34)}$$

VI.2.4 Touchet Silt Loam

Define a function in terms of the van Genuchten parameters that represents the sum of the residuals squared between the measured capillary pressure and the predicted capillary pressure for the Touchet silt loam:

$$error(Sr, \alpha, n) := \sum_{i=1}^{rows(TSL)} \left[\left(G\left(TSL_{i,2}, Sr, \alpha, n\right) - TSL_{i,1}\right)^{2}\right] \quad \text{(Eq. VI-35)}$$

Define an initial estimate of the parameters:

$$\begin{pmatrix} Sr \\ \alpha \\ n \end{pmatrix} := \begin{pmatrix} 0.001 \\ 0.01 \\ 3 \end{pmatrix} \quad \text{(Eq. VI-36)}$$

Use the Minerr function to obtain the lease squares fit to the Touchet silt loam data:

Given

$$error(Sr, \alpha, n) = 0 \quad \text{(Eq. VI-37)}$$

$$\begin{pmatrix} Sr_{TSL} \\ \alpha_{TSL} \\ n_{TSL} \end{pmatrix} := Minerr(Sr, \alpha, n) \quad \text{(Eq. VI-38)}$$

$$\begin{pmatrix} Sr_{TSL} \\ \alpha_{TSL} \\ n_{TSL} \end{pmatrix} = \begin{pmatrix} 0.360 \\ 4.775 \times 10^{-3} \\ 5.808 \end{pmatrix} \quad \text{(Eq. VI-39)}$$

Output the sum of the residuals squared:

$$\text{error}\left(Sr_{TSL}, \alpha_{TSL}, n_{TSL}\right) = 1.872 \times 10^{3} \quad \text{(Eq. VI-40)}$$

Define a function for plotting purposes:

$$Splot_{TSL} := Sr_{TSL} + \left(1 - Sr_{TSL}\right) \cdot f_{plot} \quad \text{(Eq. VI-41)}$$

The data sets have now been fitted individually. The residual saturation (Sr) for each set is inferred from the data. The results of the analysis are presented in Figure VI-1.

VI.2.5 Nondimensional Capillary Pressure Correlation Using Leverett's Nondimensional Group

The next analysis applies Leverett's nondimensional group (Leverett 1941, p. 159) to the four data sets. It collapses the data reasonably well, with the volcanic sand providing the major deviation from the group. It compares favorably with Leverett's drainage curve for clean unconsolidated sands (Leverett 1941, Figure 4).

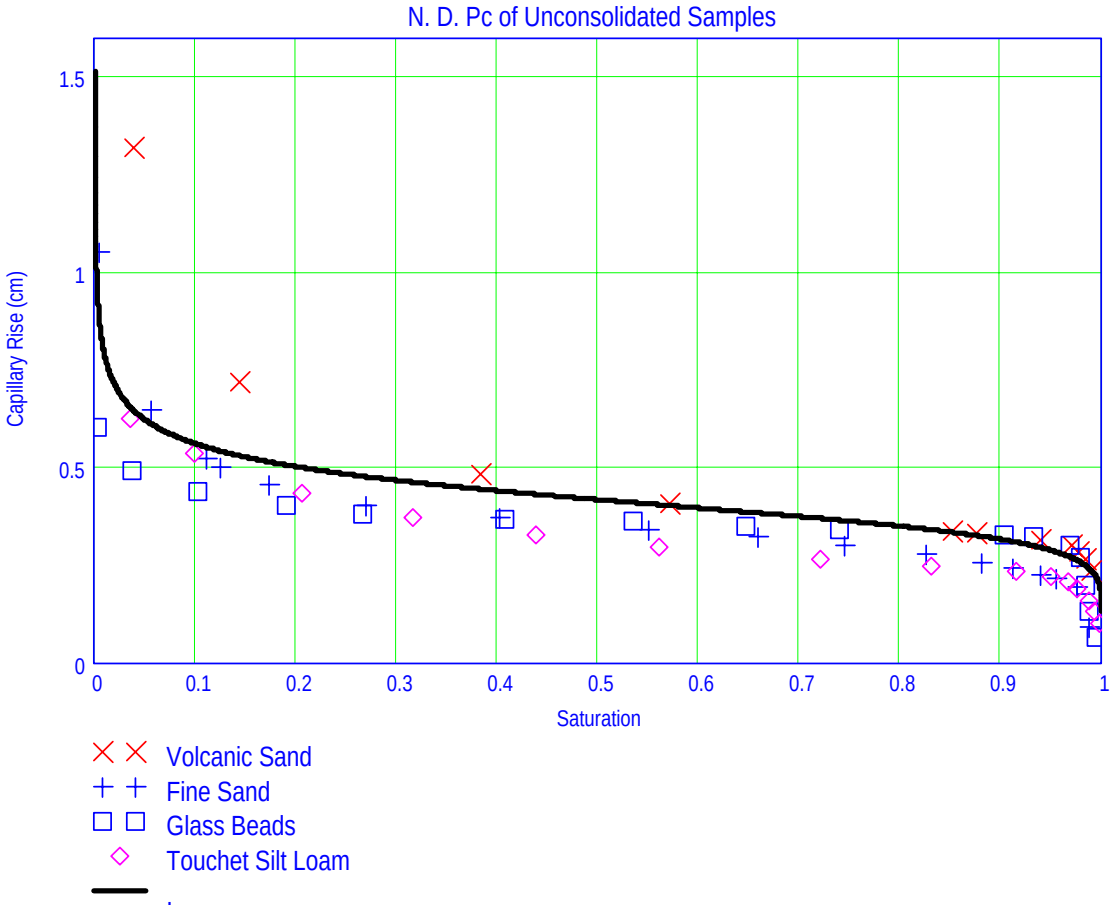

Figure VI-1. Capillary Rise of Unconsolidated Samples

Composite Set

Define the function using the := notation for assigning a function:

$$G2\left(S_{eff}, \alpha, n\right) := \frac{1}{\alpha}\cdot\left(S_{eff}^{\frac{n}{1-n}} - 1\right)^{\frac{1}{n}} \qquad \text{(Eq. VI-42)}$$

Define the nondimensional parameter for analysis (Leverett 1941, p. 159).

$$G2 = \frac{P_c}{\sigma_w}\cdot\sqrt{\frac{k}{\phi}} \qquad \text{(Eq. VI-43)}$$

Define a function in terms of the dimensionless capillary pressure and the nondimensional van Genuchten parameters that represents the sum of the residuals squared between the measured dimensionless capillary pressure and the predicted dimensionless capillary pressure for all data sets:

$$\begin{aligned} error(\alpha, n) := & \sum_{i=1}^{rows(VS)} \left[\left[G2\left(\frac{VS_{i,2} - Sr_{VS}}{1 - Sr_{VS}}, \alpha, n\right) - \left(\frac{VS_{i,1}\cdot cm\cdot\rho\cdot g}{\sigma_w}\cdot\sqrt{\frac{k_{VS}}{\phi_{VS}}}\right)\right]^2\right] \ldots \\ & + \sum_{i=1}^{rows(FS)} \left[\left[G2\left(\frac{FS_{i,2} - Sr_{FS}}{1 - Sr_{FS}}, \alpha, n\right) - \left(\frac{FS_{i,1}\cdot cm\cdot\rho\cdot g}{\sigma_w}\cdot\sqrt{\frac{k_{FS}}{\phi_{FS}}}\right)\right]^2\right] \ldots \\ & + \sum_{i=1}^{rows(GB)} \left[\left[G2\left(\frac{GB_{i,2} - Sr_{GB}}{1 - Sr_{GB}}, \alpha, n\right) - \left(\frac{GB_{i,1}\cdot cm\cdot\rho\cdot g}{\sigma_w}\cdot\sqrt{\frac{k_{GB}}{\phi_{GB}}}\right)\right]^2\right] \ldots \\ & + \sum_{i=1}^{rows(TSL)} \left[\left[G2\left(\frac{TSL_{i,2} - Sr_{TSL}}{1 - Sr_{TSL}}, \alpha, n\right) - \left(\frac{TSL_{i,1}\cdot cm\cdot\rho\cdot g}{\sigma_w}\cdot\sqrt{\frac{k_{TSL}}{\phi_{TSL}}}\right)\right]^2\right] \end{aligned} \qquad \text{(Eq. VI-44)}$$

$$i := 1 .. rows(VS)$$

Define an initial estimate of the parameters:

$$\begin{pmatrix} \alpha \\ n \end{pmatrix} := \begin{pmatrix} 4 \\ 2.3 \end{pmatrix} \qquad \text{(Eq. VI-45)}$$

Use the Minerr function to obtain the lease squares fit to the volcanic sand data:

$$\text{Given}$$

$$\text{error}(\alpha, n) = 0 \qquad \text{(Eq. VI-46)}$$

$$\begin{pmatrix} \alpha_{comp} \\ n_{comp} \end{pmatrix} := \text{Minerr}(\alpha, n) \qquad \text{(Eq. VI-47)}$$

$$\begin{pmatrix} \alpha_{comp} \\ n_{comp} \end{pmatrix} = \begin{pmatrix} 2.455 \\ 8.013 \end{pmatrix} \qquad \text{(Eq. VI-48)}$$

Output the sum of the residuals squared:

$$j := 1 .. \text{rows}(FS)$$

$$k := 1 .. \text{rows}(GB)$$

$$\text{error}(\alpha_{comp}, n_{comp}) = 4.054 \qquad \text{(Eq. VI-49)}$$

Define a function for plotting purposes:

$$Splot_{comp} := f_{plot}$$

$$l := 1 .. \text{rows}(TSL) \qquad \text{(Eq. VI-50)}$$

The results of the analysis are presented in Figure VI-2.

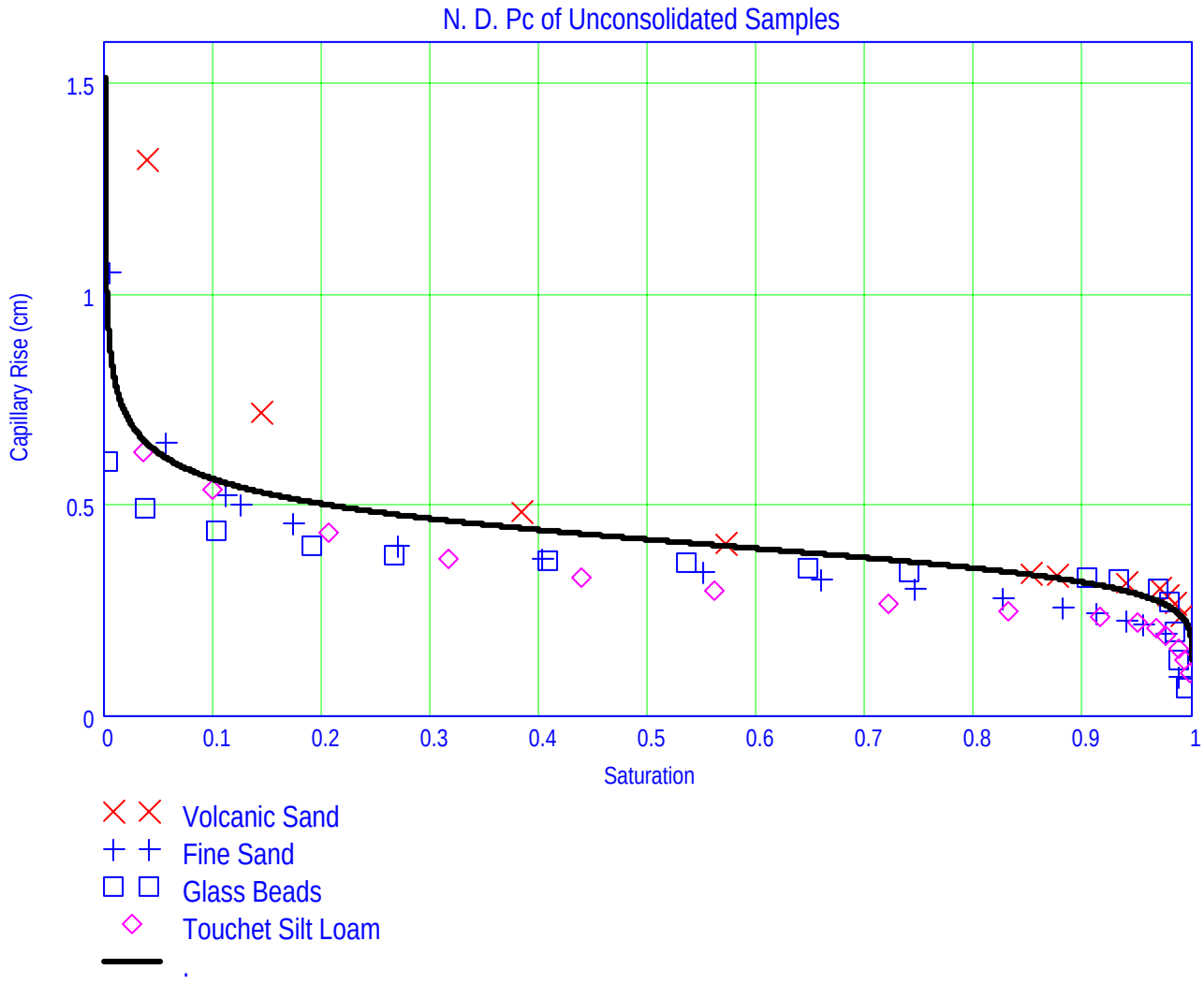

Figure VI-2. Nondimensional Capillary Pressure for Unconsolidated Samples

INTENTIONALLY LEFT BLANK

ATTACHMENT VII

VERIFICATION OF THE MATHCAD CALCULATIONS USING MICROSOFT EXCEL

INTENTIONALLY LEFT BLANK

Attachment VII - Verification of the Mathcad Calculations Using Microsoft Excel

This attachment presents an independent verification of the Mathcad 2001 Professional error functions presented in Attachment VI that are used for curve fitting to volcanic sand, fine sand, glass beads, and Touchet silt loam individually, and then collectively by transforming the capillary rise data to a nondimensional capillary rise. Microsoft Excel is used to perform curve fitting to the van Genuchten retention relationship. The Solver is an add-in function in Microsoft Excel. The Solver can minimize a target cell that involves multiple cell variables that might be subject to multiple constraints. The Solver is used specifically to solve for several variables under the constraint for a target value. In this case, the minimization of the least squares of the capillary rise is the target value for curve fitting. Tables VII-1 through VII-4 present individual curve fits to the data for volcanic sand, fine sand, glass beads, and Touchet silt loam from the measurements by Brooks and Corey (1964, Appendix 3, Table 1), as presented in Attachment VI. The results of the Microsoft Excel analysis for these materials are in agreement with the Mathcad 2001 Professional results presented in Attachment VI.

The nondimensional curve fit presented in Attachment VI requires identification of the porosity and permeability of each of these materials (Attachment VI, Figure VI-2), and the properties of water. Table VII-5 presents these properties (Incropera and DeWitt 1996, p. 846). The van Genuchten curve fit parameters are presented in Table VII-6. Table VII-7 presents the nondimensionalized data used to determine the van Genuchten parameters.

Table VII-1a. van Genuchten Curve Fit Parameters for Volcanic Sand

Parameter	Value	Units
Saturation at Complete Saturation	1.000	(no units)
Residual Saturation (Sr)	0.156	(no units)
Alpha (α)	0.021	$bars^{-1}$
n	4.413	(no units)
m	0.773	(no units)

NOTES: The sum of the residuals is 5.37E+02.

Table VII-1b. Retention Analysis for Volcanic Sand

Saturation	Capillary Rise [1] (cm)	Predicted Capillary [2] Rise	Residuals Squared
0.99	24	1.89E+01	2.60E+01
0.986	27	2.04E+01	4.33E+01
0.98	29	2.22E+01	4.65E+01
0.974	31	2.36E+01	5.50E+01
0.948	32	2.78E+01	1.74E+01
0.895	34	3.32E+01	5.95E-01
0.875	34.4	3.48E+01	1.73E-01
0.638	42	4.92E+01	5.24E+01
0.479	49.6	5.95E+01	9.90E+01
0.277	73.8	8.41E+01	1.06E+02
0.188	135.4	1.26E+02	9.03E+01
0.158	273.2	2.73E+02	5.61E-02

NOTES: [1]The capillary pressure is determined from Equation 6-22.
[2]The capillary rise is determined from the minimization of the least squares using the Microsoft Excel Solver as explained in the text.

Table VII-2a. van Genuchten Curve Fit Parameters for Fine Sand

Parameter	Value	Units
Saturation at Complete Saturation	1.000	(no units)
Residual Saturation (Sr)	0.170	(no units)
Alpha (α)	0.010	$bars^{-1}$
n	5.664	(no units)
m	0.823	(no units)

NOTES: The sum of the residuals is 6.75E+02.

Table VII-2b. Retention Analysis for Fine Sand

Saturation	Capillary Rise [1] (cm)	Predicted Capillary Rise [2]	Residuals Squared
0.99	25.6	4.53E+01	3.90E+02
0.98	55.6	5.14E+01	1.79E+01
0.962	61.6	5.78E+01	1.46E+01
0.95	63.6	6.08E+01	7.66E+00
0.926	69.6	6.56E+01	1.61E+01
0.901	73.6	6.95E+01	1.67E+01
0.855	79.6	7.53E+01	1.84E+01
0.788	85.6	8.22E+01	1.17E+01
0.716	91.6	8.87E+01	8.50E+00
0.627	97.6	9.64E+01	1.41E+00
0.503	105.6	1.08E+02	6.12E+00
0.393	115.4	1.21E+02	3.66E+01
0.314	129.6	1.36E+02	3.79E+01
0.273	143.4	1.47E+02	1.31E+01
0.262	148.8	1.51E+02	4.48E+00
0.217	184.2	1.76E+02	7.44E+01
0.174	300.2	3.00E+02	4.31E-02

NOTES: [1] The capillary pressure is determined from Equation 6-22.
[2] The capillary rise is determined from the minimization of the least squares using the Microsoft Excel Solver as explained in the text.

Table VII-3a. van Genuchten Curve Fit Parameters for Glass Beads

Parameter	Value	Units
Saturation at Complete Saturation	1.000	(no units)
Residual Saturation (Sr)	0.096	(no units)
Alpha (α)	0.016	$bars^{-1}$
n	10.271	(no units)
m	0.903	(no units)

NOTES: The sum of the residuals is 1.33E+03.

Table VII-3b. Retention Analysis for Glass Beads

Saturation	Capillary Rise [1] (cm)	Predicted Capillary Rise [2]	Residuals Squared
0.995	11.8	3.71E+01	6.40E+02
0.989	23.6	4.01E+01	2.72E+02
0.985	35.6	4.13E+01	3.28E+01
0.98	47.6	4.25E+01	2.58E+01
0.971	53.8	4.41E+01	9.34E+01
0.938	57.6	4.77E+01	9.77E+01
0.912	58.6	4.95E+01	8.23E+01
0.764	60.8	5.57E+01	2.64E+01
0.681	62	5.81E+01	1.52E+01
0.579	64.2	6.09E+01	1.09E+01
0.465	65.4	6.41E+01	1.69E+00
0.337	67.8	6.84E+01	4.04E-01
0.269	71.4	7.15E+01	1.96E-02
0.19	78	7.71E+01	8.57E-01
0.13	87.6	8.65E+01	1.21E+00
0.099	107	1.13E+02	3.21E+01
0.097	300.8	1.27E+02	3.03E+04

NOTES: [1] The capillary pressure is determined from Equation 6-22.
[2] The capillary rise is determined from the minimization of the least squares using the Microsoft Excel Solver as explained in the text.

TableVII-4a. van Genuchten Curve Fit Parameters for Touchet Silt Loam

Parameter	Value
Saturation at Complete Saturation	1.000
Residual Saturation(Sr)	0.360
Alpha (α) (1/cm)	4.775E-03
n	5.808
m	0.828

TableVII-4a. van Genuchten Retention Analysis Results

Saturation	Capillary Rise [1] (cm)	Predicted Capillary Rise [2]	Residuals Squared
0.998	65.6	8.02E+01	2.13E+02
0.995	85.6	9.40E+01	7.02E+01
0.992	105.6	1.02E+02	1.30E+01
0.984	125.6	1.15E+02	1.08E+02
0.978	135.6	1.22E+02	1.87E+02
0.967	145	1.31E+02	1.91E+02
0.946	155.6	1.44E+02	1.41E+02
0.892	164.6	1.65E+02	1.49E-01
0.821	175.4	1.85E+02	9.21E+01
0.719	195.6	2.10E+02	2.03E+02
0.641	215.2	2.30E+02	2.07E+02
0.562	246	2.54E+02	5.65E+01
0.492	285.2	2.83E+02	4.63E+00
0.424	354	3.35E+02	3.67E+02
0.383	414.4	4.19E+02	1.83E+01

NOTES: [1] The capillary pressure is determined from Equation 6-22.
[2] The capillary rise is determined from the minimization of the least squares using the Microsoft Excel Solver as explained in the text.

Table VII-5. Properties Used in the Analysis

Parameter	Symbol	Value	Unit
Water Density	ρ	998	kg/m^3
Acceleration	g	9.802	m/sec^2
Surface Tension	σ_w	72	dynes/cm

Table VII-6. van Genuchten Curve Fit Parameters

Parameter	Symbol	Value
Saturation at Complete Saturation		1.000
van Genuchten Alpha (α) (1/cm)	α	2.459E+00
n	n	8.013
m	m	0.875

Table VII-7. Nondimensional Retention Analysis

Material[1]	Saturation	Effective Saturation[2]	Capillary Rise(cm) Hydrocarbon	Capillary Rise(cm) Water[3]	Nondimensional Capillary Rise	Predicted Nondimensional Capillary Rise	Residuals Squared
Verification			1.20E+01	2.40E+01	2.34E-01		
Volcanic Sand	9.90E-01	9.88E-01	1.20E+01	2.40E+01	2.34E-01	2.38E-01	2.14E-05
	9.86E-01	9.83E-01	1.35E+01	2.70E+01	2.63E-01	2.49E-01	2.01E-04
	9.80E-01	9.76E-01	1.45E+01	2.90E+01	2.82E-01	2.60E-01	4.88E-04
	9.74E-01	9.69E-01	1.55E+01	3.10E+01	3.02E-01	2.69E-01	1.06E-03
	9.48E-01	9.38E-01	1.60E+01	3.20E+01	3.11E-01	2.95E-01	2.82E-04
	8.95E-01	8.76E-01	1.70E+01	3.40E+01	3.31E-01	3.25E-01	3.89E-05
	8.75E-01	8.52E-01	1.72E+01	3.44E+01	3.35E-01	3.33E-01	3.13E-06
	6.38E-01	5.71E-01	2.10E+01	4.20E+01	4.09E-01	4.01E-01	5.48E-05
	4.79E-01	3.83E-01	2.48E+01	4.96E+01	4.83E-01	4.43E-01	1.54E-03
	2.77E-01	1.43E-01	3.69E+01	7.38E+01	7.18E-01	5.29E-01	3.58E-02
	1.88E-01	3.79E-02	6.77E+01	1.35E+02	1.32E+00	6.47E-01	4.50E-01
	1.58E-01	2.37E-03	1.37E+02	2.73E+02	2.66E+00	9.63E-01	2.87E+00
Fine Sand	9.90E-01	9.88E-01	1.28E+01	2.56E+01	8.96E-02	2.39E-01	2.22E-02
	9.80E-01	9.76E-01	2.78E+01	5.56E+01	1.95E-01	2.61E-01	4.37E-03
	9.62E-01	9.54E-01	3.08E+01	6.16E+01	2.16E-01	2.83E-01	4.58E-03
	9.50E-01	9.40E-01	3.18E+01	6.36E+01	2.23E-01	2.94E-01	5.06E-03
	9.26E-01	9.11E-01	3.48E+01	6.96E+01	2.44E-01	3.10E-01	4.38E-03
	9.01E-01	8.81E-01	3.68E+01	7.36E+01	2.58E-01	3.23E-01	4.24E-03
	8.55E-01	8.25E-01	3.98E+01	7.96E+01	2.78E-01	3.41E-01	3.95E-03
	7.88E-01	7.45E-01	4.28E+01	8.56E+01	2.99E-01	3.63E-01	4.02E-03
	7.16E-01	6.58E-01	4.58E+01	9.16E+01	3.20E-01	3.83E-01	3.87E-03
	6.27E-01	5.51E-01	4.88E+01	9.76E+01	3.41E-01	4.06E-01	4.11E-03
	5.03E-01	4.01E-01	5.28E+01	1.06E+02	3.69E-01	4.39E-01	4.82E-03
	3.93E-01	2.69E-01	5.77E+01	1.15E+02	4.04E-01	4.75E-01	5.13E-03
	3.14E-01	1.73E-01	6.48E+01	1.30E+02	4.53E-01	5.13E-01	3.52E-03
	2.73E-01	1.24E-01	7.17E+01	1.43E+02	5.02E-01	5.41E-01	1.55E-03
	2.62E-01	1.11E-01	7.44E+01	1.49E+02	5.21E-01	5.51E-01	9.09E-04
	2.17E-01	5.66E-02	9.21E+01	1.84E+02	6.44E-01	6.10E-01	1.21E-03
	1.74E-01	4.82E-03	1.50E+02	3.00E+02	1.05E+00	8.70E-01	3.25E-02

Table VII-7. Nondimensional Retention Analysis (Continued)

Material[1]	Saturation	Effective Saturation[2]	Capillary Rise(cm) Hydrocarbon	Capillary Rise(cm) Water[3]	Nondimensional Capillary Rise	Predicted Nondimensional Capillary Rise	Residuals Squared
Glass Beads	9.95E-01	9.94E-01	5.90E+00	1.18E+01	6.62E-02	2.16E-01	2.26E-02
	9.89E-01	9.88E-01	1.18E+01	2.36E+01	1.32E-01	2.39E-01	1.14E-02
	9.85E-01	9.83E-01	1.78E+01	3.56E+01	2.00E-01	2.49E-01	2.40E-03
	9.80E-01	9.78E-01	2.38E+01	4.76E+01	2.67E-01	2.58E-01	8.16E-05
	9.71E-01	9.68E-01	2.69E+01	5.38E+01	3.02E-01	2.70E-01	9.72E-04
	9.38E-01	9.31E-01	2.88E+01	5.76E+01	3.23E-01	2.99E-01	5.78E-04
	9.12E-01	9.03E-01	2.93E+01	5.86E+01	3.29E-01	3.14E-01	2.25E-04
	7.64E-01	7.39E-01	3.04E+01	6.08E+01	3.41E-01	3.64E-01	5.49E-04
	6.81E-01	6.47E-01	3.10E+01	6.20E+01	3.48E-01	3.85E-01	1.41E-03
	5.79E-01	5.34E-01	3.21E+01	6.42E+01	3.60E-01	4.09E-01	2.42E-03
	4.65E-01	4.08E-01	3.27E+01	6.54E+01	3.67E-01	4.37E-01	5.00E-03
	3.37E-01	2.66E-01	3.39E+01	6.78E+01	3.80E-01	4.76E-01	9.26E-03
	2.69E-01	1.90E-01	3.57E+01	7.14E+01	4.00E-01	5.05E-01	1.09E-02
	1.90E-01	1.03E-01	3.90E+01	7.80E+01	4.37E-01	5.57E-01	1.43E-02
	1.30E-01	3.66E-02	4.38E+01	8.76E+01	4.91E-01	6.50E-01	2.53E-02
	9.90E-02	2.22E-03	5.35E+01	1.07E+02	6.00E-01	9.72E-01	1.38E-01
	9.70E-02	9.97E-06	1.50E+02	3.01E+02	1.69E+00	2.10E+00	1.72E-01
Touchet Silt Loam	9.98E-01	9.97E-01	3.28E+01	6.56E+01	9.91E-02	2.01E-01	1.05E-02
	9.95E-01	9.92E-01	4.28E+01	8.56E+01	1.29E-01	2.26E-01	9.33E-03
	9.92E-01	9.88E-01	5.28E+01	1.06E+02	1.60E-01	2.40E-01	6.43E-03
	9.84E-01	9.75E-01	6.28E+01	1.26E+02	1.90E-01	2.62E-01	5.19E-03
	9.78E-01	9.66E-01	6.78E+01	1.36E+02	2.05E-01	2.73E-01	4.61E-03
	9.67E-01	9.48E-01	7.26E+01	1.45E+02	2.19E-01	2.88E-01	4.66E-03
	9.46E-01	9.16E-01	7.78E+01	1.56E+02	2.35E-01	3.07E-01	5.22E-03
	8.92E-01	8.31E-01	8.23E+01	1.65E+02	2.49E-01	3.40E-01	8.24E-03
	8.21E-01	7.20E-01	8.77E+01	1.75E+02	2.65E-01	3.69E-01	1.07E-02
	7.19E-01	5.61E-01	9.78E+01	1.96E+02	2.96E-01	4.03E-01	1.16E-02
	6.41E-01	4.39E-01	1.08E+02	2.15E+02	3.25E-01	4.30E-01	1.10E-02
	5.62E-01	3.16E-01	1.23E+02	2.46E+02	3.72E-01	4.61E-01	7.99E-03
	4.92E-01	2.06E-01	1.43E+02	2.85E+02	4.31E-01	4.98E-01	4.51E-03
	4.24E-01	1.00E-01	1.77E+02	3.54E+02	5.35E-01	5.60E-01	6.07E-04
	3.83E-01	3.59E-02	2.07E+02	4.14E+02	6.26E-01	6.52E-01	6.51E-04
Sum of Residuals							3.99E+00

NOTES: 1 See Attachment V for the data.
2 The effective saturation is defined as the ratio (S-Sr)(1-Sr)
3 According to Brooks and Corey (1964, Equation 17, p. 9), the capillary rise of water was about twice that of the hydrocarbon used in the measurements.
4 Equation 4.22 is applied the the capillary rise (cm) to convert to a nondimensional capillary rise.

INTENTIONALLY LEFT BLANK

ATTACHMENT VIII

HYDROLOGIC PROPERTIES OF ENGINEERED BARRIER SYSTEM COMPONENTS USED FOR NUFT RUNS

INTENTIONALLY LEFT BLANK

Attachment VIII - Hydrologic Properties of Engineered Barrier System Components Used for NUFT Runs

Tables VIII-1 and VIII-2 present the hydrologic and thermal properties of the waste package, the drip shield, and the drift air required to run the NUFT model. Since this analysis evaluates advection versus diffusion in the invert at ambient temperature, in the absence of drift seepage, these inputs serve only as placeholders necessary to initiate the NUFT simulations and do not impact the non-thermal analysis presented in this document.

Table VIII-1. Hydrologic Properties of Engineered Barrier System Components

Component	Porosity (ϕ)	Permeability (m^2)	Tortuosity Factor
Waste Package	0.0	0.0	0.0
Drip Shield	0.0	0.0	0.0
Air	0.990	1e-08	1.0

Table VIII-2. Thermal Properties of Engineered Barrier System Components

Component	Thermal Conductivity (W/(m·K))	Specific Heat Capacity (J/(kg·K)	Mass Density (kg/m^3)
Waste Package[1]	10.1	414.0	8690
Drip Shield[2]	20.708	540.82	4512.00
Air[3]	0.0263	1.007	1.61

Source: BSC 2001d, Table 5-10, 5-11, 5-14, and 5-15

NOTES: [1] Values are for waste package at 46°C made from Alloy 22.
[2] Values are for drip shield at 100°C made from titanium Grade 7.
[3] Values are from Incropera and DeWitt 1996.

INTENTIONALLY LEFT BLANK

ATTACHMENT IX

COMPARISON OF TUFF MATRIX HYDROLOGIC PROPERTIES

INTENTIONALLY LEFT BLANK

Attachment IX - Comparison of Tuff Matrix Hydrologic Properties

The information in this attachment comes from DTN: LB990861233129.001 and DTN: LB0207REVUZPRP.002.

The tuff matrix hydrologic properties for TSw35 and TSw36 inputs used in this analysis (DTN: LB990861233129.001) are compared to more recent data (DTN: LB0207REVUZPRP.002). Although there are some differences in moisture potential at low and intermediate saturations, the moisture potential at high saturations of interest for this analysis, are equivalent.

Table IX-1. Comparison of Tuff Matrix Hydrologic Properties for TSw35 and TSw36.

Parameter	TSw36 [1]	TSw35[1]	TSw35[2]	TSw36 (Tptpln)
Porosity of the rock matrix in an individual grain (ϕ_{matrix})	0.112	0.131	0.131	0.103
Full Saturation * (S_s)	1.0	1.0	1.0	1.0
Residual Saturation (S_r)	0.18	0.12	0.12	0.20
[3]Saturated Volumetric Moisture Content (θ_s)	0.112	0.131	0.131	0.103
Residual Volumetric Moisture Content (θ_r)	0.02016	0.0157	0.0157	0.0206
van Genuchten Air-Entry Parameter (α) 1/Pa	3.55E-6	6.44E-6	1.66E-05	2.84×10^{-7}
van Genuchten Parameter (m)	0.380	0.236	0.216	0.442
[5]van Genuchten Parameter (n)	1.612	1.309E-9	1.280	1.750
Intrinsic Permeability (k) m^2	5.71E-18	3.04E-17	3.7E-17	2.3×10^{-20}

NOTES: [1] DTN: LB990861233129.001.
[2] DTN: LB0207REVUZPRP.002. Values reported in *Calibrated Properties Model* (BSC 2003c).
[3] θ_s is a calculated value. See Section 6.
[4] θ_r is a calculated value. See Section 6.
[5] The value of n is given by 1/(1-m) (Fetter 1993, p. 172).

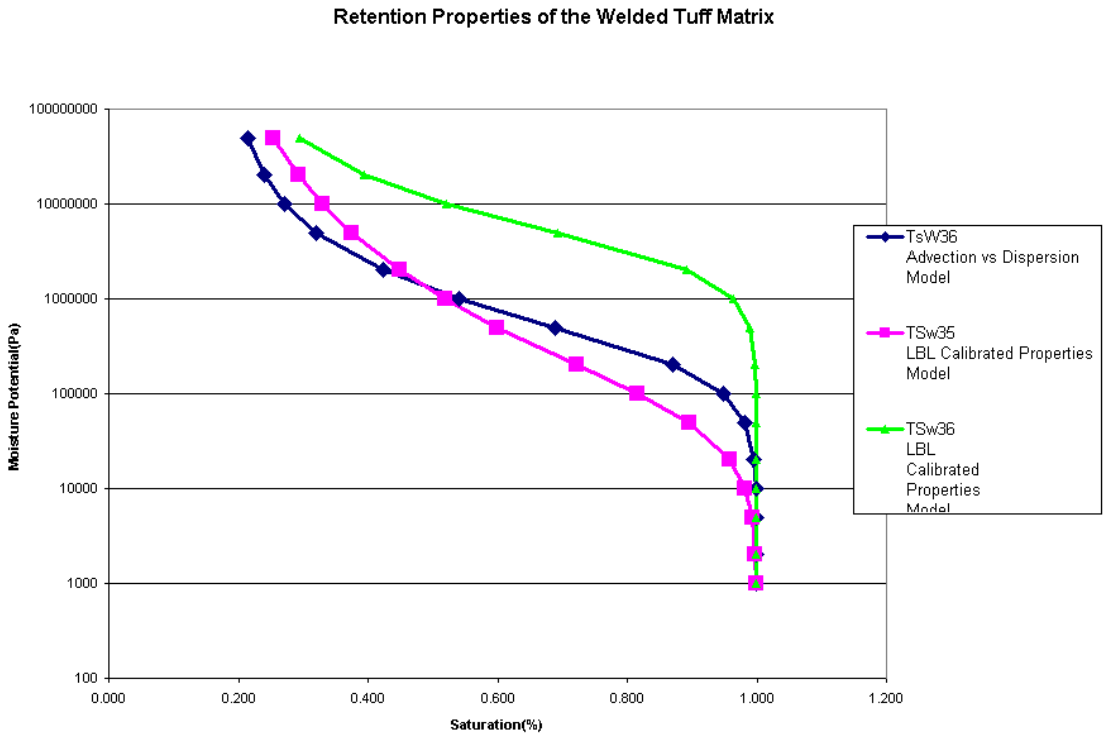

DTN: LB990861233129.001
LB0207REVUZPRP.002

Figure IX-1. Retention Properties for Welded Tuff

ATTACHMENT X

LIQUID FLUX PATTERNS IN MATRIX COMPONENT OF INVERT AND ROCK MATRIX AND IN THE INTERGRANULAR COMPONENT OF INVERT AND ROCK FRACTURES FOR THE CAMPBELL AND VAN GENUCHTEN GRAIN SIZE RETENTION RELATIONS

INTENTIONALLY LEFT BLANK

The purpose of the NUFT analyses presented in this attachment is to provide a detailed calculation of the occurrence of water and advection in the unsaturated media of the invert. The NUFT calculation provides an analysis of advection and the retention of water in both the intergranular and intragranular pore space of the invert. These calculations show that for the properties adopted for analysis for the moisture potential at the repository horizon that the fine pore space within the crushed tuff grains retains water while the coarse pore space between the particles of crushed tuff is free of water. Figures X-1 through X-18 corroborate the concept of one-dimensional transport and shows where water flows in the invert. The colors show different zones of flow. Note that the arrows show the general direction of flow but not magnitude. Also note that flow does not occur in the open void space of the drift, and that this is an artifact of the XTOOL plotting routine.

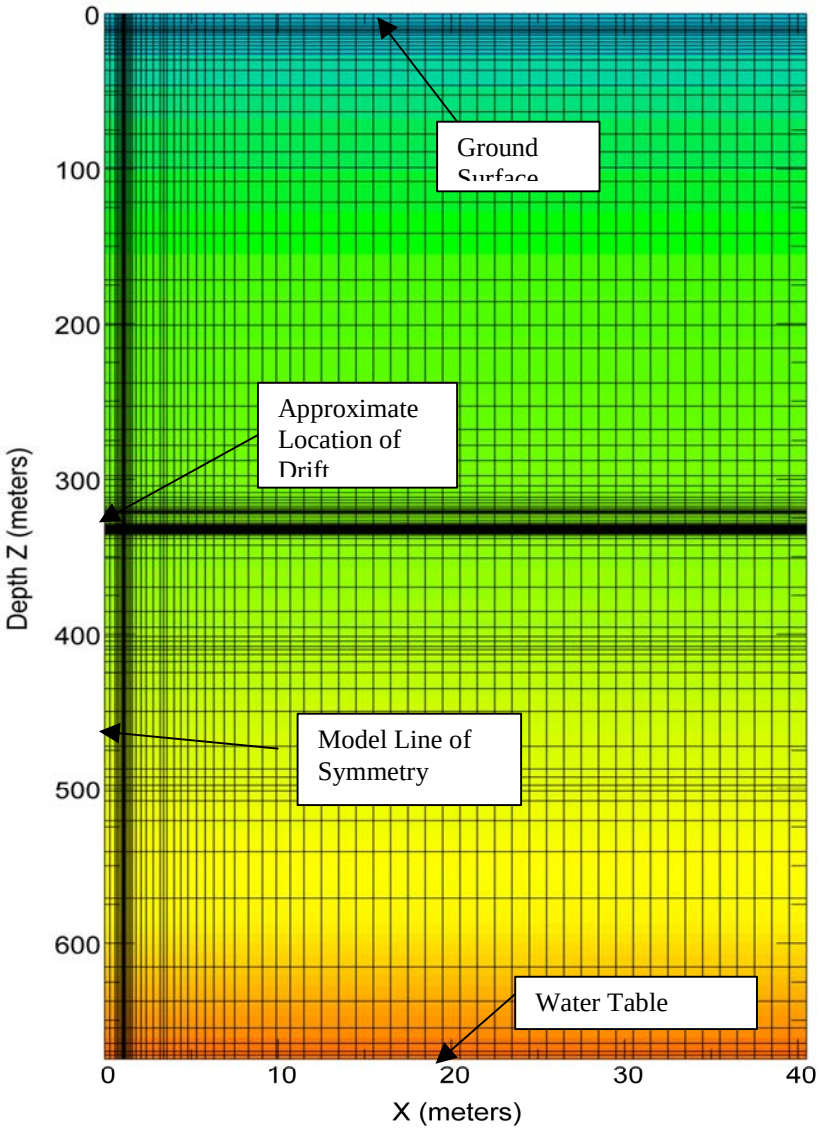

Figure X-1. NUFT Simulation Grid

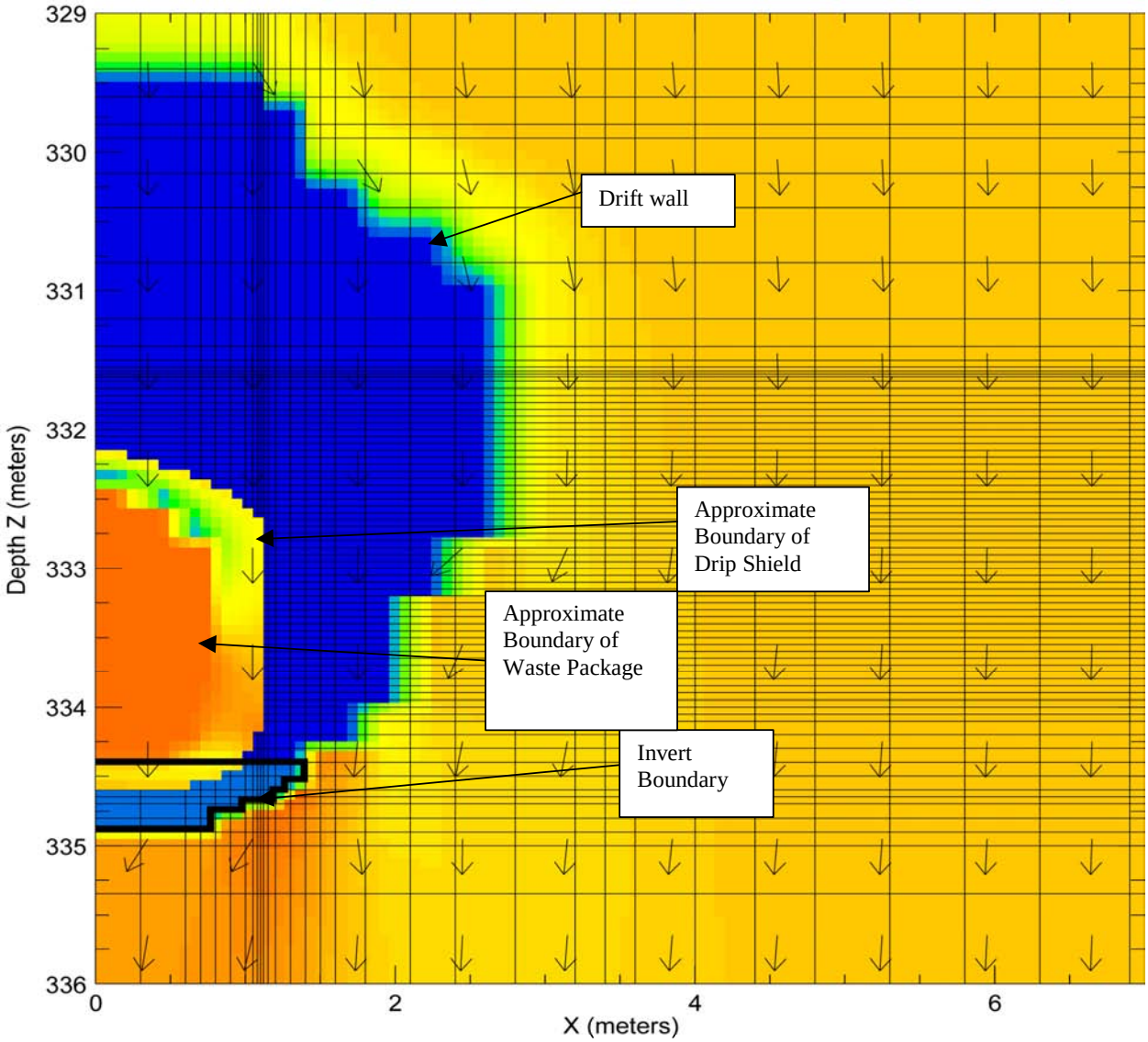

Figure X-2a. Liquid Flux Pattern in Rock Fractures Around the Drift

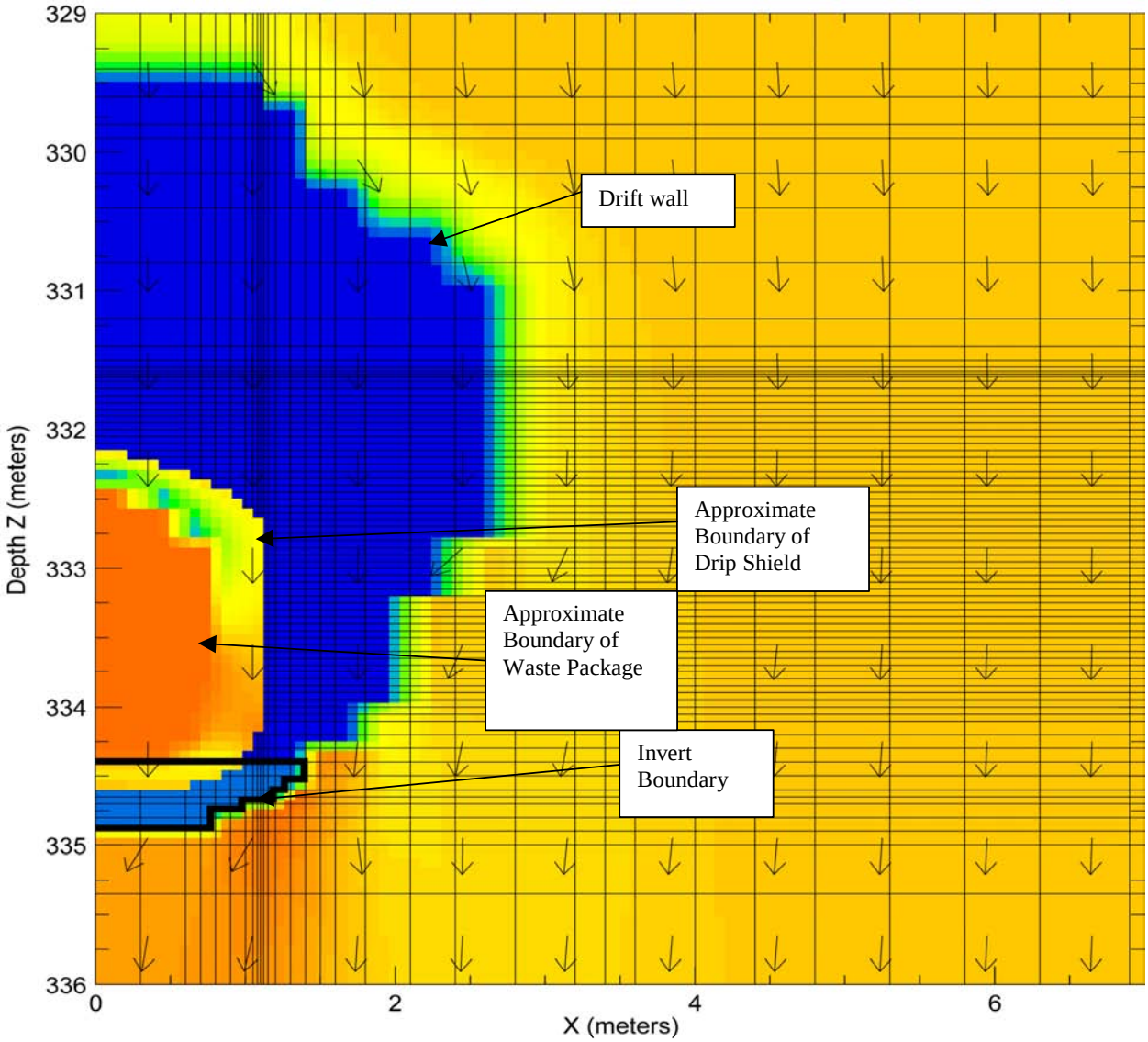

Figure X-2b. Liquid Flux Pattern in Rock Matrix Around the Drift

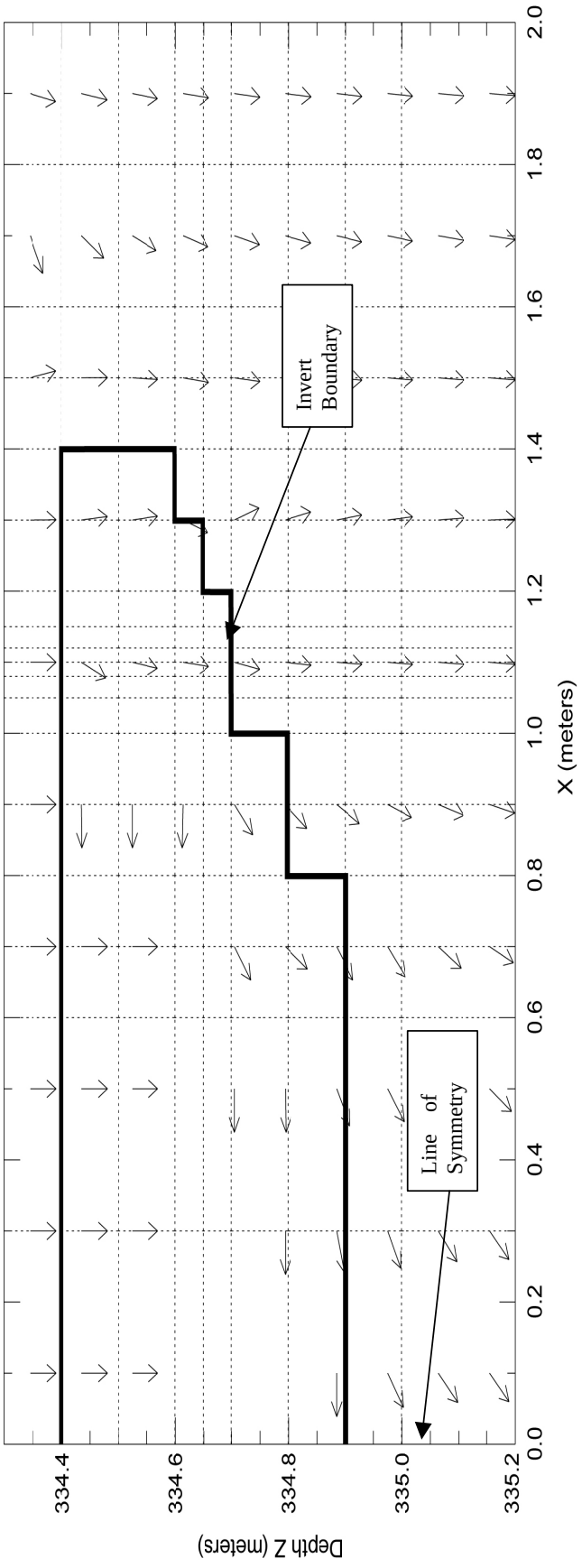

NOTE: Arrows show general flow directions, but do not represent magnitude of flow.

Figure X-3. Liquid Flux Pattern in Intergranular Component of Invert and Rock Fractures for the van Genuchten 0.317-mm Grain Size Retention Relation

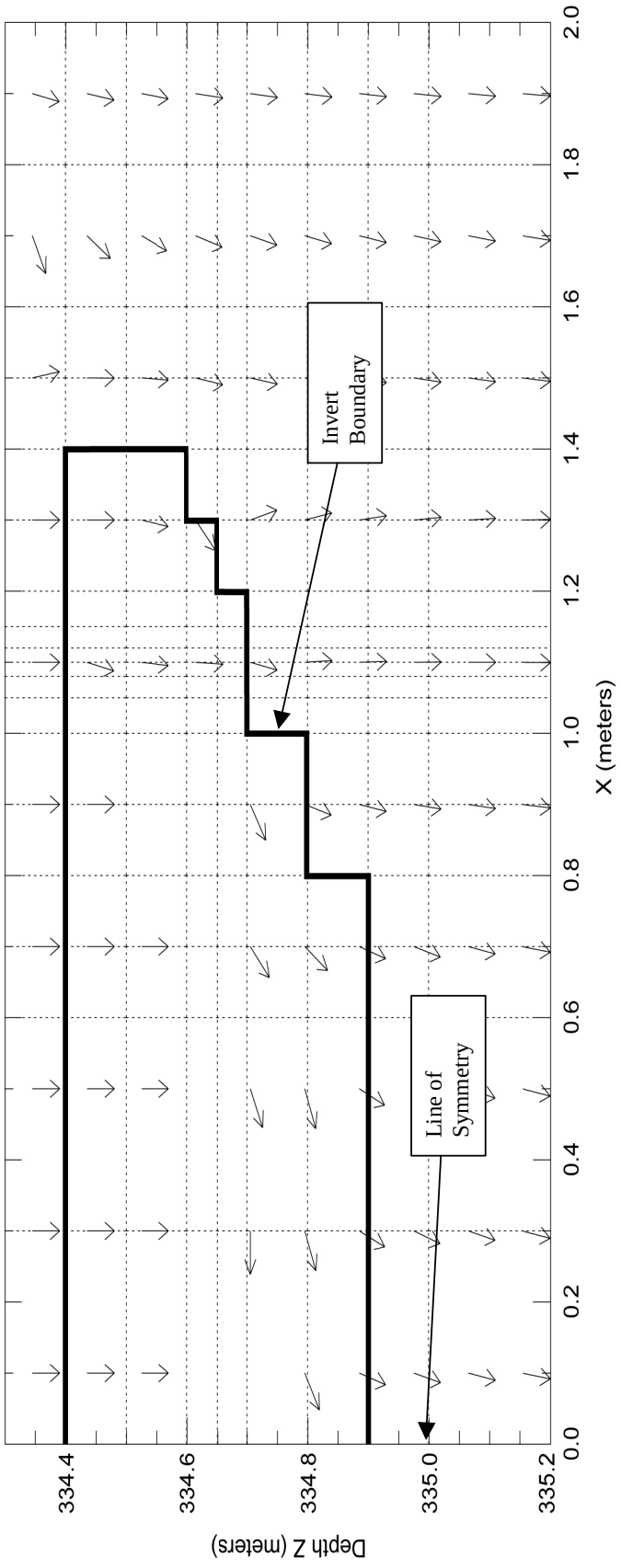

NOTE: Arrows show general flow directions, but do not represent magnitude of flow.

Figure X-4. Liquid Flux Pattern in Intergranular Component of Invert and Rock Fractures for the van Genuchten 3-mm Grain Size Retention Relation

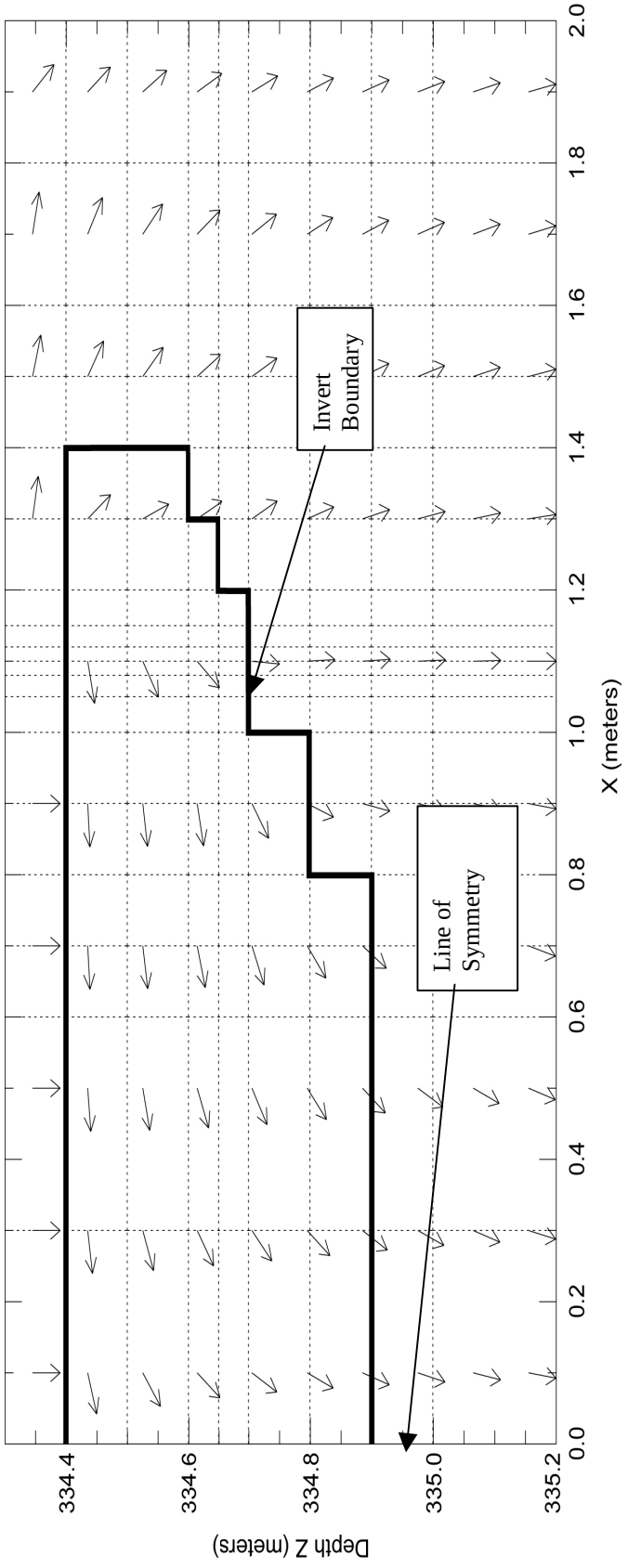

NOTE: Arrows show general flow directions, but do not represent magnitude of flow.

Figure X-5. Liquid Flux Pattern in Matrix Component of Invert and Rock Matrix for the van Genuchten 0.317-mm Grain Size

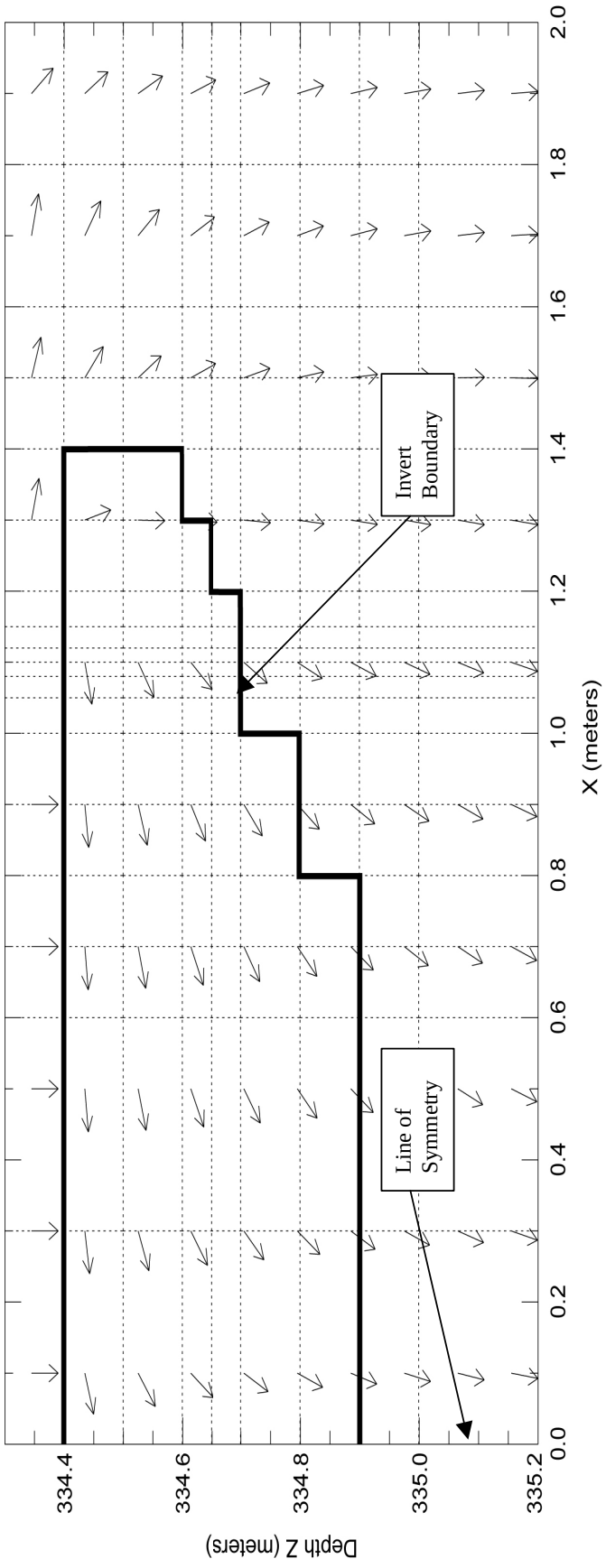

NOTE: Arrows show general flow directions, but do not represent magnitude of flow.

Figure X-6. Liquid Flux Pattern in Matrix Component of Invert and Rock Matrix for the van Genuchten 3-mm Grain Size Retention Relation

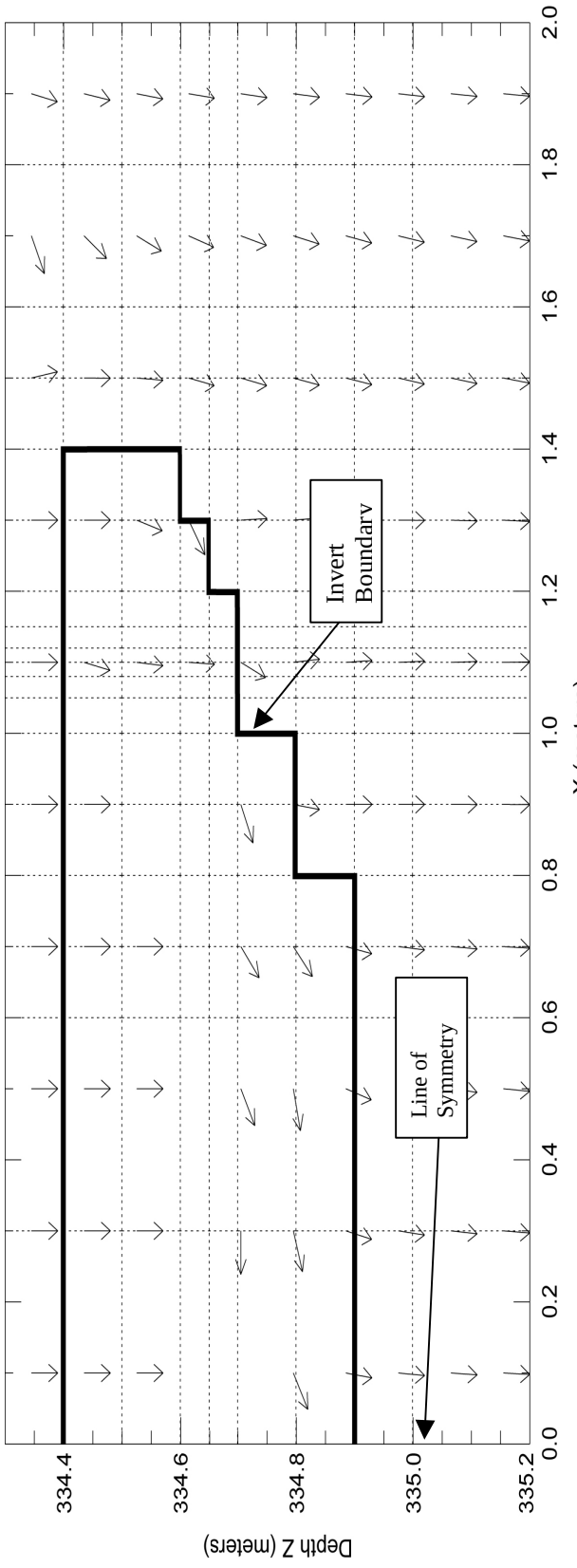

NOTE: Arrows show general flow directions, but do not represent magnitude of flow.

Figure X-7. Liquid Flux Pattern in Intergranular Component of Invert and Rock Fractures for the van Genuchten 10-mm Grain Size Retention Relation

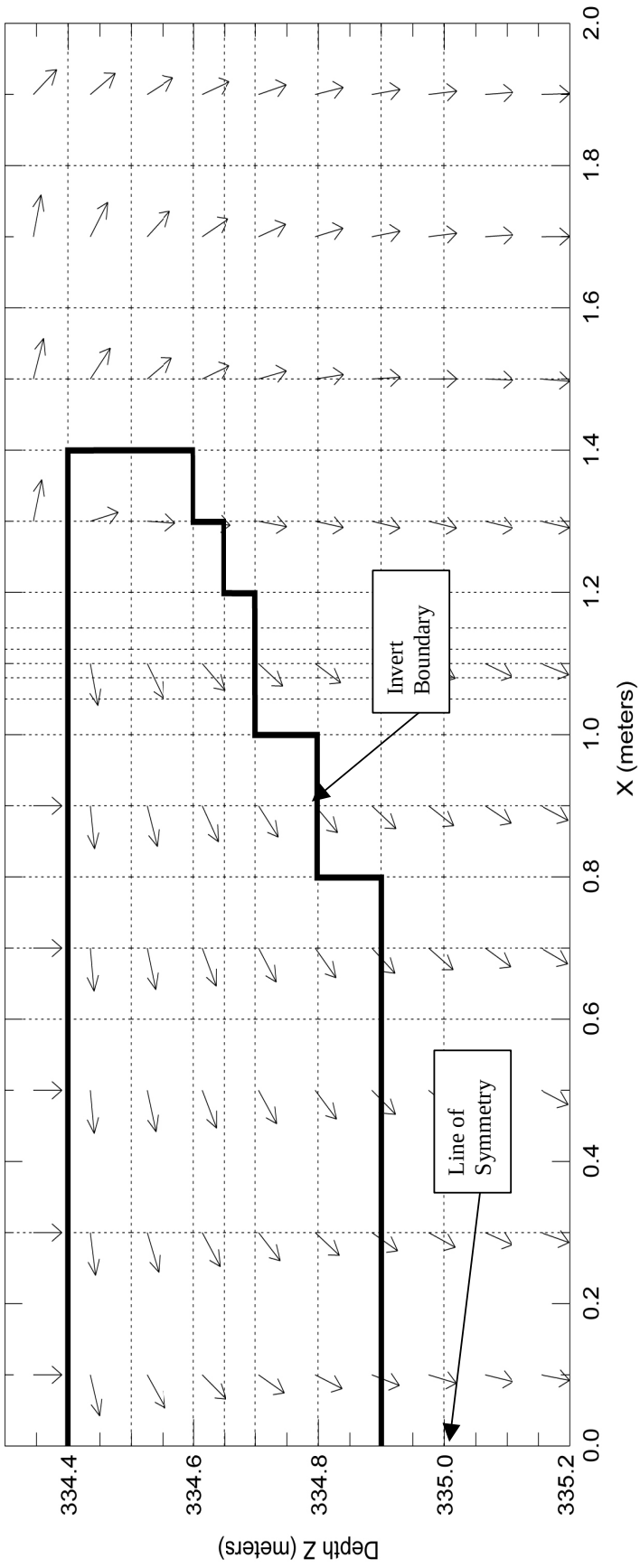

NOTE: Arrows show general flow directions, but do not represent magnitude of flow.

Figure X-8. Liquid Flux Pattern in Matrix Component of Invert and Rock Matrix for the van Genuchten 10-mm Grain Size Retention Relation

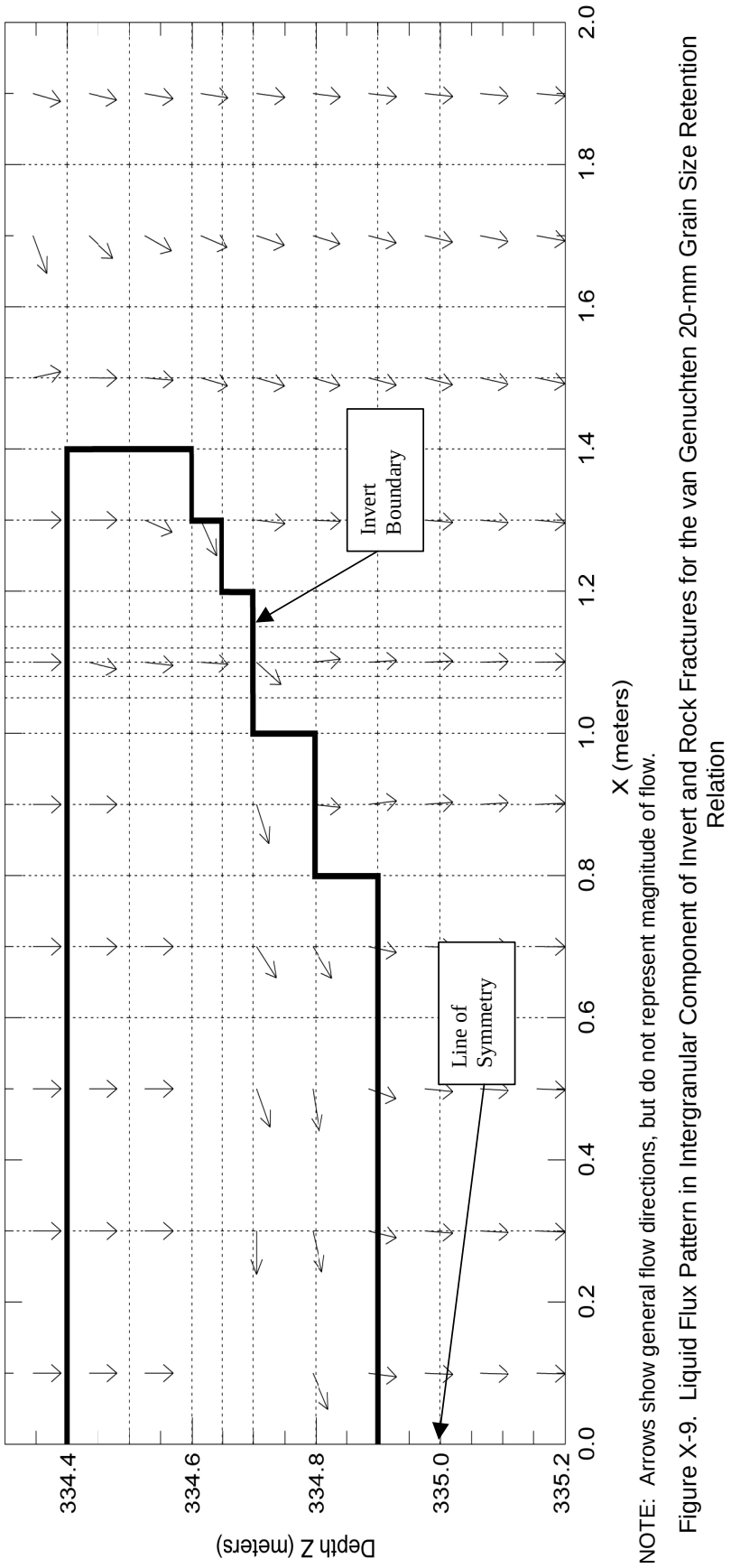

NOTE: Arrows show general flow directions, but do not represent magnitude of flow.

Figure X-9. Liquid Flux Pattern in Intergranular Component of Invert and Rock Fractures for the van Genuchten 20-mm Grain Size Retention Relation

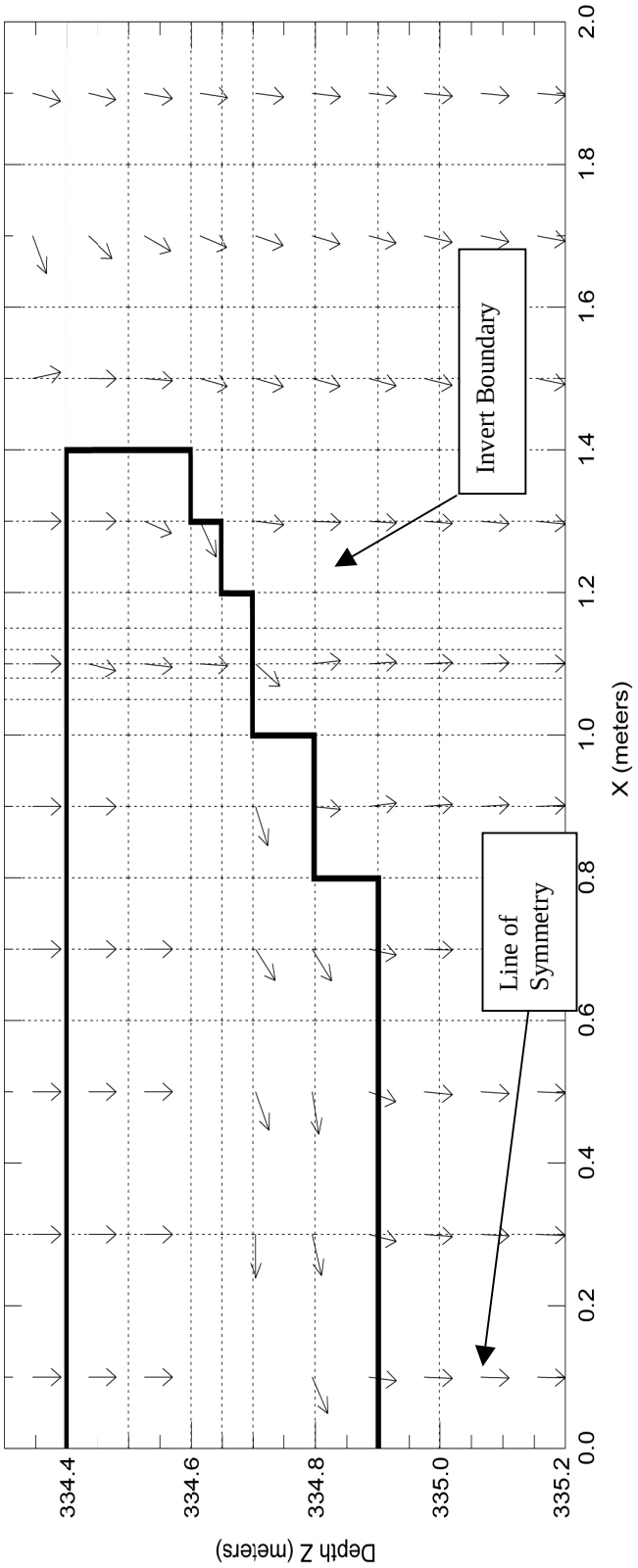

NOTE: Arrows show general flow directions, but do not represent magnitude of flow.

Figure X-10. Liquid Flux Pattern in Matrix Component of Invert and Rock Matrix for the van Genuchten 20-mm Grain Size Retention Relation

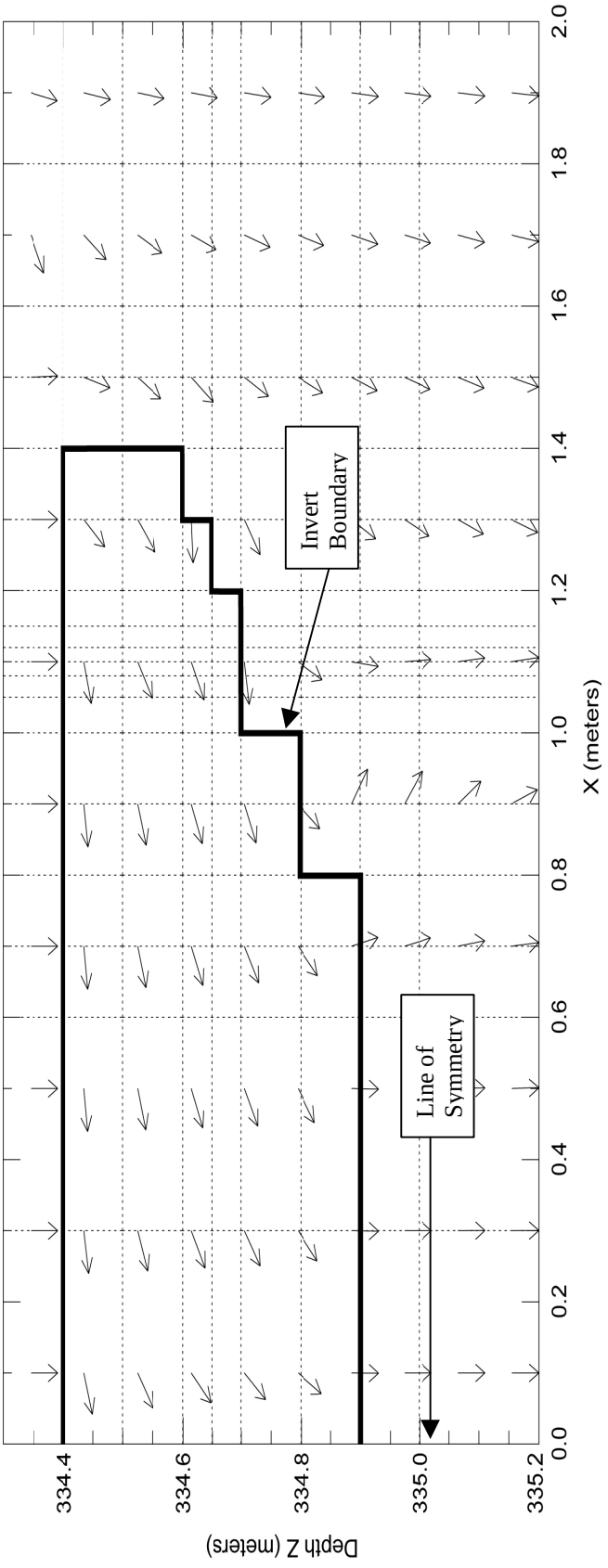

NOTE: Arrows show general flow directions, but do not represent magnitude of flow.

Figure X-11. Liquid Flux Pattern in Intergranular Component of Invert and Rock Fractures for the Campbell 0.317-mm Grain Size Retention Relation

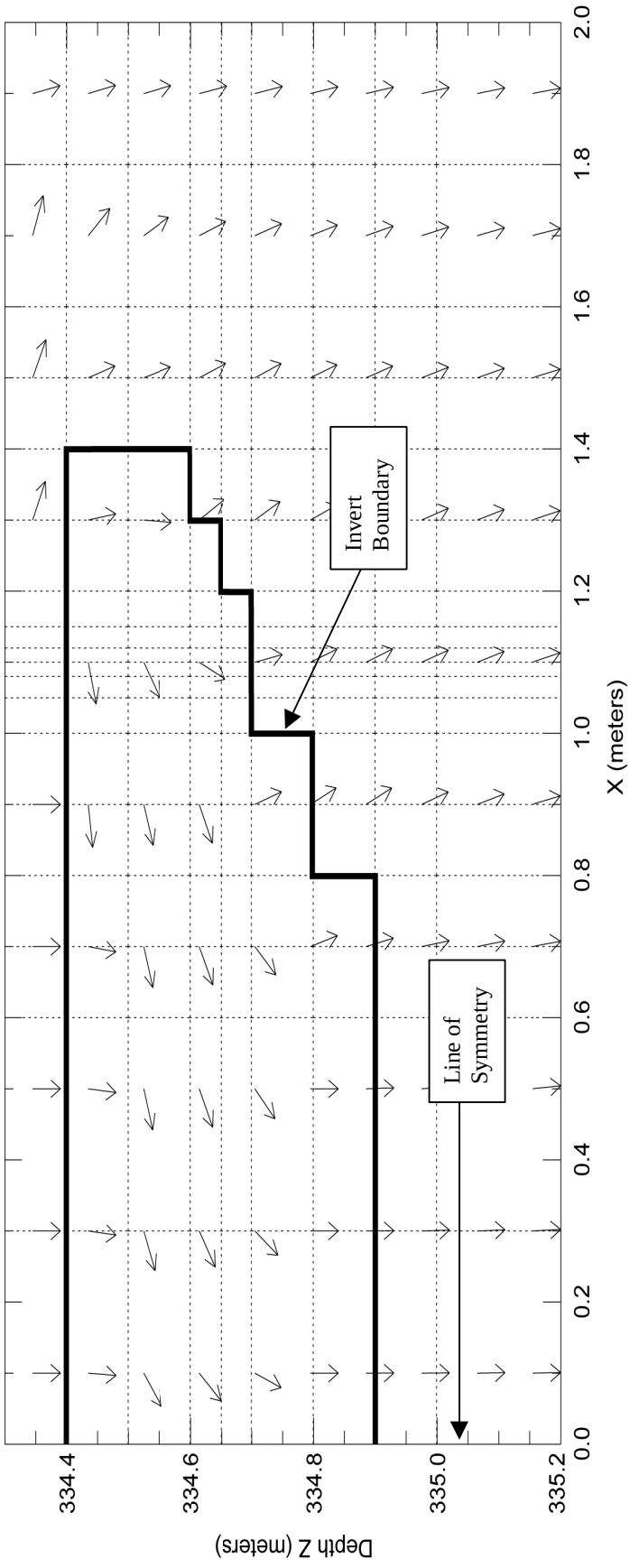

NOTE: Arrows show general flow directions, but do not represent magnitude of flow.

Figure X-12. Liquid Flux Pattern in Matrix Component of Invert and Rock Matrix for the Campbell 0.317-mm Grain Size Retention Relation

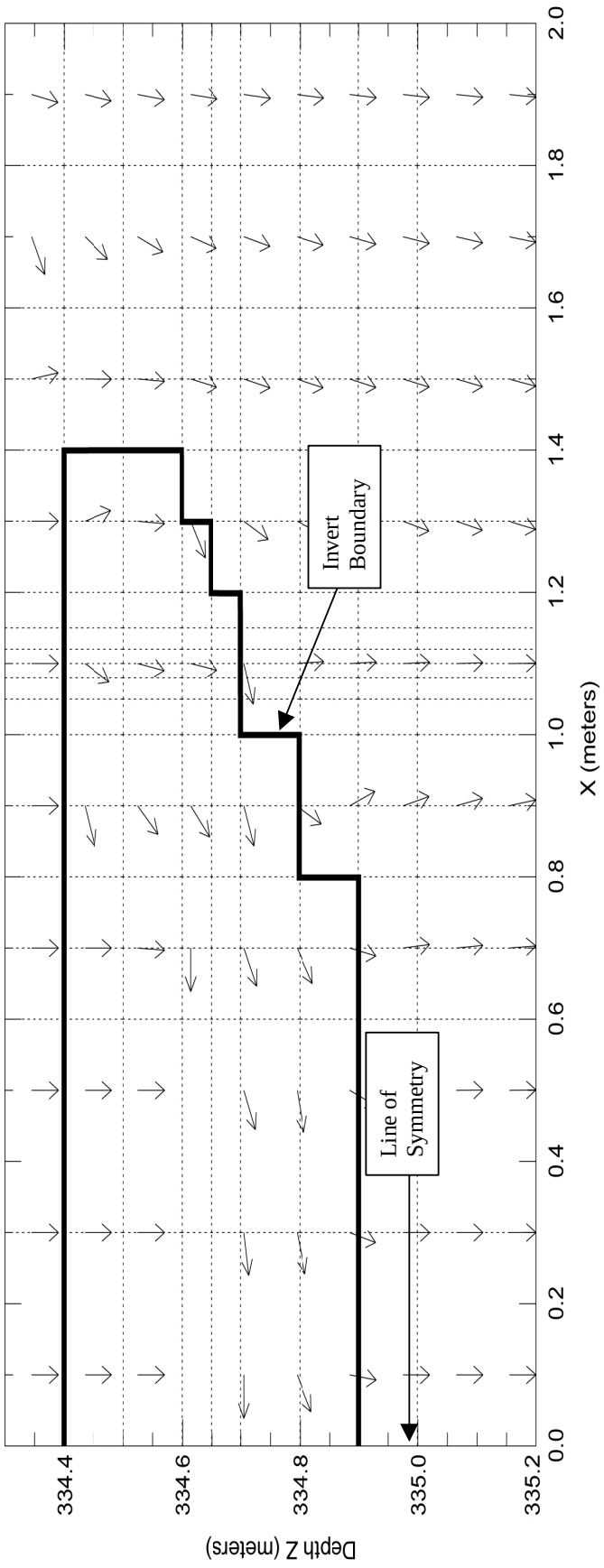

NOTE: Arrows show general flow directions, but do not represent magnitude of flow.

Figure X-13. Liquid Flux Pattern in Intergranular Component of Invert and Rock Fractures for the Campbell 3-mm Grain Size Retention Relation

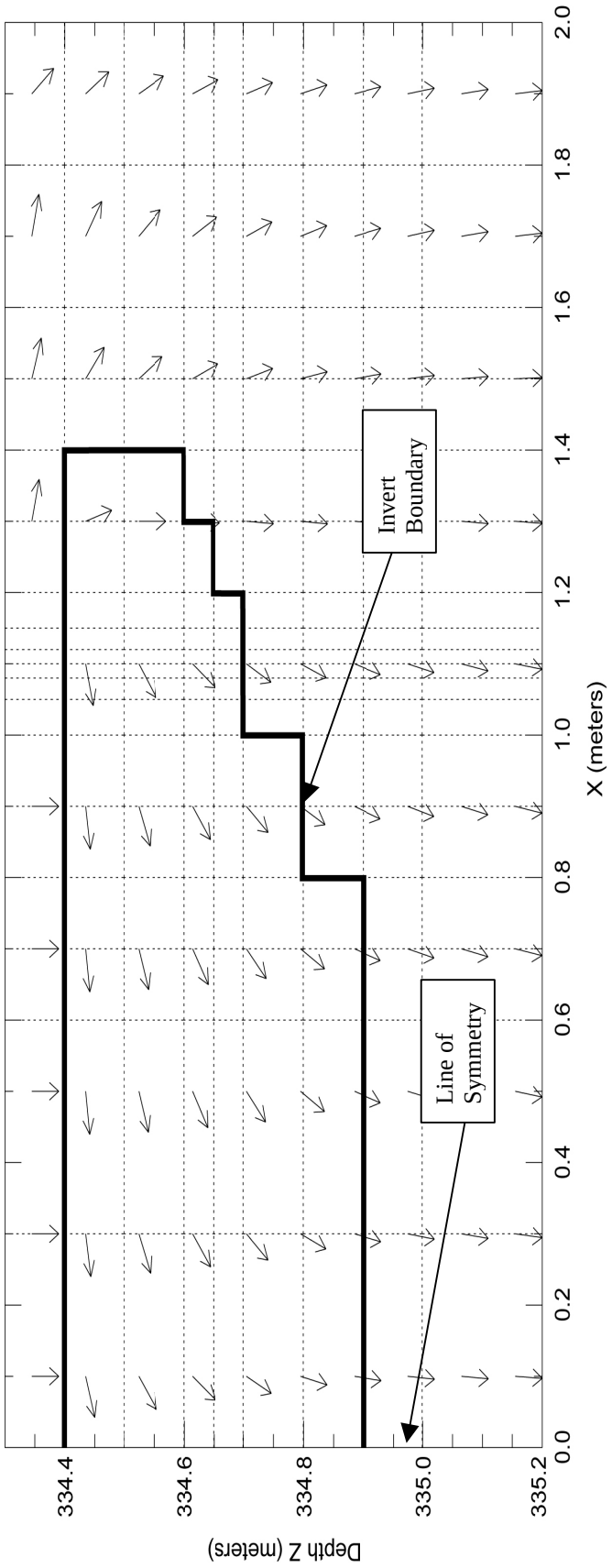

NOTE: Arrows show general flow directions, but do not represent magnitude of flow.

Figure X-14. Liquid Flux Pattern in Matrix Component of Invert and Rock Matrix for the Campbell 3-mm Grain Size Retention Relation

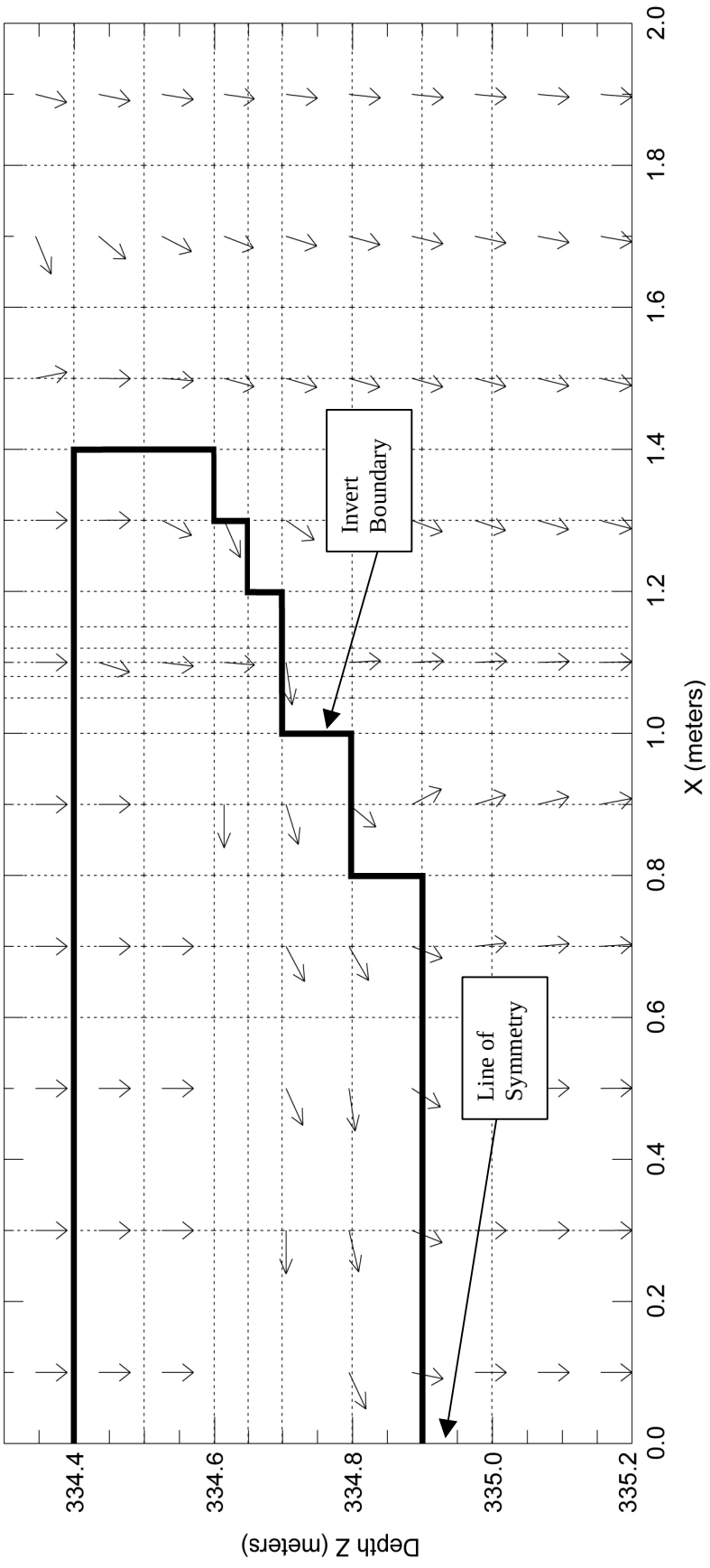

NOTE: Arrows show general flow directions, but do not represent magnitude of flow.

Figure X-15. Liquid Flux Pattern in Intergranular Component of Invert and Rock Fractures for the Campbell 10-mm Grain Size Retention Relation

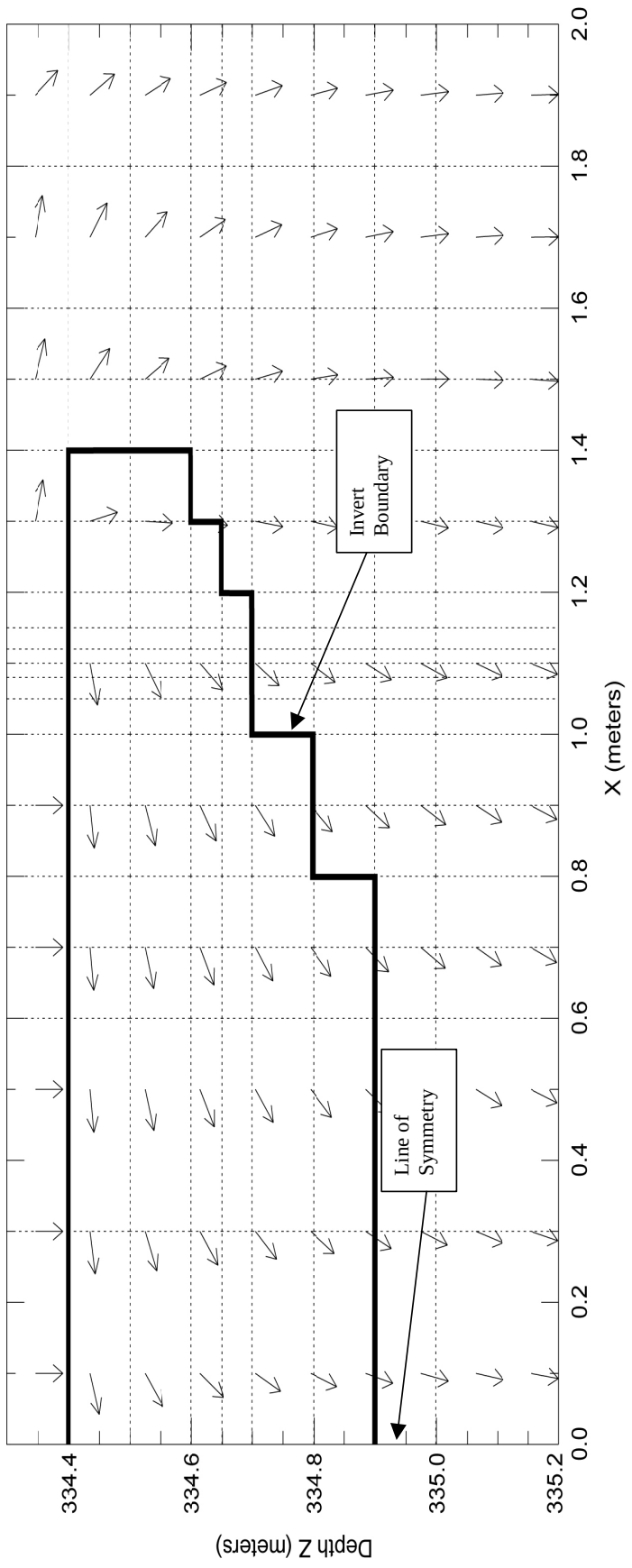

NOTE: Arrows show general flow directions, but do not represent magnitude of flow.

Figure X-16. Liquid Flux Pattern in Matrix Component of Invert and Rock Matrix for the Campbell 10-mm Grain Size Retention Relation

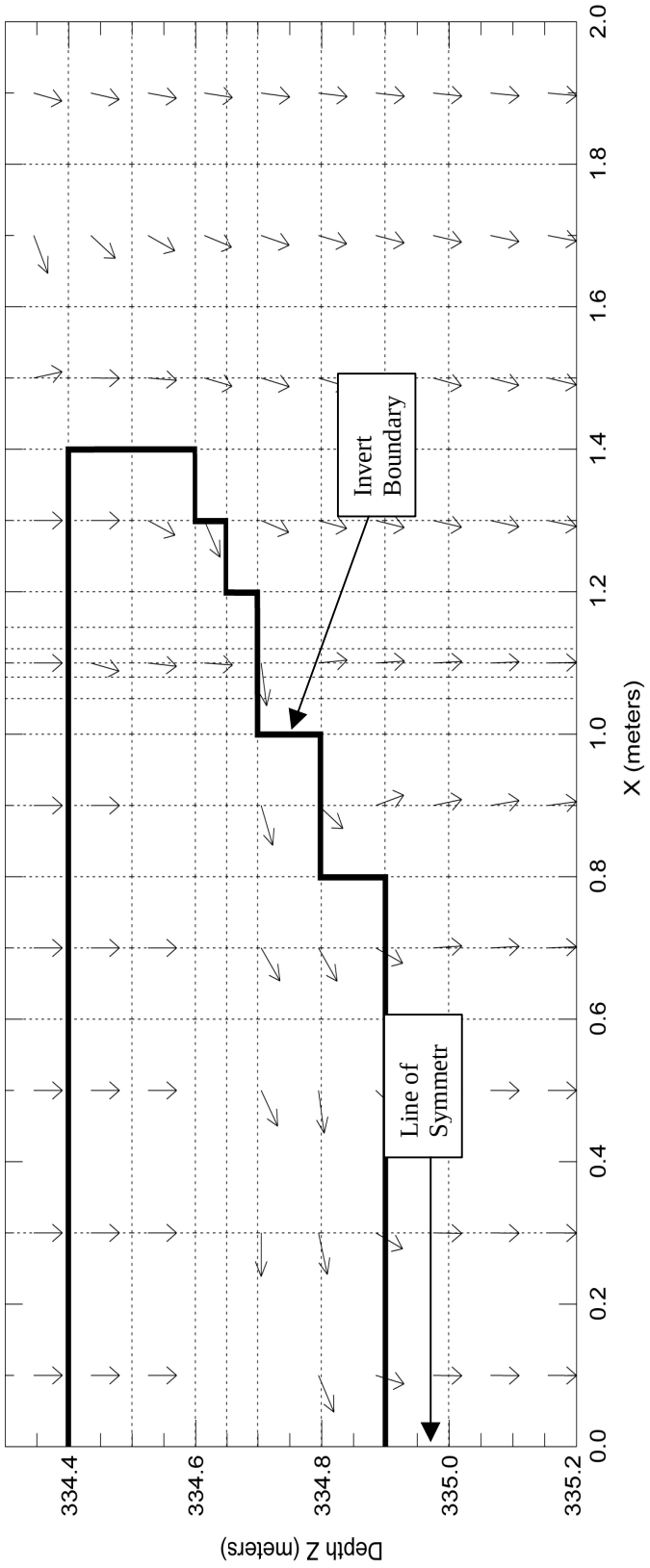

NOTE: Arrows show general flow directions, but do not represent magnitude of flow.

Figure X-17. Liquid Flux Pattern in Intergranular Component of Invert and Rock Fractures for the Campbell 20-mm Grain Size Retention Relation

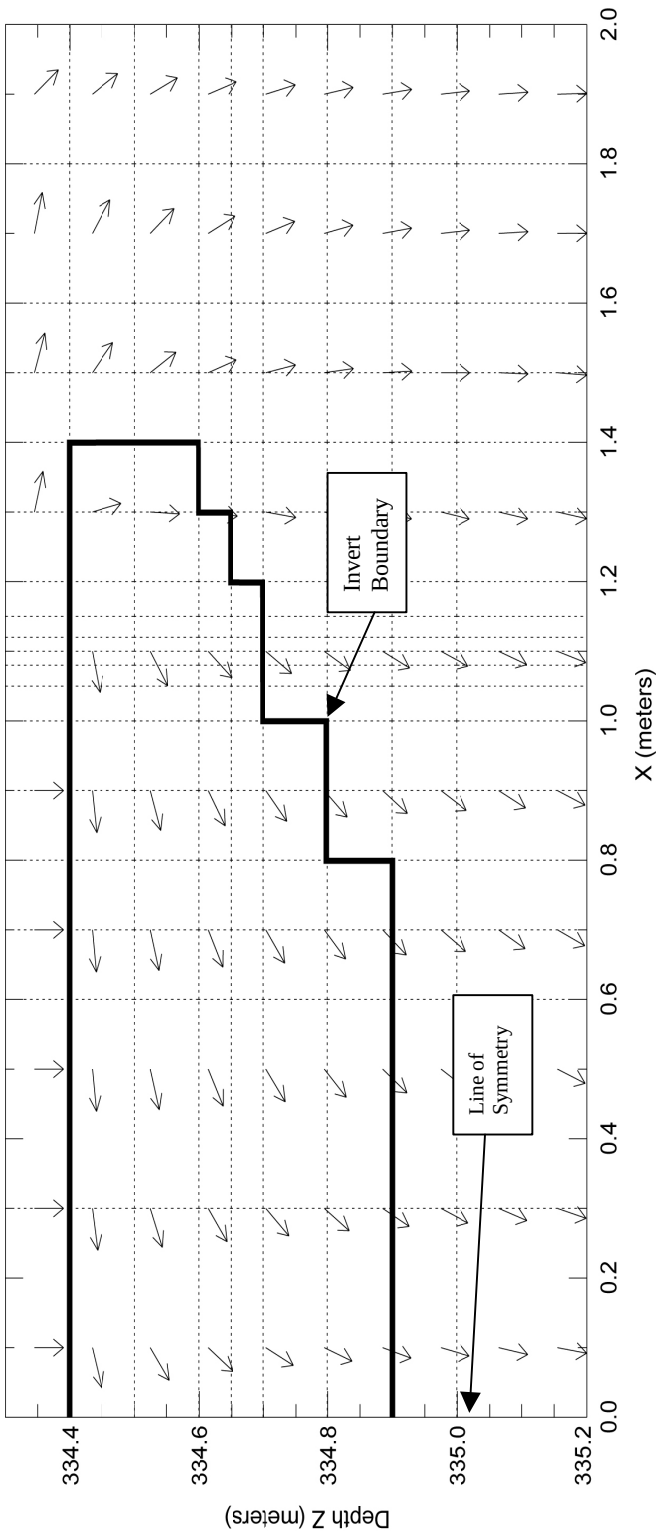

NOTE: Arrows show general flow directions, but do not represent magnitude of flow.

Figure X-18. Liquid Flux Pattern in Matrix Component of Invert and Rock Matrix for the Campbell 20-mm Grain Size Retention Relation

INTENTIONALLY LEFT BLANK

ATTACHMENT XI

HYDROLOGIC AND THERMAL PROPERTIES OF THE INVERT

INTENTIONALLY LEFT BLANK

Attachment XI - Hydrologic and Thermal Properties of the Invert

Crushed tuff is selected for the invert to provide geochemical compatibility with the surrounding host rock. The basis for the selection of the crushed is that the material provides diffusion-barrier performance when transport from the waste package to the rock floor is diffusion dominated. This could occur if a waste package is breached but the protecting drip shield is intact, so that the invert ballast material immediately below the drip shield is unsaturated and protected from advective flow from other engineered barrier components.

Crushed welded tuff sieved between 2.0 and 4.75 mm (Section 6.3) has been selected for pilot testing and the properties are described below for this material. The final design may require a different size distribution or material type, or both.

XI.1 BULK DENSITY AND POROSITY

The invert material is crushed tuff from the Tptpll lithostratigraphic unit that is part of the TSw2 thermal/mechanical unit. The repository host horizon is located mainly in the TSw2 unit. The invert material hydrological properties are presently unavailable for the Tptpll formation. It is valid to substitute the Tptpmn properties in place of Tptpll values because they are both part of the TSw2 thermal/mechanical unit. The matrix porosities of these materials are similar , and this would mean the crushed materials would have similar retention characteristics.

The USGS measured the bulk density, water retention, and unsaturated hydraulic conductivity. These properties were measured in conjunction with the UFA measurements as described subsequently. The hydrologic and geotechnical properties for the crushed tuff are taken from DTN: GS980808312242.015. These data sets are illustrated in Figures XI-1 and XI-2. The curve fits to the retention data shown in these figures are presented in Attachment XVI.

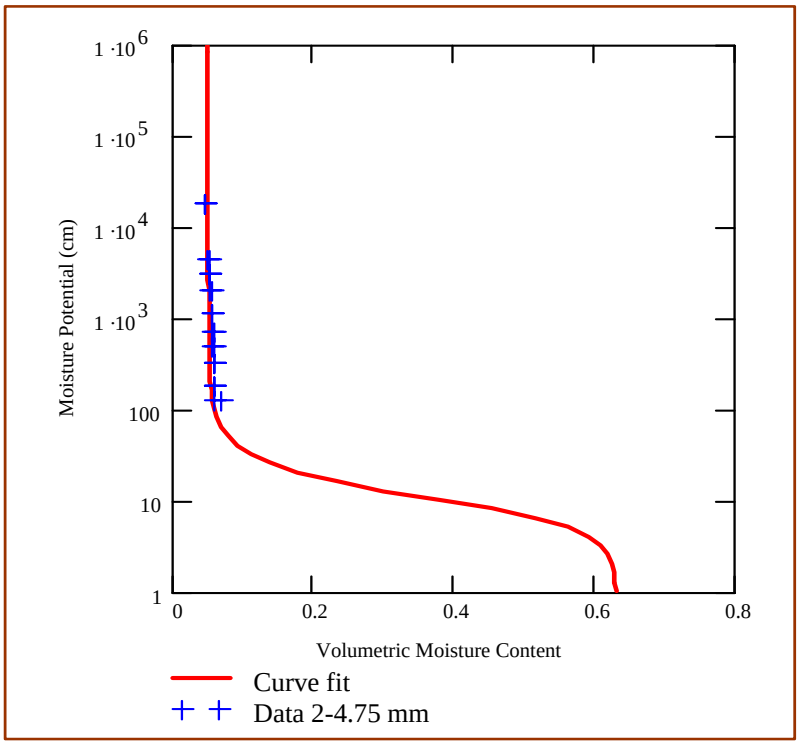

DTN: GS980808312242.015

NOTE: See Attachment XVI for the curve fit.

Figure XI-1. Moisture Retention Relationship for the Invert

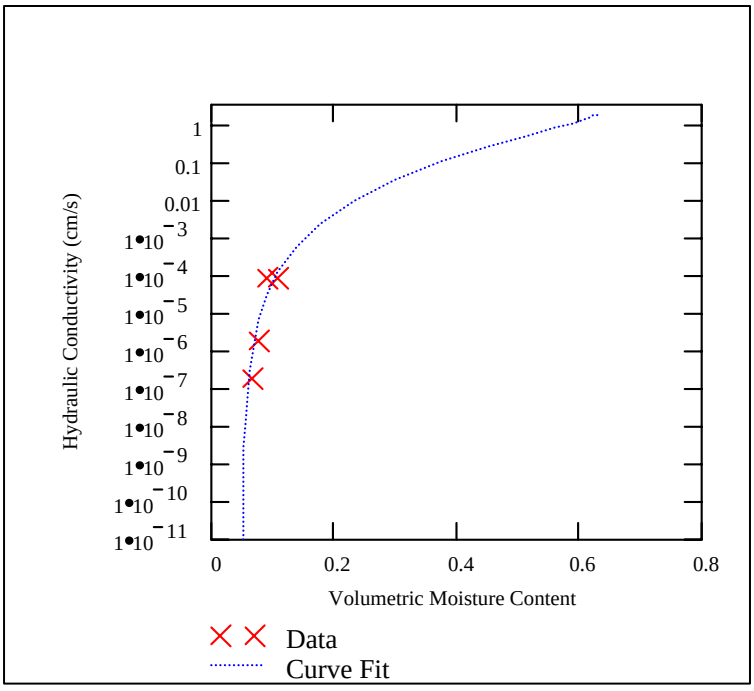

DTN: GS980808312242.015

Figure XI-2. Unsaturated Hydraulic Conductivity versus Volumetric Moisture Content for the Invert

For materials sieved between 2.00 and 4.75 mm, used for hydraulic conductivity measurements, the measured dry bulk density was 1.15 g/cm^3, as presented in *Water Distribution and Removal Model* (CRWMS M&O 2001b, Attachment XIV). The grain density is 2.53 gm/cm^3 as presented in *Water Distribution and Removal Model* (CRWMS M&O 2001b, Attachment XIV). Calculate the porosity using the soil phase convention of setting the volume of the solids (Vs) equal to 1.0 cm^3, developing a formula for the bulk density, and then calculating the volume of the voids. The dry bulk density (ρ) is defined as in the *Water Distribution and Removal Model* (CRWMS M&O 2001b, Attachment XIV):

$$\rho = G_s V_s / V_t \quad \text{(Eq. XI-1)}$$

where

ρ = Dry bulk mass density (g/cm^3)
G_s = Specific gravity of solids
V_s = Solids volume (cm^3)
V_t = Total volume (cm^3)

Substituting in for the total volume which is equal to the volume of the solids and volume of the voids ($V_t = Vs + V_v$):

$$\rho = G_s V_s / (V_s + V_v) \quad \text{(Eq. XI-2)}$$

where

V_v = Void volume (cm^3)

Substituting in the values for G_s, ρ, and V_s:

$$1.15\ \text{cm}^3 = 2.53\ \text{gm/cm}^3\ (1.0\ \text{cm}^3) / (1.0\ \text{cm}^3 + V_v) \quad \text{(Eq. XI-3)}$$

Solve for V_v:

$$V_v = (2.53/1.15 - 1.0)\ \text{cm}^3 \quad \text{(Eq. XI-4)}$$

$$V_v = 1.20\ \text{cm}^3 \quad \text{(Eq. XI-5)}$$

Solving for the porosity (ϕ):

$$\phi = 1.20/(1.0 + 1.20) = 0.55 \quad \text{(Eq. XI-6)}$$

XI.2 MOISTURE RETENTION

Moisture retention measurements were performed on the crushed tuff using the UFA measurements (CRWMS M&O 1996, Appendix C).

The UFA consists of an ultracentrifuge with a constant ultra low flow pump that provides fluid to the sample through a rotating seal assembly and microdispersal system. The volumetric moisture content (θ) as a function of the moisture potential (ψ) can be determined by allowing the sample to drain until the moisture potential equals the centrifugal force per unit area divided by the unit

weight in a state of equilibrium. The sample is then weighed to determine the volumetric moisture content (θ).

The moisture retention data obtained from the two methods can be plotted and a curve fitting performed for the retention model based upon the van Genuchten two-parameter model n and m (m=1-1/n) (Fetter 1993, p. 172). Define the moisture potential (capillary pressure divided by weight density) versus moisture content relation:

$$\theta = \left[1 + \left(|\psi \cdot \alpha|^{n}\right]^{-m} \cdot (\theta_s - \theta_r) + \theta_r \right. \quad \text{(Eq. XI-7)}$$

where

- n = van Genuchten curve-fitting parameter
- m = van Genuchten curve-fitting parameter
- α = van Genuchten or exponential curve-fitting parameters (cm^{-1})
- θ = Volumetric moisture con
- θ_r = Residual volumetric moisture content
- θ_s = Saturated volumetric moisture content and
- ψ = Moisture potential (cm of water)

Substituting the value of (m) into Equation XI-7 for the two-parameter model, gives:

$$\theta = \left[1 + \left(|\psi \cdot \alpha|^{n}\right)\right]^{-1-\frac{1}{n}} \cdot (\theta_s - \theta_r) + \theta_r \quad \text{(Eq. XI-8)}$$

The estimated curve-fitting parameters are from Attachment XIV of *Water Distribution and Removal Model* (CRWMS M&O 2001b):

$$\theta_r = 0.05$$

$$\alpha_i = 0.12 \text{ (1/cm)}$$

$$n_i = 2.75$$

From the definition of van Genuchten m (m = 1-1/n) given above:

$$1 - \frac{1}{2.75} = 0.64$$

The residual saturation equals the residual moisture content divided by the porosity (0.05/0.55) = 0.091. The satiated saturation is by definition.

Note that the measurements were performed near the residual moisture saturation. To establish the curve at higher moisture contents, the volumetric moisture content at saturation was estimated from the porosity, as presented in *Water Distribution and Removal Model* (CRWMS M&O 2001b, Attachment XIV). The volumetric moisture content θ_s equals the porosity of 0.63 which corresponds to the loose state. It should be noted that while the UFA testing was

performed on the crushed tuff in a loose state (ϕ = 0.63) than what would be anticipated in the repository (ϕ = 0.55) allowing for consolidation over time, the moisture retention scaled to the saturation level would not be significantly different.

XI.3 INTRINSIC PERMEABILITY

The saturated hydraulic conductivity (K_s) of the invert is estimated from the curve fitting analysis presented in *Water Distribution and Removal Model* (CRWMS M&O 2001b, Attachment XV) using the combined UFA unsaturated hydraulic conductivity (K_u) to moisture potential (ψ) and retention measurements. The calculated value from *Water Distribution and Removal Model* (CRWMS M&O 2001b, Attachment XV) is 0.60 cm/sec. This value corresponds to an approximate intrinsic permeability conversion value of 6.0×10^{-6} cm^2 or 6.0×10^{-10} m^2 (Freeze and Cherry 1979, p. 29).

XI.4 RELATIVE PERMEABILITY

The UFA test apparatus described above can be used to determine the relationship between the unsaturated hydraulic conductivity (K_u) and volumetric moisture content through a direct application of Darcy's Law (CRWMS M&O 1996, Appendix C). By measuring the flow rates to 0.001 ml/hr and measuring the effluent collected from the sample in a volumetrically calibrated chamber that determines volumetric moisture content (θ), the unsaturated hydraulic conductivity can be determined from the ratio of the flow rate to the centrifugal force per unit volume (CRWMS M&O 1996, p. C-2).

The relationship of the unsaturated hydraulic conductivity with volumetric moisture content is given by Jury et al. (1991, p. 109):

$$K(\theta) = K_s \cdot \left(\frac{\theta-\theta_r}{\theta_s-\theta_r}\right)^{\frac{1}{2}} \cdot \left[1-\left[1-\left(\frac{\theta-\theta_r}{\theta_s-\theta_r}\right)^{\frac{1}{1-\frac{1}{n}}}\right]^{\left(1-\frac{1}{n}\right)}\right]^2 \qquad \text{(Eq. XI-9)}$$

where

K_s is the saturated hydraulic conductivity (cm/sec)

The relative permeability function scales the saturated conductivity (K_s) to allow the unsaturated hydraulic conductivity function to be determined as shown in Figure XI-2.

The wetting-phase relative permeability as a function of moisture potential for this model is restated from Fetter (1993 , p. 182, Equation 4.17). The unsaturated hydraulic conductivity (wetting-phase relative permeability times saturated hydraulic conductivity) as a function of moisture potential is from *Water Distribution and Removal Model* (CRWMS M&O 2001b, Attachment XIV). The relative permeability function scales the saturated conductivity (K_s) to allow the unsaturated hydraulic conductivity function to be determined for crushed tuff as shown in Figure XI-3.

XI.5 THERMAL PROPERTIES

The rock grain specific heat for crushed tuff is estimated to be 948 J/(kg·K). The specific heat for the crushed tuff with a porosity of 0.55 and a bulk density of 1.15 g/cm^3 equals the specific heat of the grains since specific heat capacity depends on mass which is independent of volume. The volumetric heat (C_p) equals the specific heat (C_s) 948 J/(kg·K) times the bulk density (ρ) 1.15 g/cm^3. The thermal emissivity of the invert is taken equal to the emissivity for quartz on a rough surface 0.93 (Holman 1997, p. 649).

Additional measurements (DTN: GS000483351030.003) of geotechnical and thermal properties have been performed to characterize the thermal properties of crushed tuff. Also, it includes thermal-property measurements of oven dry samples of crushed tuff using the Thermolink Probe. This device uses a dual-probe, short-duration, heat pulse technique to simultaneously measure the volumetric specific heat and thermal diffusivities of granular materials. The measurements were performed for a "fine" crushed tuff, and "4-10" crushed tuff. The average properties are summarized in Table XI-1 for oven dry conditions at ambient temperature.

Table XI-1. Summary of Thermolink Results for Crushed Tuff

Material	Volumetric Specific Heat (J/cm^3/K)	Thermal Conductivity (W/m/K)	Thermal Diffusivity (mm^2/s)	Temperature (°C)
4-10 Crushed Tuff	0.930 ± 0.074	0.16 ± 0.01	0.175 ± 0.014	17.3 ± 1.0
Fine Crushed Tuff Group 1	0.919 ± 0.061	0.14 ± 0.01	0.153 ± 0.005	24.0 ± 2.4
Fine Crushed Tuff Group 2	0.972 ± 0.036	0.16 ± 0.01	0.159 ± 0.007	19.2 ± 0.17

DTN: GS000483351030.003

Crane et al. (1977) compared a number of models to the results of experimental studies. These included the model developed by Willhite et al. (1962) and the Dietz model. The Dietz model is a Fourier model for thermal conductivity of a packed bed. The Dietz model considered a special case of the packed bed-hexagonal array of touching spheres. However, it was found that the resulting expression for the effective bed conductivity was only a weak function of bed geometry, allowing the expression to be applied to a variety of packings.

These models were evaluated by comparing the predicted values for thermal conductivity on a separate and independent set of data developed by Saxena et al. (1986). Saxena et al. performed thermal conductivity measurements on porous materials. Measurements of effective thermal conductivity of these materials were made using three different experimental methods via the thermal probe method. The thermal probe method reported by Saxena et al. consisted of a line heat source method in which a steel hypodermic needle of length 10 cm and outer diameter 0.125 cm is used as the source and sensor for temperature (Saxena et al. 1986).

The measured data are regressed against the predicted data as presented in *Water Distribution and Removal Model* (CRWMS M&O 2001b, Attachment XIV) and illustrated in Figure XI-4. The plot shows the ratio of the thermal conductivity to the continuous or gas phase thermal conductivity for measured data and predicted values for the Dietz model, as presented in *Water*

Distribution and Removal Model (CRWMS M&O 2001b, Attachment XIV). The Dietz model was found to produce a better result for this data.

The results of the analysis on the data by Saxena et al. (1986) over a range of porosities are presented in Figure XI-4. Also, Figure XI-4 shows a data point for crushed tuff using the grain thermal conductivity for TSw34 as discussed below.

The Dietz model (Equation XI-11) can be applied to measured data for crushed tuff (TSw34) performed by the YMP. The value for the solids phase thermal conductivity for welded tuff is given in *Water Distribution and Removal Model* (CRWMS M&O 2001b, Table 4-5) as 1.56 W/(m·K). Considering the air thermal conductivity is given by Chapman (1974, p. 593) is 0.029 W/(m·K) at 60°C, the calculated value for thermal conductivity of crushed tuff is predicted to be 0.15 W/(m·K) which compares reasonably well with the measured values presented in Table XI-1.

The Dietz model can be used to predict the thermal conductivity under saturated conditions by substituting the value of thermal conductivity for water into Equation XI-11. Considering the water thermal conductivity given by Chapman (1974, p. 586) at 60°C, the value is 0.65 W/(m·K) as determined in *Water Distribution and Removal Model* (CRWMS M&O 2001b, Attachment XIV). Substituting in this value yields a value for thermal conductivity under saturated conditions of 1.03 W/(m·K) as determined in *Water Distribution and Removal Model* (CRWMS M&O 2001b, Attachment XIV).

The volumetric heat capacity under saturated conditions may be estimated by simple volumetric averaging. According to Jury et al. (1991, p. 179):

$$C_c = X_a \cdot C_a + X_w \cdot C_w + \sum_{j=1}^{N} X_{s_j} \cdot C_{s_j} \qquad \text{(Eq. XI-11)}$$

where

C_c = Average volumetric heat capacity
X_a = Void fraction of air
X_w = Void fraction of water
X_{sj} = Void fraction of the j^{th} solids component
C_a = Heat capacity per unit volume of the air
C_w =Heat capacity per unit volume of the water
C_{sj} = Heat capacity per unit volume of the j^{th} solids component

Note that NUFT will calculate the volume averaged specific heat capacity based upon the volume fractions and their respective volumetric heats for the solids, water, and air. The following calculation is provided for reference only, and illustrates how specific heat, and thermal diffusivity would change when the degree of saturation is increased from zero to one.

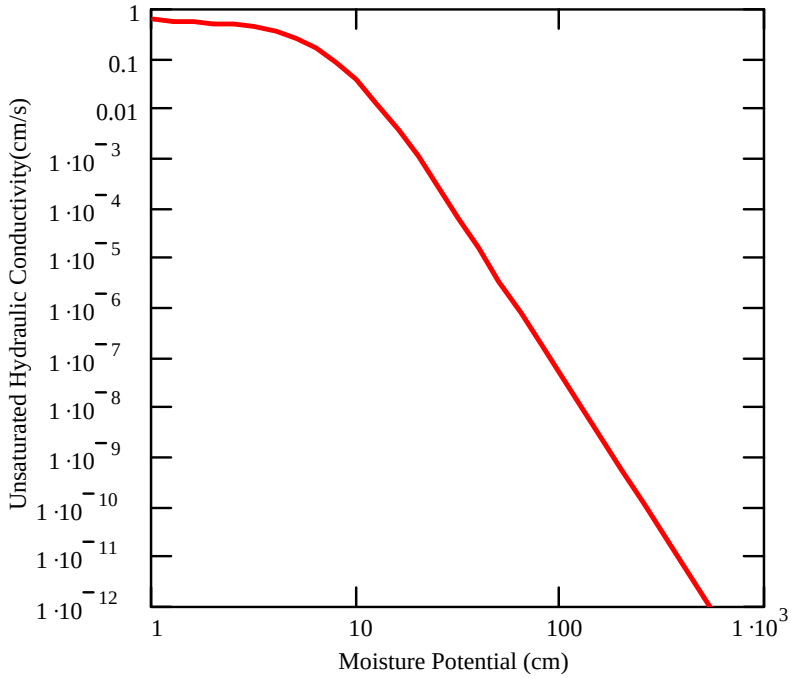

Source: CRWMS M&O 2001b, Attachment XIV

Figure XI-3. Unsaturated Hydraulic Conductivity versus Moisture Potential for the Invert

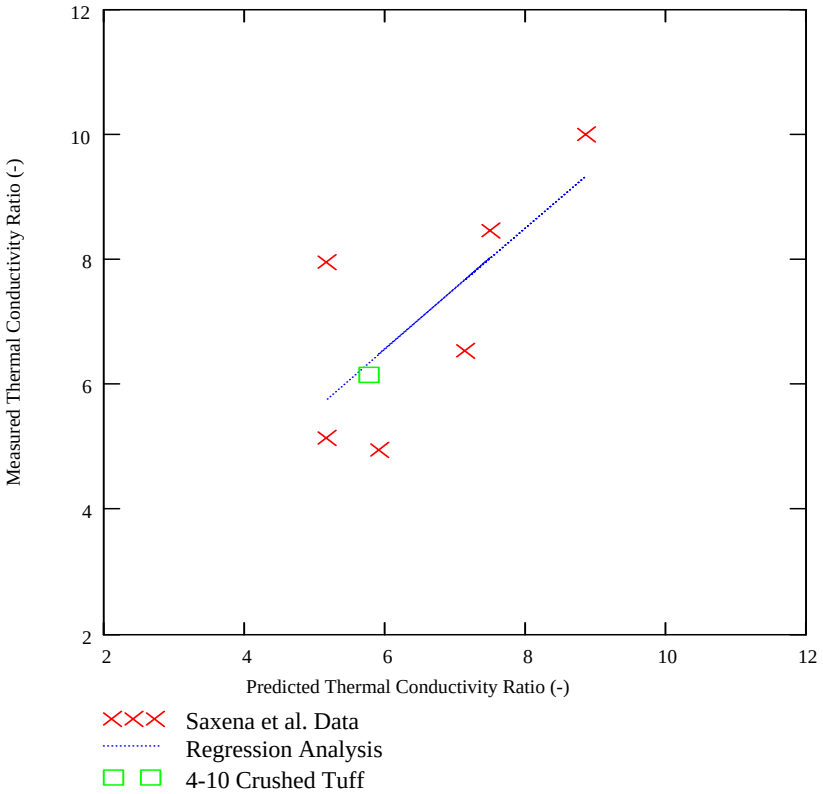

Figure XI-4. Comparison of Experimental Results with Calculated Thermal Conductivity for the Dietz Model

Calculate the volumetric heat capacity for air. From Chapman (1974, p. 593), the properties of air at 60°C (140°F) are given as:

$$Cp_a = 0.2409 \cdot \frac{BTU}{lb \cdot R}$$

$$\rho_a = 0.06614 \cdot \frac{lb}{ft^3}$$

Converting to the SI system of units:

$$Cp_a = 1009 \cdot \frac{J}{kg \cdot K}.$$

$$\rho_a = 1.059 \cdot \frac{kg}{m^3}$$

Calculate the volumetric heat capacity for air:

$$C_a = Cp_a \cdot \rho_a$$

$$C_a = 1069.0 \cdot \frac{J}{m^3 \cdot K}$$

Calculate the volumetric capacity of the tuff from Equation X-11 under dry conditions by considering 4-10 crushed tuff that has a volumetric heat capacity of 0.930 J/(cm^3 K) for TSw34 (CRWMS M&O 2001b, Table XI-3). The air void fraction is determined from Figure 6-1 from the ratio of 1.23/(1+1.23) = 0.55. Converting the value to SI units, the equation to be solved is:

$$9.30 \cdot 10^5 = C_a \cdot X_a + (1 - X_a) \cdot C_s \qquad \text{(Eq. XI-12}$$

Solving for C_s, the value of 2.07×10^6 J/(m^3 K) is obtained which is approximately twice the value for the porous crushed tuff (9.30×10^5 J/(m^3 K). As noted by Jury et al. (1991, p. 180), the volumetric heat capacity of air is small.

Consider now the properties of water. From Chapman (1974, p. 586) at a temperature of 60°C (140°F):

$$Cp_w = 0.998 \cdot \frac{BTU}{lb \cdot R}$$

$$\rho_w = 61.39 \cdot \frac{lb}{ft^3}$$

Converting to SI units:

$$Cp_w = 4178 \cdot \frac{J}{kg \cdot K}$$

$$\rho_w = 983.4 \cdot \frac{kg}{m^3}$$

The calculated volumetric heat capacity for water (C_w) is 4.11×10^6 J/(m^3 K). Substituting in Equation XI-12, the volumetric heat capacity under saturated conditions is given by:

$$X_w \cdot C_w + (1 - X_w) \cdot C_s = 3.19 \cdot 10^6 \cdot \frac{J}{m^3 \cdot K} \qquad \text{(Eq. XI-13)}$$

The volumetric heat capacity is increased by an approximate factor of three when compared to the volumetric heat capacity under dry conditions, as presented in Table XI-3.

From *Water Distribution and Removal Model* (CRWMS M&O 2001b), the value for the saturated thermal conductivity(k_{sat}) is 1.03 W/(m·K). The thermal diffusivity under saturated conditions is estimated from the thermal diffusivity relationship (Jury et al. 1991, p. 178):

$$\alpha = k_{sat} / C$$

The calculated thermal diffusivity under saturated conditions is 0.32 mm^2/s. The thermal diffusivity for the wet case increased by a factor of two when compared to the values for the dry case in Table XI-3.

ATTACHMENT XII

CALCULATION OF THE DIFFUSION COEFFICIENT FOR THE DRIPPING CASE

INTENTIONALLY LEFT BLANK

Attachment XII - Calculation of the Diffusion Coefficient for the Dripping Case

Attachment XII contains summary calculations for the estimate of the diffusion coefficient for the dripping case for a waste package flow rate of 1 m^3 per year. The attachment contains the "step by step" method that can be used to calculate the diffusion coefficient for the range of particle sizes of from 0.3 to 20 mm.

A sensitivity study was developed to evaluate the diffusion coefficient over a broad range of percolation rates. Table XII-1 summarizes the diffusion analysis developed on the basis of the approach presented in Attachment XII. The analysis shows that over a broad range of percolation rates that the intergranular water content remains "low" with the coarse pore space remaining dry. When the diffusion relationship presented in Equation 6-16 is used to calculate the diffusion coefficient, the diffusion coefficient is calculated to be on the order of 10^{-8} to 10^{-7} cm^2/sec in the invert.

A summary of the diffusion coefficients for the dripping case is presented in Figure XII-1.

Table XII-1. Summary of Diffusion Coefficients for the Dripping Case

Waste Package Flow Rate	(m3/yr)	0.01	0.1	1	10	100	1000	10000
Flux Rate (Jw)	mm/yr	0.385	3.85	38.5	385	3850	38500	385000
Particle Sizes	0.3	9.21E-08	9.45E-08	9.99E-08	1.13E-07	1.45E-07	2.29E-07	6.84E-07
	3	9.07E-08	9.12E-08	9.22E-08	9.47E-08	1.01E-07	1.14E-07	1.49E-07
	10	9.05E-08	9.07E-08	9.11E-08	9.21E-08	9.43E-08	1.01E-07	1.59E-07
	20	9.05E-08	9.06E-08	9.10E-08	9.20E-08	9.44E-08	1.01E-07	1.18E-07

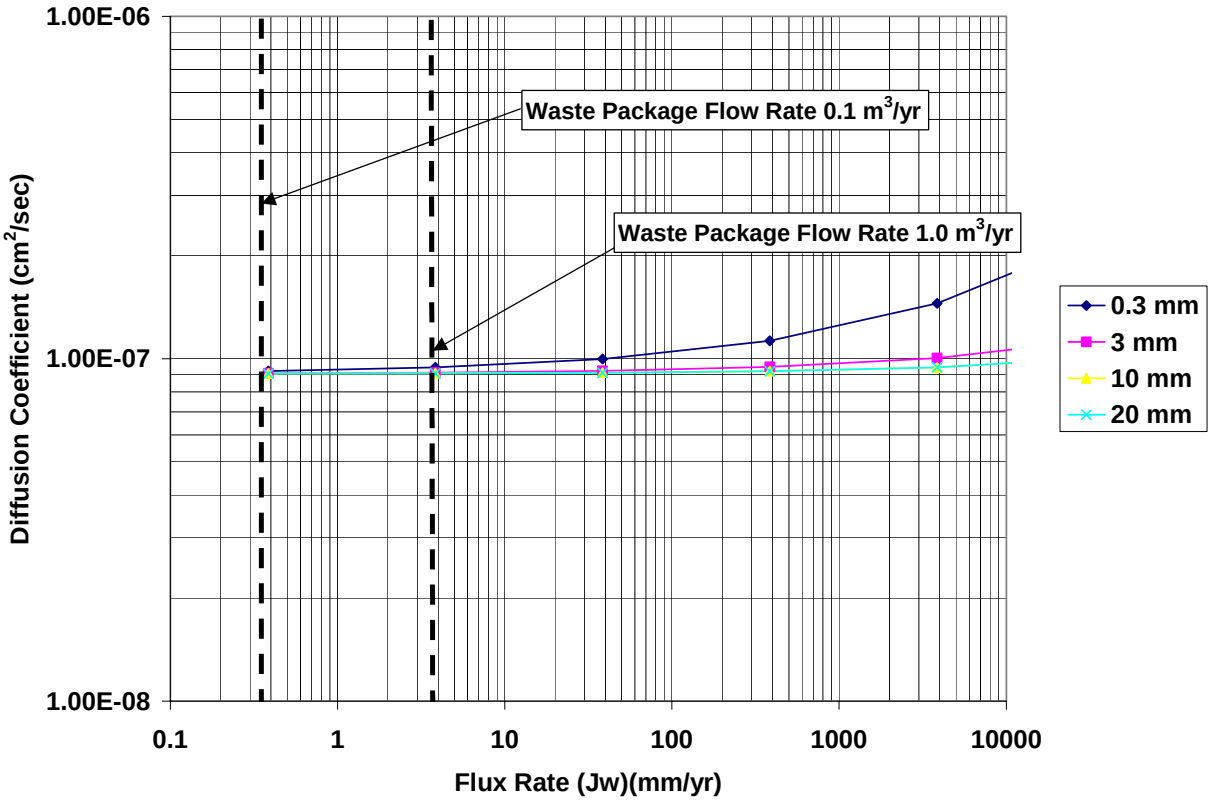

Figure XII-1. Summary of Diffusion Coefficients for the Dripping Case Over a Range of Percolation Rates

ATTACHMENT XIII

DERIVATION OF THE FORMULAS FOR THE CALCULATION OF THE BULK VOLUMETRIC MOISTURE CONTENT

INTENTIONALLY LEFT BLANK

Attachment XIII - Derivation of the Formulas for the Calculation of the Bulk Volumetric Moisture Content

This attachment presents a derivation of the formulas to be applied for the bulk volumetric moisture content that are used to calculate the diffusion coefficient in the invert for the dripping case, and the nondripping case. The first derivation considers the dripping case.

XIII.1 DERIVATION FOR THE DRIPPING CASE

The following parameters are considered for the dripping case (Table 4-3).

$\theta_{intergrain} := 0.051$

$\phi_{intergrain} := 0.45$

$\theta := .051$

$\phi_{matrix} := 0.131$

$\theta_r := 0.05$

$\theta_s := \phi_{intergrain}$

Consider the phase diagram for the matrix, and solve for the volume of the voids within the crushed tuff particles. Consider the soil mechanics convention of expressing the volume of the solids equal to one.

The matrix porosity as would be determined on core samples is defined as the volume of the matrix voids divided by the total volume (Jury et al. 1991, p. 29): Solve for the volume of the matrix.

$$\frac{V_{matrix}}{1 + V_{matrix}} = \phi_{matrix}$$

$$V_{matrix} := \frac{\phi_{matrix}}{\left(1 - \phi_{matrix}\right)}$$

$V_{matrix} = 0.151$

Now calculate the volume between the grains. From the fundamental definition of porosity for the coarse pore space:

$$\frac{V_{intergrain}}{1 + V_{matrix} + V_{intergrain}} = \phi_{intergrain}$$

$$V_{intergrain} := -\phi_{intergrain} \cdot \frac{\left(1 + V_{matrix}\right)}{\left(-1 + \phi_{intergrain}\right)}$$

$V_{intergrain} = 0.942$

Now consider the definition of the saturation for the coarse pore space. The saturation is defined in terms of the volumetric moisture content of the coarse pore space as (Fetter 1993, p. 182):

$$S_e := \frac{\theta - \theta_r}{\theta_s - \theta_r}$$

$S_e = 0.25\%$

This represents the saturation of the intergranular pore space. Now calculate the bulk density on the basis of the phase diagram assuming the fine intragranular pore space is saturated with water.

$V_w := S_e \cdot V_{intergrain}$

$V_w = 2.354 \cdot 10^{-3}$

$V_{matrix} = 0.151$

$V_{intergrain} = 0.942$

The bulk volumetric moisture content is defined as:

$$\theta_{Bulk} := \frac{V_w + V_{matrix}}{1 + V_{intergrain} + V_{matrix}}$$

$\theta_{Bulk} = 0.073$

$$\theta_{Bulk} := \frac{\phi_{intergrain} \cdot \left(1 + \frac{\phi_{matrix}}{1 - \phi_{matrix}}\right) \cdot \frac{1}{1 - \phi_{intergrain}} \cdot \left(\frac{\theta - \theta_r}{\phi_{intergrain} - \theta_r}\right) + \frac{\phi_{matrix}}{1 - \phi_{matrix}}}{1 + \left[\phi_{intergrain} \cdot \left(1 + \frac{\phi_{matrix}}{1 - \phi_{matrix}}\right) \cdot \frac{1}{1 - \phi_{intergrain}}\right] + \frac{\phi_{matrix}}{1 - \phi_{matrix}}}$$

$\theta_{Bulk} = 0.073$

XIII.2 DERIVATION FOR THE NONDRIPPING CASE

Now consider the nondripping case. In this case the coarse pore space has a zero saturation as determined, and the fine pore space may by partially saturated. Therefore, S_e = zero, and $\theta_{intergrain} = \theta_r$.

For purposes of calculation, assume that due to drying, the fine pore space in the invert is at 80 percent saturation.

$$S_{matrix} := 0.80$$

Calculate the bulk volumetric moisture content.

$$\theta_{Bulk} := \frac{0 + S_{matrix} \cdot V_{matrix}}{1 + V_{intergrain} + V_{matrix}}$$

$$\theta_{Bulk} = 0.058$$

Develop a formula for the calculation of the bulk water content.

$$\theta_{Bulk} = \frac{\left(\frac{\theta_{matrix} - \theta_{rmatrix}}{\phi_{matrix} - \theta_{rmatrix}}\right) \cdot \frac{\phi_{matrix}}{1 - \phi_{matrix}}}{1 + \phi_{intergrain} \cdot \left[\left(1 + \frac{\phi_{matrix}}{1 - \phi_{matrix}}\right) \cdot \frac{1}{1 - \phi_{intergrain}}\right] + \frac{\phi_{matrix}}{1 - \phi_{matrix}}}$$

$$\theta_{Bulk} := \frac{S_{matrix} \cdot \frac{\phi_{matrix}}{1 - \phi_{matrix}}}{1 + \phi_{intergrain} \cdot \left[\left(1 + \frac{\phi_{matrix}}{1 - \phi_{matrix}}\right) \cdot \frac{1}{1 - \phi_{intergrain}}\right] + \frac{\phi_{matrix}}{1 - \phi_{matrix}}}$$

$$\theta_{Bulk} = 0.058$$

INTENTIONALLY LEFT BLANK

ATTACHMENT XIV

TSPA CALCULATION OF THE DIFFUSION COEFFICIENT FOR THE DRIPPING CASE

INTENTIONALLY LEFT BLANK

Attachment XIV - TSPA Calculation of the Diffusion Coefficient for the Dripping Case

Develop a Mathcad 2001 TSPA-LA Abstraction to be used to assess the diffusion properties for the dripping case.

XIV.1 INPUT THE TABLE LOOKUP FOR THE UNSATURATED HYDRAULIC CONDUCTIVITY AS A FUNCTION OF MOISTURE POTENTIAL

The table lookup includes the four particle sizes. The lookup is contained on Worksheet Conductivity of Attachment IV.

Table XIV-1. Table LookUp

Moisture Potential (bars)	Hydraulic Conductivity (cm/sec)				
	Tuff Matrix	Crushed Tuff			
		dm =0.317 mm	dm = 3.0 mm	dm = 10.0 mm	dm = 20.0 mm
0.00001	6.24655E-09	0.184	16.47999988	183.093696	729.1073774
0.0002	6.23415E-09	0.184	16.47998446	182.2521233	397.4660442
0.001	6.17408E-09	0.183999998	15.16743525	8.5956E-05	4.56172E-10
0.0015	6.14714E-09	0.183999966	4.536805636	3.14417E-08	1.6582E-13
0.002	6.12358E-09	0.183999745	0.115992667	1.14088E-10	6.0155E-16
0.005	6.01436E-09	0.183835865	2.81183E-09	1.92525E-18	1.01515E-23
0.01	5.88112E-09	0.162813422	3.70878E-15	2.53888E-24	1.35981E-29
0.02	5.68014E-09	0.000502335	4.89062E-21	3.39937E-30	2.02283E-34
0.05	5.25441E-09	1.07748E-11	8.2659E-29	1.2231E-35	5.44857E-36
0.1	4.75272E-09	1.42106E-17	1.56708E-34	1.36209E-36	5.91883E-37
0.2	4.03656E-09	1.87389E-23	7.34321E-37	1.79037E-37	7.49958E-38

Reverse the order for the table lookup:

$$\text{Table\_Lookup} := \text{reverse}(\text{Table\_Lookup})$$

Note that the first column is in bars, and the remaining columns are in cm/sec.

XIV.2 LOG-LOG INTERPOLATION FUNCTIONS

Define the Log-Log Interpolation functions. Use the Mathcad interpolation functions for this analysis. Transform to log space for interpolation.

$$i := 1..\text{rows}(\text{Table\_Lookup})$$
$$j := 1..\text{cols}(\text{Table\_Lookup})$$
$$\text{Log\_Table\_Lookup}_{i,j} := \log\left(\text{Table\_Lookup}_{i,j}\right)$$

$$\text{Log\_Table\_Lookup} = \begin{pmatrix} -0.699 & -8.394 & -22.727 & -36.134 & -36.747 & -37.125 \\ -1.000 & -8.323 & -16.847 & -33.805 & -35.866 & -36.228 \\ -1.301 & -8.279 & -10.968 & -28.083 & -34.913 & -35.264 \\ -1.699 & -8.246 & -3.299 & -20.311 & -29.469 & -33.694 \\ -2.000 & -8.231 & -0.788 & -14.431 & -23.595 & -28.867 \\ -2.301 & -8.221 & -0.736 & -8.551 & -17.716 & -22.993 \\ -2.699 & -8.213 & -0.735 & -0.936 & -9.943 & -15.221 \\ -2.824 & -8.211 & -0.735 & 0.657 & -7.502 & -12.780 \\ -3.000 & -8.209 & -0.735 & 1.181 & -4.066 & -9.341 \\ -3.699 & -8.205 & -0.735 & 1.217 & 2.261 & 2.599 \\ 0.000 & -8.204 & -0.735 & 1.217 & 2.263 & 2.863 \end{pmatrix}$$

$$\text{Inter\_Function\_03}(x) := \text{linterp}\left(\text{Log\_Table\_Lookup}^{\langle 3 \rangle}, \text{Log\_Table\_Lookup}^{\langle 1 \rangle}, x\right)$$

$$\text{Inter\_Function\_3}(x) := \text{linterp}\left(\text{Log\_Table\_Lookup}^{\langle 4 \rangle}, \text{Log\_Table\_Lookup}^{\langle 1 \rangle}, x\right)$$

$$\text{Inter\_Function\_10}(x) := \text{linterp}\left(\text{Log\_Table\_Lookup}^{\langle 5 \rangle}, \text{Log\_Table\_Lookup}^{\langle 1 \rangle}, x\right)$$

$$\text{Inter\_Function\_20}(x) := \text{linterp}\left(\text{Log\_Table\_Lookup}^{\langle 6 \rangle}, \text{Log\_Table\_Lookup}^{\langle 1 \rangle}, x\right)$$

XIV.3 WASTE PACKAGE FLOW RATE AND CROSS SECTIONAL AREA

Input the waste package flow rate and the waste package cross sectional area.

$$\text{Q\_Waste\_Package} := 0.1 \cdot \frac{m^3}{yr}$$

The waste package area is taken from *Seepage Model for PA Including Drift Collapse* (CRWMS M&O 2000d, Section 6.3.1)

$$\text{A\_Waste\_Package\_Plan} := 28.05\,m^2$$

XIV.4 FLUX RATE CALCULATION

Calculate the flux rate through the invert.

$$J_w := \frac{\text{Q\_Waste\_Package}}{\text{A\_Waste\_Package\_Plan}}$$

$$J_w = 1.130 \times 10^{-8} \frac{cm}{sec}$$

$$J_w = 3.565 \frac{mm}{yr}$$

XIV.5 SOLUTION FOR MOISTURE POTENTIAL

Solve for the moisture potential for each case. Note that a power function is defined to cover a broad range of values.

$\psi_1 := 10^{\text{Inter\_Function\_03}\left(\log\left(J_w \cdot \frac{\text{sec}}{\text{cm}}\right)\right)}$

$\psi_1 = 0.034851878638221$

$\psi_2 := 10^{\text{Inter\_Function\_3}\left(\log\left(J_w \cdot \frac{\text{sec}}{\text{cm}}\right)\right)}$

$\psi_2 = 0.004649532359782$

$\psi_3 := 10^{\text{Inter\_Function\_10}\left(\log\left(J_w \cdot \frac{\text{sec}}{\text{cm}}\right)\right)}$

$\psi_3 = 0.001580705181856$

$\psi_4 := 10^{\text{Inter\_Function\_20}\left(\log\left(J_w \cdot \frac{\text{sec}}{\text{cm}}\right)\right)}$

$\psi_4 = 0.000828715173741$

XIV.6 SOLUTION OF VOLUMETRIC MOISTURE CONTENT

Solve for the volumetric moisture content. We first input the constants for the van Genuchten relationship (see Table 6-2).

$i := 1..4$

$\alpha_i :=$

65.91
624.
2080.
4160.

$n_i := 8.013$

$\theta_{r_i} := 0.05$

$\theta_{s_i} := 0.45$

Calculate the m value for the three parameter van Genuchten relationship:

$mv_i := 1 - \frac{1}{n_i}$

XIV.7 SOLVE FOR THE VOLUMETRIC MOISTURE CONTENT FROM THE VAN GENUCHTEN RETENTION RELATIONSHIP FROM FETTER (1993, P.172)

$$\theta_i := \theta_{r_i} + \frac{\left(\theta_{s_i} - \theta_{r_i}\right)}{\left[1 + \left(\alpha_i \cdot \psi_i\right)^{n_i}\right]^{mv_i}}$$

$$\theta = \begin{pmatrix} 0.051 \\ 0.050 \\ 0.050 \\ 0.050 \end{pmatrix}$$

XIV.8 SOLUTION OF EFFECTIVE WATER CONTENT

Calculate the effective water content based upon the fine pore structure being saturated with water, and the coarse pore structure have the water content shown above. Assign the matrix porosity ϕ_m to 0.131 (Table 4-3 for TSw35 tuff) and assume that the fine pore structure is saturated with water. From Attachment XIII, the following formula is developed for the dripping case.

$$\phi_{matrix} := 0.131$$

$$\phi_{intergrain} := 0.45$$

$$\theta_{Bulk_i} := \frac{\phi_{intergrain}\left(1 + \frac{\phi_{matrix}}{1 - \phi_{matrix}}\right) \cdot \frac{1}{1 - \phi_{intergrain}} \cdot \left(\frac{\theta_i - \theta_{r_i}}{\phi_{intergrain} - \theta_{r_i}}\right) + \frac{\phi_{matrix}}{1 - \phi_{matrix}}}{1 + \left[\phi_{intergrain}\left(1 + \frac{\phi_{matrix}}{1 - \phi_{matrix}}\right) \cdot \frac{1}{1 - \phi_{intergrain}}\right] + \frac{\phi_{matrix}}{1 - \phi_{matrix}}}$$

$$\theta_{Bulk_i} = \begin{pmatrix} 0.073 \\ 0.072 \\ 0.072 \\ 0.072 \end{pmatrix}$$

XIV.9 SOLUTION OF SOIL-LIQUID DIFFUSION COEFFICIENT

Calculate the soil-liquid diffusion coefficient from Equation 6-16, and accounting for an increased temperature to 45°C as calculated in Attachment III, Equations III-6 and III-7:

$$T_0 := 25 + 273.15$$

$$T := 45 + 273.15$$

$$10^{\frac{1.3272\cdot(293.15-T_0)-0.001053\cdot(T_0-293.15)^2}{T_0-168.15}-\left[\frac{1.3272\cdot(293.15-T)-0.001053\cdot(T-293.15)^2}{T-168.15}\right]} = 1.494$$

$$D_{sl_i} := 2.30\cdot 10^{-5}\cdot\frac{cm^2}{sec}\cdot 1.494\cdot(\theta_i)^{1.863}$$

$$D_{sl_i} := 3.44\cdot 10^{-5}\cdot\frac{cm^2}{sec}\cdot(\theta_{Bulk_i})^{1.863}$$

$$D_{sl} = \begin{pmatrix} 2.648\times 10^{-7} \\ 2.578\times 10^{-7} \\ 2.568\times 10^{-7} \\ 2.566\times 10^{-7} \end{pmatrix} \frac{cm^2}{sec}$$

INTENTIONALLY LEFT BLANK

ATTACHMENT XV

CALCULATION OF THE THICKNESS OF THE INVERT FOR ANALYSIS

INTENTIONALLY LEFT BLANK

Attachment XV - Calculation of the Thickness of the Invert for Analysis

The analysis in this report (Section 6.10) provides a breakthrough analysis for radionuclides through invert. The following analysis takes information on the geometry of the invert as determined from the current repository design to calculate an average thickness of the invert. A second analysis is then performed to estimate the maximum settlement that would occur. Note that the analysis is conservative because the invert foundation will be engineered to place the crushed tuff near its critical void ratio, and this would reduce the amount of settlement with time. Nevertheless, the thickness of the invert during the postclosure period is estimated. The emplacement drift configuration is shown on *Repository Design Project, Repository/PA IED Emplacement Drift Configuration 1 of 2* (BSC 2003d) and references *Repository Design, Emplacement Drift Steel Invert Plan and Details* (BSC 2001c, Figure 5). The dimension shown from center to center of the rail system on the typical invert elevation is 2.95 m. The thickness of the invert is shown as 0.806 m. Calculate the thickness of the invert considering that the emplacement drift radius is 2.75 m. Figure XV-1 shows the coordinate system and dimensions for the calculations. The distance from the centerline of the drift to the top of the invert is 1.94 m.

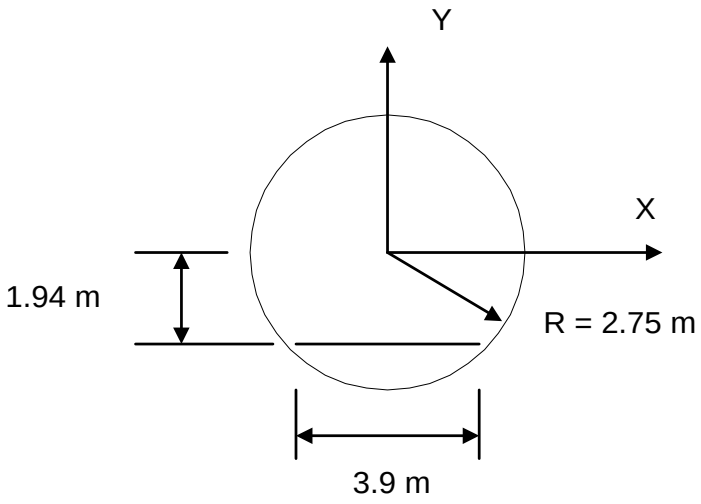

Source: BSC 2001c; BSC 2003d

Figure XV-1. Invert Geometry

The equation of a circle is given by:

$$X^2 + Y^2 = R^2 \qquad \text{(Eq. XV-1a)}$$

where

- X x coordinate,
- Y y coordinate, and
- R radius (2.75 m)

The invert thickness is given by the expression:

$$\sqrt{R^2 - x^2} = 1.94$$

Using the equation solve for the point when y = 0:

$$\sqrt{R^2 - x^2} - 1.94 = 0$$

The value for X_0 equals 1.949 m. Use integral calculus to solve for the average depth of the invert. From integral calculus

$$\int \sqrt{R^2 - x^2}\, dx = \frac{x}{2} \cdot \sqrt{R^2 - x^2} + \frac{R^2}{2} \cdot \operatorname{asin}\left(\frac{x}{R}\right)$$

$$\int 1.94\ dx = 1.94 \cdot x$$

Evaluating the definite integral for the area.

$$\left(\frac{x_0}{2} \cdot \sqrt{R^2 - x_0^2} + \frac{R^2}{2} \cdot \operatorname{asin}\left(\frac{x_0}{R}\right)\right) - \left(\frac{0}{2} \cdot \sqrt{R^2 - 0^2} + \frac{R^2}{2} \cdot \operatorname{asin}\left(\frac{0}{R}\right)\right) - \left(1.94 \cdot x_0\right) = 1.088$$

The average height is given as by the area divided by the value for x0.

$$\frac{\left(\frac{x_0}{2} \cdot \sqrt{R^2 - x_0^2} + \frac{R^2}{2} \cdot \operatorname{asin}\left(\frac{x_0}{R}\right)\right) - \left(\frac{0}{2} \cdot \sqrt{R^2 - 0^2} + \frac{R^2}{2} \cdot \operatorname{asin}\left(\frac{0}{R}\right)\right) - \left(1.94 \cdot x_0\right)}{x_0} = 0.558$$

The calculated value for the thickness of the invert is 0.558 m. Consider the maximum potential settlement that might occur with time. This report considers materials that have a range of particles from 0.3 to 20 mm. According to *Foundation Engineering Handbook* (Winterkorn and Fang 1975, p. 84), the materials would classify as a poorly graded sand (SP). Considering these materials and the potential for some settlement with time, the invert thickness used in these calculations is 0.5 m.

ATTACHMENT XVI

MOISTURE RETENTION FOR CRUSHED TUFF

INTENTIONALLY LEFT BLANK

Attachment XVI - Moisture Retention for Crushed Tuff

The analysis method is presented in *Water Diversion Model* (CRWMS M&O 2000c, Section 3 and Attachment V).

Table XVI-1. van Genuchten Curve Fit Parameter Results for the Invert

Parameter	Value	Unit
Moisture Content at Saturation (θ_s)	0.63	(no units)
Residual Moisture Content (θ_r)	0.05	(no units)
α_i	117.00	$bars^{-1}$
n_i	2.75	(no units)
m	0.64	(no units)
Sum of Residuals	5.25E-04	(no units)

NOTE: The α parameter is calculated as 0.12 cm^{-1}.

Note that the parameters are calculated using the Microsoft Excel Equation Solver based upon the sum of the residuals as given above from Table XVI-2.

Table IV-2. Retention Analysis Results for the Invert

Volumetric Moisture Content	Moisture Potential (bars)	Predicted Moisture Content	Residuals
0.068	0.121	0.057	1.29E-04
0.059	0.174	0.054	2.52E-05
0.058	0.309	0.052	3.49E-05
0.057	0.483	0.051	3.03E-05
0.056	0.696	0.051	2.24E-05
0.055	1.090	0.051	1.51E-05
0.053	1.930	0.051	3.83E-06
0.052	3.020	0.051	9.60E-07
0.050	4.350	0.051	1.02E-06
0.045	17.400	0.051	3.60E-05
0.060	0.121	0.057	1.14E-05
0.060	0.174	0.054	3.63E-05
0.059	0.309	0.052	4.77E-05
0.058	0.483	0.051	4.23E-05
0.058	0.696	0.051	4.54E-05
0.056	1.090	0.051	2.38E-05
0.054	1.930	0.051	8.74E-06
0.054	3.020	0.051	8.88E-06
0.052	4.350	0.051	9.79E-07
0.047	17.400	0.051	1.60E-05

NOTE: Volumetric moisture content and moisture potential are obtained from Attachment XI and DTN: GS980808312242.015 for crushed tuff.

Equation IV-1 is used for calculating the predicted moisture content.

Residuals are calculated as the square of the difference between the actual volumetric moisture content and the predicted moisture content.

INTENTIONALLY LEFT BLANK

ATTACHMENT XVII

ESTIMATE OF THE BOUNDARY BETWEEN ADVECTION AND DIFFUSION

Attachment XVII - Estimate of the Boundary Between Advection and Diffusion

This attachment presents an analysis to estimate the boundary between a diffusion dominated mass transfer and an advection dominated mass transfer in the invert. Section 6.2 developed the relations describing advection and hydrodynamic dynamic dispersion restated as:

Liquid Advection (bulk flow or convection)

$$J_{lc} = J_w \cdot C_L \qquad \text{(Eq. XVII-1)}$$

where

J_{lc} is the liquid advection flux (m/s)
J_w is the vertical Darcy flux rate (m/s)
C_L is the solute concentration of the solute at location x = 0 (mg/L)

Soil-Liquid Diffusion

$$J_{sl} = -D_{sl} \cdot \frac{dC_L}{dz} \qquad \text{(Eq. XVII-2)}$$

where

J_{sl} = soil liquid flux (m/sec)
J_w = vertical darcy flux (m/sec)
Z = vertical coordinate (m)

Note that the second equation can be written as an approximation across the invert.

$$J_{sl} \approx -D_{sl} \cdot \frac{C_L}{L} \qquad \text{(Eq. XVII-3)}$$

where

L = length in the vertical direction

Noting that the ratio of advective transport to diffusive transport:

$$Pec = \frac{J_w \cdot L}{D_{sl}} \qquad \text{(Eq. XVII-4)}$$

where

Pec = Peclet Number

The dimensionless Peclet Number can then be defined as the ratio of the advective transport to the diffusive transport (Fetter 1993, p. 54):

$$Pec = \frac{v_x \cdot L}{D_{sl}} \qquad \text{(Eq. XVII-5)}$$

It should be noted that the Peclet Number as calculated in this manner is a relative index of the ratio of advective to diffusive transport, and that the transition from a diffusion dominated system to an advective dominated system depends on the characteristic length used in the analysis. Fetter (1993, p. 55) defines the average diameter of the particles in cm. However, in this analysis the vertical length of the invert is selected as a more meaningful index.

In the following analysis, the critical Peclet Number is determined as the value of pore velocity that would result in the fifty percent breakthrough occurring in approximately one half the time.

The analysis estimates the critical Peclet Number for diffusion to occur. In this calculation, the contaminant transport equation for breakthrough is used to perform a diffusion analysis. The 50 percent breakthrough is defined. The demarcation between diffusion and advection occurs for a pore velocity that is one-half of this value. The velocity is selected to result in a breakthrough at the specified time of 250 years.

Consider diffusion alone. From Attachment III:

$$D_{sl} = 1.707 \times 10^{-7} \frac{cm^2}{sec}$$

The breakthrough for diffusion alone is presented in Figure XVII-1. The fifty percent breakthrough time is about 500 years.

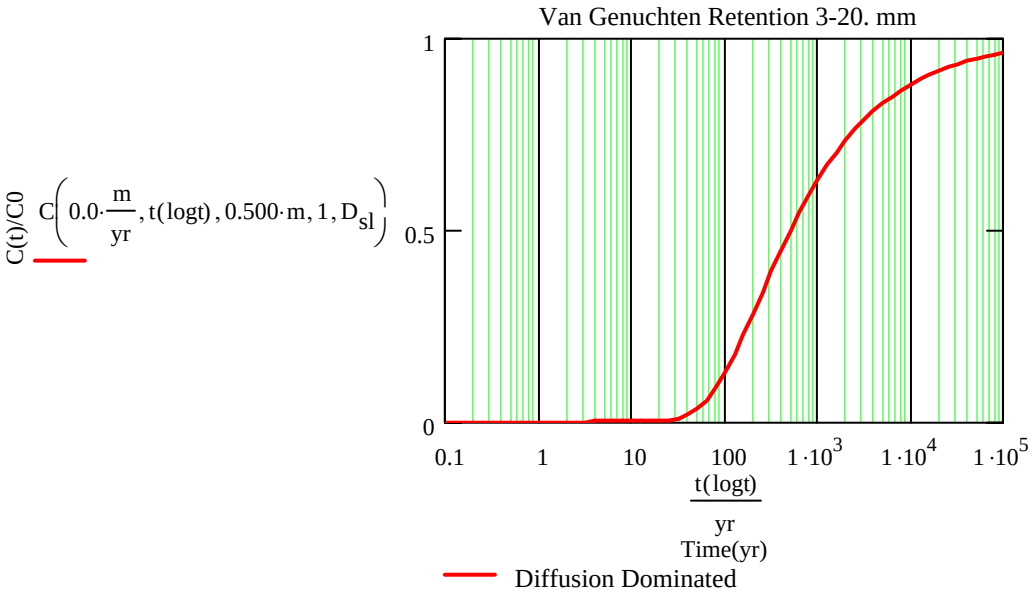

Figure XVII-1. Breakthrough for a Diffusion Dominated System

Calculate the velocity that results in a fifty percent breakthrough of 250 years. From Equations 6-12 and 6-13 for a pore water velocity of 0.85 mm per year:

$$V_L := 0.85 \cdot \frac{mm}{yr}$$

$$D_L := \lambda \cdot V_L + D_{sl}$$

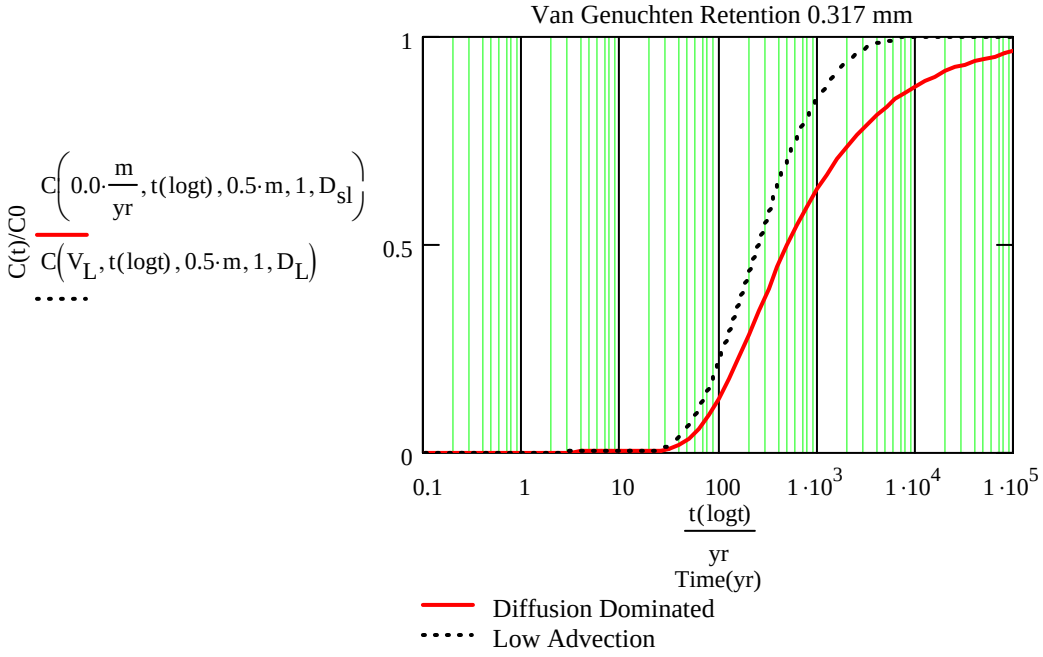

Figure XVII-2. Breakthrough Analysis for Advection-Diffusion with Fifty Percent Breakthrough Occurring After 250 Years

The results of the calculation are presented in Figure XVII-2. Calculate the critical Peclet Number based upon this velocity and the maximum depth of the invert using Equation XVII-4.

$$\frac{V_L \cdot 0.5 \cdot m}{D_{sl}} = 0.8$$

The critical Peclet Numbers based upon this criterion is about 0.8. Use this Peclet Number in the analysis.

An analysis was performed to calculate Peclet Numbers from the NUFT analysis for the case of 35 mm per year with the nondimensional van Genuchten parameters, and the Campbell parameters for particle sizes of 3 mm and 10 mm, respectively. Figure XVII-3 presents the profile of the Darcy Flux within the invert close the open drift. The Darcy Flux is calculated from the NUFT pore water velocity results by multiplying by the cross-sectional flow area within the pore space. The cross-sectional area approximately equals the saturation (S) times the porosity (θ). It is seen that the percolation fluxes expressed in mm per year are less than the saturated percolation flux of about 3 mm per year.

Figure XVII-4 presents the Peclet Number for these analyses for comparision of the value in which diffusion controls as presented above. The analysis shows that the approximate thickness of the diffusion controlled invert is approximately 0.1 m or about twenty percent of the 0.5 m thick invert.

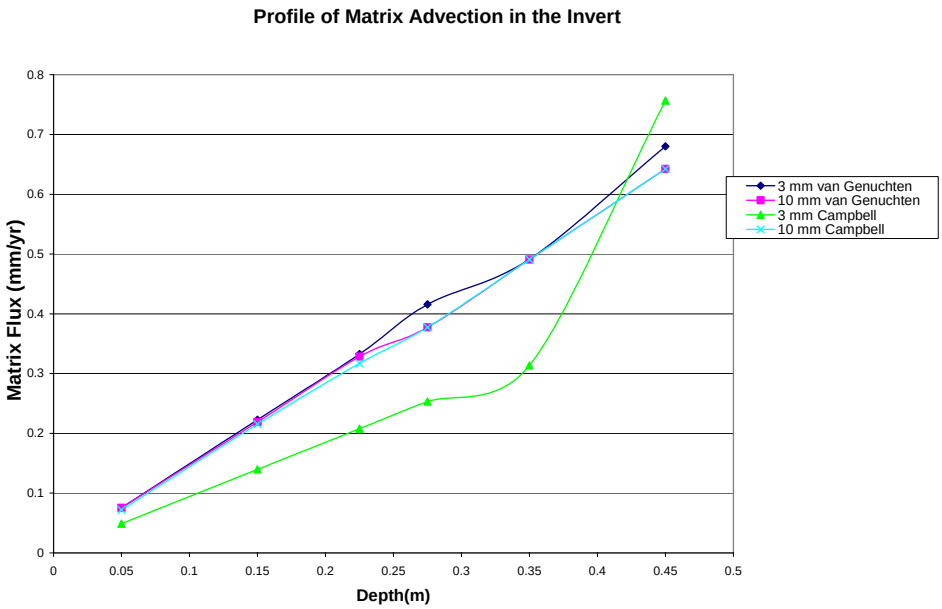

Figure XVII-3. Profile of Matrix Advection in the Invert

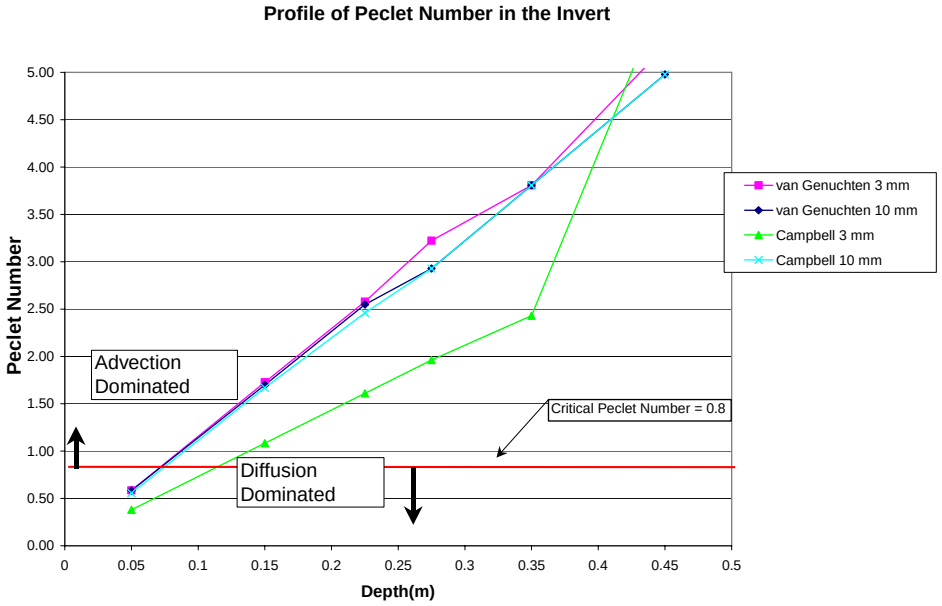

Figure XVII-4. Profile of the Peclet Number in the Invert

INTENTIONALLY LEFT BLANK

ATTACHMENT XVIII

ALTERNATE POREWATER VELOCITY CALCULATION

Attachment XVIII - Alternate Pore Water Velocity Calculation

This attachment presents an alternate analysis of the flow distribution in the invert. The invert was analyzed with intragranular matrix retention and intrinsic matrix permeability equal to the properties of the host horizon, and with intergranular properties selected on the basis of the Brooks and Corey data (Sections 4.1.1 and 4.1.2) that is named the nondimensionalized van Genuchten properties in this report. The Campbell properties were used as an alternate model, and the NUFT results (Section 6.8) showed very similar behavior to the nondimensionalized van Genuchten properties in which the crushed tuff intragranular matrix showed high saturation, and the intergranular porosity was free of water.

The results of this analysis are also consistent with the results presented in Figure 6.3.4 of *Drift-Scale Radionuclide Transport* (BSC 2003f) that shows similar behavior in the matrix host rock for similar hydrologic properties sets. In one analysis reported in Figure 6.3.4, the far field flux rate was selected as 10 mm per year which is lower than the far field flux of 35 mm per year used in the NUFT analysis. The percolation rate of 10 mm per year, according to Figure 6.3.4, would result in a lower saturation than the higher saturation presented in this analysis. Figure 6.3.4 shows that the saturation is approximately 0.87. Input the fluid properties for analysis (Incropera and DeWitt 1996, p. 846 and Table 6-2):

$$\rho := 1000 \frac{kg}{m^3}$$

$$\mu := 8.935\,10^{-4} \cdot \frac{N \cdot s}{m^2}$$

Now substituting in the relationship of hydraulic conductivity to intrinsic permeability that converts a saturated intrinsic permeability (k) to a saturated hydraulic conductivity (Ks) (Freeze and Cherry 1979, p. 27):

$$K_s := 5.71 \cdot 10^{-18} \cdot m^2 \cdot \frac{\rho \cdot g}{\mu}$$

$$K_s = 6.267 \times 10^{-9} \frac{cm}{sec}$$

$$K_s = 1.978 \frac{mm}{yr}$$

The matrix saturated hydraulic conductivity equal about 2.0 mm per year. Substituting in the following properties from Table 4-4 (TSw35):

$S := 0.87$
$\theta_r := 0.0157$
$\theta_s := \text{~~0.112~~}\ 0.131$ QBC 8/23/03
$m := 0.236$

From Jury et al. (1991, p. 109):

$$S = \frac{\theta - \theta_r}{\theta_s - \theta_r} \qquad \text{(Eq. XVIII-1)}$$

Solving for θ:

$$\theta := \left[S + \frac{1}{(\theta_s - \theta_r)} \cdot \theta_r \right] \cdot (\theta_s - \theta_r) \qquad \text{(Eq. XVIII-2)}$$

$$\theta = 0.116$$

Solving for the unsaturated hydraulic conductivity and substituting into the van Genuchten relation for unsaturated hydraulic conductivity (Jury et al. 1991, p. 109):

$$K(S) := K_s \cdot S^{\frac{1}{2}} \cdot \left[1 - \left(1 - S^{\frac{1}{m}} \right)^{m} \right]^2 \qquad \text{(Eq. XVIII-3)}$$

$$K(S) = 0.056 \frac{mm}{yr}$$

The calculated value for matrix percolation flux is approximately 0.1 mm per year. This value is in approximate agreement with the matrix percolation flux of 0.15 mm per year reported in Figure 6.3-4 of *Drift-Scale Radionuclide Transport* (BSC 2003f). It should be noted that small variations in matrix saturation might result in large variations in flux, because the unsaturated matrix hydraulic conductivity is a strong nonlinear function of volumetric moisture content or saturation. In addition, differences in temperature affect unsaturated hydraulic conductivity between the two analyses.

The results reported in Figure 6.3-4 of *Drift-Scale Radionuclide Transport* (BSC 2003f) indicate that the open drift behaves like an impermeable inclusion with flow being diverted around the inclusion. The analysis results (Section 6.7 and Attachment IX) show a similar behavior in flow being diverted around the open drift.

The crushed tuff matrix flow results can be interpreted with the aid of a closed form analytical solution for flow around an inclusion (CRWMS M&O 2001b, Attachment XII). The report developed a closed form solution for flow. From Attachment XII, Equations XII-9 and XII-10:

$$p_i = -\omega \cdot \frac{2 \cdot k_o}{k_i + k_o} \cdot r \cdot \cos(\theta) \qquad \text{(Eq. XVIII-4)}$$

$$r \le a$$

$$p_o = -\omega \cdot \left[1 - \frac{(k_i - k_o)}{k_i + k_o} \cdot \frac{a^2}{r^2} \right] \cdot r \cdot \cos(\theta) \qquad r \geq a \qquad \text{(Eq. XVIII-5)}$$

where

p_i = capillary pressure within an inclusion
p_o = capillary pressure outside an inclusion
r = radius from the center of the inclusion
ω = Darcy flux in the direction of flow
k_i = unsaturated intrinsic permeability within the inclusion
k_o = unsaturated intrinsic permeability outside the inclusion
a = radius of the inclusion

Consider the partial derivatives (from Beyer 1987, p. 205):

$$\theta = \operatorname{atn}\left(\frac{y}{x}\right)$$
$$r = \sqrt{x^2 + y^2} \qquad \text{(Eq. XVIII-6)}$$

$$u = \frac{y}{x}$$
$$\frac{d}{dx} u = \frac{-y}{x^2} \qquad \text{(Eq. XVIII-7)}$$

$$\theta = \operatorname{atn}(u) \qquad \text{(Eq. XVIII-8)}$$

$$\frac{d}{dx}\theta \quad \frac{1}{1 + u^2} \cdot \frac{d}{dx} u \qquad \text{(Eq. XVIII-9)}$$

$$\frac{d}{dx}\theta \quad \frac{1}{1 + \left(\frac{y}{x}\right)^2} \cdot \frac{-y}{x^2}$$

$$\frac{d}{dx}\theta \quad \frac{-y}{\left(x^2 + y^2\right)} \qquad \text{(Eq. XVIII-10)}$$

$$\frac{d}{dx} r = \frac{1}{\left(x^2 + y^2\right)^{\left(\frac{1}{2}\right)}} \cdot x$$
$$r = \sqrt{x^2 + y^2} \qquad \text{(Eq. XVIII-11)}$$

Consider the derivative with respect to y:

$$\frac{d}{dy}\theta = \frac{1}{1+\left(\frac{y}{x}\right)^2}\cdot\frac{d}{dy}\frac{y}{x} \qquad \text{(Eq. XVIII-12)}$$

$$\frac{d}{dy}\theta = \frac{1}{1+\left(\frac{y}{x}\right)^2}\cdot\frac{1}{x}$$

$$\frac{d}{dy}r = \frac{1}{\left(x^2+y^2\right)^{\left(\frac{1}{2}\right)}}\cdot y \qquad \text{(Eq. XVIII-13)}$$

For the case inside the inclusion, the derivative is trivial:

$$\frac{d}{dx}p_i = -\omega\cdot\frac{2\cdot k_o}{k_i+k_o}\cdot 1 \qquad \text{(Eq. XVIII-14)}$$

For the case outside the inclusion:

$$p_o = -\omega\cdot\left[1-\frac{\left(k_i-k_o\right)}{k_i+k_o}\cdot\frac{a^2}{r^2}\right]\cdot r\cdot\cos(\theta) \qquad \text{(Eq. XVIII-15)}$$

$$r \geq a$$

$$p_o = -\omega\cdot\left[r-\frac{\left(k_i-k_o\right)}{k_i+k_o}\cdot\frac{a^2}{r}\right]\cdot 1\cdot\cos(\theta) \qquad \text{(Eq. XVIII-16)}$$

Use the chain rule:

$r \geq a$

$$\frac{d}{dx}p_o = -\omega\cdot\left[1+\frac{\left(k_i-k_o\right)}{\left(k_i+k_o\right)}\cdot\frac{a^2}{r^2}\right]\cdot\frac{x}{\sqrt{x^2+y^2}}\cdot\cos(\theta) - \omega\cdot\left[r-\frac{\left(k_i-k_o\right)}{k_i+k_o}\cdot\frac{a^2}{r}\right]\cdot -\sin(\theta)\cdot\frac{-y}{\left(x^2+y^2\right)} \qquad \text{(Eq. XVIII-17)}$$

Substitute the definitions for sin and cos:

$$\frac{d}{dx}p_o = -\omega\cdot\left[1+\frac{\left(k_i-k_o\right)}{\left(k_i+k_o\right)}\cdot\frac{a^2}{r^2}\right]\cdot\frac{x}{\sqrt{x^2+y^2}}\cdot\frac{x}{r} - \omega\cdot\left[r-\frac{\left(k_i-k_o\right)}{k_i+k_o}\cdot\frac{a^2}{r}\right]\cdot\frac{-y}{r}\cdot\frac{-y}{\left(x^2+y^2\right)} \qquad \text{(Eq. XVIII-18)}$$

$$\frac{d}{dx}p_o = -\omega\cdot\left[1+\frac{\left(k_i-k_o\right)}{\left(k_i+k_o\right)}\cdot\frac{a^2}{r^2}\right]\cdot\frac{x}{\sqrt{x^2+y^2}}\cdot\frac{x}{\sqrt{x^2+y^2}} - \omega\cdot\left[1-\frac{\left(k_i-k_o\right)}{k_i+k_o}\cdot\frac{a^2}{r^2}\right]\cdot\frac{y^2}{\left(x^2+y^2\right)} \qquad \text{(Eq. XVIII-19)}$$

This agrees with Equation XII-56 of *Water Distribution and Removal Model* (CRWMS M&O 2001b):

$$\frac{d}{dx}p_o = -\omega\cdot\left[1 + \frac{(k_i - k_o)}{(k_i + k_o)}\cdot\frac{a^2}{r^2}\right]\cdot\frac{x^2}{r^2} - \omega\cdot\left[1 - \frac{(k_i - k_o)}{k_i + k_o}\cdot\frac{a^2}{r^2}\right]\cdot\frac{y^2}{r^2} \qquad \text{(Eq. XVIII-20)}$$

Take the derivative with respect to y:

$$\frac{d}{dy}p_o = -\omega\cdot\left[1 + \frac{(k_i - k_o)}{(k_i + k_o)}\cdot\frac{a^2}{r^2}\right]\cdot\frac{y}{\sqrt{x^2 + y^2}}\cdot\cos(\theta) - \omega\cdot\left[r - \frac{(k_i - k_o)}{k_i + k_o}\cdot\frac{a^2}{r}\right]\cdot -\sin(\theta)\cdot\left[\frac{1}{1 + \left(\frac{y}{x}\right)^2}\cdot\frac{1}{x}\right] \qquad \text{(Eq. XVIII-21)}$$

Substitute the definitions for sin and cos:

$$\frac{d}{dy}p_o = -\omega\cdot\left[1 + \frac{(k_i - k_o)}{(k_i + k_o)}\cdot\frac{a^2}{r^2}\right]\cdot\frac{y}{\sqrt{x^2 + y^2}}\cdot\frac{x}{r} - \omega\cdot\left[r - \frac{(k_i - k_o)}{k_i + k_o}\cdot\frac{a^2}{r}\right]\cdot\frac{-y}{r}\cdot\left[\frac{1}{1 + \left(\frac{y}{x}\right)^2}\cdot\frac{1}{x}\right] \qquad \text{(Eq. XVIII-22)}$$

Calculate the approximate area of inclusion. From Attachment XV:

$\text{Area\_Invert} := 2\cdot 1.088$

$\text{Area\_Invert} = 2.176$

$\text{Area\_Drift} := \pi\cdot 2.75^2$

$\text{Area\_Drift} = 23.758$

$\text{Area\_Inclusion} := \text{Area\_Drift} - \text{Area\_Invert}$

$\text{Area\_Inclusion} = 21.582$

$\pi\cdot a^2 - \text{Area\_Inclusion}$

has solution(s)

$$a := \frac{1}{\pi}\cdot(\pi\cdot\text{Area\_Inclusion})^{\frac{1}{2}}$$

$a = 2.621$

The calculated radius is 2.62 m. Set the farfield flow in the matrix equal to 1.31 mm per year consistent with the NUFT analysis. Set the external hydraulic conductivity equal to one, and the gradient in the farfield equal to one for a deep water table. See Jury et al. 1993 p. 127), [DIRS 102010]. The internal hydraulic conductivity is set to zero.

$a := 2.621$

$k_o := 1.31\cdot\frac{mm}{yr}$

$k_i := 0\cdot\frac{mm}{yr}$

$\omega := -1.0$

$$v_x(x,y) := k_o \cdot \left[-\omega \cdot \left[1 + \frac{(k_i - k_o)}{(k_i + k_o)} \cdot \frac{a^2}{(x^2 + y^2)} \right] \cdot \frac{x^2}{(x^2 + y^2)} - \omega \cdot \left[1 - \frac{(k_i - k_o)}{(k_i + k_o)} \cdot \frac{a^2}{(x^2 + y^2)} \right] \cdot \frac{y^2}{(x^2 + y^2)} \right]$$

(Eq. XVIII-23)

$$v_y(x,y) := -k_o \cdot \left[-\omega \cdot \left[1 + \frac{(k_i - k_o)}{(k_i + k_o)} \cdot \frac{a^2}{(x^2 + y^2)} \right] \cdot \frac{y}{x^2 + y^2} \cdot \frac{x}{1} - \omega \cdot \left[\sqrt{x^2 + y^2} - \frac{(k_i - k_o)}{k_i + k_o} \cdot \frac{a^2}{\sqrt{x^2 + y^2}} \right] \cdot \frac{-y}{\sqrt{x^2 + y^2}} \cdot \left[\frac{1}{1 + \left(\frac{y}{x}\right)^2} \cdot \frac{1}{x} \right] \right]$$

(Eq. XVIII-24)

Perform an analysis out to about four times the diameter.

Input the porewater velocity profile from NUFT analysis Attachment II and XVII. The data are from Figure XVII-2:

$$\text{Array\_Invert} := \begin{pmatrix} 0.05 & 0.075516768 \\ 0.15 & 0.222774466 \\ 0.225 & 0.332607053 \\ 0.275 & 0.415758816 \\ 0.35 & 0.491351328 \\ 0.45 & 0.680332608 \end{pmatrix}$$

Consider a column of elements 0.15 meters from the centerline.

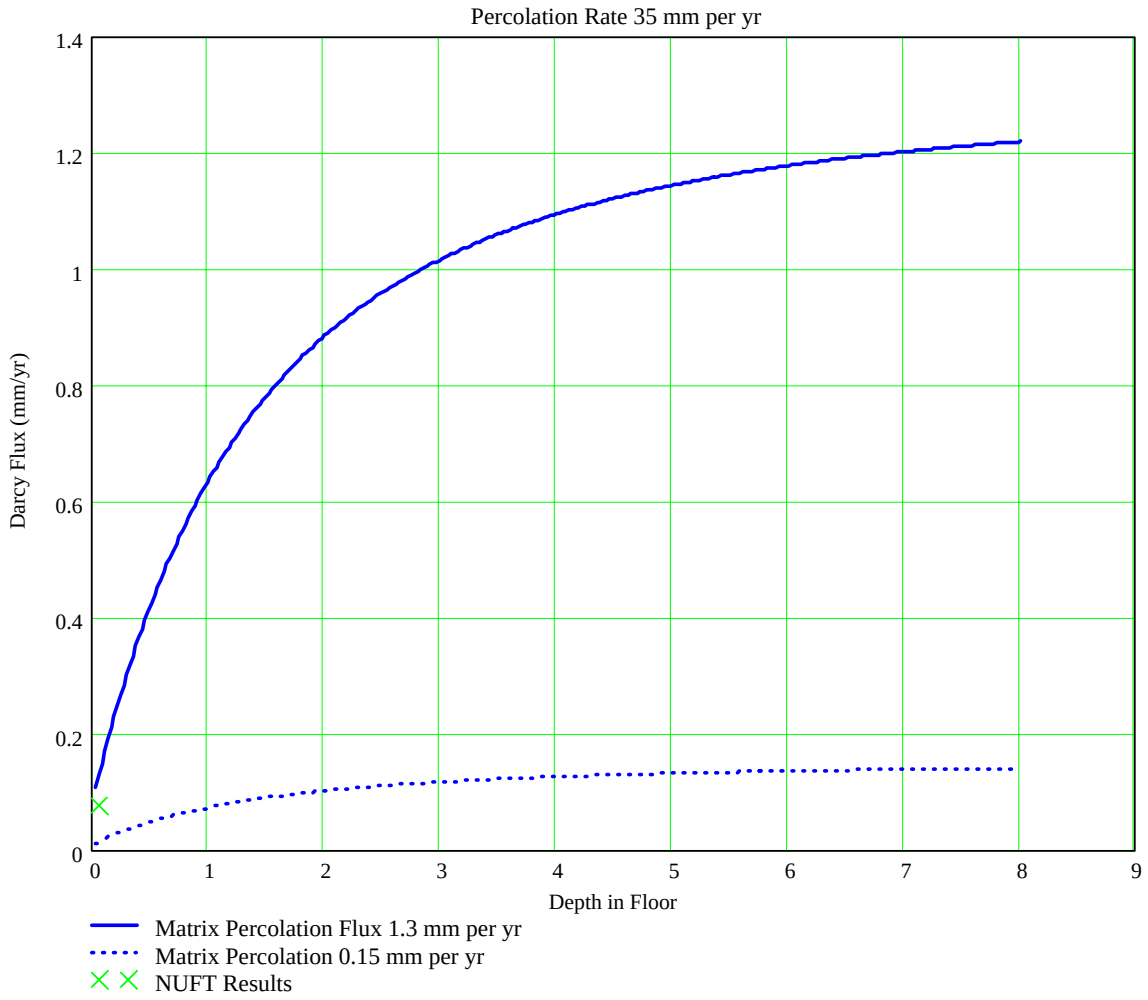

Figure XVIII-1. Comparison of a Closed Form Solution for Matrix Flow at Saturation with the Results of the NUFT Analysis

Figure XVIII-1 shows the results of a comparison of the fluxes in the invert to the closed form solution for far field matrix flow around an inclusion. This far field flow is approximately 1.3 mm per year consistent with NUFT analysis. The figure shows that the Darcy fluxes in the invert at a percolation rate of 35 mm per year are near saturation, and are responding to the impermeable inclusion as represented by the emplacement drift.

ATTACHMENT XIX

CD-ROMS WITH INPUT AND OUTPUT FILES

INTENTIONALLY LEFT BLANK